Configurations of Lagrangians, fundamental domains and discrete subgroups of PU(2,1).

Julien Paupert

UNIVERSITÉ PARIS 6

PIERRE ET MARIE CURIE

Thèse de Doctorat

Spécialité : Mathématiques

présentée par

Julien PAUPERT

pour obtenir le grade de Docteur de l'Université Paris 6

Configurations de lagrangiens, domaines fondamentaux et sous-groupes discrets de $PU(2,1)$

Configurations of Lagrangians, fundamental domains and discrete subgroups of $PU(2,1)$

Soutenue le mardi 29 novembre 2005 devant le jury composé de

Yves BENOIST	(ENS Paris)	
Elisha FALBEL	(Paris 6)	Directeur
John PARKER	(Durham)	
Frédéric PAULIN	(ENS Paris)	Rapporteur
Jean-Jacques RISLER	(Paris 6)	

Rapporteur non présent à la soutenance : William GOLDMAN (Maryland)

Remerciements

Tout d'abord, merci à mon directeur de thèse, Elisha Falbel, pour tout le temps et l'énergie qu'il m'a consacrés.

Merci ensuite à William Goldman et à Frédéric Paulin d'avoir accepté de rapporter cette thèse; à Yves Benoist, John Parker et Jean-Jacques Risler d'avoir bien voulu participer au jury.

Merci en particulier à Frédéric Paulin et à John Parker pour les nombreuses corrections et améliorations qu'ils ont suggérées.

Pour les nombreuses et enrichissantes conversations mathématiques durant ces années de thèse, je voudrais remercier particulièrement Martin Deraux et Pierre Will, ainsi que les membres du groupuscule de géométrie hyperbolique complexe de Chevaleret, Marcos, Masseye et Florent.

Merci également de nouveau à John Parker et à Richard Wentworth pour les conversations que nous avons eues et les explications qu'ils m'ont données lors de leurs visites à Paris.

Je voudrais enfin remercier particulièrement deux enseignants qui m'ont donné envie de faire des maths puis de continuer: M. Monnet qui a réussi en deux ans de lycée à nous montrer des "vraies" maths et à nous les faire apprécier, ainsi que Laurent Coppey qui m'a montré la beauté des actions géométriques de groupes en Licence.

Quant aux remerciements d'ordre personnel, je les ferai de vive voix.

Contents

0.1 Introduction en français 6
0.2 Introduction in english 12

1 Geometric preliminaries **21**
1.1 Complex hyperbolic space 22
1.1.1 Definition, models and structures 22
1.1.2 Isometries 23
1.2 Subspaces and configurations 23
1.2.1 Totally geodesic subspaces 23
1.2.2 Geodesic triangles 24
1.2.3 Configurations of Lagrangians 26
1.3 Isometries 28
1.3.1 Classification of isometries 28
1.3.2 Elliptic isometries 29

2 Fundamental domains for finite groups of $U(2)$ and configurations of Lagrangians **33**
2.1 Introduction 34
2.2 Lagrangian subspaces and $\mathbb{R}$-reflections 34
2.3 Lagrangian pairs 41
2.3.1 Groups generated by two $\mathbb{R}$-reflections 41
2.3.2 Representations of an $\mathbb{R}$-reflection by matrices 42
2.4 An example: the group 3[3]3 42
2.4.1 Action on $\mathbb{C}P^1$ 43
2.4.2 $\mathbb{R}$-reflections 44
2.4.3 Presentations and diagrams 46
2.4.4 Fundamental domains 47
2.5 Other two-generator subgroups of $U(2)$ 47
2.5.1 The strategy 48
2.5.2 Explicit decomposition of reflection groups 49
2.6 Appendix: explicit decomposition of reflection groups 53

3 New constructions of fundamental polyhedra for Mostow's lattices **60**
3.1 Introduction 61
3.2 Complex hyperbolic space 63
3.2.1 Bisectors 65

3.2.2 The group $\Gamma(p,t)$ . . . 69
3.2.3 A canonical hexagon . . . 72
3.2.4 Computing the vertices of the hexagon . . . 73
3.3 Description of a fundamental polyhedron Π in $\mathbf{H}^2_{\mathbb{C}}$ . . . 75
3.3.1 The core hexagon . . . 77
3.3.2 The 3-faces H and H' . . . 77
3.3.3 The whole polyhedron Π . . . 79
3.3.4 The remaining 3-faces . . . 80
3.4 Topology and combinatorial structure of Π . . . 81
3.5 Using Poincaré's polyhedron theorem . . . 84
3.5.1 Side-pairings . . . 85
3.5.2 Cycles and orbits of faces . . . 86
3.5.3 Verifying the tessellation conditions . . . 87
3.6 Beyond the critical phase shift . . . 98
3.7 Comparison with Mostow's domains . . . 99
3.8 Appendix: list of faces and combinatorial structure of Π . . . 100

4 Elliptic triangle groups in $PU(2,1)$, Lagrangian triples and momentum maps 104
4.1 Introduction . . . 105
4.2 Elliptic triangle groups, a polygon of configurations . . . 106
4.2.1 Introduction . . . 106
4.2.2 The group product: a group-valued momentum map . . . 108
4.2.3 Walls and reducible groups . . . 109
4.2.4 Chambers and irreducible groups . . . 116
4.2.5 Which chambers are full ? . . . 118
4.3 Configurations of Lagrangian triples . . . 124
4.3.1 Lagrangian triples vs. elliptic triangles . . . 126
4.3.2 Parametrizing the configurations . . . 130
4.4 Examples and experimental pictures . . . 136
4.4.1 The two generators are complex reflections in a point . . . 137
4.4.2 One generator is a complex reflection in a point . . . 137
4.4.3 The two generators are complex reflections: a non-convex example . . . 138
4.4.4 One generator is a complex reflection: families containing Mostow's lattices $\Gamma(p,t)$ . . . 138
4.4.5 Generic examples . . . 138
4.5 The search for discrete groups: experimental aspects . . . 140
4.5.1 Families containing Mostow's lattices $\Gamma(p,t)$ . . . 142
4.5.2 Families containing $\mathbb{R}$-Fuchsian groups . . . 145

5 Groupes triangulaires elliptiques dans $PU(2,1)$, triplets de lagrangiens et applications moment 150
5.1 Introduction . . . 151
5.2 Groupes triangulaires elliptiques, un polygone de configurations . . . 152
5.2.1 Introduction . . . 152
5.2.2 Le produit de groupe: une application moment à valeurs dans le groupe . 154

5.2.3 Murs et groupes réductibles 155
5.2.4 Chambres et groupes irréductibles 163
5.2.5 Quelles chambres sont pleines ? 164
5.3 Configurations de triplets lagrangiens 171
5.3.1 Triplets lagrangiens vs. triangles elliptiques 172
5.3.2 Un paramétrage des configurations 177
5.4 Exemples et images expérimentales 183
5.4.1 Les deux générateurs sont des réflexions complexes par rapport à un point 184
5.4.2 L'un des générateurs est une réflexion complexe par rapport à un point . 184
5.4.3 Les deux générateurs sont des réflexions complexes: un exemple non convexe 184
5.4.4 L'un des générateurs est une réflexion complexe: familles contenant les réseaux $\Gamma(p,t)$ de Mostow 185
5.4.5 Exemples génériques 187
5.5 A la recherche des groupes discrets: aspects expérimentaux 189
5.5.1 Familles contenant les réseaux $\Gamma(p,t)$ de Mostow 190
5.5.2 Familles contenant des groupes $\mathbb{R}$-fuchsiens 193

0.1 Introduction en français

Ce travail se situe dans le cadre encore assez peu exploré des groupes discrets d'isométries de l'espace hyperbolique complexe, et en particulier des réseaux de $PU(2,1)$.

L'étude des sous-groupes discrets des groupes de Lie semisimples est un sujet maintenant classique et bien développé (voir par exemple les livres [Rag] et [Mar2] ou les exposés introductifs [Mos3], [Pan]). Une distinction fondamentale s'opère entre les sous-groupes discrets de covolume fini, ou *réseaux*, et ceux de covolume infini, tant pour les questions qui se posent que pour les méthodes d'approche possibles (le covolume d'un sous-groupe Γ d'un groupe de Lie G est la mesure de Haar du quotient G/Γ). Typiquement, on peut espérer classer les réseaux qui sont beaucoup moins nombreux que leurs homologues de covolume infini, une notion cruciale étant celle d'*arithméticité*. Dans les cas qui nous intéressent où l'espace symétrique associé est à courbure négative, les réseaux sont des points isolés dans un gros espace (précisément, le théorème de rigidité forte de Mostow dit que dans ces cas, les représentations d'un groupe donné Γ dont l'image est un réseau de G sont des point isolés dans l'espace des représentations $Hom(\Gamma, G)/G$). A l'opposé, les représentations discrètes de covolume infini admettent en général des déformations, dont l'étude est un sujet riche et fascinant. On pourra par exemple se reporter aux articles de Weil ([W1], [W2]) ou au mémoire [LM] pour la théorie générale des déformations, ainsi que [GM] pour le cas hyperbolique complexe. Le cas des représentations de groupes de surfaces est particulièrement riche, voir [Gol1], [Gol2] ainsi que [H], [Lab] pour les représentations dans $SL(n,\mathbb{R})$, et [Tol], [GKL] pour celles dans $PU(n,1)$. Mentionnons enfin à ce propos la famille des groupes triangulaires de réflexions (complexes) dans $PU(2,1)$ dont l'étude a été initiée pour le cas des triangles idéaux dans [GolPar] et qui fait depuis l'objet de nombreuses recherches, voir par exemple le panorama [Sz1]. On s'intéressera ici plutôt aux réseaux, mais les méthodes géométriques par lesquelles on espère trouver de nouveaux sous-groupes discrets de $PU(2,1)$ (voir en particulier le dernier chapitre) peuvent a priori fournir des exemples des deux types.

Il existe une construction générale de réseaux dans un groupe de Lie semisimple, due à Borel et Harish-Chandra, qui généralise la situation classique du réseau $SL(n,\mathbb{Z})$ dans $SL(n,\mathbb{R})$ (voir l'article original [BHC] ou le traité introductif [WM] pour la construction exacte et différents exemples). Un réseau qui peut s'obtenir par ce biais est dit *arithmétique*; cette approche permet en particulier de montrer que tout groupe de Lie semisimple admet des réseaux, cocompacts et non cocompacts (Γ est dit cocompact si G/Γ est compact). D'autres exemples classiques de réseaux arithmétiques sont les groupes de Bianchi $SL(2,\mathcal{O}_d) \subset SL(2,\mathbb{C})$ formés des matrices ayant leurs coefficients dans un anneau d'entiers quadratique imaginaire $\mathcal{O}_d$ tel que les entiers de Gauss $\mathbb{Z}[i]$ ou les entiers d'Eisenstein $\mathbb{Z}[e^{2i\pi/3}]$; ceux-ci ressemblent beaucoup aux premiers exemples de Picard dans $SU(2,1)$ dont nous reparlerons plus bas.

Comme premier exemple de réseau non-arithmétique, considérons les groupes triangulaires de réflexions dans le plan hyperbolique $H^2_{\mathbb{R}} \simeq H^1_{\mathbb{C}}$ (plan de Poincaré). Ces groupes sont engendrés par les réflexions par rapport aux côtés d'un triangle géodésique de ce plan; il n'est pas difficile de voir que si les angles de ce triangle ont pour mesure $\pi/p, \pi/q, \pi/r$ avec $p,q,r \in \mathbb{Z} \cup \{\infty\}$ (conditions de Coxeter) alors le groupe en question est un sous-groupe discret de $PSL(2,\mathbb{R}) \simeq SO_0(2,1)$ et le triangle en est un domaine fondamental. On sait, par la con-

dition sur les angles d'un triangle en courbure négative, qu'un tel triangle est réalisable dans $H^2_{\mathbb{R}}$ dès que $1/p + 1/q + 1/r < 1$; on dispose donc d'une famille dénombrable de tels triangles non-isométriques dont les groupes ne sont pas conjugués dans $SL(2, \mathbb{R})$. Or il n'y a parmi ces groupes qu'un nombre fini de réseaux arithmétiques (voir par exemple [Tak]), l'exemple le plus connu étant le groupe modulaire $PSL(2, \mathbb{Z})$ qui est contenu avec indice 2 dans le groupe triangulaire avec $(p, q, r) = (2, 3, \infty)$. Il y a donc dans $PSL(2, \mathbb{R})$ une famille dénombrable de réseaux non arithmétiques.

Il se trouve que cette situation est très rare, mais qu'elle n'est pas liée aux phénomènes de basse dimension. Margulis a démontré en 1974 une conjecture de Selberg (affinée par Piatetski-Shapiro, voir [Mos3]) affirmant que **si le rang réel de G est au moins 2**, alors tous les réseaux irréductibles de G sont arithmétiques (Margulis a en fait démontré la propriété plus forte de *supperrigidité* pour ces réseaux, voir [Mar1] ou [GP]). Le rang réel de G est la dimension maximale d'un sous-groupe diagonalisable sur $\mathbb{R}$ (ou "tore déployé sur $\mathbb{R}$"); géométriquement, c'est la dimension maximale d'un espace euclidien plongé isométriquement dans l'espace symétrique associé, d'image simplement connexe (voir [WM]). Ainsi les groupes de rang réel 0 sont les groupes compacts (dont les sous-groupes discrets sont les sous-groupes finis); quant aux groupes simples connexes de rang réel 1, ce sont à indice fini près les suivants, par la classification d'Elie Cartan:

$$SO(n, 1) \qquad SU(n, 1) \qquad Sp(n, 1) \qquad F_4^{-20}$$

(le dernier étant une forme du groupe exceptionnel F_4), qui agissent par isométries sur les espaces symétriques suivants:

$$H^n_{\mathbb{R}} \qquad H^n_{\mathbb{C}} \qquad H^n_{\mathbb{H}} \qquad H^2_{\mathbb{O}}$$

lesquels sont les espaces hyperboliques respectivement réel, complexe, et quaternionique de dimension n ainsi que le plan hyperbolique sur les octonions de Cayley. Les résultats de superrigidité de Margulis ont été étendus aux deux derniers cas par les travaux de Corlette ([Cor]) et Gromov-Schoen ([GS]); restent donc les cas hyperboliques réel et complexe.

Dans le cas de la géométrie hyperbolique réelle, on sait fabriquer des groupes discrets engendrés par des réflexions, de façon analogue à celle des groupes triangulaires du plan. En l'occurrence, on dispose dans $H^n_{\mathbb{R}}$ d'hyperplans (hypersurfaces réelles totalement géodésiques) et de réflexions associées; considérant une famille finie $H_1, ..., H_k$ de tels hyperplans et le groupe engendré par leurs réflexions, on peut montrer comme ci-dessus que si les angles diédraux $(\widehat{H_i, H_j})$ ont tous une mesure de la forme π/n_{ij} avec $n_{ij} \in \mathbb{Z} \cup \{\infty\}$, alors le groupe de réflexions associé est discret et le polyèdre découpé par les hyperplans en est un domaine fondamental (un tel polyèdre est appelé *polyèdre de Coxeter*). Malheureusement, cette construction ne fournit des réseaux qu'en basses dimensions. Les premiers exemples en dimension 3 (dans $SO(3, 1)$) sont dus à Makarov, qui a construit des réseaux non cocompacts dont certains sont non arithmétiques (voir [Mak]). Vinberg a ensuite initié une étude systématique des tels polyèdres (voir [Vin1] et [Vin2] p. 198–210), dont il ressort les faits remarquables suivants:

- (Vinberg) Il n'existe pas de polyèdre de Coxeter compact dans $H^n_{\mathbb{R}}$ pour $n \geqslant 30$.

- (Prokhorov-Khovanskij) Il n'existe pas de polyèdre de Coxeter de volume fini dans $H^n_{\mathbb{R}}$ pour $n \geqslant 996$.

Les bornes données par ces énoncés sont assez larges (surtout la deuxième); les exemples connus sont en dimension au plus 8 pour le premier cas, et au plus 21 pour le deuxième.

Par contre, Gromov et Piatetski-Shapiro ont donné une construction générale, qu'ils appellent *hybridation* de deux variétés hyperboliques (voir [GPS] ainsi que [Mar2], [Vin2] et [WM]), et qui fournit en toute dimension des exemples de réseaux non arithmétiques dans $SO(n,1)$, cocompacts et non cocompacts.

Quant au cas de $SU(n,1)$, toutes les questions que nous avons évoquées sont encore largement ouvertes, même dans les plus petites dimensions. Ceci est dû en grande partie au fait qu'il n'y a pas en géométrie hyperbolique complexe d'hypersurface (réelle) totalement géodésique, et en particulier pas de notion naturelle de polyèdre ou de groupe de réflexions analogue au cas hyperbolique réel (ou euclidien). Cette situation rend ardues non seulement les constructions de sous-groupes discrets dans $SU(n,1)$, mais aussi celles de domaines fondamentaux pour l'action d'un tel groupe. Les substituts possibles dont on dispose dans $H^n_{\mathbb{C}}$ sont les *réflexions complexes* (ou $\mathbb{C}$-réflexions), isométries holomorphes fixant une hypersurface complexe totalement géodésique (une copie de $H^{n-1}_{\mathbb{C}} \subset H^n_{\mathbb{C}}$) et les *réflexions réelles* (ou $\mathbb{R}$-réflexions) qui sont des involutions antiholomorphes fixant un sous-espace lagrangien (une copie de $H^n_{\mathbb{R}} \subset H^n_{\mathbb{C}}$). La plupart des exemples connus à ce jour sont des sous-groupes engendrés par des réflexions complexes, ou bien des constructions arithmétiques. L'utilisation de $\mathbb{R}$-réflexions et des plans lagrangiens correspondants est très récente (elle a été introduite par Falbel et Zocca dans [FZ] en 1999) et est l'un des fils conducteurs de cette thèse; nous en reparlerons plus bas.

Les premières constructions de réseaux dans $SU(2,1)$ remontent à la fin du XIX^e siècle et sont dues à Picard; il est frappant que ce sont encore presque les seules connues à ce jour. Les premiers exemples de Picard sont de nature arithmétique, dans l'esprit des groupes de Bianchi mentionnés précédemment, à savoir qu'il considère dans [Pic1] les sous-groupes $SU(2,1,\mathcal{O}_d) \subset SU(2,1)$ formés des matrices dont tous les coefficients sont dans l'anneau d'entiers $\mathcal{O}_d$ (quadratique et purement imaginaire: d est négatif et sans facteur carré), tel que les entiers de Gauss $\mathbb{Z}[i]$ ou les entiers d'Eisenstein $\mathbb{Z}[e^{2i\pi/3}]$. Il n'est pas difficile de voir qu'un tel sous-groupe est un réseau non cocompact (voir [McR]); par contre il est intéressant de noter que la détermination explicite d'un domaine fondamental pour ces groupes (qui en fournit entre autres une présentation) est délicate et fait l'objet de travaux actuels même dans les cas les plus classiques des entiers de Gauss et Eisenstein (voir [FPar]).

Plus surprenante est la deuxième construction de Picard, issue des groupes de monodromie des fonctions (méromorphes d'une variable complexe) dites *hypergéométriques* (voir [Pic2] et [DM] pour un langage plus moderne), qui produit un sous-groupe de $PU(2,1)$ engendré par trois réflexions complexes. On considère maintenant $PU(2,1)$ (quotient d'ordre 3 de $SU(2,1)$) qui est plus naturel géométriquement: c'est le groupe des isométries holomorphes de $H^2_{\mathbb{C}}$. Cette construction est liée à l'espace des modules des quintuplets de points sur la sphère de Riemann $\mathbb{C}P^1$, ainsi qu'aux métriques euclidiennes à singularités coniques sur la sphère étudiées par

Thurston dans [Th] (voir aussi [Par]). Picard a énoncé des conditions suffisantes pour assurer la discrétude du sous-groupe ainsi obtenu (conditions obtenues par une étude géométrique); son étudiant Le Vavasseur a énuméré tous les paramètres satisfaisant à ces conditions (dans [LeV]), qui sont essentiellement au nombre de 27. Les 27 réseaux correspondants sont maintenant connus sous le nom de *réseaux de Picard*; parmi eux, 7 sont non arithmétiques. Cette observation est due à Deligne et Mostow (la notion n'était même pas en germe à l'époque de Picard), lorsqu'ils ont repris et systématisé l'approche hypergéométrique de Picard un siècle plus tard, dans [DM]. Ils ont obtenu par cette méthode des réseaux dans $PU(n,1)$ pour $n \leqslant 5$; il est intéressant de noter qu'en dimension 2, ils arrivent exactement aux 27 réseaux de Picard (bien qu'utilisant une condition de discrétude plus faible que la sienne) et que le seul autre exemple non arithmétique de leur liste est un réseau non compact dans $PU(3,1)$.

Entre-temps, à la fin des années 1970, Mostow avait étudié de nouveaux exemples de sous-groupes de $PU(2,1)$ engendrés par trois réflexions complexes d'ordre p ($p = 3,4,5$), qu'il note $\Gamma(p,t)$ (t étant un paramètre réel). Son étude ([M1]) repose sur une analyse détaillée de l'action géométrique du groupe sur $H^2_{\mathbb{C}}$, d'où il dégage des conditions de discrétude ainsi que la description d'un domaine fondamental le cas échéant. Ces exemples, encore très mal compris, constituent l'autre fil conducteur de cette thèse. L'approche originale de Mostow est la construction d'un domaine fondamental par la méthode de Dirichlet, qui consiste à considérer, pour le choix d'un point "central" p_0, l'ensemble des points de $H^2_{\mathbb{C}}$ plus près de p_0 que de tout autre point de son orbite. Cette approche a l'avantage de la généralité et de la simplicité de principe, mais elle est très peu maniable en pratique. En l'occurrence, l'objet de base de cette construction est l'ensemble des points équidistants de deux points donnés (p_0 et l'une de ses images), que Mostow a appelé *bisecteur*; ces objets jouissent de propriétés géométriques remarquables, comme les deux feuilletages en $\mathbb{C}$-plans et en $\mathbb{R}$-plans (voir [Gol3]), mais leurs intersections sont très difficiles à comprendre. Par exemple, l'un des buts du livre de Goldman [Gol3] est de comprendre précisément l'intersection de deux bisecteurs; voir également le troisième chapitre de cette thèse (en particulier son introduction) pour les problèmes liés à cette construction.

Ceci est l'un des aspects du problème de la construction de polyèdres dans $H^2_{\mathbb{C}}$, en particulier de leurs faces de codimension 1. Comme on l'a dit, le problème majeur est l'absence d'hyperplans (ou hypersurfaces réelles totalement géodésiques), qui n'ont pas de substitut naturel. Différentes constructions d'hypersurfaces sont apparues, la nature de celles-ci étant liée au type du sous-groupe considéré. Schwartz en a décrit différents types (en 2002) dans son panorama [Sz1]; une idée commune à toutes ces constructions est l'utilisation de $\mathbb{C}$-plans ou de $\mathbb{R}$-plans (et leurs bords, les $\mathbb{C}$-cercles et $\mathbb{R}$-cercles du groupe de Heisenberg $H^3 = \partial H^2_{\mathbb{C}}$) pour feuilleter les hypersurfaces comme dans le cas des bisecteurs.

C'est ici que les $\mathbb{R}$-réflexions apparaissant dans le groupe jouent un rôle crucial, selon le principe général qu'un domaine fondamental le plus naturel possible doit s'appuyer sur les lieux des points fixes de certains éléments du groupe. On gagne ainsi de l'information géométrique en décomposant les générateurs d'un groupe d'isométries en produit de $\mathbb{R}$-réflexions, ce qui est un thème récurrent dans cette thèse. Un exemple classique de cette situation est celui des groupes triangulaires du plan (hyperbolique, euclidien ou sphérique), engendrés par deux rotations que l'on décompose en produit de réflexions pour déterminer l'ordre du produit (et le troisième

angle du triangle délimité par les droites de réflexion, lequel est un domaine fondamental pour le groupe). Un autre exemple apparaît dans notre analyse des réseaux de Mostow au chapitre 3 (voir [DFP]), où nous remarquons qu'un groupe légèrement plus gros que le réseau est engendré par deux isométries qui se décomposent en produit de trois $\mathbb{R}$-réflexions; les $\mathbb{R}$-plans correspondants apparaissaient en filigrane dans l'article de Mostow (typiquement, certains quintuplets de sommets de son polyèdre fondamental étaient contenus dans un de ces $\mathbb{R}$-plan) mais sans qu'il en ait eu conscience (voir à cet égard la figure 14.2 p. 239 de [M1]). Ceci nous a permis de simplifier la structure du polyèdre fondamental en introduisant des 2-faces contenues dans ces $\mathbb{R}$-plans.

Le plan de cette thèse se déroule de la façon suivante. Chaque chapitre est conçu de façon indépendante, comportant introduction et bibliographie propres (pour utiliser un anglicisme, disons qu'ils se contiennent eux-mêmes). Après un court chapitre de préliminaires géométriques dans $H^2_{\mathbb{C}}$ (pour lesquels le lecteur pourra également se reporter au livre de Goldman [Gol3]), nous étudions le type le plus simple de groupes discrets, à savoir les groupes finis. Dans notre cadre, ces groupes fixent un point de $H^2_{\mathbb{C}}$ et sont donc conjugués à des sous-groupes de $U(2)$; il s'agit d'un problème vectoriel dans $\mathbb{C}^2$, mais qui contient déjà une géométrie très riche. Une des motivations de cette étude était de comprendre la brique élémentaire des réseaux de Mostow, les groupes finis engendrés par deux des trois réflexions complexes fondamentales (c'est l'exemple du groupe 3[3]3 dans les notations de Coxeter, que nous étudions en détail). Nous décrivons précisément le rôle des $\mathbb{R}$-plans dans ce cadre, et construisons des domaines fondamentaux au bord de la boule unité de $\mathbb{C}^2$ qui s'appuient sur des arcs des $\mathbb{R}$-cercles correspondants. On y détaille les conditions sous lesquelles une $\mathbb{R}$-réflexion donnée décompose une transformation elliptique de $H^2_{\mathbb{C}}$ (au sens où cette dernière s'écrit comme le produit de la $\mathbb{R}$-réflexion en question et d'une autre $\mathbb{R}$-réflexion), et on en déduit entre autres le résultat suivant:

Théorème 1 *Tout sous-groupe fini de $U(2)$ est sous-groupe d'indice 2 d'un groupe engendré par des $\mathbb{R}$-réflexions. Plus précisément:*

- *Tout sous-groupe à deux générateurs de $U(2)$ est sous-groupe d'indice 2 d'un groupe engendré par 3 $\mathbb{R}$-réflexions. Il existe génériquement un cercle de tels groupes, et un 2-tore dans les cas dégénérés.*

- *Les sous-groupes finis exceptionnels de $U(2)$ qui ne sont pas engendrés par 2 éléments sont sous-groupe d'indice 2 d'un groupe engendré par 4 $\mathbb{R}$-réflexions.*

Ce deuxième chapitre est un travail commun avec E. Falbel, et a fait l'objet d'une publication ([FPau]) dans *Geometriae Dedicata*.

Le chapitre suivant consiste en une étude détaillée des réseaux $\Gamma(p,t)$ de Mostow, s'appuyant sur les observations mentionnées ci-dessus que ces réseaux comportent naturellement des $\mathbb{R}$-réflexions. Nous construisons principalement un nouveau polyèdre fondamental Π, plus simple que celui de Mostow, mais surtout qui permet d'employer des arguments géométriques synthétiques évitant le recours massif à l'ordinateur pour les preuves, ce que faisait Mostow dans [M1]. On pourra également lire l'introduction détaillée à ce chapitre pour diverses motivations et prolongements, ainsi que pour les notations. $\tilde{\Gamma}(p,t)$ désigne le groupe engendré par l'une des trois réflexions complexes génératrices (R_1 par exemple) et l'isométrie J qui permute

cycliquement ces trois réflexions; il contient $\Gamma(p,t)$ avec indice 1 ou 3. On peut résumer nos résultats dans l'énoncé suivant:

Théorème 2 *Le groupe $\tilde{\Gamma}(p,t) \subset PU(2,1)$, avec $p = 3, 4, \text{ou} 5$ et $|t| < \frac{1}{2} - \frac{1}{p}$, est discret si $k = (\frac{1}{4} - \frac{1}{2p} + \frac{t}{2})^{-1}$ et $l = (\frac{1}{4} - \frac{1}{2p} - \frac{t}{2})^{-1}$ sont dans $\mathbb{Z}$. Dans ce cas Π est un domaine fondamental avec appariements de faces J, R_1, R_2, R_2R_1, R_1R_2 et les relations de cycle donnent la présentation suivante du groupe:*

$$\tilde{\Gamma}(p,t) = \langle J, R_1, R_2 \mid J^3 = R_1^p = R_2^p = J^{-1}R_2JR_1^{-1} = R_1R_2R_1R_2^{-1}R_1^{-1}R_2^{-1}$$

$$= (R_2R_1J)^k = ((R_1R_2)^{-1}J)^l = I\rangle.$$

Ce troisième chapitre est un travail en commun avec M. Deraux et E. Falbel, et a fait l'objet d'une publication ([DFP]) dans *Acta Mathematica*.

Le dernier chapitre constitue une première étape dans la recherche de nouveaux groupes discrets dans une famille que nous appellerons *groupes triangulaires elliptiques*. Ce sont les groupes engendrés par deux transformations elliptiques A et B (c'est-à-dire ayant chacune un point fixe dans $H^2_{\mathbb{C}}$) dont le produit AB est également elliptique. De la même façon que l'on utilise la caractérisation des triangles du plan (hyperbolique, euclidien ou sphérique) pour comprendre les groupes engendrés par deux rotations, on aura besoin ici de la caractérisation des classes de conjugaison que parcourt le produit AB lorsque A et B sont chacun dans une classe de conjugaison fixée. Les classes de conjugaison de transformations elliptiques de $H^2_{\mathbb{C}}$ sont caractérisées par une paire d'angles (non ordonnée), donc la question se ramène à l'étude de l'image dans la surface $\mathbb{T}^2/\mathfrak{S}_2$ de l'application $\tilde{\mu}$, qui est la composée de l'application produit du groupe restreinte au produit de deux classes de conjugaison fixées, suivie de la projection du groupe sur ses classes de conjugaison. Ceci est une occurrence d'application moment associée à une action quasi-hamiltonnienne sur une variété symplectique, généralisation du cadre hamiltonien classique définie dans [AMM] (voir également [Sf] pour plus de détails). Le chapitre est consacré à la détermination de cette image, ainsi qu'à la question analogue en termes de $\mathbb{R}$-plans, à savoir la classification des configurations de triplets de $\mathbb{R}$-plans s'intersectant deux à deux dans $H^2_{\mathbb{C}}$. Notre analyse repose sur la description détaillée de l'ensemble W_{red} des *murs réductibles* (i.e. les points images de paires (A,B) engendrant un groupe linéaire réductible), qui séparent la surface $\mathbb{T}^2/\mathfrak{S}_2$ en polygones convexes appelés *chambres*. On obtient entre autres le résultat suivant, qui rappelle le théorème classique de convexité d'Atiyah-Guillemin-Sternberg (voir [A], [GS1], [GS2]) :

Théorème 3 *Soient C_1 et C_2 deux classes de conjugaison elliptiques dans $PU(2,1)$, dont une au moins n'est pas une classe de réflexions complexes. Alors l'image de l'application $\tilde{\mu}$ dans $\mathbb{T}^2/\mathfrak{S}_2$ est une réunion de chambres fermées, contenant au voisinage de chaque sommet totalement réductible l'enveloppe convexe des murs réductibles qui contiennent ce sommet.*

Notons que ces questions sont également motivées par l'étude des réseaux de Mostow dans la mesure où chacune de ses familles $\Gamma(p,t)$ avec p fixé rentre exactement dans ce cadre, en tant que segment dans l'un des polygones images. Ceci distingue une famille géométrique plus vaste à laquelle appartiennent les réseaux de Mostow, et dans laquelle nous espérons découvrir d'autres exemples. Nous terminons en proposant quelques candidats explicites.

0.2 Introduction in english

The setting of this thesis is the still rather unexplored area of discrete groups of isometries of complex hyperbolic space, in particular that of lattices in $PU(2,1)$.

The study of discrete subgroups of semisimple Lie groups is a now classical and well-developed subject (see for instance the books [Rag] and [Mar2] or the introductory expositions [Mos3] and [Pan]). A fundamental difference exists between discrete subgroups of finite covolume, or *lattices*, and those of infinite covolume, concerning the questions which arise as well as the methods to explore them (the *covolume* of a subgroup Γ of a Lie group G is the Haar measure of the quotient G/Γ). Typically, one can expect a classification of lattices which are much less abundant than their infinite covolume counterparts, a crucial notion being that of *arithmeticity*. In our particular case of interest where the associated symmetric space has non-negative sectional curvature, lattices are isolated points in a big space (more precisely, Mostow's strong rigidity theorem states that, in that case, representations of a given group Γ whose image is a lattice in G are isolated points of the representation space $Hom(\Gamma, G)/G$). In contrast, discrete representations with infinite covolume can in general be deformed, and the study of these deformations is a rich and fascinating subject. The general theory of these deformations can be found for instance in Weil's articles ([W1], [W2]) or the memoir [LM]; see also [GM] for the complex hyperbolic case. The case of representations of surface groups is especially rich, as can be seen in [Gol1], [Gol2] as well as [H], [Lab] for representations in $SL(n,\mathbb{R})$ and [Tol], [GKL] for those in $PU(n,1)$. Another case of special interest in $PU(2,1)$ is that of (complex) reflection triangle groups, the study of which started with the ideal triangles of [GolPar] and continues to inspire much research, see the survey [Sz1]. We will be more concerned with lattices, but the geometric methods by which we hope to produce new examples of discrete groups (see the last chapter) may a priori yield examples from both types.

There exists a general construction of lattices in a semisimple Lie group, due to Borel and Harish-Chandra, which generalizes the classical situation of the lattice $SL(n,\mathbb{Z}) \subset SL(n,\mathbb{R})$ (see the original article [BHC] or the introductory treatise [WM] for the exact construction and various examples). A lattice which can be obtained by those means is called *arithmetic*; this approach proves among other things that every semismple Lie group contains lattices, cocompact and non cocompact (Γ is said to be cocompact if G/Γ is compact). Other classical examples of arithmetic lattices include Bianchi's groups $SL(2,\mathcal{O}_d) \subset SL(2,\mathbb{C})$ comprising matrices whose entries are all in an imaginary quadratic ring of integers $\mathcal{O}_d$, such as the Gaussian integers $\mathbb{Z}[i]$ or the Eisenstein integers $\mathbb{Z}[e^{2i\pi/3}]$; these are very similar to Picard's first examples in $PU(2,1)$ which we will mention below.

For our first examples of nonarithmetic lattices, consider the reflection triangle groups in the hyperbolic plane $H^2_{\mathbb{R}} \simeq H^1_{\mathbb{C}}$ (or Poincaré plane). These groups are generated by the reflections in the sides of a geodesic triangle of this plane; it is not difficult to see that if the angles of this triangle have measures $\pi/p, \pi/q, \pi/r$ with $p,q,r \in \mathbb{Z} \cup \{\infty\}$ (Coxeter's conditions) then the group in question is a discrete subgroup of $PSL(2,\mathbb{R}) \simeq SO_0(2,1)$ and the triangle is a fundamental domain for its action on the plane. Now we know, by the condition on the angles of a triangle in nonnegative curvature, that such a triangle exists in $H^2_{\mathbb{R}}$ provided that $1/p + 1/q + 1/r < 1$; we thus have a countable family of such non-isometric triangles

whose reflection groups are non-conjugate in $SL(2,\mathbb{R})$. However, there is only a finite number of arithmetic lattices among these groups (see for instance [Tak]), the most famous example being the modular group $PSL(2,\mathbb{Z})$ which is contained with index 2 in the triangle group with $(p,q,r) = (2,3,\infty)$. There is thus a countable collection of nonarithmetic lattices in $PSL(2,\mathbb{R})$.

It so happens that this situation is very rare, but not because of phenomena related to low dimension. Margulis proved in 1974 a conjecture of Selberg (refined by Piatetski-Shapiro, see [Mos3]) which states that **if the real rank of G is greater than 2** then all irreducible lattices in G are arithmetic (in fact, Margulis proved that these lattices have the stronger property of *superrigidity*, see [Mar1] or [GP]). The real rank of G is the maximal dimension of an $\mathbb{R}$-split torus (a subgroup consisting of matrices which can simultaneously be written in diagonal form over $\mathbb{R}$); geometrically, it is the maximal dimension of an isometrically embedded Euclidian space with simply-connected image in the associated symmetric space (see [WM]). Thus the groups with real rank 0 are the compact groups (whose discrete subgroups are the finite subgroups); as for simple connected groups of real rank one, these are, up to finite index, by Elie Cartan's classification:

$$SO(n,1) \qquad SU(n,1) \qquad Sp(n,1) \qquad F_4^{-20}$$

(the latter being a form of the exceptional group F_4), acting by isometries on the following symmetric spaces:

$$H^n_{\mathbb{R}} \qquad H^n_{\mathbb{C}} \qquad H^n_{\mathbb{H}} \qquad H^2_{\mathbb{O}}$$

which are hyperbolic spaces of dimension n over the reals, complex numbers, quaternions respectively, and the hyperbolic plane over the Cayley octonions. Margulis' superrigidity results wer extended to the two latter cases by the work of Corlette ([Cor]) and Gromov-Schoen ([GS]); remain only the cases of real and complex hyperbolic geometry.

In the case of real hyperbolic geometry, we know how to construct discrete groups generated by reflections in a manner analogous to that of the previous triangle groups of the plane. The reason for this is that there are in $H^n_{\mathbb{R}}$ hyperplanes (i.e. totally geodesic real hypersurfaces) with associated reflections; considering a finite collection $H_1, ..., H_k$ of such hyperplanes and the group generated by their reflections, one can show as above that if the dihedral angles $(\widehat{H_i, H_j})$ all have measure π/n_{ij} with $n_{ij} \in \mathbb{Z} \cup \{\infty\}$, then the associated reflection group is discrete and has as a fundamental domain the polyhedron cut out by the hyperplanes (such a polyhedron is called a *Coxeter polyhedron*). Unfortunately, this construction only yields lattices in small dimensions. The first examples in dimension 3 (in $SO(3,1)$) are due to Makarov, who constructed non-cocompact lattices among which some are nonarithmetic (see [Mak]). Vinberg then initiated a systematic study of such polyhedra (see [Vin1] and [Vin2] pp. 198–210) which revealed the following remarkable facts:

- (Vinberg) Compact Coxeter polyhedra do not exist in $H^n_{\mathbb{R}}$ for $n \geqslant 30$.
- (Prokhorov-Khovanskij) Coxeter polyhedra of finite volume do not exist in $H^n_{\mathbb{R}}$ for $n \geqslant 996$.

The bounds given by these results are wide (especially the second); known examples are in dimensions up to 8 for the first case, and 21 for the second.

On the other hand, Gromov and Piatetski-Shapiro have given a general construction, which they call *hybridation* of two hyperbolic manifolds (see [GPS] as well as [Mar2], [Vin2] and [WM]), which yields examples of nonarithmetic lattices in $SO(n,1)$ in all dimensions, cocompact and non-cocompact.

As for the case of $SU(n,1)$, all the questions we have raised remain wide open, even in the smallest dimensions. This is mostly due to the fact that there are no totally geodesic real hypersurfaces in complex hyperbolic geometry, and in particular no natural notion of polyhedra or reflection groups as in the real hyperbolic (or Euclidian) case. This situation makes it difficult to construct not only discrete subgroups of $SU(n,1)$, but also fundamental polyhedra for such groups. Possible substitutes in $H^n_{\mathbb{C}}$ are *complex reflections* (or $\mathbb{C}$-reflections) which are holomorphic isometries fixing pointwise a totally geodesic complex hypersurface (a copy of $H^{n-1}_{\mathbb{C}} \subset H^n_{\mathbb{C}}$), and *real reflections* (or $\mathbb{R}$-reflections) which are antiholomorphic involutions fixing pointwise a Lagrangian subspace (a copy of $H^n_{\mathbb{R}} \subset H^n_{\mathbb{C}}$). Most examples up to now are generated by complex reflections, or are arithmetic constructions. The use of $\mathbb{R}$-reflections and of the corresponding Lagrangian planes is very recent (it was introduced by Falbel and Zocca in [FZ] in 1999) and is one of the guiding principles of this thesis; we will mention this again below.

The first constructions of lattices in $SU(2,1)$ go back to the end of the XIXth century and are due to Picard; it is striking that they are still almost the only known examples. Picard's first examples are of an arithmetic nature, in the spirit of the Bianchi groups; namely he considered in [Pic1] the groups $SU(2,1,\mathcal{O}_d) \subset SU(2,1)$ comprising the matrices whose entries are all in the imaginary quadratic ring of integers $\mathcal{O}_d$ (d is square-free and negative), such as the Gaussian integers $\mathbb{Z}[i]$ or the Eisenstein integers $\mathbb{Z}[e^{2i\pi/3}]$. It is not difficult to see that such a subgroup is a non-cocompact lattice (see [McR]); however it is interesting to note that the explicit determination of a fundamental domain for these groups (providing for instance a presentation) is delicate and is the subject of contemporary research even in the most classical cases of the Gaussian and Eisenstein integers.

More surprising is Picard's second construction coming from monodromy groups of the so-called *hypergeometric* functions, which are meromorphic functions of a complex variable (see [Pic2] and [DM] for a more modern language), which produces a subgroup of $PU(2,1)$ generated by three complex reflections. We now consider $PU(2,1)$ (a quotient of order 3 of $SU(2,1)$) which is more natural geometrically, as the group of holomorphic isometries of $H^n_{\mathbb{C}}$. This construction is related to the moduli space of quintuples of points on the Riemann sphere $\mathbb{C}P^1$, as well as to Euclidian cone metrics on the sphere studied by Thurston in [Th] (see also [Par]). Picard stated conditions sufficient to ensure dicreteness of the corresponding group (conditions which he obtained through a geometric analysis); his student Le Vavasseur enumerated all the parameters saisfying these conditions (in [LeV]), which amount essentially to 27 cases. The 27 corresponding lattices are now known as the *Picard lattices*; among them, 7 are nonarithmetic. This observation is due to Deligne and Mostow (the notion was not even

burgeoning in Picard's time), when they rewrote and made systematic Picard's hypergeometric approach a century later in [DM]. They obtained by this method lattices in $PU(n,1)$ for $n \leqslant 5$; it is interesting to note that in dimension 2 they find exactly the 27 Picard lattices (although using a weaker discreteness condition) and that the only other nonarithmetic lattice of their list is a non-cocompact example in $PU(3,1)$.

In the meantime, at the end of the 1970's, Mostow had studied new examples of subgroups of $PU(2,1)$ generated by three complex reflections of order p ($p = 3, 4, 5$), which he denoted by $\Gamma(p,t)$ (t being a real parameter). His investigation [M1] is based on a detailed analysis of the geometric action of the group on $H^2_{\mathbb{C}}$, from which he infers discreteness conditions as well as the description of a fundamental domain when this is the case. These examples, still poorly understood, are the other guiding principle of this thesis. Mostow's original approach is the construction of a fundamental domain by Dirichlet's method, which consists in the consideration, for a "central" point p_0, of the set of points closer to p_0 than to any other point in its orbit. This approach has the advantages of generality and simplicity of principle, but it is very hard to use in practice. Namely, the basic object in this construction is the set of points equidistant from two given points (p_0 and one of its translates), which Mostow called a *bisector*. These objects enjoy remarkable geometric properties, such as the double foliation by $\mathbb{C}$-planes and $\mathbb{R}$-planes (see [Gol3]), but their intersections are difficult to understand. For instance, one of the goals of Goldman's book [Gol3] is to understand these intersections; see also the third chapter of this thesis (in particular its introduction) for problems related to this construction.

This is one of the aspects of the difficulty of constructing polyhedra in $H^2_{\mathbb{C}}$, in particular their codimension-1 faces. As we have mentioned, the major problem is the absence of hyperplanes (or totally geodesic real hypersurfaces), which have no natural substitute. Different constructions of hypersurfaces have appeared, the nature of which is linked to the type of the group in question. Schwartz has described some different examples (in 2002) in his survey [Sz1]; an idea shared by all these constructions is the use of $\mathbb{C}$-planes and $\mathbb{R}$-planes (and their boundaries, the $\mathbb{C}$-circles and $\mathbb{R}$-circles of the Heisenberg group $H^3 = \partial H^2_{\mathbb{C}}$) to foliate the hypersurfaces as in the case of bisectors.

This is where the $\mathbb{R}$-reflections which appear in the group play a crucial role, according to the general principle by which the most natural fundamental domain for a group rests upon the fixed-point loci of certain elements of the group. We thus gain some geometric information by decomposing the generators of a group of isometries as products of $\mathbb{R}$-reflections, which is a recurring theme in this thesis. A classic example of this situation is that of triangle groups of the plane (hyperbolic, Euclidian, or spherical), generated by two rotations which one decomposes as a product of reflections to determine the order of the product (and the third angle of the triangle bounded by the reflecting lines, which is a fundamental domain for the group). Another example arises in our investigation of Mostow's lattices in chapter 3 (see [DFP]), where we notice that a group slightly bigger than his lattice is generated by two isometries which decompose as a product of three $\mathbb{R}$-reflections. The corresponding $\mathbb{R}$-planes could be seen by transparency in Mostow's article (typically, certain quintuples of vertices of his domain were contained in one of these $\mathbb{R}$-planes), whithout his noticing them (see for this aspect figure 14.2 on p. 239 of [M1]). This allowed us to simplify the structure of the fundamental polyhedron by introducing some 2-faces contained in these $\mathbb{R}$-planes.

The thesis is organized as follows. Each chapter is conceived to be self-contained, with its own introduction and bibliography. After a short chapter of geometric preliminaries in $H^2_{\mathbb{C}}$ (for which the reader may also refer to Goldman's book [Gol3]), we investigate the simplest kind of discrete groups, namely finite groups. In our setting, these groups are conjugate to subgroups of $U(2)$; it is thus a linear question in $\mathbb{C}^2$, but which already contains some rich geometric aspects. One of the motivations for this study was to understand the elementary building block of Mostow's lattices, the finite groups generated by two of the three fundamental complex reflections (this is the example of the group 3[3]3 in Coxeter's notation, which we study in detail). We describe precisely the role of $\mathbb{R}$-planes in that setting, and construct fundamental domains in the boundary of the unit ball of $\mathbb{C}^2$ based upon arcs of the corresponding $\mathbb{R}$-circles. We detail the conditions under which a given $\mathbb{R}$-reflection decomposes an elliptic isometry of $H^2_{\mathbb{C}}$ (in the sense where the latter can be written as the product of the given $\mathbb{R}$-reflection with another $\mathbb{R}$-reflection), and infer among other things the following result:

Theorem 0.2.1 *Every finite subgroup of $U(2)$ is of index 2 in a group generated by $\mathbb{R}$-reflections. More precisely:*

- *Every two-generator subgroup of $U(2)$ is of index 2 in a group generated by 3 $\mathbb{R}$-reflections.*
- *The exceptional finite subgroups of $U(2)$ which are not generated by two elements are of index 2 in a group generated by 4 $\mathbb{R}$-reflections.*

This second chapter is a joint work with E. Falbel and has been published in *Geometriae Dedicata* ([FPau]).

The next chapter consists in a detailed analysis of Mostow's lattices $\Gamma(p,t)$, based on the aforementioned observation that these lattices naturally contain $\mathbb{R}$-reflections. We construct a new fundamental domain Π which is simpler than Mostow's, but mostly which allows the use of synthetic geometric arguments which spare the resort to massive computer use for the proofs as in [M1]. Further motivations and ramifications can be found in the detailed introduction to that chapter, as well as some notation. $\tilde{\Gamma}(p,t)$ denotes the group generated by one of the complex reflections, say R_1 and the isometry J which cyclically permutes these three reflections; it contains $\Gamma(p,t)$ with index 1 or 3. We can sum up our results in the following:

Theorem 0.2.2 *The group $\tilde{\Gamma}(p,t) \subset PU(2,1)$, for $p = 3, 4, \text{or} 5$ and $|t| < \frac{1}{2} - \frac{1}{p}$, is discrete if $k = (\frac{1}{4} - \frac{1}{2p} + \frac{t}{2})^{-1}$ and $l = (\frac{1}{4} - \frac{1}{2p} - \frac{t}{2})^{-1}$ are in $\mathbb{Z}$. In that case Π is a fundamental domain with side pairings given by J, R_1, R_2, R_2R_1, R_1R_2 and the cycle relations give the following presentation of the group*

$$\tilde{\Gamma}(p,t) = \langle J, R_1, R_2 \mid J^3 = R_1^p = R_2^p = J^{-1}R_2JR_1^{-1} = R_1R_2R_1R_2^{-1}R_1^{-1}R_2^{-1}$$
$$= (R_2R_1J)^k = ((R_1R_2)^{-1}J)^l = I\rangle.$$

This third chapter is a joint work with M. Deraux and E. Falbel and has been published in *Acta Mathematica* ([DFP]).

The last chapter is a first step in the search for new discrete groups in a family which we will call *elliptic triangle groups*. These are the groups generated by two elliptic isometries A and B

(i.e. each having a fixed point inside $H^2_{\mathbb{C}}$) whose product AB is also elliptic. In the same way that we use the characterization of triangles of the plane (hyperbolic, Euclidian, or spherical) to understand the groups generated by two rotations, we will need the characterization of which conjugacy classes the product AB can be in when A and B are each in a fixed conjugacy class. Elliptic conjugacy classes in $PU(2,1)$ are characterized by an unordered angle pair, so that the question is the determination of the image in the surface $\mathbb{T}^2/\mathfrak{S}_2$ of the map $\tilde{\mu}$, which is the composite of the group product (restricted to the product of fixed conjugacy classes), followed by projection from the group to its conjugacy classes. This is an occurrence of a momentum map associated with a quasi-Hamiltonian group action on a symplectic manifold, generalizing the classical Hamiltonian setting and defined in [AMM] (see also [Sf] for more details). The chapter is devoted to the explicit determination of the image, as well as the counterpart in terms of $\mathbb{R}$-planes, namely the question of classifying triples of $\mathbb{R}$-planes intersecting pairwise inside $H^2_{\mathbb{C}}$. Our analysis rests upon a detailed description of the collection W_{red} of *reducible walls* (i.e. those points which are images of pairs (A,B) generating a reducible linear group), which disconnect the surface $\mathbb{T}^2/\mathfrak{S}_2$ into a union of open convex polygons which we call *chambers*. We obtain among other things the following result, which is reminiscent of the classical convexity theorem of Atiyah-Guillemin-Sternberg (see [A], [GS1], [GS2]):

Theorem 0.2.3 *Let C_1 and C_2 be two elliptic conjugacy classes in $PU(2,1)$, at least one of which is not a class of complex reflections. Then the image of the map $\tilde{\mu}$ in $\mathbb{T}^2/\mathfrak{S}_2$ is a union of closed chambers, containing in a neighborhood of each totally reducible vertex the convex hull of the reducible walls containing that vertex.*

Note that these questions were also motivated by the study of Mostow's lattices in the respect that each of his families $\Gamma(p,t)$ with fixed p is part of our setting, sitting as a segment inside of the momentum polygon. This distinguishes a larger geometric family to which these lattices belong, and among which we hope to find other examples. We finish by suggesting some explicit candidates.

Bibliography

[A] M. F. Atiyah; *Convexity and commuting Hamiltonians*. Bull. London Math. Soc. **14(1)** (1982), 1–15.

[AMM] A. Alekseev, A. Malkin, E. Meinrenken; *Lie group valued moment maps*. J. Diff. Geom. **48(3)** (1998), 445–495.

[BHC] A. Borel, Harish-Chandra; *Arithmetic subgroups of algebraic groups*. Ann. Math. **75(2)** (1962), 485–535.

[Cor] K. Corlette; *Archimedean superrigidity and hyperbolic geometry*. Ann. Math. **135(1)** (1992), 165–182.

[DM] P. Deligne, G. D. Mostow; *Monodromy of hypergeometric functions and non-lattice integral monodromy*. Publ. Math. IHES **63** (1986), 5–89.

[DFP] M. Deraux, E. Falbel, J. Paupert; *New constructions of fundamental polyhedra in complex hyperbolic space*. Acta Math. **194** (2005), 155–201.

[FPar] E. Falbel, J. Parker; *Geometry of the Eisenstein-Picard modular group*. To appear in Duke Math. Journal (2006).

[FPau] E. Falbel, J. Paupert; *Fundamental domains for finite subgroups in $U(2)$ and configurations of Lagrangians*. Geom. Dedicata **109** (2004), 221–238.

[FZ] E. Falbel, V. Zocca; *A Poincaré's polyhedron theorem for complex hyperbolic geometry*. J. Reine Angew. Math. **516** (1999), 138–158.

[Gol1] W. M. Goldman; *The symplectic nature of fundamental groups of surfaces*. Adv. in Math. **54** (1984), 200–225.

[Gol2] W. M. Goldman; *Representations of fundamental groups of surfaces*. In: Geometry and Topology, Proceedings, Univ. of Maryland (1983-1984), J. Alexander and J. Harer (eds.). Lecture Notes in Math. **1167**, Springer-Verlag (1985), 95–117.

[Gol3] W. M. Goldman; Complex hyperbolic geometry. Oxford Mathematical Monographs. Oxford University Press (1999).

[GKL] W. M. Goldman, M. E. Kapovich, B. Leeb; *Complex hyperbolic manifolds homotopy equivalent to a Riemann surface*. Comm. Anal. Geom. **9** (2001), 61–95.

[GM] W. M. Goldman, J. J. Millson; *Local rigidity of discrete groups acting on complex hyperbolic space*. Invent. Math. **88** (1987), 495–520.

[GolPar] W. M. Goldman, J. R. Parker; *Complex hyperbolic ideal triangle groups*. J. reine angew. Math. **425** (1992), 71–86.

[GP] M. Gromov, P. Pansu; *Rigidity of lattices: an introduction*. Geometric topology: recent developments, Montecatini Terme 1990. Lecture Notes **1504**, Springer (1991), 39–137.

[GPS] M. Gromov, I. Piatetski-Shapiro; *Non-arithmetic groups in Lobachevsky spaces*. Publ. Math. IHES **66** (1987), 93–103.

[GS] M. Gromov, R. Schoen; *Harmonic maps into singular spaces and p-adic superrigidity for lattices in groups of rank 1*. Publ. Math. IHES **76** (1992), 165–246.

[GS1] V. Guillemin, S. Sternberg; *Convexity properties of the moment mapping*. Invent. Math. **67(3)** (1982), 491–513.

[GS2] V. Guillemin, S. Sternberg; *Convexity properties of the moment mapping II*. Invent. Math. **77(3)** (1984), 533–546.

[H] N. J. Hitchin; *Lie groups and Teichmuller space*. Topology **31** (1992), 449–473.

[Lab] F. Labourie; *Anosov flows, surface groups and curves in projective space*. Preprint (2003).

[LeV] R. Le Vavasseur; *Sur le système d'équations aux dérivées partielles simultanées auxquelles satisfait la série hypergéométrique à deux variables* $\mathrm{F}_1(\alpha, \beta, \beta', \gamma; x, y)$. Annales de la faculté des sciences de Toulouse Sér. 1 **7 (3-4)** (1893), 1–205.

[LM] A. Lubotsky, A. R. Magid; Varieties of representations of finitely generated groups. Memoirs of the AMS **336** (1985).

[Mak] V. S. Makarov; *On a class of discrete groups in Lobachevsky space having an unbounded fundamental domain of finite measure*. Dokl. Akad. Nauk. SSSR **167** (1966), 30–33.

[Mar1] G. A. Margulis; *Discrete groups of motions of manifolds of non-positive curvature*. Proc. Int. Congr. Math., Vancouver 1974, vol. 2, 21–34.

[Mar2] G. A. Margulis; Discrete subgroups of semisimple Lie groups. Springer (1991).

[McR] D. B. McReynolds; Arithmetic lattices in $SU(n, 1)$. Preprint (2005).

[Mos1] G. D. Mostow; *On a remarkable class of polyhedra in complex hyperbolic space*. Pacific J. Math. **86** (1980), 171–276.

[Mos2] G. D. Mostow; *Generalized Picard lattices arising from half-integral conditions*. Publ. Math. IHES **63** (1986), 91–106.

[Mos3] G. D. Mostow; *Discrete subgroups of Lie groups*. *In* Elie Cartan et les Mathématiques d'aujourd'hui. Société Mathématique de France. Astérisque, hors série (1985), 289–309.

[Pan] P. Pansu; *Sous-groupes discrets des groupes de Lie: rigidité, arithméticité*. Séminaire Bourbaki, exposé 778 (1993-94). Astérisque **227**, Soc. Math. de France (1995), 69–105.

[Par] J. Parker; *Cone metrics on the sphere and Livné's lattices*. Preprint (2005).

[Pic1] E. Picard; *Sur des formes quadratiques ternaires indéfinies à indéterminées conjuguées et sur les fonctions hyperfuchsiennes correspondantes*. Acta Math. **5** (1884), 121–182.

[Pic2] E. Picard; *Sur les fonctions hyperfuchsiennes provenant des séries hypergéométriques de deux variables*. Ann. ENS III **2** (1885), 357-384.

[Rag] M. S. Raghunathan; Discrete subgroups of Lie groups. Ergebnisse der Mathematik **68**. Springer-Verlag (1972).

[Sf] F. Schaffhauser; Decomposable representations and Lagrangian submanifolds of moduli spaces associated to surface groups. Thesis, Université Paris 6, 2005.

[Sz] R. E. Schwartz; *Complex hyperbolic triangle groups*. Proceedings of the International Congress of Mathematicians, Vol. II (Beijing, 2002), 339–349, Higher Ed. Press, Beijing, 2002.

[Tak] K. Takeuchi; *Arithmetic triangle groups*. J. Math. Soc. Japan **29(1)** (1977), 91–106.

[Th] W. P. Thurston; *Shapes of polyhedra and triangulations of the sphere*. Geometry and Topology Monographs **1**, the Epstein Birthday Schrift (1998), 511–549.

[Tol] D. Toledo; *Representations of surface groups on complex hyperbolic space*. J. Diff. Geom. **29** (1989), 125–133.

[Vin1] E. B. Vinberg; *Discrete groups generated by reflections in Lobachevsky spaces*. Mat. Sb. (NS) **72(114)** (1967), 471–488.

[Vin2] E. B. Vinberg (ed.); Geometry II, Encyclopaedia of Math. Sc. **29**. Springer-Verlag (1993).

[W1] A. Weil; *Discrete subgroups of Lie groups I*. Ann. Math. **72** (1960), 369–384.

[W2] A. Weil; *Discrete subgroups of Lie groups II*. Ann. Math. **75** (1962), 578–602.

[WM] D. Witte Morris; Introduction to arithmetic groups. Preliminary version (2003).

Chapter 1

Geometric preliminaries

In this chapter we review some basic features of complex hyperbolic geometry which will be needed later on; we will mainly focus on the case of (complex) dimension 2. Most of the material is standard, and can be found for instance in Goldman's book [G], Parker's notes [P] or the earlier article of Chen and Greenberg [CG]. The parts which are not standard are section 1.2.3, concerning configurations of Lagrangian planes (which uses in particular the angle pair between two intersecting Lagrangian planes defined by Falbel and Zocca in [FZ]), as well as section 1.3.2 which relates the angle pair of an elliptic motion of $H^2_{\mathbb{C}}$ with the more familiar trace invariant investigated by Goldman. In fact, the only new result is proposition 1.2.2, which compares the Riemannian angle between two geodesics with the angle pair of any two Lagrangians each containing one of the geodesics. As a corollary we obtain an obstruction on the possible angle pairs for a triple of Lagrangian planes, which we will use in chapter 4.

1.1 Complex hyperbolic space

1.1.1 Definition, models and structures

Complex hyperbolic space $H^n_{\mathbb{C}}$ can be defined as the symmetric space $PU(n,1)/U(n)$ associated with the Lie group $PU(n,1)$ (we consider the latter rather than $SU(n,1)$ to get rid of the center and thus obtain a faithful action on the space). Now $H^n_{\mathbb{C}}$ can be seen as a domain (a connected open set) in the complex projective space $\mathbb{C}P^n$ as follows. Consider $\mathbb{C}^{n,1}$, the vector space $\mathbb{C}^{n+1}$ equipped with a non-degenerate Hermitian form of signature $(n,1)$ which we denote $\langle\cdot,\cdot\rangle$. Then for $\mathbf{z}\in\mathbb{C}^{n,1}$ the Hermitian product $\langle z,z\rangle$ is real, so that $\mathbb{C}^{n,1}$ is the disjoint union of the three following sets:

$$\begin{aligned} V_- &= \{\mathbf{z}\in\mathbb{C}^{n,1}|\langle\mathbf{z},\mathbf{z}\rangle<0\}\\ V_0 &= \{\mathbf{z}\in\mathbb{C}^{n,1}|\langle\mathbf{z},\mathbf{z}\rangle=0\}\\ V_+ &= \{\mathbf{z}\in\mathbb{C}^{n,1}|\langle\mathbf{z},\mathbf{z}\rangle>0\}\end{aligned}$$

Note that these subspaces are homogeneous (i.e. invariant under multiplication by scalars); $H^n_{\mathbb{C}}$ is then the image in $\mathbb{C}P^n$ of the negative cone V_- under the projectivization map:

$$\pi : C^{n+1}\setminus\{0\}\longrightarrow\mathbb{C}P^n$$

Moreover the boundary $\partial H^n_{\mathbb{C}}$ of $H^n_{\mathbb{C}}$ (which can be defined intrinsically) is identified with the image $\pi(V_0\setminus\{0\})$ of the null cone.

Different choices of Hermitian forms will lead to different models of complex hyperbolic space. We will here use mostly the *ball model* of $H^2_{\mathbb{C}}$. This is given by the Hermitian form defined by $\langle\mathbf{w},\mathbf{z}\rangle=\mathbf{w}^*.J.\mathbf{z}$ where J is the diagonal matrix $Diag(1,1,-1)$ (and * denotes the conjugate transpose). Then, in the affine chart

$$\begin{aligned}\mathbb{C}^2 &\hookrightarrow \mathbb{C}P^2\\ (z_1,z_2) &\longmapsto \pi((z_1,z_2,1)),\end{aligned}$$

$H^2_{\mathbb{C}}$ is the unit ball $\{(z_1,z_2)\in\mathbb{C}^2|\ |z_1|^2+|z_2|^2<1\}$. Other examples of Hermitian forms are discussed in [P]. Also, we follow Mostow in the study of his lattices $\Gamma(p,t)$ by using a Hermitian form which varies with p and t (see chapter 3).

As an open set of $\mathbb{C}P^n$, $H^n_{\mathbb{C}}$ inherits a Kähler structure; in particular it possesses a symplectic structure, a Riemannian structure, and a complex structure (see [G] p. 52 for the relations and compatibility between these); they can all be expressed in terms of Hermitian linear algebra in $\mathbb{C}^{n,1}$. For instance, the Riemannian metric on $H^n_{\mathbb{C}}$ (or Bergman metric) is given by the following distance formula. The distance $\rho(w,z)$ between two points $w,z \in H^n_{\mathbb{C}}$ can be written (normalizing so that the metric has constant holomorphic curvature -1):

$$\cosh^2\left(\frac{\rho(w,z)}{2}\right) = \frac{\langle \mathbf{w},\mathbf{z}\rangle\ \langle \mathbf{z},\mathbf{w}\rangle}{\langle \mathbf{w},\mathbf{w}\rangle\ \langle \mathbf{z},\mathbf{z}\rangle}$$

where $\mathbf{w},\mathbf{z} \in \mathbb{C}^{n,1}$ are lifts of w,z respectively.

1.1.2 Isometries

The subgroup $U(n,1)$ of $GL(n,\mathbb{C})$ preserving the Hermitian form acts on $H^n_{\mathbb{C}}$ (because it preserves $V_- \subset \mathbb{C}^{n,1}$); however all scalar matrices $\lambda.\mathrm{Id}$ ($\lambda \in U(1)$) have trivial action so that we are interested in the quotient $PU(n,1) = U(n,1)/U(1)$. It follows from the above distance formula that this group acts on $H^n_{\mathbb{C}}$ by isometries; the same formula implies that complex conjugation on the coordinates is also an isometry (the latter is an example of what we will call $\mathbb{R}$-*reflections*). These describe all of the isometries of $H^n_{\mathbb{C}}$ in the following sense (see [P]):

Proposition 1.1.1 *The group of holomorphic isometries of $H^n_{\mathbb{C}}$ is $PU(n,1)$; all other isometries are antiholomorphic and are obtained by composing an element of $PU(n,1)$ with complex conjugation.*

1.2 Subspaces and configurations

1.2.1 Totally geodesic subspaces

A *complex line* (or $\mathbb{C}$-*plane*) of $H^2_{\mathbb{C}}$ is the intersection with $H^2_{\mathbb{C}}$ of a complex projective line of $\mathbb{C}P^2$ (when this intersection is not empty). Such a $\mathbb{C}$-plane is an embedded copy of $H^1_{\mathbb{C}}$ (more precisely, in the ball model, it carries the Poincaré model of the hyperbolic plane, with constant curvature -1, see [G] and [P]). Each $\mathbb{C}$-plane C is also the fixed-point set of a one-parameter family of (holomorphic) isometries, called $\mathbb{C}$-*reflections*; these are the images in $PU(2,1)$ of the stabilizer in $U(2,1)$ of a complex plane above C. One of these $\mathbb{C}$-reflections is an involution, so that $\mathbb{C}$-planes are totally geodesic.

$PU(2,1)$ acts transitively on the set of $\mathbb{C}$-planes, with isotropy group a conjugate of $P(U(1)\times U(1,1))$.

A *Lagrangian plane* (or $\mathbb{R}$-*plane*) is a maximal totally real subspace of $H^2_{\mathbb{C}}$. This means that it is the projective image of a real 3-subspace $\tilde{L}$ of $\mathbb{C}^{2,1}$ such that $\langle v,w\rangle \in \mathbb{R}$ for all $v,w \in \tilde{L}$ (and such that $\tilde{L} \cap H^2_{\mathbb{C}} \neq \emptyset$). Such an $\mathbb{R}$-plane is an embedded copy of $H^2_{\mathbb{R}}$ (more precisely, in the ball model, it carries the Klein-Beltrami model of the hyperbolic plane, with constant curvature $-1/4$, see [G] and [P]). Each $\mathbb{R}$-plane is also the fixed-point set of a unique (antiholomorphic) isometry, which is an involution; such an involution is called an $\mathbb{R}$-*reflection*. In particular, $\mathbb{R}$-planes are also totally geodesic. The standard example of an $\mathbb{R}$-reflection is

complex conjugation, which can be written in the ball model (or in any affine model defined by a real Hermitian matrix):

$$\sigma_0 \ : \ (z_1, z_2) \longmapsto (\overline{z_1}, \overline{z_2})$$

whose fixed-point set is the standard $\mathbb{R}$-plane:

$$L_0 = \{(z_1, z_2) \in H^2_{\mathbb{C}} \mid z_1, z_2 \in \mathbb{R}\}$$

$PU(2,1)$ acts transitively on the set of $\mathbb{R}$-planes, with isotropy a conjugate of $PO(2,1)$.

These are the only non-obvious totally geodesic subspaces of $H^2_{\mathbb{C}}$:

Theorem 1.2.1 *The complete totally geodesic submanifolds of $H^2_{\mathbb{C}}$ are points, geodesic lines, $\mathbb{C}$-planes and $\mathbb{R}$-planes.*

Goldman sketches a proof (pp. 82–84 of [G]) of the general result in $H^n_{\mathbb{C}}$, whose only complete totally geodesic submanifolds are complex linear subspaces and totally real totally geodesic subspaces.

This has an important consequence for the study of geometric group actions in $H^n_{\mathbb{C}}$, namely the fact that there do not exist hyperplanes, i.e. totally geodesic real hypersurfaces. In particular there is no natural notion of polyhedra in these spaces.

1.2.2 Geodesic triangles

We recall a few facts about geodesic triangles in $H^2_{\mathbb{C}}$ in order to obtain an obstruction on the angle pairs in a triple of $\mathbb{R}$-planes intersecting pairwise inside $H^2_{\mathbb{C}}$. We will mostly need an explicit expression for one of the angles, as well as the general fact in nonpositive curvature that the angle sum in such a triangle is less than π. Our main reference for this section is Brehm's article [B].

We begin with a quick dimension count for the space of triangles. Each point in $H^2_{\mathbb{C}}$ depends on four parameters, so that the space of triples of points is of dimension 12. Now we normalize by the action of $PU(2,1)$ which is of dimension 8, so that the space of triples of points up to isometry is of dimension 4.

We now write an explicit normal form for such triples of points, which we will use to compute the angle at the origin. We start with three points A, B and C in $H^2_{\mathbb{C}}$, and bring point A to the origin $O = (0,0)$ of the ball. Then, the action of $PU(2,1)$ being transitive on geodesics through a given point, bring point B to the real half-axis $\{(0,t) | t \in]0;1[\}$. Using the isotropy of this geodesic (rotation on the first coordinate), we bring the third point to (z_1, z_2) with $z_1 \in]0;1[$. Then, if the three points are not colinear, there is no more holomorphic isotropy (in fact, using complex conjugation, we can also suppose that $Im(z_2) > 0$, but this will have no effect on the angle we are interested in). We then denote:

$$A = (0,0), B = (0,t), C = (z_1, z_2) \text{ with } t, z_1 \in]0;1[.$$

This normal form is analogous to that used by Brehm; we have made this specific choice because of the $\mathbb{R}$-planes containing the various pairs of points.

The geometry of the triangle translates in terms of the Hermitian products of three vectors X, Y, and Z in $\mathbb{C}^{2,1}$ above the three points A, B and C. To simplify the expressions, we normalize so that:

$$\langle X, X\rangle = \langle Y, Y\rangle = \langle Z, Z\rangle = -1$$

We thus choose:

$$X = (0, 0, 1), Y = (0, \frac{t}{\tau}, \frac{1}{\tau}), Z = (\frac{z_1}{\rho}, \frac{z_2}{\rho}, \frac{1}{\rho})$$

with:

$$\tau := \sqrt{1 - t^2},\ \rho := \sqrt{1 - |z_1|^2 - |z_2|^2}$$

The various Hermitian products are then:

$$\langle X, Y\rangle = -\frac{1}{\tau}$$

$$\langle X, Z\rangle = -\frac{1}{\rho}$$

$$\langle Y, Z\rangle = \frac{t\overline{z_2} - 1}{\tau\rho}$$

so that the Hermitian triple product, which is a fundamental invariant of the triangle, is written:

$$T := \langle X, Y\rangle\langle Y, Z\rangle\langle Z, X\rangle = \frac{t\overline{z_2} - 1}{\tau^2\rho^2}$$

There are two angular invariants usually attached to a pair of geodesic rays emanating from a point $A \in H^2_{\mathbb{C}}$, which Goldman calls *real angle* and *complex angle*. Geometrically, these are respectively the Riemannian angle $\lambda(A)$ between the two geodesics, and the angle $\phi(A)$ between the $\mathbb{C}$-planes containing the geodesics. We will consider for now only the Riemannian angle $\lambda(A)$.

In concrete terms, we identify the tangent space $T_A H^2_{\mathbb{C}}$ with $X^{\perp} \subset \mathbb{C}^{2,1}$, subspace on which the restriction of the Hermitian form is positive definite. Then the Riemannian structure in $T_A H^2_{\mathbb{C}}$ is simply the real part of this Hermitian form. Consider two unitary vectors $u_1, u_2 \in T_A H^2_{\mathbb{C}}$ tangent to the geodesic rays. Then, with the above notation, we have:

$$\cos\lambda(A) = Re(\langle u_1, u_2\rangle)$$

$$(\text{analogously, } \cos\phi(A) = |\langle u_1, u_2\rangle|).$$

The product in which we are interested is then written in terms of X, Y, Z as (the conjugate of Brehm's expression):

$$\langle u_1, u_2\rangle = \frac{\langle X, Y\rangle\langle Y, Z\rangle\langle Z, X\rangle + |\langle X, Y\rangle|^2|\langle X, Z\rangle|^2}{(|\langle X, Y\rangle|^2 - 1)^{\frac{1}{2}}(|\langle X, Z\rangle|^2 - 1)^{\frac{1}{2}}|\langle X, Y\rangle||\langle X, Z\rangle|}$$

Replacing the various products by their expression in our normal form, we obtain:

$$\cos\lambda(A) = \frac{Re(z_2)}{(|z_1|^2 + |z_2|^2)^{\frac{1}{2}}}$$

This is all we will need for later, as well as the following classical result for which the reader can refer for instance to [BGS] (p. 6):

Proposition 1.2.1 *Let A, B and C be three points in a Riemannian manifold of negative curvature (not necessarily constant), and $\lambda(A)$, $\lambda(B)$ and $\lambda(C)$ be (measures in $[0, \pi[$ of) the three Riemannian angles between the geodesic segments at each vertex. Then:*

$$\lambda(A) + \lambda(B) + \lambda(C) < \pi$$

1.2.3 Configurations of Lagrangians

We will now define the angle pair between two intersecting $\mathbb{R}$-planes of $H^2_{\mathbb{C}}$, and relate it to the angle between any two geodesics, one being in each $\mathbb{R}$-plane. See chapter 2 and [N] for more details about pairs of $\mathbb{R}$-planes, and chapter 4 for triples.

Given two $\mathbb{R}$-planes L_1 and L_2 intersecting in a point of $H^2_{\mathbb{C}}$ and σ_1, σ_2 the associated $\mathbb{R}$-reflections, the composite map $\sigma_2 \circ \sigma_1$ is holomorphic and has a fixed point inside of $H^2_{\mathbb{C}}$. It is thus conjugate in $PU(2,1)$ to an element of $U(2)$ (the stabilizer of the origin in the ball model), which is semisimple with two unitary eigenvalues $e^{2i\theta_1}$, $e^{2i\theta_2}$. The unordered pair $\{\theta_1, \theta_2\}$ with $\theta_i \in \mathbb{R}/\pi\mathbb{Z}$ will be called *angle pair* of the ordered pair of $\mathbb{R}$-planes (L_1, L_2). Such a pair characterizes the pair (L_1, L_2) up to holomorphic isometry.

We now recall from [N] (p. 74) the following fundamental result (note that bringing the intersection point to the origin transforms the $\mathbb{R}$-planes to vectorial Lagrangians in $\mathbb{C}^2$):

Lemma 1.2.1 *Let L_1 and L_2 be two Lagrangians in $\mathbb{C}^2$, with angle pair $\{\theta_1, \theta_2\}$. Then there exists an orthonormal basis (v_1, v_2) of L_1 such that $(e^{i\theta_1}v_1, e^{i\theta_2}v_2)$ is an orthonormal basis of L_2.*

We now show the main result of this section:

Proposition 1.2.2 *Let L_1 and L_2 be two intersecting $\mathbb{R}$-planes, with angle pair $\{\theta_1, \theta_2\}$ ($\theta_i \in [0, \pi[$) and let $g_1 \subset L_1$, $g_2 \subset L_2$ be two intersecting geodesics, with Riemannian angle $\lambda \in [0, \pi[$. Then the following inequality holds:*

$$|\cos\lambda| \leqslant \mathrm{Max}(|\cos\theta_1|, |\cos\theta_2|)$$

In other words:

$$\mathrm{Min}\{\theta_1, \theta_2, \pi - \theta_1, \pi - \theta_2\} \leqslant \lambda \leqslant \mathrm{Max}\{\theta_1, \theta_2, \pi - \theta_1, \pi - \theta_2\}$$

Before proving the proposition, we deduce the result which we are interested in, which follows immediately from the previous angle-sum property:

Proposition 1.2.3 *Let L_1, L_2, L_3 be three pairwise intersecting $\mathbb{R}$-planes with angle pairs $\{\theta_1, \theta_2\}$, $\{\theta_3, \theta_4\}$, $\{\theta_5, \theta_6\}$ ($\theta_i \in [0, \pi[$). Then the following inequality holds:*

$$\sum_{i=1,3,5} \mathrm{Min}\{\theta_i, \theta_{i+1}, \pi - \theta_i, \pi - \theta_{i+1}\} < \pi$$

Proof. Bring the intersection point of the two $\mathbb{R}$-planes L_1 and L_2 to be the origin 0, and L_1 the standard Lagrangian $\{(x, y) \in H^2_{\mathbb{C}} \mid x, y \in \mathbb{R}\}$. Then, by Nicas' lemma, there exists an orthonormal basis (v_1, v_2) of L_1 such that $(e^{i\theta_1}v_1, e^{i\theta_2}v_2)$ is an orthonormal basis of L_2. A (direct) orthonormal basis of L_1 being of the form:

$$v_1 = \begin{pmatrix} \cos\varphi \\ \sin\varphi \end{pmatrix} \; v_2 = \begin{pmatrix} -\sin\varphi \\ \cos\varphi \end{pmatrix}$$

with $\varphi \in [0, 2\pi[$, L_2 will be of the form:

$$L_2(\varphi) = \begin{pmatrix} e^{i\theta_1}\cos\varphi & -e^{i\theta_2}\sin\varphi \\ e^{i\theta_1}\sin\varphi & e^{i\theta_2}\cos\varphi \end{pmatrix} \cdot L_1$$

Recall now that the Riemannian angle in question is given by:

$$\cos\lambda = \frac{Re(z_2)}{(|z_1|^2 + |z_2|^2)^{\frac{1}{2}}}$$

where here

$$Re(z_2) = x\sin\varphi\cos\theta_1 + y\cos\varphi\cos\theta_2$$

and we can suppose that $|z_1|^2 + |z_2|^2 = x^2 + y^2 = 1$ (taking the extremal points to be on the boundary sphere).

It only remains to bound the following function of $\varphi, \psi \in [0, 2\pi[$ (writing $x = \cos\psi$ and $y = \sin\psi$):

$$\cos\lambda = f_{\theta_1,\theta_2}(\varphi, \psi) = \cos\psi\sin\varphi\cos\theta_1 + \sin\psi\cos\varphi\cos\theta_2$$

Taking partial derivatives, we see that:

$$\begin{cases} \frac{\partial f}{\partial \psi} &= -\sin\psi\sin\varphi\cos\theta_1 + \cos\psi\cos\varphi\cos\theta_2 \\ \frac{\partial f}{\partial \varphi} &= \cos\psi\cos\varphi\cos\theta_1 - \sin\psi\sin\varphi\cos\theta_2 \end{cases}$$

These two expressions cannot be simultaneously be null if $\cos\theta_1 \neq \cos\theta_2$, so that the extremal values of the function must be on the sides of the square, where its values are:

$$f_{\theta_1,\theta_2}(\varphi, 0) = \sin\varphi\cos\theta_1$$

$$f_{\theta_1,\theta_2}(0, \psi) = \sin\psi\cos\theta_2$$

This proves the proposition. □

1.3 Isometries

1.3.1 Classification of isometries

As in the more familiar case of plane hyperbolic geometry, holomorphic isometries of $H^2_{\mathbb{C}}$ fall into three main classes, according to the position of their fixed point(s) in the ball. An element of $PU(2,1)$ is said to be:

- *elliptic* if it has a fixed point inside $H^2_{\mathbb{C}}$.
- *parabolic* if it has a single fixed point on the boundary $\partial H^2_{\mathbb{C}}$.
- *loxodromic* if it has exactly two fixed points on the boundary $\partial H^2_{\mathbb{C}}$.

These three cases exhaust all possibilities.

It is very useful to have concrete criteria to decide which class a given isometry belongs to. We will now present two such criteria, the first, due to Chen and Greenberg, being in terms of the Jordan normal form and eigenvalues of any corresponding matrix representative in $U(2,1)$, and the second, analogous to the trace criterion in plane hyperbolic geometry and due to Goldman, in terms of the trace of a representative in $SU(2,1)$. Note that fixed points in $\mathbb{C}P^2$ of a projective transformation are given by the eigenvectors of any matrix representative. We will say that an eigenvalue is of *negative type* if its eigenspace intersects the negative cone of the Hermitian form (this corresponds to fixed points inside $H^2_{\mathbb{C}}$), and positive if not.

Proposition 1.3.1 (see [CG] p. 72) *Let A be a matrix in $U(2,1)$, and g the associated isometry in $PU(2,1)$. Then:*

- *g is elliptic $\iff$ A is semisimple with eigenvalues of norm 1.*
- *g is loxodromic $\iff$ A is semisimple with exactly one eigenvalue of norm 1 (the two others then have inverse norms).*
- *g is parabolic $\iff$ A is not semisimple. It then has eigenvalues of norm 1.*

Chen and Greenberg also detail conditions under which two isometries of a given class are conjugate in $PU(2,1)$; we will only state this in the case of elliptic isometries in the next section.

We now state Goldman's trace criterion; note that in this case the matrix representative must be in $SU(2,1)$. We now need to distinguish among elliptic isometries the *regular elliptic* isometries, whose associated matrices have distinct eigenvalues, and the *special elliptic* ones whose associated matrices have a repeated eigenvalue. We will see what this means geometrically in the next section. We will say that an isometry is unipotent if its matrix representatives have three equal eigenvalues; a parabolic isometry which is not unipotent will be called *elliptoparabolic* (it then has a unique stable $\mathbb{C}$-plane). C_3 will denote the set of the three cube roots of unity in $\mathbb{C}$.

Proposition 1.3.2 (see [G] p. 204) *Let A be a matrix in $SU(2,1)$ and $g \in PU(2,1)$ be the associated isometry of $H^2_{\mathbb{C}}$. Let f be the real polynomial of a complex variable defined by:*

$$f(\tau) = |\tau|^4 - 8Re(\tau^3) + 18|\tau|^2 - 27$$

Then:

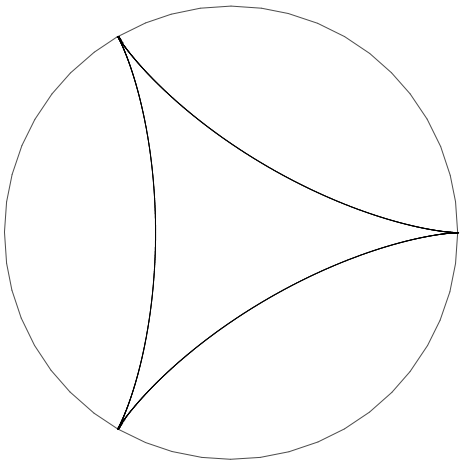

Figure 1.1: The null-locus of the polynomial f inscribed in the circle of radius 3 centered at the origin

- *g is regular elliptic* $\iff f(tr(A)) < 0$.
- *g is loxodromic* $\iff f(tr(A)) > 0$.
- *g is special elliptic or ellipto-parabolic* $\iff f(tr(A)) = 0$ *and* $tr(A) \notin 3C_3$.
- *g is unipotent* $\iff tr(A) \in 3C_3$.

The null-locus of the polynomial f can be seen in figure 1.1.

1.3.2 Elliptic isometries

We now define the main invariant of an elliptic conjugacy class in $PU(2,1)$, which is an unordered angle pair (we have in fact already used this notion to define the angle pair of a pair of $\mathbb{R}$-planes). Let g be an elliptic isometry of $H^2_{\mathbb{C}}$; by bringing a fixed point of g to the origin O of the ball, we see that g is conjugate in $PU(2,1)$ to an element in the stabilizer $U(2)$ of O, which in turn is conjugate in $U(2)$ to a diagonal matrix with eigenvalues of norm 1. We can thus choose a matrix representative A to be in the standard (for the ball model) embedding of $U(2)$:

$$\begin{array}{ccc} U(2) & \hookrightarrow & U(2,1) \\ \begin{pmatrix} a & b \\ c & d \end{pmatrix} & \longmapsto & \begin{pmatrix} a & b & 0 \\ c & d & 0 \\ 0 & 0 & 1 \end{pmatrix} \end{array}$$

in the following diagonal form :

$$A = \begin{pmatrix} e^{i\theta_1} & 0 & 0 \\ 0 & e^{i\theta_2} & 0 \\ 0 & 0 & 1 \end{pmatrix}$$

The unordered pair $\{\theta_1, \theta_2\}$ with $\theta_i \in \mathbb{R}/2\pi\mathbb{Z}$ is the *angle pair* of the elliptic isometry g. Geometrically, when both angles are non-null and distinct, g has exactly 2 stable $\mathbb{C}$-planes which pass through its isolated fixed point. These correspond to the images of the eigenspaces of a representative in $U(2)$. g acts on each of these $\mathbb{C}$-planes as a rotation, one with angle θ_1 and the other with angle θ_2.

We now relate this angle pair to the point of view of Chen-Greenberg; it then follows from their characterization of elliptic conjugacy classes that:

Proposition 1.3.3 *Two elliptic isometries of $H^2_{\mathbb{C}}$ are conjugate $\iff$ they have same angle pair.*

If g is an elliptic isometry with a matrix representative $A \in U(2,1)$, then by proposition 1.3.1 A is semisimple with eigenvalues of norm 1, one of which is of negative type, say $e^{i\theta_3}$. Then:

$$A \sim \begin{pmatrix} e^{i\theta_1} & 0 & 0 \\ 0 & e^{i\theta_2} & 0 \\ 0 & 0 & e^{i\theta_3} \end{pmatrix} \sim \begin{pmatrix} e^{i(\theta_1-\theta_3)} & 0 & 0 \\ 0 & e^{i(\theta_2-\theta_3)} & 0 \\ 0 & 0 & 1 \end{pmatrix}$$

where the first $\sim$ sign denotes conjugacy in $U(2,1)$ and the second denotes equivalence by a scalar multiplication. The angle pair of such an element is thus $\{\theta_1 - \theta_3, \theta_2 - \theta_3\}$ (note that the eigenvalue of negative type plays a special role). Applying the criterion of conjugacy from [CG] gives us the proposition.

We now give three examples of elliptic isometries of special types, along with a geometric characterization of each type:

- elliptic isometries with angles $\{0, \theta\}$ are called *complex reflections*. They have a fixed $\mathbb{C}$-plane (and act on all orthogonal $\mathbb{C}$-planes by rotation of θ).
- elliptic isometries with angles $\{\theta, \theta\}$ are called *complex reflections in a point*. They have an isolated fixed point and preserve all $\mathbb{C}$-planes through this point (acting by rotation of θ).
- elliptic isometries with angles $\{\theta, -\theta\}$ are called *real rotations* (the name is not standard). They are the only ones which preserve an $\mathbb{R}$-plane, apart from complex reflections of order 2 (which have angles $\{0, \pi\}$).

We finish by showing the link between the angle pair of an elliptic isometry (which as an unordered pair of angles lives in the surface $\mathbb{T}^2/\mathfrak{S}_2$) and the corresponding trace of one of its three matrix representatives in $SU(2,1)$ (which lives in Goldman's triangle T_G of figure 1.1 but is only defined up to multiplication in C_3, so that it lives in fact in T_G/C_3). There is a map:

$$\tau : \mathbb{T}^2/\mathfrak{S}_2 \longrightarrow T_G/C_3$$

given by the trace. For instance, one of the representatives in T_G of $\tau(\{\theta_1, \theta_2\})$ is:

$$e^{i\frac{2\theta_1-\theta_2}{3}} + e^{i\frac{2\theta_2-\theta_1}{3}} + e^{-i\frac{\theta_1+\theta_2}{3}}$$

as can be seen by normalizing the diagonal matrix with entries $e^{i\theta_1}, e^{i\theta_2}, 1$ in $SU(2,1)$. This map is three-to-one from $(\mathbb{T}^2 \setminus (\Delta \cup (\{0\} \times S^1) \cup (S^1 \times \{0\})))/\mathfrak{S}_2$ to the interior of T_G/C_3 (this

corresponds to regular elliptic elements), except at the central point of angles $\{\frac{2\pi}{3}, -\frac{2\pi}{3}\}$ which is the only point of trace 0. On the boundary it is one-to-one.

Bibliography

[BGS] W. Ballmann, M. Gromov, V. Schroeder; Manifolds of Nonpositive Curvature. Birkhaüser Progress in Math. vol. 61, 1985.

[B] Brehm, Ulrich; *The shape invariant of triangles and trigonometry in two-point homogeneous spaces*. Geom. Dedicata **33** (1990), 59–76.

[CG] S. Chen, L. Greenberg; *Hyperbolic spaces*. In Contributions to Analysis. Academic Press, New York (1974), 49–87.

[FZ] E. Falbel, V. Zocca; *A Poincaré's polyhedron theorem for complex hyperbolic geometry*. J. reine angew. Math. **516** (1999), 133–158.

[G] W. M. Goldman; Complex Hyperbolic Geometry. Oxford Mathematical Monographs. Oxford Science Publications (1999).

[N] A. J. Nicas; *Classifying pairs of Lagrangians in a Hermitian vector space*. Topology Appl. **42** (1991), 71–81.

[P] J. R. Parker; Notes on complex hyperbolic geometry, preliminary version (2003).

Chapter 2

Fundamental domains for finite groups of $U(2)$ and configurations of Lagrangians

This chapter is a joint work with Elisha Falbel and has been published in *Geometriae Dedicata* (see reference [FPau] in the bibliography of the introduction).

2.1 Introduction

Finite subgroups of $U(2)$, of the group $\widehat{U(2)}$ obtained by adjoining complex conjugation to $U(2)$, and more generally of $O(4)$ have been enumerated (see [CS, C, D] for lists and discussions on that problem). It contains two important classes of subgroups, namely, those generated by complex reflections and those which are index two subgroups of groups generated by involutions fixing a Lagrangian subspace of $\mathbb{C}^2$. We show in fact that all finite subgroups of $U(2)$ are of the second type (th. 2.1). This will follow from the fact that almost all finite subgroups of $U(2)$ have two generators (see th. 2.3), and the main goal in this paper is to obtain a description of these groups in terms of Lagrangian reflections. In particular we describe fundamental domains for those groups which are adapted to the Lagrangian decomposition and seem much simpler than previous fundamental domains (sections 4.4 and 5.1.3). Previous fundamental domains for some of those finite groups were obtained by Mostow in [M] in view of applications in complex hyperbolic geometry. Fundamental domains in the hyperbolic case for some groups generated by Lagrangian reflections were studied in [FZ].

It is interesting to note that, in our construction, the boundary of the fundamental domain is made out of pieces which are foliated by complex lines or Lagrangian planes and sometimes both and they show that recent constructions of fundamental domains in complex hyperbolic geometry (cf. [S]) appear naturally in the realm of finite groups.

2.2 Lagrangian subspaces and $\mathbb{R}$-reflections

Let $\mathbb{C}^n$ be the n-dimensional complex vector space which we will consider together with its standard Hermitian metric given by $\langle z, w\rangle = z_1\bar{w}_1 + \cdots + z_n\bar{w}_n$. We write the real and imaginary decomposition of the Hermitian metric

$$\langle z, w\rangle = g(z, w) - i\omega(z, w)$$

thus defining the standard symplectic form ω on $\mathbb{C}^n$ compatible with the Hermitian metric. The complex structure $J : \mathbb{C}^n \to \mathbb{C}^n$ defined by $Jz = iz$ satisfies the following relation

$$g(z, w) = \omega(z, Jw).$$

Let $U(n)$ be the unitary group of $\mathbb{C}^n$ relative to $\langle\, ,\rangle$, $O(2n)$ the orthogonal group of $\mathbb{C}^n$ relative to g and $Sp(n)$ the symplectic group of $\mathbb{C}^n$ relative to ω. Then by definition of $\langle\, ,\rangle$, we have $U(n) = O(2n) \cap Sp(n)$. It follows that J is a map that is both orthogonal and symplectic.

Definition 2.2.1 *A real subspace L of $\mathbb{C}^n$ is said to be* Lagrangian *if its orthogonal $L^{\perp_\omega}$ with respect to ω is L itself.*

Equivalently, L is isotropic with respect to ω and of maximal dimension with respect to this property. A real subspace W of $\mathbb{C}^n$ is said to be *totally real* if $\langle u, v\rangle \in \mathbb{R}$ for all $u, v \in W$. A

real subspace L of $\mathbb{C}^n$ is therefore Lagrangian if and only if it is totally real and of maximal dimension with respect to this property. Thus Lagrangians in $\mathbb{C}^n$ are none other than $\mathbb{R}^n$-planes (see [G]). Equivalently again, L is Lagrangian if and only if its orthogonal with respect to g is $L^{\perp_g} = JL$. In particular, given a Lagrangian subspace L of $\mathbb{C}^n$, we have the following g-orthogonal decomposition $\mathbb{C}^n = L \oplus JL$. That decomposition enables us to associate to every Lagrangian L an $\mathbb{R}$-linear map

$$\begin{array}{rccc} \sigma_L : & \mathbb{C}^n & \longrightarrow & \mathbb{C}^n \\ & x + Jy & \longmapsto & x - Jy \end{array}$$

Definition 2.2.2 *A Lagrangian reflection (or $\mathbb{R}$-reflection) is an involution in $\mathbf{O}(2n)$ which fixes a Lagrangian subspace L and acts as $-I$ on $J(L)$.*

Observe that

1. A Lagrangian reflection is a skew-symplectic ($\omega(\sigma_L(z), \sigma_L(w)) = -\omega(z, w)$) and anti-holomorphic map ($\sigma_L \circ J = -J \circ \sigma_L$).
2. Reciprocally, if an anti-holomorphic map fixes a Lagrangian space L, it acts on $J(L)$ by $-I$.
3. If n is even the Lagrangian reflections are in $\mathbf{SO}(2n)$,
4. In complex dimension 1, Lagrangian reflections coincide with real reflections in lines,
5. Lagrangian reflections are in $\widehat{\mathbf{U}}(n) \subset \mathbf{O}(2n)$, the group generated by $\mathbf{U}(n)$ and the conjugation $z \mapsto \bar{z}$.

Denoting by $L(n)$ the $\frac{n(n+1)}{2}$-dimensional manifold of all Lagrangian subspaces of $\mathbb{C}^n$ (the *Lagrangian grassmannian* of $\mathbb{C}^n$), we have defined a map

$$\begin{array}{rcl} L(n) & \to & \widehat{\mathbf{U}}(n) \\ L & \to & \sigma_L. \end{array}$$

Proposition 2.2.1 (cf. [N, FMS]) *Given two Lagrangian subspaces L_1 and L_2 there exists a unique $g_{12} \in U(n)$ such that $L_2 = g_{12}L_1$ satisfying the following conditions:*

1. *the eigenvalues are unitary complex numbers $e^{i\lambda_j}$ verifying $\pi > \lambda_1 \geq \cdots \lambda_n \geq 0$*
2. *there exists an orthonormal basis for L_1 which is a basis of eigenvectors for g_{12}.*

A corollary of this proposition is given by the following classification of pairs of Lagrangians:

Proposition 2.2.2 ([N]) *Pairs of Lagrangian subspaces in $\mathbb{C}^n$ are classified up to unitary transformations by a list $(\lambda_1, \cdots, \lambda_n)$, with $\pi > \lambda_1 \geq \cdots \lambda_n \geq 0$.*

The vector $(\lambda_1, \cdots, \lambda_n)$ will be called *angle between* L_1 and L_2. Note that the angle between L_2 and L_1 is $(\pi - \lambda_n, \cdots, \pi - \lambda_1)$ (in the case $\lambda_i > 0$). Sometimes we will write the angle between L_1 and L_2 without fixing a particular convention for the eigenvalues. To relate the angle with the inversions associated to the Lagrangians we use the following proposition which is a consequence of proposition 1. We refer to [FMS] for a proof.

Proposition 2.2.3 *Let g_{12} be the unique unitary map sending L_1 to L_2 defined in the above proposition. Then:*

$$g_{12}^2 = \sigma_2 \circ \sigma_1$$

Let $L_0 = \mathbb{R}^n$ be the standard real plane in $\mathbb{C}^n$ and σ_0 its corresponding $\mathbb{R}$-reflection.

Definition 2.2.3 *Let $L \subset \mathbb{C}^n$ be a Lagrangian subspace and σ its corresponding $\mathbb{R}$-reflection. The matrix of $\sigma \circ \sigma_0$ with respect to the canonical basis is called the Souriau matrix of L (or of σ).*

We introduce the following terminology:

Definition 2.2.4 *If a unitary transformation U is expressed as a product $\sigma_2\sigma_1$ of two $\mathbb{R}$-reflections in $\mathbb{R}^n$-planes L_1 and L_2, we say that L_1 (or L_2)* decomposes *U.*

Note that the second $\mathbb{R}^n$-plane is then uniquely determined.

Proposition 2.2.4 *Let U be a unitary transformation of $\mathbb{C}^n$, and C_1,...,C_k its eigenspaces with dimensions n_1,...,n_k. Then an $\mathbb{R}^n$-plane L decomposes $U \iff L \cap C_i$ is a Lagrangian subspace in C_i for all i. The space of such $\mathbb{R}^n$-planes is isomorphic to $U(n_1)/O(n_1) \times ... \times U(n_k)/O(n_k)$. In particular:*

- *If U is a multiple of identity, then any $\mathbb{R}^n$-plane decomposes U.*
- *If U has n distinct eigenvalues, let C_1,..., C_n be its eigenspaces. Then an $\mathbb{R}^n$-plane L decomposes $U \iff L \cap C_i$ is a real line for all i. There exists an n-torus of such $\mathbb{R}^n$-planes.*

This proposition follows from Nicas' diagonalization lemma (prop. 1). We use this result to simultaneously decompose two unitary elements (in view of dimension 2, we are only concerned with the two particular cases above):

Proposition 2.2.5 *Let U_1, U_2 be unitary transformations of $\mathbb{C}^n$, each with distinct eigenvalues, and let C_1,..., C_n, C'_1,..., C'_n be their respective eigenspaces. Then an $\mathbb{R}^n$-plane L simultaneously decomposes U_1 and $U_2 \iff L \cap C_i$ and $L \cap C'_i$ are real lines for all i.*

The case of dimension 2 is special because any pair of unitary transformations can be simultaneously decomposed into $\mathbb{R}$-reflections,as we will see below. We begin by recalling a few facts about the behavior of $\mathbb{R}$-planes of $\mathbb{C}^2$ under projectivisation, for which the reader can refer to [FMS].

Let:

$$\pi : \mathbb{C}^2 - \{0\} \longrightarrow \mathbb{C}P^1$$

denote projectivisation, inducing a surjective morphism:

$$\tilde{\pi} : U(2) \longrightarrow SO(3).$$

If C_i is a $\mathbb{C}$-plane (i. e. a complex line) and L_j an $\mathbb{R}$-plane, then $\pi(C_i)$ is a point in $\mathbb{C}P^1$ which we denote c_i, and $\pi(L_j)$ is a great circle in $\mathbb{C}P^1$ which we denote l_j. Moreover their relative position is as follows:

- $c_i \in l_j \Longleftrightarrow C_i \cap L_j$ is a real line
- $c_i \notin l_j \Longleftrightarrow C_i \cap L_j = \{0\}$

We can state now the

Theorem 2.2.1 *Every finite subgroup of $U(2)$ admits an index 2 supergroup in $\widehat{U(2)}$ generated by $\mathbb{R}$-reflections. In fact:*

- *Every two-generator subgroup of $U(2)$ admits an index 2 supergroup in $\widehat{U(2)}$ generated by 3 $\mathbb{R}$-reflections. There exists generically a circle of such groups, and a 2-torus in the degenerate cases.*
- *The exceptional finite subgroups of $U(2)$ which are not generated by 2 elements ($\langle 2q, 2, 2\rangle_m$ with m even, see theorem 2.2.3) admit an index 2 supergroup in $\widehat{U(2)}$ generated by 4 $\mathbb{R}$-reflections.*

Proof. We will only prove the first part for now; the case of the exceptional family $\langle 2q, 2, 2\rangle_m$ (m even), will be handled in the last section where we give an explicit decomposition into $\mathbb{R}$-reflections.

The case of two generators can be seen in $\mathbb{C}P^1$ as follows. Assuming that the generators U_1, U_2 each have distinct eigenvalues, their eigenspaces project to two pairs of antipodal points in $\mathbb{C}P^1$, and there exists a great circle l containing these points (l is unique if the four points are distinct, that is if U_1 and U_2 have distinct eigenspaces). This means that any $\mathbb{R}$-plane L above l intersects the four eigenspaces along a real line, and thus simultaneously decomposes U_1 and U_2. □

Remark: Theorem 4.1 in [F] gives an incomplete classification. In the course of the proof the imprimitive groups were neglected. Also, the primitive family $(\mathbf{C}_{6m}/\mathbf{C}_{2m}; \mathbf{T}/\mathbf{V})$ was excluded because $\mathbf{T}$ was not generated by pure quaternions. In fact, $\mathbf{T}$ is a subgroup of index 2 of $\mathbf{O}$, a group generated by pure quaternions and this is admissible in the proof.

It remains to see which finite subgroups of $U(2)$ can be generated by two elements; to this effect, we recall Du Val's classification of finite subgroups of $U(2)$ among those of $SO(4)$ (they comprise the 9 first types of his list, [D] p. 57, see also [C] p. 98). We will use Du Val's notations, writing elements of $U(2)$ as pairs (l, r) with $l \in U(1)$ and $r \in SU(2)$ (which we write as a unit quaternion under an implicit isomorphism), with the relations $(l, r) = (-l, -r)$; and subgroups of $U(2)$ as $\Gamma = (L/L_K; R/R_K)$ where $L_K \lhd L \subset U(1)$ and $R_K \lhd R \subset SU(2)$ are defined as follows:

$$L_K = \{l \in U(1) \,|\, (l, 1) \in \Gamma\}$$

$$R_K = \{r \in SU(2) \,|\, (1, r) \in \Gamma\}$$

$$L = \{l \in U(1) \,|\, \exists\, r \in SU(2), (l, r) \in \Gamma\}$$

$$R = \{r \in SU(2) \,|\, \exists\, l \in U(1), (l, r) \in \Gamma\}$$

Γ is then recovered from L_K, L, R_K, R, fixing an isomorphism
$\phi : L/L_K \longrightarrow R/R_K$, as:

$$\Gamma = \{(l, r) \in L \times R \,|\, \phi(\bar{l}) = \bar{r}\}$$

The boldface letters $\mathbf{C}_k$, $\mathbf{D}_k$, $\mathbf{T}$, $\mathbf{O}$, $\mathbf{I}$, $\mathbf{V}$ indicate subgroups of $SU(2)$ which are double covers of the corresponding groups in $SO(3)$ (the cyclic, dihedral, tetrahedral, octahedral, icosahedral groups and the classical quaternion group of order 8). The subscript notation, such as in $\langle p, 2, 2\rangle_m$, is made explicit in the table below and indicates a group where $L = L_K$ and $R = R_K$ (its double cover is a direct product).

These notations established, the classification is:

Theorem 2.2.2 (see [D], [C]) *The finite subgroups of $U(2)$ are*

1. $(\mathbf{C}_{2m}/\mathbf{C}_f; \mathbf{C}_{2n}/\mathbf{C}_g)_d$
2. $\langle p, 2, 2\rangle_m = (\mathbf{C}_{2m}/\mathbf{C}_{2m}; \mathbf{D}_p/\mathbf{D}_p)$
3. $(\mathbf{C}_{4m}/\mathbf{C}_{2m}; \mathbf{D}_p/\mathbf{C}_{2p})$ *and* $(\mathbf{C}_{4m}/\mathbf{C}_m; \mathbf{D}_p/\mathbf{C}_p)$, *$m$ and p odd*
4. $(\mathbf{C}_{4m}/\mathbf{C}_{2m}; \mathbf{D}_{2p}/\mathbf{D}_p)$
5. $\langle 3, 3, 2\rangle_m = (\mathbf{C}_{2m}/\mathbf{C}_{2m}; \mathbf{T}/\mathbf{T})$
6. $(\mathbf{C}_{6m}/\mathbf{C}_{2m}; \mathbf{T}/\mathbf{V})$
7. $\langle 4, 3, 2\rangle_m = (\mathbf{C}_{2m}/\mathbf{C}_{2m}; \mathbf{O}/\mathbf{O})$
8. $(\mathbf{C}_{4m}/\mathbf{C}_{2m}; \mathbf{O}/\mathbf{T})$
9. $\langle 5, 3, 2\rangle_m = (\mathbf{C}_{2m}/\mathbf{C}_{2m}; \mathbf{I}/\mathbf{I})$

Type 1 consists of the reducible groups (those that fix a decomposition $\mathbb{C}^2 = V_1 \oplus V_2$), types 2-4 of the irreducible imprimitive groups (those that stabilize a decomposition $\mathbb{C}^2 = V_1 \oplus V_2$, see [ST]), and types 5-9 of the irreducible primitive groups.
We can now state which of the above groups are generated by two elements:

Theorem 2.2.3 *All finite subgroups of $U(2)$ can be generated by two elements, except for one exceptional family. More precisely:*

- *Any finite subgroup of $U(2)$ whose projection in $SO(3)$ is different from an "even" dihedral group $(2q, 2, 2)$ is a 2-generator subgroup.*
- *Among those groups which project to $(2q, 2, 2)$ (types 2, 3, and 4 in Du Val's classification), all are 2-generator subgroups but one exceptional family in type 2, namely $\langle 2q, 2, 2\rangle_m = (\mathbf{C}_{2m}/\mathbf{C}_{2m}; \mathbf{D}_{2q}/\mathbf{D}_{2q})$ with m even.*

Proof. We use the projection $\tilde{\pi}$ introduced above, which gives us the short exact sequence:

$$1 \longrightarrow U(1) \longrightarrow U(2) \xrightarrow{\tilde{\pi}} SO(3) \longrightarrow 1$$

or for a finite subgroup Γ of $U(2)$:

$$1 \longrightarrow Z(\Gamma) \longrightarrow \Gamma \xrightarrow{\tilde{\pi}} G \longrightarrow 1$$

Now the finite subgroups G of $SO(3)$ are well known: they are either cyclic or triangular of type $(p,2,2)$, $(3,3,2)$, $(4,3,2)$ or $(5,3,2)$, all generated by two rotations. The main result is the following:

Lemma 2.2.1 *If G is generated by g_1 and g_2 such that $g_1^{r_1} = g_2^{r_2} = 1$ with r_1 and r_2 relatively prime, then Γ is generated by two elements.*

Indeed, choose at first γ_1 and γ_2 to be arbitrary preimages of g_1 and g_2 under $\tilde{\pi}$. Since $g_1^{r_1} = g_2^{r_2} = 1$, there exist $l_1, l_2 \in \mathbb{Z}$ such that $\gamma_1^{r_1} = z^{l_1}$ and $\gamma_2^{r_2} = z^{l_2}$, where z is a generator of the cyclic center $Z(\Gamma)$.
Now, for different preimages $\gamma_1' = z^{a_1}.\gamma_1$ and $\gamma_2' = z^{a_2}.\gamma_2$, we write:

$$(z^{a_1}.\gamma_1)^{r_1}.(z^{a_2}.\gamma_2)^{r_2} = z^{a_1 r_1 + a_2 r_2 + l_1 + l_2}$$

Then, r_1 and r_2 being relatively prime, there exist $a_1, a_2 \in \mathbb{Z}$ such that $a_1 r_1 + a_2 r_2 = 1 - l_1 - l_2$; for such a choice of a_1 and a_2, we have $z = (\gamma_1')^{r_1}.(\gamma_2')^{r_2}$ so that the group generated by γ_1' and γ_2', containing z and projecting to G, is the entire Γ. This proves the lemma, and settles all cases but that where G is the even dihedral group $(2q,2,2)$, which we now examine separately. We start by giving generating triples for the 3 types in question (we write elements of $SU(2)$ as unitary quaternions, the quaternion q corresponding to right multiplication by q in $\mathbb{C}^2$):

Lemma 2.2.2

- $\langle 2q,2,2\rangle_m = (\mathbf{C}_{2m}/\mathbf{C}_{2m}; \mathbf{D}_{2q}/\mathbf{D}_{2q})$ *(type 2) is generated by* $a = (e^{i\pi/m}, 1)$, $b = (1, e^{i\pi/2q})$ *and* $c = (1, j)$.
- $(\mathbf{C}_{4m}/\mathbf{C}_{2m}; \mathbf{D}_{2q}/\mathbf{C}_{4q})$ *(type 3) is generated by* $a = (e^{i\pi/m}, 1)$, $b = (1, e^{i\pi/2q})$ *and* $c = (e^{i\pi/2m}, j)$.
- $(\mathbf{C}_{4m}/\mathbf{C}_{2m}; \mathbf{D}_{2q}/\mathbf{D}_{q})$ *(type 4) is generated by* $a = (e^{i\pi/m}, 1)$, $b = (e^{i\pi/2m}, e^{i\pi/2q})$ *and* $c = (1, j)$.

The lemma is easily proven: the first type is obvious, and in the two other cases the subgroups L_K, R_K are of index 2 in L, R. We then notice that in type 3 a and b generate the direct product $L_K \times R_K$ so that we only need to add any element of $\Gamma \setminus L_K \times R_K$ such as c to obtain Γ. The last case is analogous except that $L_K \times R_K$ is generated by a, c and $b^2 a^{-1}$.
Now in most cases these generating triples can be reduced to 2 elements:

Lemma 2.2.3

- $\langle 2q,2,2\rangle_m = (\mathbf{C}_{2m}/\mathbf{C}_{2m}; \mathbf{D}_{2q}/\mathbf{D}_{2q})$ *(type 2) is generated by* ac *and* b *<u>when m is odd</u>.*
- $(\mathbf{C}_{4m}/\mathbf{C}_{2m}; \mathbf{D}_{2q}/\mathbf{C}_{4q})$ *(type 3) is generated by* b *and* c.

- $(\mathbf{C}_{4m}/\mathbf{C}_{2m};\mathbf{D}_{2q}/\mathbf{D}_q)$ *(type 4) is generated by* ac *and* b.

We simply show that the previous 3 generators can be written in terms of the new pair.
In the first case, we write: $(ac)^m = a^m c^m = c^{m+2}$ so that when m is odd, this is c or c^{-1} (c has order 4).
In the second case, we compute: $c^{2m+2} = (e^{i(\pi+\pi/m)}, (-1)^{m+1})$ which is equal to a if m is even or $a.(-1,1) = ab^{2q}$ if m is odd.
In the third case, we compute:

$$b.(ac)^{-1}.b.ac = (e^{i\pi/m}, e^{i\pi/2q}.(-j).e^{i\pi/2q}.j) = (e^{i\pi/m}, 1) = a$$

The only case that remains is the family $\langle 2q,2,2\rangle_m = (\mathbf{C}_{2m}/\mathbf{C}_{2m};\mathbf{D}_{2q}/\mathbf{D}_{2q})$ with m even, which behaves differently:

Lemma 2.2.4 *None of the groups* $\langle 2q,2,2\rangle_m = (\mathbf{C}_{2m}/\mathbf{C}_{2m};\mathbf{D}_{2q}/\mathbf{D}_{2q})$ *with* m *even can be generated by two elements.*

We prove this first for the smallest group $\langle 2,2,2\rangle_2 = (\mathbf{C}_4/\mathbf{C}_4;\mathbf{D}_2/\mathbf{D}_2)$, then extend the result to the other groups in the family by showing that they all project onto this group.
We have seen in a straightforward manner that the group $\langle 2,2,2\rangle_2$ (of order 16, whose elements are in $\{\pm 1,\pm i\}\times\{\pm 1,\pm i,\pm j,\pm k\}$ modulo $(-1,-1)$) cannot be generated by a pair of its elements, by testing different pairs (in fact, this group has many symmetries and the only relevant candidates are of the type $(1,i),(i,j)$ or $(i,i),(i,j)$, which both generate a subgroup of order 8).
We then define, for m even, an application $s : \langle 2q,2,2\rangle_m \longrightarrow \langle 2,2,2\rangle_2$ by sending $a = (e^{i\pi/m},1)$ to $a^{m/2} = (i,1)$, $b = (1,e^{i\pi/2q})$ to $b^q = (1,i)$ and $c = (1,j)$ to itself. In fact this only defines an application $\tilde{s}$ from the free group over $\{a,b,c\}$ to $\langle 2,2,2\rangle_2$; that s is well-defined and is a morphism comes from the fact that we know a presentation of $\langle 2q,2,2\rangle_m$ in terms of the generators a,b,c and that $\tilde{s}$ is compatible with all the relations involved. These are (with redundancy):

$$a^{2m} = b^{4q} = c^4 = 1$$

$$a^m = b^{2q} = c^2 \text{ (the central (1,-1))}$$

$$cbc^{-1} = b^{-1} \text{ and } [a,b] = [a,c] = 1$$

The relations are easy to write in this case because a,b,c are of the form $(1,r)$ or $(l,1)$. This concludes the proof of the lemma and the theorem, for if $\langle 2q,2,2\rangle_m$ were generated by two elements g_1 and g_2, then $\langle 2,2,2\rangle_2$ would be generated by $s(g_1)$ and $s(g_2)$.
We finish by making the remark that our proof relies on Du Val's classification, which is slightly incomplete as pointed out in [C] and [CS]. However the missing groups do not interfere with our result, because Coxeter's type 3' (p. 98) projects to $(p,2,2)$ with p odd, whereas Conway and Smith add subgroups in $SO(4)\setminus U(2)$. □

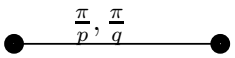

2.3 Lagrangian pairs

2.3.1 Groups generated by two $\mathbb{R}$-reflections

In order to classify finite groups generated by two $\mathbb{R}$-reflections we observe first that the angle between the two Lagrangians should be of the form

$$(\frac{\pi q_1}{p_1}, \cdots, \frac{\pi q_n}{p_n})$$

where $\frac{q_i}{p_i}$ are reduced fractions satisfying $1 > \frac{q_1}{p_1} \geq \cdots \frac{q_n}{p_n} \geq 0$. If $n = 1$ it is clear that we can find generators with angle of the form $\frac{\pi}{p}$. The normal form for the angle between two generators in higher dimensions is essentially given by the chinese remainder theorem.

Suppose the Lagrangians L_1 and L_2 form an angle $(\frac{\pi q_1}{p_1}, \cdots, \frac{\pi q_n}{p_n})$. We define the following map

$$(L_1, L_2) \mapsto \frac{\pi q_1}{p_1} + \cdots + \frac{\pi q_n}{p_n} \in [0, n\pi[$$

Different generators are obtained by taking a power of g_{12}^2; computing its eigenvalues we obtain

$$g_{12}^{2k} \mapsto [\frac{\pi k q_1}{p_1}] + \cdots + [\frac{\pi k q_n}{p_n}] \in [0, n\pi[$$

where $[\frac{\pi k q_1}{p_1}]$ is the representative of $\frac{\pi k q_1}{p_1} \mod \pi\mathbb{Z}$ in $[0, \pi[$.

We choose k to be one with minimal image under the above map. Clearly, if the p_i are pairwise prime the chinese remainder theorem implies that the minimal choice (unique in that case) is a generator and is given precisely by $(\frac{2\pi}{p_1}, \cdots, \frac{2\pi}{p_n})$.

In dimension 2 we can list all possibilities:

1. $\theta_1 = 2\pi/p_1$ and $\theta_2 = 2\pi/p_2$, with $(p_1, p_2) = 1$.

2. $\theta_1 = 2\pi/p_1$ and $\theta_2 = 2\pi q_2/p_2$, with $(p_1, p_2) = d \neq 1$ and $(q_2, p_2) = 1$.

This follows from the chinese remainder theorem, that is, the congruence $x \equiv a_i \ (p_i)$ (with $(p_1, p_2) = d$) has a solution if and only if $a_1 \equiv a_2 \ (d)$. Having obtained $\theta_1 = 2\pi/p_1$ by some power of the generator we ask whether another power by x satisfies $x \equiv 1 \ (p_1)$ and $xq_2 \equiv a_2 \ (p_2)$. This has a solution if and only if $q_2 \equiv a_2 \ (d)$. So one can suppose $q_2 < d$.

Given r $\mathbb{R}$-reflections, it is convenient to construct a diagram with r nodes corresponding to the generators σ_i and edges joining each pair of nodes labeled by $m(i, j)$. Here $m(i, j)$ is the angle between the given Lagrangians. For example, in the two dimensional case if two Lagrangians L_1 and L_2 have an angle $(\frac{\pi}{p}, \frac{\pi}{q})$ we can represent them by the following diagram:

2.3.2 Representations of an $\mathbb{R}$-reflection by matrices

We use throughout this section the canonical basis of $\mathbb{C}^n$. Recall that we have in $\mathbb{C}^n$ a standard $\mathbb{R}^n$-plane L_0:

$$L_0 = \{(x_1, ..., x_n) \in \mathbb{C}^n | x_i \in \mathbb{R}\}$$

whose $\mathbb{R}$-reflection is in coordinates:

$$\sigma_0 : (z_1, ..., z_n) \longmapsto (\overline{z_1}, ..., \overline{z_n})$$

This allows us to define for a single $\mathbb{R}^n$-plane L_i the invariants of a pair by considering the pair (L_0, L_i). We thus call *standard direct image matrix* for L_i any $U_i \in U(n)$ such that: $L_i = U_i L_0$ (the element U_i is defined up to the stabilizer of L_0 which is $O(2)$); we define the *Souriau map* of L_i which is the unitary map $\phi_i = \sigma_i \circ \sigma_0$ as well as the *Souriau matrix* A_i of L_i, the matrix of ϕ_i **in the canonical basis**. We will often characterize an $\mathbb{R}^n$-plane L_i by its Souriau matrix A_i, because as we will now see these matrices behave nicely under composition.

Indeed, rewrite the relation defining the Souriau map $\phi_i = \sigma_i \circ \sigma_0$ as: $\sigma_i = \phi_i \circ \sigma_0$. This is written in coordinates $z = (z_1, ..., z_n)$: $\sigma_i(z) = A_i \overline{z}$. Concretely, this allows us on one hand to obtain a parametrization of the $\mathbb{R}^n$-plane L_i as the set of solutions of the system $A_i \overline{z} = z$ (solved for instance by diagonalization in a real basis), and on the other hand to compose $\mathbb{R}$-reflections in matrix form. Indeed, if L_1 and L_2 are two $\mathbb{R}^n$-planes, we write in coordinates:

$$\sigma_2 \circ \sigma_1(z) = \sigma_2(A_1.\overline{z}) = A_2.(\overline{A_1.\overline{z}}) = A_2.\overline{A_1}.z$$

Thus the Souriau matrix of the pair (L_1, L_2) is $A_2.\overline{A_1}$; we will often use this for the decomposition of unitary (or complex hyperbolic) groups into $\mathbb{R}$-reflections. This also shows, $\mathbb{R}$-reflections being involutory, that every Souriau matrix A_i of a single $\mathbb{R}^n$-plane L_i (that is a Souriau matrix of the pair (L_0, L_i)) verifies the condition $A_i.\overline{A_i} = Id$.

Finally, it will be useful for our purposes to obtain the Souriau matrix A_i from a standard direct image matrix U_i. The relation we use is simply: $A_i = U_i.\overline{U_i^{-1}} = U_i.U_i^T$, which expresses the fact that σ_i and σ_0 are conjugated by U_i.

2.4 An example: the group $3[3]3$

The group in which we are now interested, denoted 3[3]3 by Coxeter and $(\mathbf{C}_6/\mathbf{C}_2; \mathbf{T}/\mathbf{V})$ by Du Val (type 6 in his classification), is a finite subgroup Γ of $U(2)$, of order 24, generated by two $\mathbb{C}$-reflections R_1 and R_2 in terms of which it has the presentation:

$$\Gamma = < R_1, R_2 \mid R_1^3 = R_2^3 = 1, R_1 R_2 R_1 = R_2 R_1 R_2 >$$

This group appears in Mostow as the finite subgroup fixing a point in $\mathbb{C}H^2$. We will use (especially in the determination of a fundamental domain) the fact that $Z(\Gamma)$ is cyclic of order 2, generated by $(R_1 R_2)^3$.

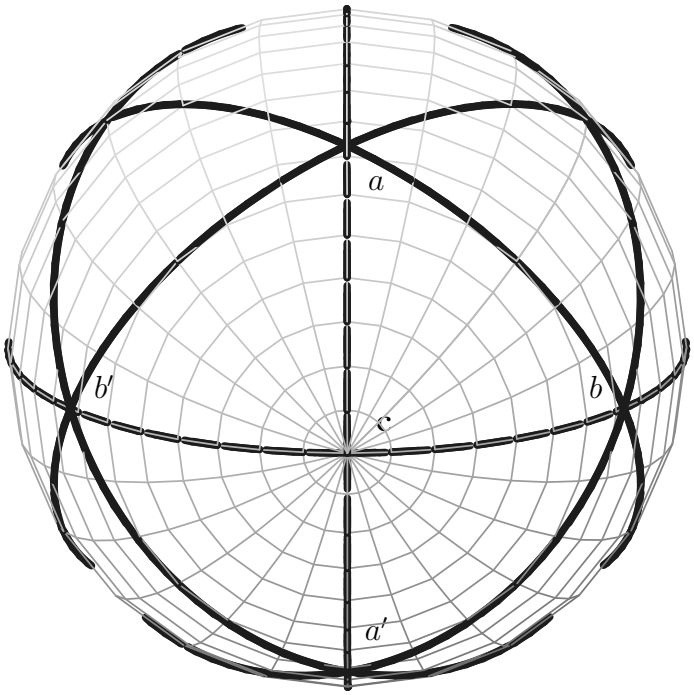

Figure 2.1: Projected Lagrangians for the group 3[3]3

2.4.1 Action on $\mathbb{C}P^1$

As we will now see, the generators R_1 and R_2 project onto two rotations $r_1, r_2 \in SO(3)$ with angles $-\frac{2\pi}{3}$ about the vertices b and b' of a spherical triangle abb' having angles $\frac{\pi}{3}$ at b and b', and $\frac{2\pi}{3}$ at the remaining vertex a (see figure 2.1). Thus, in Coxeter's notations:

$$\tilde{\pi}(3[3]3) = (3, 3, 2)$$

the latter being the group of orientation-preserving isometries of the tetrahedron (the corresponding reflection group is generated by reflections in the sides of a spherical triangle with angles $(\frac{\pi}{3}, \frac{\pi}{3}, \frac{\pi}{2})$).

The three vertices b, b' and a are projections in $\mathbb{C}P^1$ of eigenspaces of the matrices R_1, R_2, and R_2R_1 respectively. Our generators, slightly different from Coxeter's (his are above a and a' whereas ours are above b and b'), are explicitly:

$$R_1 = \frac{e^{\frac{i\pi}{3}}}{2} \begin{pmatrix} 1+i & 1+i \\ i-1 & 1-i \end{pmatrix}$$

$$R_2 = \frac{e^{\frac{i\pi}{3}}}{2} \begin{pmatrix} 1+i & -1-i \\ 1-i & 1-i \end{pmatrix}$$

The eigenvectors we have chosen, and whose images in $\mathbb{C}P^1$ are drawn in figure 2.1, are:

$$B^+ = \begin{bmatrix} \frac{1}{2}(1+\sqrt{3})(1-i) \\ 1 \end{bmatrix}$$

$$B'^+ = \begin{bmatrix} \frac{1}{2}(1+\sqrt{3})(i-1) \\ 1 \end{bmatrix}$$

$$A^+ = \begin{bmatrix} \frac{1}{2}(1+\sqrt{3})(1+i) \\ 1 \end{bmatrix}$$

2.4.2 $\mathbb{R}$-reflections

We will now determine two triples of $\mathbb{R}$-planes which decompose the group $3[3]3$: the former corresponds to writing each of the generators R_1 and R_2 as a product of $\mathbb{R}$-reflections, whereas for the latter we use the generators R_1 and R_1R_2. Explicitly, we will find $\mathbb{R}$-planes L_1, L_2, L_3, and L_4 such that:

$$\sigma_2 \circ \sigma_1 = R_1 \ , \ \sigma_1 \circ \sigma_3 = R_2$$

$$\sigma_2 \circ \sigma_1 = R_1 \ , \ \sigma_4 \circ \sigma_2 = R_1R_2$$

The second triple of $\mathbb{R}$-planes is more canonical geometrically in the sense that it projects onto the Möbius triangle abc (type (233)) instead of the Schwarz triangle abb' (type $(3\frac{3}{2}3)$), thus possessing a kind of minimality property (among the triangles in $\mathbb{C}P^1$ bounded by the projective lagrangians which are great circles).

The idea for the explicit determination of these $\mathbb{R}$-planes is very simple: their images in $\mathbb{C}P^1$ are given, we have a free S^1-parameter in the choice of the first $\mathbb{R}$-plane, the others being completely determined by the pairwise products.

We begin with L_1, above the great circle (bb'). We need only notice that with our choice of vectors B^+ and B'^+, the hermitian product $\langle B^+, B'^+ \rangle$ is real; thus $L_1 := Span_{\mathbb{R}}(B^+, B'^+)$ is an $\mathbb{R}$-plane projecting to (bb'). We will however also need the unitary matrices associated as earlier with this $\mathbb{R}$-plane, which requires a bit more calculation. Recall that we have a standard $\mathbb{R}$-plane $L_0 = \{(x,y) \in \mathbb{C}^2 | x, y \in \mathbb{R}\}$ with associated $\mathbb{R}$-reflection $\sigma_0 : (z_1, z_2) \mapsto (\overline{z_1}, \overline{z_2})$. The two (families of) unitary matrices U_1 and A_1 associated with L_1 (and its $\mathbb{R}$-reflection σ_1) are such that:

$$L_1 = U_1.L_0$$

$$\sigma_1 = A_1 \circ \sigma_0$$

As we have seen, the matrix U_1 is simply obtained by the choice of an orthonormal basis for L_1. Since we already have the basis (B^+, B'^+), we only need to orthonormalize it, for instance by a Gram-Schmidt procedure. We thus obtain:

$$U_1 = \begin{pmatrix} \frac{(1+\sqrt{3})(1-i)}{2(3+\sqrt{3})^{1/2}} & \frac{(1+\sqrt{3})(i-1)}{2(9+5\sqrt{3})^{1/2}} \\ (3+\sqrt{3})^{-1/2} & \frac{2+\sqrt{3}}{(9+5\sqrt{3})^{1/2}} \end{pmatrix}$$

We then obtain an admissible A_1 as $U_1.U_1^T$, which gives us here:

$$A_1 = \begin{pmatrix} -i & 0 \\ 0 & 1 \end{pmatrix}$$

This latter matrix is surprisingly simpler than U_1, which means that our choice of an orthonormal basis for L_1 was not very good; however we obtain the following nice parametrization:

$$L_1 = \{(e^{-\frac{i\pi}{4}}.x, y) \in \mathbb{C}^2 | x, y \in \mathbb{R}\}$$

We now proceed to find L_2 such that $\sigma_2 \circ \sigma_1 = R_1$. Rewriting this as $\sigma_2 = R_1 \circ \sigma_1$ (and applying this to coordinate-vector z as $A_2.\overline{z} = R_1.(A_1.\overline{z})$), we see that we can choose $A_2 = R_1.A_1$. Explicitly:

$$A_2 = \frac{e^{\frac{i\pi}{3}}}{2} \begin{pmatrix} 1-i & 1+i \\ 1+i & 1-i \end{pmatrix}$$

We will then obtain L_2 as the set of solutions in $\mathbb{C}^2$ of $A_2.\overline{z} = z$. This can be done by diagonalizing A_2 in a real basis. We compute the eigenvalues of A_2 which are $e^{\frac{i\pi}{3}}$ and $e^{-\frac{i\pi}{6}}$, with corresponding eigenvectors:

$$V_2^{\pm} = \begin{bmatrix} \pm 1 \\ 1 \end{bmatrix}$$

We thus obtain the parametrization:

$$L_2 = \{x.e^{\frac{i\pi}{6}}.V_2^+ + y.e^{-\frac{i\pi}{12}}.V_2^- | x, y \in \mathbb{R}\}$$

We find in the same way L_3 such that $\sigma_1 \circ \sigma_3 = R_2$. We rewrite this as $\sigma_3 = \sigma_1 \circ R_2$ and see that we can choose $A_3 = A_1.\overline{R_2}$. Explicitly:

$$A_3 = \frac{e^{-\frac{i\pi}{3}}}{2} \begin{pmatrix} -1-i & 1+i \\ 1+i & 1+i \end{pmatrix}$$

We then obtain L_3 as the set of solutions in $\mathbb{C}^2$ of $A_3.\overline{z} = z$, by diagonalizing as above A_3 in a real basis. The eigenvalues of A_3 are $e^{-\frac{i\pi}{12}}$ and $e^{\frac{5i\pi}{12}}$, with corresponding eigenvectors:

$$V_3^{\pm} = \begin{bmatrix} -1 \pm \sqrt{2} \\ 1 \end{bmatrix}$$

We obtain the parametrization:

$$L_3 = \{x.e^{-\frac{i\pi}{24}}.V_3^+ + y.e^{\frac{5i\pi}{24}}.V_3^- | x, y \in \mathbb{R}\}$$

The last $\mathbb{R}$-plane L_4 is obtained in the same way, asking that:
$\sigma_4 \circ \sigma_1 = R_1 R_2 R_1$, which gives us $A_4 = R_1.R_2.R_1.A_1$. Explicitly:

$$A_4 = \begin{pmatrix} -1 & 0 \\ 0 & i \end{pmatrix}$$

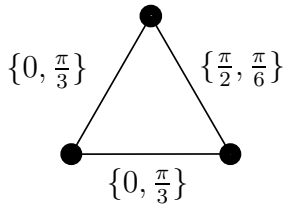

We then obtain L_4 as the set of solutions in $\mathbb{C}^2$ of $A_4.\overline{z} = z$, in the easy case where A_4 is diagonal. This gives us the following parametrization :

$$L_4 = \{(i.x, e^{\frac{i\pi}{4}}.y) \in \mathbb{C}^2 | x, y \in \mathbb{R}\}$$

2.4.3 Presentations and diagrams

Recall the above presentation for the unitary group 3[3]3:

$$\Gamma = \langle R_1, R_2 \mid R_1^3 = R_2^3 = 1, R_1R_2R_1 = R_2R_1R_2 \rangle$$

Two presentations for $\widehat{\Gamma}$, the index 2 supergroup of Γ generated by three $\mathbb{R}$-reflections, given by the two systems of generators above, are easily derived (we simply rewrite the relations in terms of the $\mathbb{R}$-reflections, and add that these are of order 2). We obtain explicitly in the first case:

$$\widehat{\Gamma} = \langle \sigma_1, \sigma_2, \sigma_3 \mid \sigma_i^2 = (\sigma_1\sigma_2)^3 = (\sigma_1\sigma_3)^3 = 1, \sigma_1.\sigma_2\sigma_3\sigma_2.\sigma_1 = \sigma_3\sigma_2\sigma_3 \rangle$$

which implies that $\sigma_2\sigma_3$ has order 6, and in the second case :

$$\widehat{\Gamma} = \langle \sigma_1, \sigma_2, \sigma_4 \mid \sigma_i^2 = (\sigma_1\sigma_2)^3 = (\sigma_1\sigma_2\sigma_4\sigma_2)^3 = 1, \sigma_1\sigma_4\sigma_1 = \sigma_2.\sigma_4\sigma_2\sigma_4.\sigma_2 \rangle$$

which implies as above that $\sigma_2\sigma_4$ has order 6.

We now write down for each of the Lagrangian triples the Coxeter-style diagrams we have introduced earlier, which contain the information characterizing each of the three intersecting pairs, that is a pair of angles (written on the edge joining the generators). Recall that these pairs are characterized by the product of the two $\mathbb{R}$-reflections, in our case:

$$\sigma_2 \circ \sigma_1 = R_1 \ , \ \sigma_1 \circ \sigma_3 = R_2$$

$$\sigma_2 \circ \sigma_1 = R_1 \ , \ \sigma_4 \circ \sigma_2 = R_1R_2$$

Computing the eigenvalues of the four corresponding matrices, we find the following diagrams for our two Lagrangian triples:

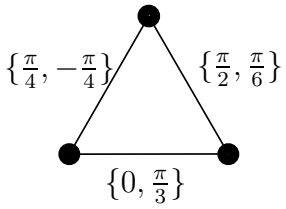

2.4.4 Fundamental domains

We now determine fundamental domains for the action of $\widehat{\Gamma}$ (and thus Γ) on $\mathbb{C}^2$, or rather on its unit ball $B^2_{\mathbb{C}}$ (in the perspective of complex hyperbolic geometry). We use the action of these groups on $\mathbb{C}P^1$ to determine these fundamental domains as (parts of) circle bundles over spherical triangles ; we thus obtain domains essentially different from Mostow's construction, the faces of our "polyhedra" not being bisectors.

Our groups Γ and $\widehat{\Gamma}$ are (finite) subgroups of $U(2)$ (resp. $\widehat{U(2)}$), so they fix the origin in $\mathbb{C}^2$ and we can choose a fundamental domain D^4 for their action on $B^2_{\mathbb{C}}$ as a cone (in half $\mathbb{R}$-lines) over a fundamental domain D^3 for their action on $\partial B^2_{\mathbb{C}} = S^3$, which we like to look at as the Heisenberg group H^3 for the same reason as above. We then determine D^3 using the Hopf fibration $H : S^3 \longrightarrow \mathbb{C}P^1$ induced by complex projectivisation; the actions of $\widehat{\Gamma}$ and Γ on S^3 and $\mathbb{C}P^1$ being equivariant with respect to H, a domain D^3 is obtained as a part of the Hopf bundle over a spherical triangle D^2, a fundamental domain in $\mathbb{C}P^1$: $D^3 \subset H^{-1}(D^2)$. We have seen that $\widehat{\Gamma}$ acts on $\mathbb{C}P^1$ as the reflection group of type (3,3,2) (with for instance the Möbius triangle abc for D^2), and that its index 2 subgroup Γ acts on $\mathbb{C}P^1$ as the rotation group of type (3,3,2) (with for instance the Schwarz triangle abb' for D^2).

It now remains to see exactly which part of this triangular prism we want to keep. Each fiber is a $\mathbb{C}$-circle (the intersection of a complex line with $\partial B^2_{\mathbb{C}}$), and the fiberwise action which remains is the one which was invisible in $\mathbb{C}P^1$, that is the action of the kernel of $\tilde{\pi} : \Gamma \longrightarrow SO(3)$, which is none other than the order 2 center $Z(\Gamma)$, acting on each fiber by a half-turn. The domain D^3 will thus be a union of half-circles obtained by cutting in half the triangular prism $H^{-1}(D^2)$, forming a sort of polyhedron with five faces (compare with the ten bisector faces obtained by Mostow). Three of these faces are (contained in something) canonical, that is the union of $\mathbb{C}$-circles above the boundary of the spherical triangle. It remains to choose how to perform the cutting to obtain the two remaining faces in a reasonable fashion (the least we can ask is that they be smooth). The best would be to use surfaces that are geometrically natural in $\partial B^2_{\mathbb{C}}$, such as bisectors [Go], however in the perspective of assembling different copies of these domains it can be useful to bear in mind the flexibility that we have in the choice of these faces.

2.5 Other two-generator subgroups of $U(2)$

The method used here relies on the fact that the unitary group which we want to decompose admits a system of two generators, and in that case is a straightforward generalization of the

example of 3[3]3. We will describe this method in a general manner, but will apply it explicitly only in two cases where the pairs of generators are given by Coxeter (in quaternionic form) namely:

- the binary polyhedral groups (that is all non-cyclic finite subgroups of $SU(2)$, [C] pp. 74-78)
- the finite groups generated by two $\mathbb{C}$-reflections ([C] pp. 98-102 and table p. 176)

These groups seem sufficiently representative, as they cover all but type 4 (and type 1 which has cyclic action on $\mathbb{C}P^1$) of Du Val's 9 types.

2.5.1 The strategy

We start off with a finite subgroup Γ of $U(2)$ with two explicit generators G_1 and G_2, and proceed to find three $\mathbb{R}$-reflections σ_i, σ_j, and σ_k such that $\widehat{\Gamma} = \langle \sigma_i, \sigma_j, \sigma_k \rangle$ contains Γ with index two.

Action on $\mathbb{C}P^1$

We begin by calculating the eigenvectors of G_1 and G_2, which give us the two (pairs of antipodal) fixed points in $\mathbb{C}P^1$; these and the eigenvalues tell us the type of action on $\mathbb{C}P^1$ (that is dihedral, tetrahedral, octahedral, or icosahedral). We only need to do this once for each type, for instance only for the binary polyhedral groups $\langle p, 2, 2 \rangle$, $\langle 3, 3, 2 \rangle$, $\langle 4, 3, 2 \rangle$ and $\langle 5, 3, 2 \rangle$.

$\mathbb{R}$-reflections

Given the two (pairs of antipodal) fixed points, we know from Prop. 5 that any $\mathbb{R}$-plane which decomposes simultaneously G_1 and G_2 projects to the only great circle in $\mathbb{C}P^1$ containing these points. Such an $\mathbb{R}$-plane is thus determined up to multiplication by $U(1)$, and the two remaining $\mathbb{R}$-planes are uniquely determined by this choice.

Fundamental domains

We have thus obtained three $\mathbb{R}$-planes whose projections to $\mathbb{C}P^1$ comprise a triangle which is part of a triangular tessellation of the sphere. Now this triangle is either an elementary triangle of this tessellation (if it is a Möbius triangle, i.e. with angles $(\frac{\pi}{p}, \frac{\pi}{q}, \frac{\pi}{r})$ with $p, q, r \in \mathbb{N}$), or a union of two or more of such triangles (it is then a Schwarz triangle, with angles $(\frac{\pi}{p}, \frac{\pi}{q}, \frac{\pi}{r})$ where one of p, q, r is in $\mathbb{Q} \setminus \mathbb{N}$). This can be seen graphically for instance. If the triangle is of Möbius type, it is a fundamental domain D^2 for the action of $\widehat{\Gamma}$ on $\mathbb{C}P^1$ (and two adjacent copies form a fundamental domain for the action of Γ on $\mathbb{C}P^1$). If not, we change a well-chosen reflection by conjugation, as in the example of 3[3]3, to obtain a Möbius triangle (or "minimal" triple of $\mathbb{R}$-planes).

We then proceed exactly as in the example, constructing the triangular prism $H^{-1}(D^2)$ in S^3 and cutting it into $|Z(\Gamma)|$ "slices" according to the cyclic action of $Z(\Gamma)$ on each fiber ($\mathbb{C}$-circle); any of these slices is then a fundamental domain D^3 for the action of Γ (resp. $\widehat{\Gamma}$) on S^3. The final fundamental domain D^4 in $\mathbb{C}^2$ (or in the unit ball of $\mathbb{C}^2$) is then simply a cone (in half-$\mathbb{R}$-lines) over D^3 based at the origin.

We have thus obtained D^4 as a 5-sided polyhedral cone over D^3, whose 5 faces are as follows:

- three "vertical" faces are parts of canonical objects, the union of $\mathbb{C}$-circles over a geodesic segment in $\mathbb{C}P^1$. Such an object is foliated both by $\mathbb{C}$-circles and $\mathbb{R}$-circles, and is part of a "Clifford torus", see [G]. These faces are four-sided.
- two "horizontal" faces (bisectors, see [Go], are possible choices or other surfaces, see [S]). These are three-sided.

2.5.2 Explicit decomposition of reflection groups

We now find triples of $\mathbb{R}$-planes for the finite subgroups of $SU(2)$ and the two-generator reflection groups in $U(2)$; we proceed according to type of action on $\mathbb{C}P^1$. The results are summarized in the following tables, where we use the digit notation for words in the $\mathbb{R}$-reflections σ_i; for instance "1321" denotes the unitary elment $\sigma_1 \circ \sigma_3 \circ \sigma_2 \circ \sigma_1$. For the $\mathbb{R}$-plane L_7, τ denotes the golden ratio $\frac{1+\sqrt{5}}{2}$.

The details for all these groups can be found in the appendix; for the sake of clarity and completeness, we will write the details for the exceptional family stated on the last line of table 2, and for this we need the decomposition of the binary dihedral group $\langle p, 2, 2\rangle$ given in the first line of the same table.

For this group $\langle p, 2, 2\rangle$, Coxeter gives the two quaternion generators $e^{i\pi/p}$ and j, corresponding to the following matrices in $SU(2)$:

$$G_1 = \begin{pmatrix} e^{i\pi/p} & 0 \\ 0 & e^{-i\pi/p} \end{pmatrix}$$

$$G_2 = \begin{pmatrix} 0 & -1 \\ 1 & 0 \end{pmatrix}$$

We apply the method described earlier to simultaneously decompose these two generators: the fixed points in $\mathbb{C}P^1$ of these elements (the projection of their eigenvectors) are, in the notation of the figure on page 13, c and $A^{-1}(c)$; the great circle containing these points is $l_{101} = \sigma_1(l_0)$, so that an $\mathbb{R}$-plane decomposing simultaneously G_1 and G_2 can only be some multiple of $L_{101} = \sigma_1(L_0)$. We thus need the Souriau matrix A_{101} of $\mathbb{R}$-reflection $\sigma_1\sigma_0\sigma_1$ (denoted 101), which is simply:

$$A_{101} = A_1\overline{A_0}A_1 = \begin{pmatrix} -1 & 0 \\ 0 & 1 \end{pmatrix}$$

$\mathbb{R}$-plane	Souriau matrix	Orthogonal basis for the $\mathbb{R}$-plane
L_0	$A_0 = \begin{pmatrix} 1 & 0 \\ 0 & 1 \end{pmatrix}$	$\begin{bmatrix} 1 \\ 0 \end{bmatrix}, \begin{bmatrix} 0 \\ 1 \end{bmatrix}$
L_1	$A_1 = \begin{pmatrix} -i & 0 \\ 0 & 1 \end{pmatrix}$	$e^{-\frac{i\pi}{4}}.\begin{bmatrix} 1 \\ 0 \end{bmatrix}, \begin{bmatrix} 0 \\ 1 \end{bmatrix}$
L_2	$A_2 = \frac{e^{\frac{i\pi}{3}}}{2}\begin{pmatrix} 1-i & 1+i \\ 1+i & 1-i \end{pmatrix}$	$e^{\frac{i\pi}{6}}.\begin{bmatrix} 1 \\ 1 \end{bmatrix}, e^{-\frac{i\pi}{12}}.\begin{bmatrix} -1 \\ 1 \end{bmatrix}$
L_3	$A_3 = \frac{e^{-\frac{i\pi}{3}}}{2}\begin{pmatrix} -1-i & 1+i \\ 1+i & 1+i \end{pmatrix}$	$e^{-\frac{i\pi}{24}}.\begin{bmatrix} -1+\sqrt{2} \\ 1 \end{bmatrix}, e^{\frac{5i\pi}{24}}.\begin{bmatrix} -1-\sqrt{2} \\ 1 \end{bmatrix}$
L_4	$A_4 = \begin{pmatrix} -1 & 0 \\ 0 & i \end{pmatrix}$	$i.\begin{bmatrix} 1 \\ 0 \end{bmatrix}, e^{\frac{i\pi}{4}}.\begin{bmatrix} 0 \\ 1 \end{bmatrix}$
L_5	$A_5 = e^{-\frac{i\pi}{12}}.\begin{pmatrix} 1 & 0 \\ 0 & 1 \end{pmatrix}$	$e^{-\frac{i\pi}{24}}.\begin{bmatrix} 1 \\ 0 \end{bmatrix}, e^{-\frac{i\pi}{24}}.\begin{bmatrix} 0 \\ 1 \end{bmatrix}$
L_6	$A_6 = \begin{pmatrix} 0 & i \\ i & 0 \end{pmatrix}$	$e^{\frac{i\pi}{4}}.\begin{bmatrix} 1 \\ 1 \end{bmatrix}, e^{-\frac{i\pi}{4}}.\begin{bmatrix} -1 \\ 1 \end{bmatrix}$
L_7	$A_7 = \frac{1}{2}\begin{pmatrix} \tau+\frac{i}{\tau} & i \\ i & \tau-\frac{i}{\tau} \end{pmatrix}$	$e^{\frac{i\pi}{6}}.\begin{bmatrix} \tau-1+2\sin\frac{\pi}{5} \\ 1 \end{bmatrix}, e^{-\frac{i\pi}{6}}.\begin{bmatrix} \tau-1-2\sin\frac{\pi}{5} \\ 1 \end{bmatrix}$
$L_8(p)$	$A_8(p) = \begin{pmatrix} -e^{-\frac{i\pi}{p}} & 0 \\ 0 & e^{\frac{i\pi}{p}} \end{pmatrix}$	$-e^{-\frac{i\pi}{2p}}.\begin{bmatrix} 1 \\ 0 \end{bmatrix}, e^{\frac{i\pi}{2p}}.\begin{bmatrix} 0 \\ 1 \end{bmatrix}$
L_9	$A_9 = \begin{pmatrix} 0 & 1 \\ 1 & 0 \end{pmatrix}$	$\begin{bmatrix} 1 \\ 1 \end{bmatrix}, i.\begin{bmatrix} -1 \\ 1 \end{bmatrix}$

Figure 2.2: $\mathbb{R}$-planes for finite groups of $U(2)$

We thus have, for suitably chosen $\mathbb{R}$-planes L_8 and L_9:

$$\begin{cases} G_1 = 101.8 \\ G_2 = 101.9 \end{cases}$$

We sum this up in the last column of the table by the notation $(101; 8; 9)$. Now we almost have the decomposition of the exceptional family $\langle 2q, 2, 2\rangle_{2m'}$, because it is obtained from $\langle 2q, 2, 2\rangle$ by simply adding the generator $G_3 = e^{i\pi/2m'}.Id$, which we denoted earlier $a = (e^{i\pi/2m'}, 1)$. Since we have in an obvious manner: $G_3 = e^{i\pi/2m'}.\sigma_8.\sigma_8$ (for instance), we obtain as claimed a decomposition of the exceptional family with 4 $\mathbb{R}$-reflections $(101; 8; 9; e^{i\pi/2m'}.8)$.

Γ	Action on $\mathbb{C}P^1$	Du Val type	Order; order of center	Generators of $\widehat{\Gamma}$
$\mathbf{D}_p = \langle p, 2, 2\rangle$	D_p	2	$4p$; 2	$(101; 8; 9)$
$\mathbf{T} = \langle 3, 3, 2\rangle$	T	5	24; 2	$(1; e^{-i\pi/3}.2; -4)$
$\mathbf{O} = \langle 4, 3, 2\rangle$	O	7	48; 2	$(5; e^{-5i\pi/6}.4; i.121)$
$\mathbf{I} = \langle 5, 3, 2\rangle$	I	9	120; 2	$(0; 6; 7)$
$p[4]2$	D_p	3 or 4	$2p^2$; p	$(101; e^{-i\pi/p}.8; -i.9)$
$3[4]3 = \langle 3, 3, 2\rangle_3$	T	5	72; 6	$(121; e^{-i\pi/3}.131; 1)$
$3[3]3$	T	6	24; 2	$(1; 2; 3)$, $(1; 2; 4)$
$3[6]2$	T	6	48; 4	$(4; e^{2i\pi/3}.121; i.1)$
$4[6]2 = \langle 4, 3, 2\rangle_4$	O	7	192; 8	$(5; e^{-7i\pi/12}.4; 121)$
$4[3]4$	O	8	96; 4	$(5; e^{-7i\pi/12}.4; e^{i\pi/12}.12121)$
$3[8]2$	O	8	144; 6	$(121; e^{-2i\pi/3}.4; 5)$
$4[4]3$	O	8	288; 12	$(4; e^{7i\pi/12}.5; e^{2i\pi/3}.121)$
$3[5]3 = \langle 5, 3, 2\rangle_3$	I	9	360; 6	$(6; e^{-i\pi/3}.7; e^{2i\pi/3}.070)$
$5[3]5 = \langle 5, 3, 2\rangle_5$	I	9	600; 10	$(0; e^{i\pi/5}.7; e^{4i\pi/5}.676)$
$3[10]2 = \langle 5, 3, 2\rangle_6$	I	9	720; 12	$(6; e^{-i\pi/3}.7; -i.0)$
$5[6]2 = \langle 5, 3, 2\rangle_{10}$	I	9	1200; 20	$(0; e^{i\pi/5}.7; i.6)$
$5[4]3 = \langle 5, 3, 2\rangle_{15}$	I	9	1800; 30	$(7; e^{-i\pi/5}.0; e^{i\pi/3}.6)$
$\langle 2q, 2, 2\rangle_{2m'}$	D_{2q}	2	$32m'q$; $4m'$	$(101; 8; 9; e^{i\pi/2m'}.8)$

Figure 2.3: Finite groups and $\mathbb{R}$-reflections. We list the irreducible subgroups of $SU(2)$, then the complex reflection groups generated by two reflections and finally the imprimitive exceptional family which is a subgroup of index two of a group generated by four Lagrangian reflections.

Bibliography

[CS] J. H. Conway, D. A. Smith ; On Quaternions and Octonions. K. Peters. 2003.

[C] H. S. M. Coxeter ; Regular Complex Polytopes. Cambridge University Press (1991).

[D] P. Du Val ; Homographies, Quaternions and Rotations. Oxford Mathematical Monographs. Oxford (1964).

[F] E. Falbel ; *Finite groups generated by involutions on Lagrangian planes of* $\mathbb{C}^2$. Canad. Math. Bull. 44 (2001), no. 4, 408–419

[FMS] E. Falbel, J.-P. Marco, F. Schaffhauser ; *Classifying triples of Lagrangians in a Hermitian vector space*. To appear in Topology and its Applications.

[FZ] E. Falbel, V. Zocca ; *A Poincaré's polyhedron theorem for complex hyperbolic geometry*. J. Reine Angew. Math. 516 (1999), 138-158.

[G] W. Goldman ; Complex Hyperbolic Geometry. Oxford Mathematical Monographs. Oxford Science Publications (1999).

[M] G. D. Mostow ; *On a remarkable class of polyhedra in complex hyperbolic space*. Pacific J. Math. 86 (1980), 171-276.

[N] A. J. Nicas ; *Classifying pairs of Lagrangians in a hermitian vector space*. Topology and its Applications 42 (1991), 71-81.

[S] R. E. Schwartz; *Complex Hyperbolic Triangle Groups*. Proceedings of the International Congress of Mathematicians, Volume 1 (2002) 339-350.

[ST] G. C. Shephard, J. A. Todd ; *Finite unitary reflection groups*. Canadian Journal of Mathematics 6 (1954), 274-304.

2.6 Appendix: explicit decomposition of reflection groups

We now find triples of $\mathbb{R}$-planes for the finite subgroups of $SU(2)$ and the two-generator reflection groups in $U(2)$; we proceed according to type of action on $\mathbb{C}P^1$. The results are summarized in table 2.3. Throughout this section, we use the digit notation for words in the $\mathbb{R}$-reflections σ_i; for instance "1321" denotes the unitary elment $\sigma_1 \circ \sigma_3 \circ \sigma_2 \circ \sigma_1$.

Dihedral groups

We start with the binary dihedral (or dicyclic) group $\langle p, 2, 2\rangle$, for which Coxeter gives the two quaternion generators $e^{i\pi/p}$ and j, corresponding to the following matrices in $SU(2)$:

$$G_1 = \begin{pmatrix} e^{i\pi/p} & 0 \\ 0 & e^{-i\pi/p} \end{pmatrix}$$

$$G_2 = \begin{pmatrix} 0 & -1 \\ 1 & 0 \end{pmatrix}$$

The fixed points in $\mathbb{C}P^1$ of these elements (the projection of their eigenvectors) are, in the notation of figure 2.1, c and $A^{-1}(c)$; the great circle containing these points is $l_{151} = \sigma_1(l_5)$ (the $\mathbb{R}$-plane L_5 is introduced below in the octahedral groups), so that an $\mathbb{R}$-plane decomposing simultaneously G_1 and G_2 can only be some multiple of $L_{151} = \sigma_1(L_5)$. We thus need the Souriau matrix A_{151} of $\mathbb{R}$-reflection 151, which is simply:

$$A_{151} = A_1\overline{A_5}A_1 = e^{i\pi/12}\begin{pmatrix} -1 & 0 \\ 0 & 1 \end{pmatrix}$$

It will be more practical to use $e^{-i\pi/12}.151$ as a common $\mathbb{R}$-reflection; we thus want $\mathbb{R}$-planes L_8 and L_9 such that:

$$\begin{cases} G_1 = e^{-i\pi/12}.151.8 \\ G_2 = e^{-i\pi/12}.151.9 \end{cases}$$

This gives us the Souriau matrices of our new $\mathbb{R}$-planes as:

$$A_8 = A_{151}.\overline{G_1} = \begin{pmatrix} -e^{-i\pi/p} & 0 \\ 0 & e^{i\pi/p} \end{pmatrix}$$

$$A_9 = A_{151}.\overline{G_2} = \begin{pmatrix} 0 & 1 \\ 1 & 0 \end{pmatrix}$$

from which we infer the parametrizations:

$$L_8 = \{(e^{-\frac{i\pi}{2p}}.x, e^{\frac{i\pi}{2p}}.y) \in \mathbb{C}^2 | x, y \in \mathbb{R}\}$$

$$L_9 = \{(x + iy, x - iy) \in \mathbb{C}^2 | x, y \in \mathbb{R}\}$$

We now have all we need to decompose the two groups of dihedral type.

- $\underline{\langle p, 2, 2\rangle}$:

  As we have just seen, $\langle p, 2, 2\rangle$ is an index 2 subgroup of the group generated by the three $\mathbb{R}$-reflections: $(e^{-i\pi/12}.151; 8; 9)$.

- $\underline{p[4]2}$:

  Coxeter gives generators R_1 and R_2:

$$\begin{cases} R_1 = e^{i\pi/p}.G_1 = e^{-i\pi/12}.151.e^{-i\pi/p}.8 \\ R_2 = i.G_2 = e^{-i\pi/12}.151.(-i).9 \end{cases}$$

  A possible triple of $\mathbb{R}$-reflections is thus: $(e^{-i\pi/12}.151; e^{-i\pi/p}.8; -i.9)$.

Tetrahedral groups

We have already done most of the work in the example of 3[3]3, where we found $\mathbb{R}$-planes L_1, L_2, L_3, and L_4 such that:

$$21 = R_1 = e^{i\pi/3}.B \ , \ 13 = R_2 = e^{i\pi/3}.B'$$

$$42 = 23 = R_1R_2 = e^{2i\pi/3}.A'$$

and satisfying also:

$$41 = R_1R_2R_1 = -C \ , \ 1321 = 1241 = R_2R_1 = e^{2i\pi/3}.A$$

where R_1, R_2 are our generators for 3[3]3, and A, A', B, B', C are in $SU(2)$, any two of them generating the binary tetrahedral group $\mathbf{T} = \langle 3, 3, 2\rangle$. This, along with some relations which we will use when needed, is enough to decompose the following four groups:

- $\underline{\mathbf{T} = \langle 3, 3, 2\rangle}$:

  We choose for instance B and C as generators for $\mathbf{T}$, and write:

$$\begin{cases} B = e^{-i\pi/3}.21 \\ C = -41 \end{cases}$$

  A possible triple of $\mathbb{R}$-reflections is thus: $(1; e^{-i\pi/3}.2; -4)$.

- $\underline{3[4]3}$:

  Coxeter gives generators G_1 and G_2:

$$\begin{cases} G_1 = e^{i\pi/3}.A = e^{-i\pi/3}.1321 = e^{-i\pi/3}.131.121 \\ G_2 = e^{i\pi/3}.B = 21 = 1.121 \end{cases}$$

  A possible triple of $\mathbb{R}$-reflections is thus: $(121; e^{-i\pi/3}.131; 1)$.

- 3[3]3:

  This is the example we have decomposed into the triples $(1;2;3)$ and $(1;2;4)$. However the generators which we have chosen, $e^{i\pi/3}.B$ and $e^{i\pi/3}.B'$, are conjugate to those listed by Coxeter, which are $e^{i\pi/3}.A$ and $e^{i\pi/3}.A'$, and for the sake of consistency we decompose here his group 3[3]3:

  $$\left\{ \begin{array}{l} G_1 = e^{i\pi/3}.A = e^{-i\pi/3}.1241 = -e^{-i\pi/3}.121.4 \\ G_2 = e^{i\pi/3}.A' = e^{-i\pi/3}.42 \end{array} \right.$$

  We have used the relation: $41 = -14$ (which comes from: $(41)^2 = C^2 = -Id$). A possible triple of $\mathbb{R}$-reflections is thus: $(4; e^{2i\pi/3}.121; e^{-i\pi/3}.2)$.

- 3[6]2:

  Coxeter's generators are:

  $$\left\{ \begin{array}{l} G_1 = e^{i\pi/3}.A = e^{-i\pi/3}.1241 = -e^{-i\pi/3}.121.4 \\ G_2 = i.C = -i.41 \end{array} \right.$$

  A possible triple of $\mathbb{R}$-reflections is thus: $(4; e^{2i\pi/3}.121; i.1)$.

Octahedral groups

The binary octahedral group $\mathbf{O} = \langle 4, 3, 2 \rangle$ contains $\mathbf{T}$ with index two and is obtained from the latter simply by adding the quaternion $\frac{1}{\sqrt{2}}(i + k)$ which corresponds to the following matrix in $SU(2)$:

$$D = \frac{1}{\sqrt{2}} \begin{pmatrix} i & i \\ i & -i \end{pmatrix}$$

The fixed points in $\mathbb{C}P^1$ of this transformation are, in the notation of figure 2.1, the midpoint d of geodesic $[ab]$ (part of the great cirle l_{121}), along with its antipodal point. We will then introduce another $\mathbb{R}$-plane L_5 passing through this point, and such that 5.121 is a multiple of D; the projected great circle l_5 is then in fact orthogonal to l_{121}, and cuts triangle (abc), of type (233), into two (234)'s. For practical reasons, we chose to impose $5.121 = i.D$ which gives us for the Souriau matrix A_5 of σ_5:

$$A_5 = iD.A_{121} = iD.A_1.\overline{A_2}.A_1 = e^{-i\pi/12}.Id$$

and the $\mathbb{R}$-plane L_5 thus admits the following parametrization:

$$L_5 = \{(e^{-\frac{i\pi}{24}}.x, e^{-\frac{i\pi}{24}}.y) \in \mathbb{C}^2 | x, y \in \mathbb{R}\}$$

It remains to see how this new $\mathbb{R}$-reflection interacts with the others appearing in the triangle, σ_1 and σ_4. We thus calculate the Souriau matrices of the two remaining pairs:

$$\sigma_5 \circ \sigma_1 \sim A_5.\overline{A_1} = e^{-i\pi/12} \begin{pmatrix} i & 0 \\ 0 & 1 \end{pmatrix}$$

$$\sigma_4 \circ \sigma_5 \sim A_4.\overline{A_5} = e^{7i\pi/12} \begin{pmatrix} i & 0 \\ 0 & 1 \end{pmatrix}$$

This last matrix $R_1 = \begin{pmatrix} i & 0 \\ 0 & 1 \end{pmatrix} = e^{i\pi/4} \begin{pmatrix} e^{i\pi/4} & 0 \\ 0 & e^{-i\pi/4} \end{pmatrix}$ is one of the generators listed by Coxeter, and corresponds to the rotation of $\pi/2$ appearing at point c.

We are now ready to list the $\mathbb{R}$-reflections for the octahedral groups, starting with **O**:

- $\underline{\mathbf{O} = \langle 4, 3, 2 \rangle}$:

  We choose two generators among A,D and $e^{-i\pi/4}R_1$, for instance the two latter:

  $$\begin{cases} G_1 = e^{-i\pi/4}R_1 = e^{-5i\pi/6}.45 \\ G_2 = D = -i.5.121 = 5.i.121 \end{cases}$$

  A possible triple of $\mathbb{R}$-reflections is thus: $(5; e^{-5i\pi/6}.4; i.121)$.

- $\underline{4[6]2 = \langle 4, 3, 2 \rangle_4}$:

  Coxeter's generators are:

  $$\begin{cases} G_1 = R_1 = e^{-7i\pi/12}.45 \\ G_2 = i.D = 5.121 \end{cases}$$

  A possible triple of $\mathbb{R}$-reflections is thus: $(5; e^{-7i\pi/12}.4; 121)$.

- $\underline{4[3]4}$:

  This example requires a bit more manipulation of words, which we will detail in part. Coxeter's generators are:

  $$\begin{cases} G_1 = R_1 = e^{-7i\pi/12}.45 \\ G_2 = A.R_1.A^{-1} \end{cases}$$

  The fixed point in $\mathbb{C}P^1$ of G_1 is c and that of G_2 is $A(c)$; the great circle containing these points is l_5 so that an $\mathbb{R}$-plane decomposing simultaneously G_1 and G_2 can only be some multiple of L_5. We thus try to rewrite G_2 as a word starting or finishing with 5:

  $$G_2 = A.R_1.A^{-1} = 1241.e^{-7i\pi/12}.45.1421 = e^{-7i\pi/12}.12.(-14).45.(-41).21$$

$$= e^{-7i\pi/12}.12.e^{2i\pi/3}54.4121 = e^{i\pi/12}12.5121$$
$$= e^{i\pi/12}.12121.5$$

We used the relations: $14 = -41$, $15 = e^{2i\pi/3}.54$ (as seen on the Souriau matrices), and $5.121 = 121.5$ (from $(1215)^2 = -D^2 = Id$).

A possible triple of $\mathbb{R}$-reflections is thus: $(5; e^{-7i\pi/12}.4; e^{i\pi/12}.12121)$.

- 3[8]2:

  Coxeter's generators are:

$$\begin{cases} G_1 = e^{i\pi/3}A = e^{2i\pi/3}.121.4 = 121.e^{-2i\pi/3}.4 \\ G_2 = i.D = 5.121 \end{cases}$$

  A possible triple of $\mathbb{R}$-reflections is thus: $(121; e^{-2i\pi/3}.4; 5)$.

- 4[4]3:

  Coxeter's generators are:

$$\begin{cases} G_1 = R_1 = e^{-7i\pi/12}.45 = 4.e^{7i\pi/12}.5 \\ G_2 = e^{i\pi/3}A = e^{2i\pi/3}.121.4 \end{cases}$$

  A possible triple of $\mathbb{R}$-reflections is thus: $(4; e^{7i\pi/12}.5; e^{2i\pi/3}.121)$.

Icosahedral groups

We must start again from the beginning for the binary icosahedral group $\mathbf{I} = \langle 5, 3, 2\rangle$, which doesn't contain any previous group (the classical icosahedral group being simple).

We have the following three (redundant) quaternion generators for $\mathbf{I}$ given by Coxeter:

$$d = \frac{1}{2}(\tau + \frac{i}{\tau} + k),\ e = \frac{1}{2}(1 + \frac{j}{\tau} + \tau k),\ f = k = de$$

where τ is the golden section $\frac{1+\sqrt{5}}{2}$. The corresponding matrices in $SU(2)$ are:

$$D = \frac{1}{2}\begin{pmatrix} \tau + \frac{i}{\tau} & i \\ i & \tau - \frac{i}{\tau} \end{pmatrix}$$

$$E = \frac{1}{2}\begin{pmatrix} 1 & \tau i - \frac{1}{\tau} \\ \frac{1}{\tau} + \tau i & 1 \end{pmatrix}$$

$$F = \begin{pmatrix} 0 & i \\ i & 0 \end{pmatrix} = E.D$$

(Notice that our isomorphism between untary quaternions and $SU(2)$ reverses order of multiplication). We compute the eigenvectors of these matrices, whose eigenvalues are $e^{\pm i\pi/5}$, $e^{\pm i\pi/3}$, and $\pm i$:

$$D^{\pm} = \begin{bmatrix} \tau - 1 \pm 2\sin\frac{\pi}{5} \\ 1 \end{bmatrix}$$

$$E^{\pm} = \begin{bmatrix} \frac{1}{\sqrt{3}}(\pm\tau \pm \frac{i}{\tau}) \\ 1 \end{bmatrix}$$

$$F^{\pm} = \begin{bmatrix} \pm 1 \\ 1 \end{bmatrix}$$

The vectors D^+, E^+, and F^+ project to an elementary (235)-triangle in $\mathbb{C}P^1$, as can be seen graphically or by computation of the hermitian products.

Now one of the $\mathbb{R}$-planes is obvious: since $D^{\pm}$ and $F^{\pm}$ have real coordinates, they all belong to our standard $\mathbb{R}$-plane L_0 (this happens because matrices D and F are unitary and symmetric). Thus we only need to find two $\mathbb{R}$-planes L_6 and L_7 such that $\pi(E^+), \pi(F^+) \in \pi(L_6)$ and $\pi(D^+), \pi(E^+) \in \pi(L_7)$. Since we already have L_0 containing $D^{\pm}$ and $F^{\pm}$, we can find the Souriau matrices A_6 and A_7 by the relations:

$$\sigma_6 \circ \sigma_0 \sim A_6.\overline{A_0} = F$$

$$\sigma_7 \circ \sigma_0 \sim A_7.\overline{A_0} = D$$

Now A_0 is identity so we immediately obtain $A_6 = F$ and $A_7 = D$. This gives us if necessary parametrizations of L_6 and L_7, by solving the systems $A_i.\overline{z} = z$ (diagonalization in a real basis), which results in:

$$L_6 = \{x.e^{\frac{i\pi}{4}}.F^+ + y.e^{-\frac{i\pi}{4}}.F^- | x, y \in \mathbb{R}\}$$

$$L_7 = \{x.e^{\frac{i\pi}{6}}.D^+ + y.e^{-\frac{i\pi}{6}}.D^- | x, y \in \mathbb{R}\}$$

It is then easy to check for the sake of completeness that: $\sigma_6 \circ \sigma_7 \sim E$. We are now ready to list the $\mathbb{R}$-reflections for the icosahedral groups, starting with **I**:

- $\underline{\mathbf{I} = \langle 5, 3, 2 \rangle}$:

  As we have just seen, a possible triple of $\mathbb{R}$-reflections is: $(0; 6; 7)$.

- $\underline{3[10]2}$:

  Coxeter's generators are:

  $$\begin{cases} G_1 = e^{i\pi/3}.E = e^{i\pi/3}.67 \\ G_2 = i.F = i.60 \end{cases}$$

  A possible triple of $\mathbb{R}$-reflections is thus: $(6; e^{-i\pi/3}.7; -i.0)$.

- 5[6]2:

  Coxeter's generators are:

$$\begin{cases} G_1 = e^{i\pi/5}.D = e^{i\pi/5}.70 \\ G_2 = i.F = i.60 \end{cases}$$

  A possible triple of $\mathbb{R}$-reflections is thus: $(0; e^{i\pi/5}.7; i.6)$.

- 5[4]3:

  Coxeter's generators are:

$$\begin{cases} G_1 = e^{i\pi/5}.D = e^{i\pi/5}.70 \\ G_2 = e^{i\pi/3}.E = e^{i\pi/3}.67 \end{cases}$$

  A possible triple of $\mathbb{R}$-reflections is thus: $(7; e^{-i\pi/5}.0; e^{i\pi/3}.6)$.

- 3[5]3:

  Coxeter's generators are:

$$\begin{cases} G_1 = e^{i\pi/3}.E = e^{i\pi/3}.67 \\ G_2 = e^{i\pi/3}.FEF^{-1} = e^{i\pi/3}.60.67.06 = -e^{i\pi/3}.070.6 \end{cases}$$

  We have used the relation $606 = -0$ which comes from $F^2 = 6060 = -Id$. A possible triple of $\mathbb{R}$-reflections is thus:

  $(6; e^{-i\pi/3}.7; e^{2i\pi/3}.070)$.

- 5[3]5:

  Coxeter's generators are:

$$\begin{cases} G_1 = e^{i\pi/5}.D = e^{i\pi/5}.70 \\ G_2 = e^{i\pi/5}.FDF^{-1} = e^{i\pi/5}.60.70.06 = -e^{i\pi/5}.0.676 \end{cases}$$

  A possible triple of $\mathbb{R}$-reflections is thus: $(0; e^{i\pi/5}.7; e^{4i\pi/5}.676)$.

This completes our list of groups.

Chapter 3

New constructions of fundamental polyhedra for Mostow's lattices

This chapter is a joint work with Martin Deraux and Elisha Falbel and has been published in *Acta Mathematica* (see reference [DFP] in the bibliography of the introduction).

3.1 Introduction

Construction of lattices in $PU(n,1)$ has been a major challenge in the last decades. In particular, in contrast with the situation in real hyperbolic space, non-arithmetic lattices have been found only in dimensions up to three (see [M1], [DM] and [M2]).

Mostow's first examples in $PU(2,1)$ were constructed by giving explicit generators, and verifying that the corresponding groups are discrete by finding a fundamental domain for their action. In complex hyperbolic space, or in any space where sectional curvature is not constant, such an approach is bound to be at least somewhat difficult since there are no totally geodesic real hypersurfaces.

Other direct proofs of discreteness have led to domains bounded by various types of hypersurfaces, each of them adapted to the situation at hand (see the constructions in [FP], [Sz1]). There is a canonical construction due to Dirichlet, where the boundary of the domain is made up of bisectors, i.e. hypersurfaces equidistant from two given points. One chooses a point p_0, and considers the set F of points closer to p_0 than to any other point in its orbit under the group. It is obvious that the group is discrete if and only if F contains a neighborhood of p_0, but the set F is in general very difficult to study or describe. Such a description amounts to solving a system of infinitely many quadratic inequalities in four variables (the real and imaginary part of the coordinates in the complex 2-ball). In particular, bisector intersections are neither transverse nor connected in general.

Nevertheless, this was the original approach taken by Mostow ([M1]) to study a remarkable class of groups, $\Gamma(p,t)$ (where $p = 3, 4, 5$ and t is a real parameter). Each of these is generated by three braiding complex reflections R_1, R_2, R_3 of order p; it is contained with finite index in the group $\tilde{\Gamma}(p,t)$ generated by R_1 and the elliptic element J which conjugates R_i into R_{i+1} (see section 3.2.2 for further details).

There are very few values of the parameter t for which $\Gamma(p,t)$ is discrete; for these values Mostow shows discreteness using Dirichlet domains, discovered by computer experimentation. They turn out to be the intersection of the three Dirichlet domains for the finite groups $\Gamma_{ij} = \langle R_i, R_j \rangle$ generated by only two of the generators R_i. The advantage of working with a finite group is obvious, namely one needs to solve a *finite* set of inequalities. However, the fact that the inequalities are quadratic is still an important difficulty, and in fact using current computer technology, it is fairly easy to convince oneself that Mostow's domains for these finite groups (see [M1], page 220) are incorrect. The missing faces, most of which do not contain the common fixed point of the finite group, are described in [De] (it turns out that many of the extra faces disappear when taking the intersection of the three domains for different finite groups).

Part of Mostow's mistake comes from the assumption that the Dirichlet domain for each of the finite groups Γ_{ij} is a cone with vertex given by its fixed point p_{ij}, which is far from being the case. Conical fundamental domains for finite subgroups of $U(2)$ have been constructed in [FPa], but these are not Dirichlet domains. Our constructions also naturally yield cone fundamental domains for Γ_{ij}, having eight cone faces over the eight faces in Figure 3.5.

The fact that these mistakes are particularly difficult to notice in Mostow's paper, and

that they seem quite difficult to fix, prompted us to write a detailed argument, using more geometric techniques. Another motivation for our work is to obtain simpler domains than the ones obtained by the Dirichlet construction, by allowing totally real 2-faces, that are necessarily excluded from Dirichlet domains (see Proposition 3.2.5).

The presence of totally real faces is related to the fact that Mostow's groups are index two subgroups of groups generated by three involutions fixing Lagrangian totally geodesic submanifolds (see section 3.2.2). This observation makes them part of a large family containing infinite covolume groups (see [FK]) and all finite subgroups of $U(2)$ (see [FPa]), among which one would expect to find other lattices as well.

We construct new fundamental polyhedra $\Pi = \Pi_{p,t}$ in $\mathbf{H}^2_{\mathbb{C}}$ for the action of $\tilde{\Gamma}(p,t)$. Our fundamental domains have the same vertices as Mostow's domains, but their higher-dimensional skeletons are simpler and more natural. All our 1-faces are geodesic segments, and many (but not all) of our 2-faces are either real or complex totally geodesic submanifolds. The 3-faces are either on bisectors, or on cones over totally geodesic submanifolds. Note that this construction is related to a fundamental domain for the Eisenstein-Picard group constructed in [FP].

The main advantage, beyond the simplification of the combinatorics of the domains (see section 3.7), is that most verifications can be phrased in concrete geometric terms and the arguments are often completely synthetic, i.e. very few calculations are needed.

In order to prove discreteness, we show that Π and its images under the group tile complex hyperbolic space, by using the appropriate version of the Poincaré polyhedron theorem. In particular, to show that Π and $\gamma\Pi$ have disjoint interior for every nontrivial group element γ, we are reduced to showing this for a finite set of group elements, provided that we can check some detailed compatibility conditions along the codimension two faces of Π.

It turns out that only the cycles of complex geodesic faces impose conditions on the parameters, known as the Picard integrality conditions. The corresponding cycle transformations are simply complex reflections, whose angle of rotation is required to be an integer fraction of π, see Proposition 3.5.4. The heart of the proof consists in a careful justification (incomplete in [Pi], and not quite satisfactory in [M1]) that these are the only conditions. The main result is the following theorem (see section 3.2.2 for the definition of the group, and section 3.3 for the description of Π):

Theorem 3.1.1 *The group $\tilde{\Gamma}(p,t) \subset PU(2,1)$, for $p = 3,4,5$ and $|t| < \frac{1}{2} - \frac{1}{p}$, is discrete if $k = (\frac{1}{4} - \frac{1}{2p} + \frac{t}{2})^{-1}$ and $l = (\frac{1}{4} - \frac{1}{2p} - \frac{t}{2})^{-1}$ are in $\mathbb{Z}$. In that case Π is a fundamental domain with side pairings given by J, R_1, R_2, R_2R_1, R_1R_2 and the cycle relations give the following presentation of the group*

$$\tilde{\Gamma}(p,t) = \langle J, R_1, R_2 \mid J^3 = R_1^p = R_2^p = J^{-1}R_2JR_1^{-1} = R_1R_2R_1R_2^{-1}R_1^{-1}R_2^{-1}$$
$$= (R_2R_1J)^k = ((R_1R_2)^{-1}J)^l = I\rangle.$$

The condition $|t| < \frac{1}{2} - \frac{1}{p}$ shall be referred to as *small phase shift*, following Mostow. In fact the conclusion of the theorem holds for large phase shift as well, but the combinatorics of the fundamental domains are then quite different. For the sake of brevity, we shall only sketch the corresponding changes in our fundamental domain, see section 3.6.

There are finitely many values of t for which the integrality conditions hold, and among the corresponding groups, seven are non arithmetic. The list is given in Remark 3.5.3 on page 97.

Our cone polyhedra turn out to be very convenient when proving that Π and $\gamma\Pi$ have disjoint interiors. In most cases we find a bisector B_γ that separates them (but these bisectors are certainly not all equidistant from a given point p_0, unlike in the Dirichlet construction). In order to verify that Π or $\gamma\Pi$ lies entirely on one side of B_γ, we carefully argue that it is enough to verify this on the level of its 1-skeleton. Note that verifications on the 0-skeleton would quite clearly not be enough to prove that our polyhedron is on one side of a bisector, since the two complementary components of a bisector are far from being convex.

Verifications on the 1-skeleton become relatively easy, as they amount to analyzing the intersection of a bisector with geodesic segments (see Lemma 3.4.2). Note that the strength of the reduction is that we only need to check the position of a finite number of geodesic segments with respect to finitely many bisectors, which in turn amounts to checking finitely many inequalities. The verifications can be done very efficiently with the aid of a computer; however our proofs are geometric and most of the time synthetic. For the case $p = 3$, the small number of calculations could in principle even be done by hand.

Going from the 1-skeleton to the 2-skeleton involves geometric arguments of general interest about the projection of totally geodesic submanifolds onto a given complex geodesic, which is usually the complex spine of the relevant bisector (see Lemma 3.2.1). The main point is to analyze when a geodesic projects onto a geodesic, as in Lemma 3.4.1. Finally, passing to the 3-skeleton is quite natural using the structure of our 3-faces, either the slice decomposition of bisectors, or the cone structure of the other faces.

The paper is organized as follows. In section 3.2 we review a number of geometric facts about complex hyperbolic space and bisectors, and give a description of the relevant groups. We construct our polyhedra $\Pi_{p,t}$ in section 3.3, and section 3.4 is devoted to a detailed verification that they have no self-intersection and are homeomorphic to a closed ball in complex hyperbolic space. In section 3.5 we prove the main theorem by verifying the conditions of the Poincaré polyhedron theorem, following the strategy outlined above. Section 3.6 states the modifications needed in order to treat all the cases from [M1], allowing $|t| \geq \frac{1}{2} - \frac{1}{p}$. Section 3.7 contains a comparison with Mostow's original fundamental domains, including some difficulties encountered with the arguments in [M1]. For the reader's convenience, the last section lists the faces of our polyhedra and their lower-dimensional skeletons.

3.2 Complex hyperbolic space

We use [Go] as a general reference for this section. Let $\langle \cdot, \cdot \rangle$ be a Hermitian form of signature $(2, 1)$ on $\mathbb{C}^3$. The set of complex lines in $\mathbb{C}^3$ on which the Hermitian form is negative definite is a model of complex hyperbolic space. One can write the distance between two points as

$$\cosh(\frac{1}{2}d([x],[y])) = \frac{|\langle x, y\rangle|}{\sqrt{\langle x, x\rangle\langle y, y\rangle}} \tag{3.2.1}$$

The factor $\frac{1}{2}$ is chosen so as to get a metric with sectional curvature between -1 and $-\frac{1}{4}$.

More explicitly, we consider a Hermitian form $\langle z, w\rangle = z^T H \bar{w}$, where H is a Hermitian matrix of signature $(2, 1)$, and the following subsets of $\mathbb{C}^3$:

$$V_0 = \left\{ z \in \mathbb{C}^3 - \{0\} \quad : \quad \langle z, z\rangle = 0 \right\},$$

$$V_- = \left\{ z \in \mathbb{C}^3 - \{0\} \quad : \quad \langle z, z \rangle < 0 \right\}.$$

Let $\pi : \mathbb{C}^3 \setminus \{0\} \to \mathbb{C}P^2$ be the canonical projection onto the complex projective space. Then $\mathbf{H}^2_{\mathbb{C}} = \pi(V_-)$ is complex hyperbolic space. In the case where

$$H = \begin{pmatrix} 1 & 0 & 0 \\ 0 & 1 & 0 \\ 0 & 0 & -1 \end{pmatrix}$$

we obtain in non-homogeneous coordinates the complex ball

$$\mathbf{H}^2_{\mathbb{C}} = \{ \ (z_1, z_2) \in \mathbb{C}^2 \mid |z_1|^2 + |z_2|^2 < 1 \ \}.$$

The group of holomorphic isometries of $\mathbf{H}^2_{\mathbb{C}}$ is then $PU(2,1)$ (the projectivisation of the unitary group of the Hermitian form), and the full group of isometries of complex hyperbolic space, which we denote $\widehat{PU(2,1)}$, is obtained by adjoining just one anti-holomorphic involution.

Anti-holomorphic involutions are also called *real reflections* ($\mathbb{R}$-*reflections*) or *Lagrangian reflections*. In the ball coordinates as above an example of such a transformation is: $(z_1, z_2) \mapsto (\bar{z}_1, \bar{z}_2)$. Their fixed point set is a totally real totally geodesic submanifold which is a Lagrangian submanifold for the symplectic structure on $\mathbf{H}^2_{\mathbb{C}}$ defined by the imaginary part of the Hermitian metric.

Given a vector v with $\langle v, v \rangle = 1$, we consider the isometry of $\mathbb{C}^3$ given by

$$R_{v,\zeta}(x) = x + (\zeta - 1)\langle x, v \rangle v \tag{3.2.2}$$

where ζ is a complex number of absolute value one. The corresponding isometry of complex hyperbolic space is called a complex reflection; it fixes the totally geodesic subspace corresponding to the linear hyperplane $v^\perp$, and rotates in the normal direction by an angle θ, where $\zeta = e^{i\theta}$.

Totally geodesic subspaces of complex hyperbolic space have the following natural description.

Proposition 3.2.1 *The complete totally geodesic subspaces of $\mathbf{H}^2_{\mathbb{C}}$ are either geodesics, fixed subsets of complex reflections (complex lines, also called $\mathbb{C}$-planes) or fixed subsets of Lagrangian reflections (Lagrangian planes, also called $\mathbb{R}$-planes).*

The following lemma describes the projection of geometrical objects into a complex line.

Lemma 3.2.1 *Let π_C be the orthogonal projection of complex hyperbolic space onto a complex line C.*

1. *The image under π_C of a polygon in a complex line is either a point or another polygon such that the angles at the vertices are preserved.*

2. *The image under π_C of a polygon in a Lagrangian plane is either contained in a geodesic, or a polygon or the union of two polygons with a common vertex.*

Proof. The first item follows from the fact that the projection is holomorphic. For the second item, suppose the image of the projection is not contained in a geodesic. The projection is either a diffeomorphism, and in that case the image is another polygon, or the projection is singular at a point. That means that the differential of the projection has a non-trivial kernel. Every vector in the kernel generates a geodesic which projects to a point; in fact such a geodesic is contained in the Lagrangian and in the complex line tangent to the vector. We then claim that there is at most one of these geodesics: if there are two of them then clearly they are ultraparallel, the common orthogonal geodesic is contained in C which therefore intersects the Lagrangian in a geodesic. This would mean that the Lagrangian projects to that geodesic, which we have ruled out. Then the singular geodesic separates the Lagrangian in two and in each half the projection is a diffeomorphism.

□

Remark 3.2.1 One can easily show, by using coordinates with center at the intersection, that if the Lagrangian intersects the complex line its projection is either a geodesic (and in that case that geodesic is precisely the intersection) or a geodesic cone in the complex line at the intersection point.

3.2.1 Bisectors

Recall that the bisector equidistant from two points x_1 and $x_2 \in \mathbf{H}^2_{\mathbb{C}}$ is given by

$$B(x_1, x_2) = \{x \in \mathbf{H}^2_{\mathbb{C}} : d(x, x_1) = d(x, x_2)\} \tag{3.2.3}$$

In what follows we will also denote by x_1 and x_2 lifts to $\mathbb{C}^3$, by a slight abuse of notation. In view of equation (3.2.1), if we normalize two vectors x_1 and x_2 to have equal norms, the bisector is simply the projectivization of the set of vectors x that satisfy

$$|\langle x, x_1\rangle| = |\langle x, x_2\rangle| \tag{3.2.4}$$

An example in the ball model is the "standard" bisector:

$$B_0 = \{(z, t) \in \mathbf{H}^2_{\mathbb{C}} : z \in \mathbb{C}, t \in \mathbb{R}\}$$

which is equidistant from $x_1 = (0, \frac{i}{2})$ and $x_2 = (0, -\frac{i}{2})$ for instance.

A bisector is a smooth real hypersurface diffeomorphic to a ball, but it is not totally geodesic. The **complex spine** Σ of $B(x_1, x_2)$ is by definition the complex geodesic that contains x_1 and x_2. The **real spine** σ is the real geodesic in Σ that is equidistant from x_1 and x_2.

Proposition 3.2.2 *1.* [**Mostow**] *B is foliated by complex geodesics of the form $\pi_\Sigma^{-1}(\{p\})$, for $p \in \sigma$. These are called the **complex slices** of B.*

2. [**Goldman**] *B is the union of all the Lagrangian planes that contain its real spine σ. These are called the **meridians** of B.*

The complex slice decomposition is quite easy to understand from equation (3.2.4), which is equivalent to saying that $x \in (x_1 - \alpha x_2)^\perp$ for some complex number α with $|\alpha| = 1$. The hyperplanes corresponding to the orthogonal complements of $x_1 - \alpha x_2$ (whenever such a vector has positive norm), are precisely the complex slices of B.

Remark 3.2.2

1. The complex slice decomposition makes it clear that a bisector is uniquely determined by its real spine.
2. The Lagrangian reflection in any meridian of B fixes its real spine, hence preserves its complex spine. It must then interchange the two points x_1 and x_2. In fact if x is on the complex spine (but not on the real spine), and μ is the Lagrangian reflection in any meridian of B, then B is equidistant from x and $\mu(x)$.

The following result gives a refinement of the statement that bisectors are not totally geodesic:

Proposition 3.2.3 (see [Go], Theorem 5.5.1) *Let B be a bisector, and $x, y \in B$. Then the real geodesic between x and y is contained in B if and only if x and y are in either a complex slice or a meridian of B.*

Intersection with complex lines

In view of the slice decomposition for bisectors, it is clear that the following result is important to understand bisector intersections.

Proposition 3.2.4 ([M1]) *Let C be a complex geodesic that is not a complex slice of a bisector B. Then $B \cap C$ is either empty or a hypercycle in the complex geodesic.*

Recall that a hypercycle in C is a curve at constant distance from a real geodesic. In particular, unless the two bisectors share a common slice, the proposition implies that their intersection is foliated by arcs of circles. Since the complex slices map into the real spine under projection onto the complex spine, one sees that each connected component of the intersection $B_1 \cap B_2$ is a disk (indeed it fibers over an interval, with intervals as fibers). It can be proven that there are at most two connected components. If the bisectors are coequidistant, more can be said:

Proposition 3.2.5 *Let B_1 and B_2 be two coequidistant bisectors, i.e such that their complex spines intersect outside their real spines. Then $B_1 \cap B_2$ is diffeomorphic to a disk. If the disk is totally geodesic then it is in a common complex slice.*

A proof of this can be found in [Go]. When the intersection is not geodesic, we call it a *Giraud disk*. Observe that, in particular, the intersection of two coequidistant bisectors cannot contain a meridian. The latter fact can be seen directly: if two equidistant bisectors $B_1 = B(x_0, x_1)$ and $B_2 = B(x_0, x_2)$ share a meridian with $\mathbb{R}$-reflection μ, then as we have just seen μ exchanges on one hand x_0 and x_1, and on the other x_0 and x_2, so that the bisectors are equal.

The following lemma characterizes complex lines intersecting a bisector in a geodesic.

Lemma 3.2.2 *Let C be a complex geodesic, and let B be a bisector with real spine σ. Suppose that C is not a complex slice of B, and $C \cap B$ is non empty. Then $C \cap B$ is a geodesic if and only if the extensions to projective space of C and σ intersect.*

Proof. Let Σ be the complex spine of B, which is the complex geodesic containing the real geodesic σ.

1. Suppose Σ and C intersect in $H^2_{\mathbb{C}}$. If the real spine goes through their intersection, then taking the origin of our ball coordinates to be that intersection point makes the equation of B linear, hence the intersection is a line through the origin, which is a geodesic.

   Conversely, if C intersects Σ outside of σ, we still take coordinates centered on σ, so that the intersection is again given by a straight line. If this line were a geodesic, it would have to be contained in a meridian of B, but then it would intersect σ in projective space (but two complex projective lines intersect in exactly one point).

2. The case where Σ and C intersect on $\partial H^2_{\mathbb{C}}$ is similar to the previous one.

3. Suppose Σ and C intersect outside of $H^2_{\mathbb{C}} \cup \partial H^2_{\mathbb{C}}$. Then these two complex geodesics have a common perpendicular complex geodesic D. We may assume that Σ is given by $z_2 = 0$, that C is $z_2 = c$, $c \neq 0$ and D is $z_1 = 0$. The real spine is either a straight line or a circle, depending on whether or not it goes through the origin.

   Note that the intersection $B \cap C$ is the intersection with C of the inverse image of σ under the linear projection $(z_1, z_2) \mapsto z_1$. Remembering that real geodesics in complex geodesics are orthogonal to the boundary, we see that $B \cap C$ is a geodesic if and only if σ is a straight line. This in turn is equivalent to saying that C and σ intersect in projective space (since any intersection would have to take place at infinity in $\mathbb{C}^2$).

□

Intersection with Lagrangian planes

The intersections of Lagrangians with bisectors have the following general property (which expresses the fact that a suitable normalisation of the coordinates gives a quadratic equation for such an intersection):

Proposition 3.2.6 *Let L be a Lagrangian which is not a meridian of the bisector B. Then $B \cap L$ is a conic in L.*

Note that singular conics can occur (two intersection lines). We describe that situation more explicitly. Using the ball coordinates, the Hermitian metric is written at $p = (b, 0)$ with b real as (see [Go])

$$\begin{bmatrix} \frac{1}{(1-b^2)^2} & 0 \\ 0 & \frac{1}{(1-b^2)} \end{bmatrix}$$

Lemma 3.2.3 *Consider coordinates of the standard bisector $\{(z,t),\ z \in \mathbb{C},\ t \in \mathbb{R}\}$, at a point $p = (b, 0)$ with $b \in \mathbb{R}$ and let two tangent vectors $v_1 = (z_1, t_1)$ and $v_2 = (z_2, t_2)$ be in T_pB.*

1. *v_i is tangent to a meridian if and only if $z_i \in \mathbb{R}$*

2. *v_1 and v_2 are tangent to a common Lagrangian if and only if $z_1\bar{z}_2 \in \mathbb{R}$.*

Proof. The first item is obvious. For the second, we need $iv_1 \perp v_2$. Computing, using the form of the metric defined above at the point $(b, 0)$,

$$g(iv_1, v_2) = Re\langle iv_1, v_2\rangle = Re\langle (iz_1, it_1), (z_2, t_2)\rangle = Re\left(iz_1\bar{z}_2\frac{1}{(1-b^2)^2} + it_1t_2\frac{1}{(1-b^2)}\right)$$

we see that the Hermitian product is purely imaginary if and only if $z_1\bar{z}_2 \in \mathbb{R}$. □

Proposition 3.2.7 *Suppose the tangent space to a Lagrangian L is contained in the tangent space to a bisector B, that is $T_pL \subset T_pB$. Then*

1. *$L \subset B$ is a meridian or*
2. *$L \cap B$ is the union of two geodesics passing through p, one being in a meridian and orthogonal to a slice which contains the other one.*

Proof. Follows from the lemma and proposition above. If L is not contained in B we first observe that the tangent space T_pL in the coordinates of the lemma contains the vector $(0, t)$ which is tangent to the meridian passing through $p = (b, 0)$. The geodesic along that vector is contained in both the meridian and L. Analogously, the vector $(z, 0)$ is tangent to the slice and the geodesic defined by it belongs to the slice and to L. The above proposition implies that there can be no more intersection. □

Lemma 3.2.4 *Let g be a geodesic in a meridian of a bisector B, ultraparallel to its real spine. Then there exists a unique slice of B which is othogonal to g; moreover it is orthogonal to the complex geodesic containing g.*

Proof. Observe that in the meridian there exists a unique geodesic orthogonal to the real spine which is also orthogonal to g. The lemma follows from the fact that orthogonal geodesics in a Lagrangian plane are contained in orthogonal complex geodesics. □

Proposition 3.2.8 *Let B be a bisector with real spine σ, and L a Lagrangian not contained in B. Suppose $L \cap B$ contains a geodesic g which is in a meridian of B but not in a slice.*

- *If g is ultraparallel to σ then $L \cap B$ contains another geodesic which is in a complex slice of B.*
- *If g intersects σ in $\mathbf{H}^2_{\mathbb{C}} \cup \partial\mathbf{H}^2_{\mathbb{C}}$ then $L \cap B = g$.*

Proof. In the first case, by the above lemma, there exists a unique slice of B orthogonal to the complex geodesic containing g. This implies that L also intersects that slice in a geodesic. In the second case, by Proposition 3.2.7, we can exclude a singular intersection because g is not orthogonal to any slice. To show that there is only one component in the intersection, in the case where g intersects σ in $\mathbf{H}^2_{\mathbb{C}}$ we can use ball coordinates such that both the bisector and the Lagrangian are linear. In the parallel case we observe that there is a point p at infinity

belonging to the boundary of both σ and L. If $L \cap B$ were to contain a point outside of g, then the geodesic joining that point to p would belong to B and L; there would then exist a complex slice of B having two points in L, therefore $L \cap B$ would contain another geodesic intersecting g, which is a contradiction.

□

We also need the following corollary to Proposition 3.2.7:

Proposition 3.2.9 *Fix four points in $\mathbf{H}^2_{\mathbb{C}}$. If three triples of these points are contained in Lagrangian planes then the four are contained in a common Lagrangian plane.*

Proof. First observe that the four triples are in fact contained in Lagrangians. Indeed, it can easily be seen (as in [Go] pg. 219), that the Cartan angular invariants of various triples among four points $x_1, x_2, x_3, x_4 \in \mathbf{H}^2_{\mathbb{C}}$ satisfy the following relation:

$$\mathbb{A}(x_1, x_2, x_3) + \mathbb{A}(x_1, x_3, x_4) = \mathbb{A}(x_1, x_2, x_4) + \mathbb{A}(x_2, x_3, x_4)$$

Consider then the tetrahedron formed by the four points. Taking opposite edges as real spines of two bisectors we obtain that the intersection contains at least the other four edges. Using Proposition 3.2.7 we conclude that if the Lagrangians do not coincide then there exists one of the faces with all edges meeting at right angles, which is a contradiction. □

3.2.2 The group $\Gamma(p, t)$

The most natural description of a complex reflection group is done by means of a Coxeter diagram, where the nodes correspond to generating reflections, and the edges translate into braiding relations between the generators. In the case of complex reflection groups, there is an extra parameter attached to each loop in the diagram, the so-called phase shift. More details on the general case can be found in [M1] or [C], but for the sake of brevity we only discuss the following special case.

Consider the groups with Coxeter diagrams of the form

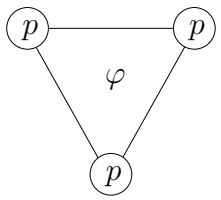

for $p = 3$, 4 or 5. Each such group is generated by three complex reflections R_1, R_2 and R_3 of order p, satisfying the braid relation

$$R_i R_j R_i = R_j R_i R_j \tag{3.2.5}$$

We write the mirror of R_j as $e_j^{\perp}$ (take $v = e_j$ and $\zeta = e^{2\pi i/p}$ in equation (3.2.2)). We may assume after rescaling the vectors e_i that $\langle e_i, e_i \rangle = 1$ and $\langle e_1, e_2 \rangle = \langle e_2, e_3 \rangle = \langle e_3, e_1 \rangle$. The

braid relation imposes a condition on the angle between the mirrors of the generating reflections, which translates as

$$|\langle e_i, e_j\rangle| = \frac{1}{2\sin\frac{\pi}{p}} \tag{3.2.6}$$

In what follows we shall write $\alpha = 1/2\sin\frac{\pi}{p}$.

The phase shift φ that appears in the above diagram corresponds to specifying the common value of the argument of the inner products $\langle e_i, e_{i+1}\rangle$, specifically we take

$$\langle e_i, e_{i+1}\rangle = -\alpha\varphi \tag{3.2.7}$$

where $|\varphi| = 1$. We follow Mostow's notation and write $\varphi^3 = e^{\pi i t}$, and denote the corresponding group by $\Gamma(p,t)$.

In the basis $\{e_1, e_2, e_3\}$, the matrix for the Hermitian form is given by

$$H = \begin{pmatrix} 1 & -\alpha\varphi & -\alpha\overline{\varphi} \\ -\alpha\overline{\varphi} & 1 & -\alpha\varphi \\ -\alpha\varphi & -\alpha\overline{\varphi} & 1 \end{pmatrix} \tag{3.2.8}$$

The existence of a triple of positive vectors e_i satisfying (3.2.7) is equivalent to the requirement that H be of signature $(2,1)$, which in turn is equivalent to

$$|t| < 3(\frac{1}{2} - \frac{1}{p}) \tag{3.2.9}$$

In what follows, we shall always use coordinates in this basis and the Hermitian form (3.2.8).

The linear transformation

$$J = \begin{pmatrix} 0 & 0 & 1 \\ 1 & 0 & 0 \\ 0 & 1 & 0 \end{pmatrix} \tag{3.2.10}$$

is clearly an isometry, which is a regular elliptic element fixing $p_0 = [1,1,1]^T$. Moreover there are three natural antiholomorphic isometric involutions σ_{ij}, given by complex conjugation of the coordinates followed by exchanging two of the standard basis vectors. For instance,

$$\sigma_{12} : [x_1, x_2, x_3]^T \mapsto [\overline{x}_2, \overline{x}_1, \overline{x}_3]^T \tag{3.2.11}$$

We will denote by L_{ij} the fixed point set of σ_{ij}, which is a Lagrangian plane by proposition 3.2.1.

One checks that R_1 is given in the basis $\{e_1, e_2, e_3\}$ by the following matrix, where $\eta = e^{\pi i/p}$,

$$R_1 = \begin{pmatrix} \eta^2 & -\eta i\overline{\varphi} & -\eta i\varphi \\ 0 & 1 & 0 \\ 0 & 0 & 1 \end{pmatrix} \tag{3.2.12}$$

Note that J conjugates R_i into R_{i+1} where indices are taken modulo 3, so that the matrices for R_2 and R_3 are easily deduced from the matrix above.

The condition that $p < 6$ is equivalent to requiring that the mirrors of two reflections R_i, R_j intersect in the ball, in a point denoted by p_{ij}. The common fixed point of R_1 and R_2 can be written as

$$p_{12} = \begin{bmatrix} \alpha\varphi + \alpha^2\overline{\varphi}^2 \\ \alpha\overline{\varphi} + \alpha^2\varphi^2 \\ 1 - \alpha^2 \end{bmatrix} \tag{3.2.13}$$

and the other p_{ij} are deduced by applying the isometry J.

We study the group $\tilde{\Gamma}(p,t)$ generated by J and R_1. It is instructive to decompose these generators as a product of antiholomorphic involutions:

$$\begin{cases} J = \sigma_{12}\sigma_{23} \\ R_1 = \sigma_{23}\tau \end{cases} \tag{3.2.14}$$

where the σ_{ij} are as in (3.2.11), and τ is by definition $\sigma_{23}R_1$. We shall write $\hat{\Gamma}(p,t)$ for the group generated by σ_{12}, σ_{23} and τ. Note that the subgroup $\tilde{\Gamma}(p,t) \subset \hat{\Gamma}(p,t)$ is the index two subgroup of holomorphic elements.

We write L_{ij} and L_τ for the fixed point set of σ_{ij} and τ, respectively.

Proposition 3.2.10 *The Lagrangians fixed by the generating antiholomorphic involutions intersect as follows:*

1. *$L_{12} \cap L_{23}$ is the isolated fixed point p_0 of J.*
2. *$L_{12} \cap L_\tau$ is the isolated fixed point p_1 of JR_1.*
3. *$L_{23} \cap L_\tau$ is a geodesic g_1, contained in the mirror of R_1.*

Proof. The first part follows from the definition of J. In order to get the second, note that JR_1 has three distinct eigenvalues, its characteristic polynomial being given by $-(\lambda+\eta i\overline{\varphi})(\lambda^2+\eta i\varphi)$. The eigenvector with negative norm is the one corresponding to $\sqrt{-\eta i\varphi} = e^{\pi i(\frac{1}{4}-\frac{1}{2p}-\frac{t}{6})}$ for $t > -(\frac{1}{2}-\frac{1}{p})$, and corresponding to $-\eta i\overline{\varphi}$ otherwise.

We now prove part 3. Since $\sigma_{23}e_1 = e_1$, σ_{23} preserves the mirror of R_1 and this implies that L_{23} intersects the mirror in a geodesic (cf. [FPa]). □

We wish to use these three Lagrangians and their intersections, of dimension 0, 1 and 2, as building blocks for a fundamental polyhedron. The first observation is that these objects define a 3-dimensional object, namely the bisector B_1 having g_1 as its real spine. This bisector then has $Fix(R_1)$ as complex spine, L_{23} and L_τ as meridians, and contains the points p_0 and p_1 so it is indeed well adapted to our configuration.

We collect the groups we introduced above in the following

Definition 3.2.1 *For any integer p and $|t| < 3(\frac{1}{2}-\frac{1}{p})$ define*

- $\hat{\Gamma}(p,t) = \langle \sigma_{12}, \sigma_{23}, \tau \rangle$

- $\tilde{\Gamma}(p,t) = \langle R_1, J\rangle \subset \hat{\Gamma}(p,t)$ *of index two.*
- $\Gamma(p,t) = \langle R_1, R_2, R_3\rangle \subset \tilde{\Gamma}(p,t)$,

where $R_1 = \sigma_{23}\tau, J = \sigma_{12}\sigma_{23}$ *and* $R_2 = JR_1J^{-1}, R_3 = J^2R_1J^{-2}$.

Note that the index of $\Gamma(p,t)$ in $\tilde{\Gamma}(p,t)$ could be one or three. Although we are not going to use the next proposition, we observe that using the main theorem we can decide, in certain cases, what the index is.

Proposition 3.2.11 (cf. [M1] lemma 16.1 pg. 244) *Let p and t as in Theorem 3.1 be such that $k = (\frac{1}{4} - \frac{1}{2p} + \frac{t}{2})^{-1}$ and $l = (\frac{1}{4} - \frac{1}{2p} - \frac{t}{2})^{-1}$ are in $\mathbb{Z}$. Then $\Gamma(p,t) \subset \tilde{\Gamma}(p,t)$ is an index 3 subgroup if k and l are both divisible by 3 and otherwise the groups are equal.*

Proof. Clearly, the quotient $\tilde{\Gamma}(p,t)/\Gamma(p,t)$ is represented by the class of J. From the main theorem we obtain the presentation with relation $(R_2R_1J)^k = I$, so

- $(R_2R_1J)^k = (R_2R_1R_3)^{2m}$ if $k = 3m$
- $(R_2R_1J)^k = (R_2R_1R_3)^{2m}R_2R_1J$ if $k = 3m+1$
- $(R_2R_1J)^k = (R_2R_1R_3)^{2m+1}R_2J^2$ if $k = 3m+2$

Therefore J is generated by R_1, R_2, R_3 if 3 does not divide k. Using the relation $((R_1R_2)^{-1}J)^l = I$ we obtain an analogous result for l. □

3.2.3 A canonical hexagon

Let B_1 be the bisector with real spine g_1, the geodesic where L_{23} and L_τ intersect. Note that its complex spine is by construction the mirror of the complex reflection R_1, and the Lagrangians L_{23} and L_τ are two of its meridians. In particular, it also contains the points $p_0 = L_{12} \cap L_{23}$ and $p_1 = L_{12} \cap L_\tau$ (see Proposition 3.2.10).

The bisector B_1 can also be described as being equidistant from two understood points. Indeed the isometry σ_{23}, which is the involution in a meridian of B_1, sends p_{12} to p_{31}. This implies that B_1 is equidistant from p_{12} and p_{31} (see Remark 3.2.2).

Recall that we would like to construct a 3-face of a fundamental domain on B_1. We need this face to intersect "well" with its neighbors, i.e. its images under short words in the group. This leads us to explore the intersection of the whole bisector B_1 with some of its images. Now R_1 stabilizes B_1 (in fact each slice is stabilized), and J cyclically permutes

$$B_1,\ B_2 := J(B_1),\ B_3 := J^2(B_1)$$

We thus study the intersection $S_\eta = B_1 \cap J(B_1)$.

The surface S_η is by construction equidistant from the three fixed points p_{12}, $p_{23} = Jp_{12}$ and $p_{31} = J^2p_{12}$. This also makes it apparent that S_η is the intersection of *any two* among the three bisectors B_1, B_2 and B_3.

Proposition 3.2.12
- *S_η is a smooth non totally geodesic disk.*

- *S_η contains 6 geodesics, arranged in a hexagon with right angles.*

The extension to projective space of the hexagon S_η is shown in Figure 3.1. Note that the hexagon appears already in Mostow but not as a face (see figure 14.1 in page 236 in [M1]). In his notation the six vertices are $s_{12}, \tilde{s}_{13}, s_{23}, \tilde{s}_{21}, s_{31}, \tilde{s}_{32}$ and are given by

$$s_{12} = \begin{bmatrix} \overline{\eta} i \varphi \\ \overline{\eta} i \overline{\varphi} \\ 1 \end{bmatrix}, \quad \tilde{s}_{21} = \begin{bmatrix} -\eta i \varphi \\ -\eta i \overline{\varphi} \\ 1 \end{bmatrix} \tag{3.2.15}$$

and $s_{23} = Js_{12}$, $s_{31} = Js_{23}$, $\tilde{s}_{32} = J\tilde{s}_{21}$, $\tilde{s}_{13} = J\tilde{s}_{32}$

The next section, which provides a proof of Proposition 3.2.12, is devoted to a more detailed analysis of this situation. It is somewhat technical and can be skipped during a first read; the reader can simply assume Proposition 3.2.12 and refer to Figure 3.1.

3.2.4 Computing the vertices of the hexagon

We now prove Proposition 3.2.12. The first part follows from Proposition 3.2.5. Indeed, the bisectors B_i and B_j are co-equidistant, since their complex spines intersect at the point p_{ij}.

In the following arguments, we shall often refer to intersections taking place in complex *projective* space rather than hyperbolic space. We denote by $\tilde{S}_\eta$ the extension to projective space of S_η, which is the set of lines $[x]$ (not necessarily negative definite with respect to the Hermitian form) such that

$$|\langle x, p_{12} \rangle| = |\langle x, p_{23} \rangle| = |\langle x, p_{31} \rangle| \tag{3.2.16}$$

It is readily checked that $\tilde{S}_\eta$ is a torus in projective space (cf. [Go], Lemma 8.3.4). Similarly, $\tilde{\sigma}_j$ denotes the extension to projective space of the real spine σ_j. It is simply the circle parameterized by $p_{ij} - \alpha p_{jk}$, $|\alpha| = 1$. It is clear from the definitions that $[x] \in \tilde{S}_\eta$ is equivalent to saying that x is orthogonal to two vectors of the form $p_{ij} - \alpha_i p_{ki}$ and $p_{ij} - \alpha_j p_{jk}$, $|\alpha_i| = |\alpha_j| = 1$.

The second statement follows from the following observations:

Proposition 3.2.13 *1. For each i, there are precisely two complex slices of B_i that intersect S_η in a geodesic. We choose vectors v_{jik} and v_{kij} polar to these two complex slices.*

2. The vectors v_{jik} and v_{kij} correspond to the two intersection points of $\tilde{\sigma}_i$ and $\tilde{S}_\eta$ in projective space.

3. $v_{ijk} \perp v_{jik}$ and $v_{ijk} \perp v_{ikj}$.

4. The union of any two adjacent sides of the hexagon is the intersection with S_η of a meridian of one of the three bisectors B_i.

The reader should keep Figure 3.1 at hand when reading the proof of the proposition. The picture of $\tilde{S}_\eta$ is drawn using spinal coordinates on $B_1 \cap B_2$, so that the complex slices of B_1, B_2 and B_3 intersect $\tilde{S}_\eta$ in vertical, horizontal, and slope one lines respectively.

Proof. Lemma 3.2.2 implies that any slice of B_i that intersects S_η in a geodesic must intersect both $\tilde{\sigma}_j$ and $\tilde{\sigma}_k$ in projective space. By the slice decomposition, their points of intersection with

the slice are orthogonal to some vector $z \in \tilde{\sigma}_i$. z is clearly contained in $\tilde{S}_\eta$, since it is orthogonal to two points from two different extended real spines.

Hence the slices C_i of B_i that intersect S_η in a geodesic are polar to points of intersection $\tilde{\sigma}_i \cap \tilde{S}_i$. Now σ_i is not contained in B_j for $j \neq i$, and it intersects (the extension) of B_j (hence $\tilde{S}_j$) in at most two points.

We now describe the intersection points $\tilde{\sigma}_j \cap \tilde{S}_\eta$. The corresponding six points appear already in [M1], and are denoted v_{ijk} (where all indices are distinct among 1, 2 and 3). We give the coordinates of two of them, the other ones being deduced by applying J and the according cycle in the indices:

$$v_{123} = \begin{bmatrix} -\eta i\overline{\varphi} \\ 1 \\ \overline{\eta} i\varphi \end{bmatrix}, \quad v_{321} = \begin{bmatrix} \overline{\eta} i\overline{\varphi} \\ 1 \\ -\eta i\varphi \end{bmatrix} \tag{3.2.17}$$

These vectors have geometric meaning, namely v_{ijk} can be checked to be orthogonal to the mirrors of a complex reflections given by $J^{\pm 1} R_j R_k$, where the power is 1 if $k = j+1$ and -1 if $k = j-1$.

Using (3.2.13), one verifies that

$$p_{12} + \eta i\varphi p_{23} = \alpha^2(\eta^2\varphi^2 + \overline{\eta} i\overline{\varphi}) v_{123} \tag{3.2.18}$$

$$p_{12} - \overline{\eta} i\varphi p_{23} = \alpha^2(\overline{\eta}^2\varphi^2 - \eta i\overline{\varphi}) v_{321} \tag{3.2.19}$$

which implies that v_{123} and v_{321} are indeed on the extended real spine of B_2. Similarly, applying J, we see that v_{ijk} is on the extended real spine of B_j. Another unenlightening computation yields

$$\langle v_{123}, p_{12} \rangle = \overline{\eta} i\varphi\kappa \tag{3.2.20}$$

$$\langle v_{123}, p_{23} \rangle = -\eta i\overline{\varphi}\kappa \tag{3.2.21}$$

$$\langle v_{123}, p_{31} \rangle = \kappa \tag{3.2.22}$$

$$\langle v_{321}, p_{12} \rangle = -\eta i\varphi\kappa \tag{3.2.23}$$

$$\langle v_{321}, p_{23} \rangle = \overline{\eta} i\overline{\varphi}\kappa \tag{3.2.24}$$

$$\langle v_{321}, p_{31} \rangle = \kappa \tag{3.2.25}$$

where $\kappa = \det(H) = 1 - 3\alpha^2 - \alpha^3(\varphi^3 + \overline{\varphi}^3)$. Note that all the complex numbers from equation (3.2.20) have the same absolute value, so v_{123} and v_{321} are in $\tilde{S}_\eta$, see (3.2.16). The above result remains true for any v_{ijk} simply by applying the 3-cycle J.

This proves parts 1 and 2 of the proposition. We now check the orthogonality claim, namely that two successive spikes of the star of Figure 3.1 are represented by orthogonal vectors. We only check that v_{321} and v_{312} are orthogonal (the other orthogonality properties are easily deduced from this one). This follows at once from direct calculation, but a better interpretation is that the group contains a number of pairs of commuting complex reflections. Namely, $v_{312}^\perp$ is the mirror of $J^{-1}R_1R_2$, and $v_{321}^\perp$ is the mirror of JR_2R_1. Now these two mirrors are orthogonal, since

$$(J^{-1}R_1R_2)(JR_2R_1) = J^{-1}R_1JJ^{-1}R_2JR_2R_1 = R_3R_1R_2R_1 \tag{3.2.26}$$

$$(JR_2R_1)(J^{-1}R_1R_2) = JR_2J^{-1}JR_1J^{-1}R_1R_2 = R_3R_2R_1R_2 \tag{3.2.27}$$

and these two are equal because of the braiding relation (these commutation relations become more transparent in the description of the groups given in [DM]).

It can be checked that, for $|t| < \frac{1}{2} - \frac{1}{p}$, all v_{ijk} are positive vectors, so that $v_{312}^{\perp} \cap v_{321}^{\perp}$ is a negative line. The corresponding point in complex hyperbolic space is denoted by s_{12} in [M1]. Similarly, there is a point $\tilde{s}_{21}$ which can be described as $v_{123}^{\perp} \cap v_{213}^{\perp}$.

One can compute explicit homogeneous coordinates for these points, and obtain expression (3.2.15). Coordinates for the other four vertices of the hexagon are easily obtained from s_{12} and $\tilde{s}_{21}$ by applying the symmetry J, namely $s_{23} = Js_{12}$, $s_{31} = Js_{23}$, $\tilde{s}_{32} = J\tilde{s}_{21}$, $\tilde{s}_{13} = J\tilde{s}_{32}$.

It follows from the above orthogonality property that the complex geodesics that contain two successive sides of the hexagon are orthogonal, hence the real geodesics themselves must be orthogonal. The orthogonality of the complex geodesics also implies that two successive sides of the hexagon are contained in a totally real 2-plane, which must then be a meridian of one of the three bisectors intersecting in the Giraud disk (indeed it contains two points of its extended real spine). This gives part 4. □

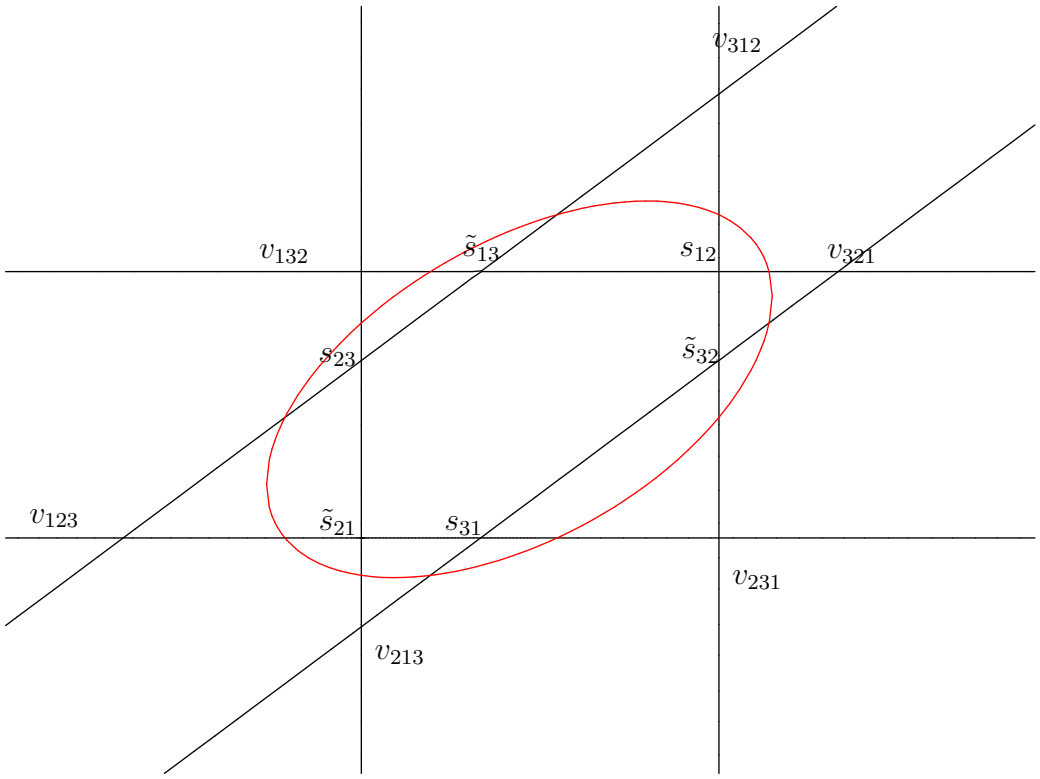

Figure 3.1: A right angled geodesic hexagon on the Giraud disk $B_1 \cap B_2 \cap B_3$, for $t = 1/18$. The figure shows a neighborhood of the disk in its torus extension to projective space.

3.3 Description of a fundamental polyhedron Π in $\mathbf{H}^2_{\mathbb{C}}$

Our fundamental domain is a polyhedron Π constructed as a cone at a point p_{12} over the union of two 3-cells named H and H' intersecting in a hexagonal 2-cell η.

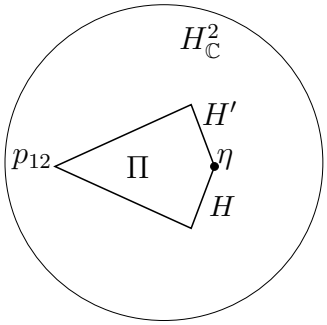

Figure 3.2: A schematical view of the fundamental domain. The two 3-faces H and H' intersect in a 2-face (an hexagon) η. The domain is a geodesic cone from p_{12}.

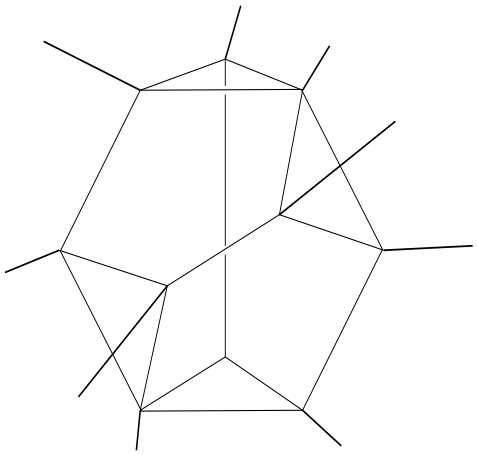

Figure 3.3: The boundary of the fundamental domain is a sphere divided into 10 cells. The cone point p_{12} is represented at infinity and only two of the 3-cells are finite. They correspond to H and H' and intersect in a hexagon. There are 4 pentagonal prisms and 4 tetrahedra containing p_{12} as a vertex. The 1-cells are all geodesics.

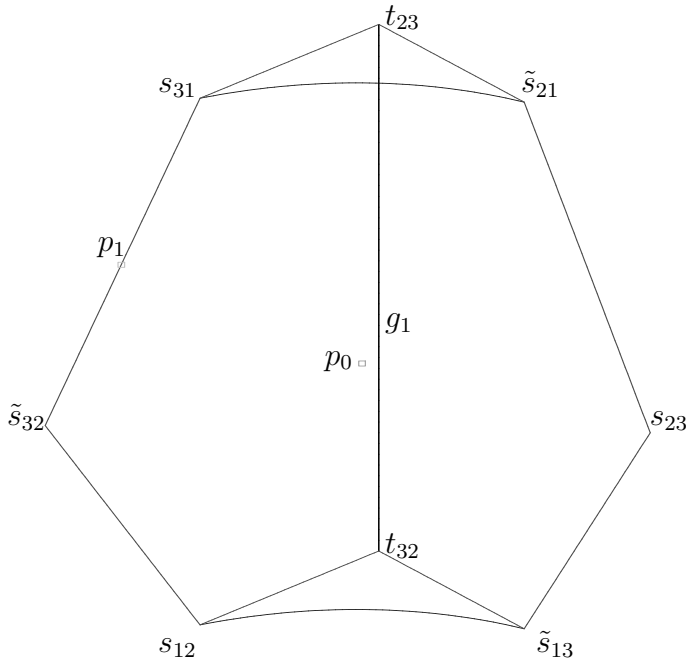

Figure 3.4: The 3-face H in the bisector B_1. One of its 2-faces is the hexagon η contained in the intersection $B_1 \cap J(B_1)$.

3.3.1 The core hexagon

In order to construct the first 3-faces of the fundamental domain we recall that the intersection $S_\eta = B_1 \cap J(B_1)$ is a topological disc which contains 6 geodesics, arranged along a hexagon with right angles, see Proposition 3.2.12. We thus define a 2-face η of our polyhedron to be the part of the surface S_η bounded by the hexagon; this 2-face is contained in two 3-faces which we now define, H in B_1 and H' in $B_1' = J(B_1)$. Here in and in what follows, we denote

$$B_1,\ B_1' := J(B_1),\ B_1'' := J^2(B_1)$$

3.3.2 The 3-faces H and H'

We first take a closer look at the position of the hexagon in the first bisector B_1. We have:

- s_{12}, s_{31} and $\tilde{s}_{32}$ are in the meridian L_τ.
- $\tilde{s}_{13}, s_{23}$ and $\tilde{s}_{21}$ are in the meridian $R_1(L_\tau)$.
- s_{31} and $\tilde{s}_{21}$ are in a common slice.
- s_{12} and $\tilde{s}_{13}$ are in a common slice.

The situation can be seen on Figure 3.4 , where we use coordinates on B_1 adapted to the bisector structure, in the sense that the (real) spine is the vertical axis, slices are horizontal planes and meridians are vertical planes containing the axis. We call such coordinates *spinal coordinates* on B_1.

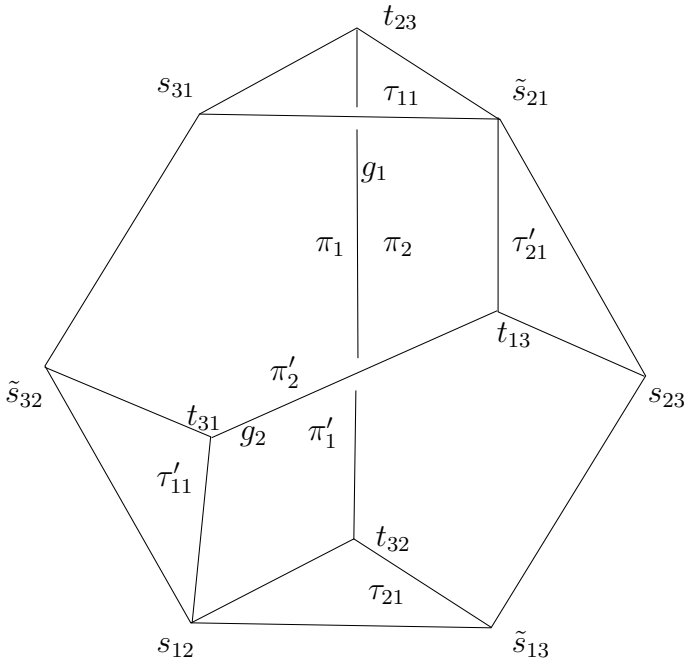

Figure 3.5: The core part $H \cup H'$ in $B_1 \cup B'_1$. The pentagonal 2-cells π_1 and π_2 contain the spine g_1 and π'_1 and π'_2 contain the spine g_2. The side pairing transformation which interchanges H and H' is J.

We are now ready to complete the 3-face H by adding two vertices, t_{23} and t_{32} in Mostow's notation. They are given by the projection onto the spine of B_1 of the two slices containing the pairs $(s_{31}, \tilde{s}_{21})$, and $(s_{12}, \tilde{s}_{13})$ respectively. An elementary computation gives the following formulas:

$$t_{23} = \begin{bmatrix} \alpha|\varphi - \eta i\overline{\varphi}^2|^2 \\ \varphi - \eta i\overline{\varphi}^2 \\ \overline{\varphi} + \overline{\eta} i\varphi^2 \end{bmatrix}, \quad t_{32} = \begin{bmatrix} \alpha|\overline{\varphi} - \eta i\varphi^2|^2 \\ \varphi + \overline{\eta} i\overline{\varphi}^2 \\ \overline{\varphi} - \eta i\varphi^2 \end{bmatrix} \tag{3.3.1}$$

We then enclose H by adding four 2-faces:

- two $\mathbb{C}$-planar geodesic triangles, $\tau_{11} = (t_{23}, s_{31}, \tilde{s}_{21})$ in the "top" slice and $\tau_{21} = (t_{32}, s_{12}, \tilde{s}_{13})$ in the "bottom" slice,
- two $\mathbb{R}$-planar geodesic right-angled pentagons, $\pi_1 = (t_{23}, s_{31}, \tilde{s}_{32}, s_{12}, t_{32})$ in the meridian L_τ, and $\pi_2 = (t_{23}, \tilde{s}_{21}, s_{23}, \tilde{s}_{13}, t_{32})$ in the meridian $R_1(L_\tau)$.

It is natural to construct this wedge from the spine g_1 because R_1 acts on the bisector B_1 by rotation around its spine. These five 2-faces enclose a region in B_1 which is our first 3-face H. Now the next face H' is easily derived: we simply consider $H' = J(H)$ in $B'_1 = J(B_1)$. This new face, isometric to H, is glued to H along the 2-face η (with a rotation of $\frac{2\pi}{3}$ in the orientation of the picture) and it only has two new vertices $t_{31} = J(t_{23})$ and $t_{13} = J(t_{32})$ which are on the spine of B'_1.
We have thus closed the 2-face η in the sense that it belongs to two 3-faces; we eventually want to close all the 2-faces we have introduced, which is what we now do.

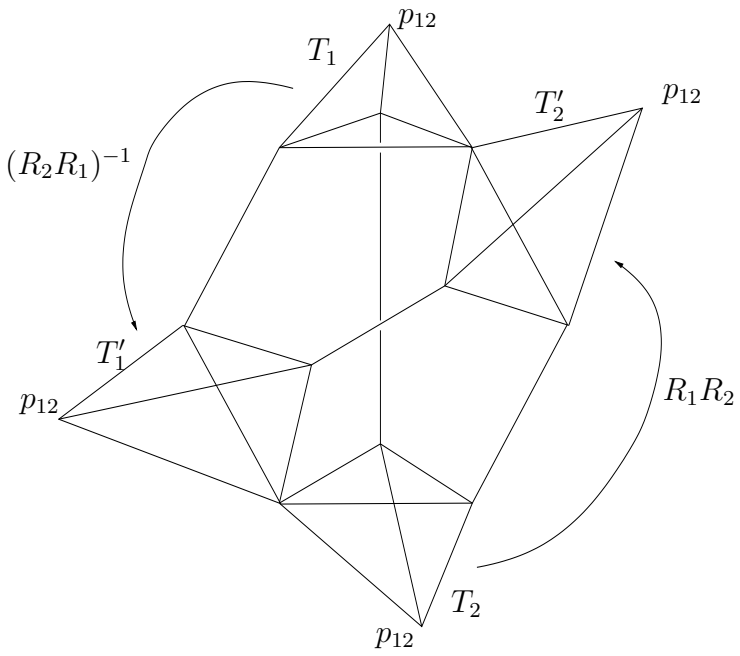

Figure 3.6: The 4 tetrahedra in the boundary of the polyhedron Π actually have the common vertex p_{12}. Shown are the corresponding side-pairings transformations.

3.3.3 The whole polyhedron Π

Recall from section 3.2.2 that p_{12} is the intersection of the mirrors of R_1 and R_2 (see equation 3.2.13). Alternatively, it can be seen as the intersection of the complex spines of the two bisectors we have used so far, B_1 and B_1'.
We then construct our polyhedron Π as the geodesic cone over the "core" part $H \cup H'$ from the point p_{12}. We use the notation:

$$Cone(\alpha) = \bigcup_{q \in \alpha} [p_{12}q]$$

where $[pq]$ denotes the geodesic segment from p to q. So that

$$\Pi := Cone(H \cup H')$$

This is analogous to the construction in [FP] for the Eisenstein-Picard modular group, where the cone vertex was at infinity.
With this construction, the interior of Π is the cone over the interior of $H \cup H'$, and its boundary is the cone over the boundary of $H \cup H'$, together with $H \cup H'$. Thus the boundary of Π consists in ten 3-faces: H, H' and eight faces of two combinatorial types, tetrahedra (cones over a triangle) and pentagonal pyramids (cones over a pentagon). We will see in fact that these two types are also geometrically different, because the tetrahedra live in bisectors whereas the pentagonal pyramids do not.
What is less obvious, and which we leave to the next section, is that this construction does not yield any unwanted intersection between the faces. We first describe the remaining 3-faces.

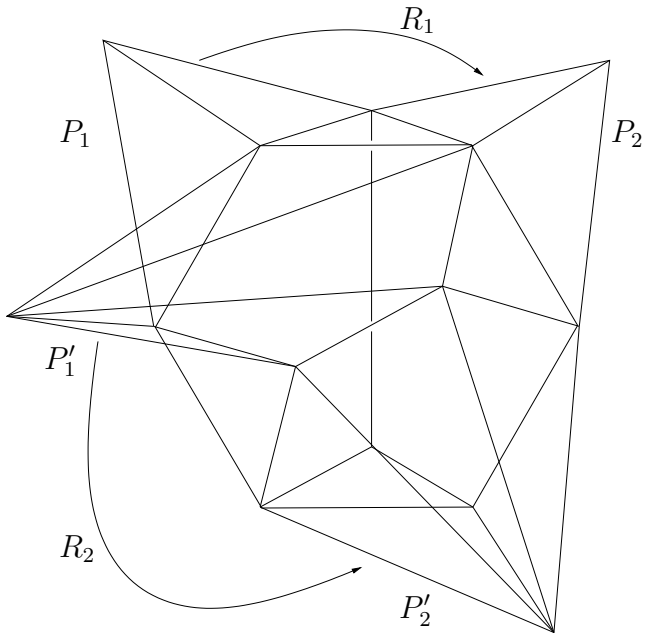

Figure 3.7: The 4 pentagonal pyramids in the boundary of Π and their side-pairing tranformations. Again, they are defined as cones to the common vertex p_{12}

3.3.4 The remaining 3-faces

Description of a tetrahedron

The "top" and "bottom" triangles τ_{11} and τ_{21} are not isometric (unless $t = 0$), however the tetrahedra based on them have the same structure so that we need only describe the tetrahedron T_1 based on τ_{11}.
Recall that $\tau_{11} = (t_{23}, s_{31}, \tilde{s}_{21})$ is $\mathbb{C}$-planar. Now when we add the point p_{12}, we obtain a special configuration:

Lemma 3.3.1 *The triangles $\tau_{12} = (t_{23}, s_{31}, p_{12})$ and $\tau_{13} = (t_{23}, \tilde{s}_{21}, p_{12})$ are $\mathbb{R}$-planar.*

Proof. This can be seen by computing the two Hermitian triple products. Another proof is obtained by observing that the complex geodesics containing $[t_{23}, s_{31}]$ and $[t_{23}, p_{12}]$ respectively, are orthogonal. Indeed, by construction, the first one is a slice of B_1 and the second is the complex spine of B_1. □

This shows that three faces of the tetrahedron are naturally reconstructed from its vertices; there remains some flexibility in the choice of the fourth face, and we have chosen the union of geodesics from p_{12} to the opposite edge (this ensures that this face is in common with the neighboring pentagonal pyramid). We can moreover see the following:

Lemma 3.3.2 *The tetrahedron T_1 is contained in a (unique) bisector.*

Proof. We need to find a bisector B such that the $\mathbb{R}$-planar triangles τ_{12} and τ_{13} are each in a meridian of B and such that the $\mathbb{C}$-planar triangle τ_{11} is in a slice. This is possible because the

geodesic $(t_{23}p_{12})$ common to both $\mathbb{R}$-planes (which is the only possible spine) lives in a $\mathbb{C}$-plane orthogonal to the possible slice. □

Description of a pentagonal pyramid

We also have a priori two isometry classes of pentagonal pyramids, however they share the same structure and we only describe the pyramid P_1 based on the $\mathbb{R}$-planar pentagon π_1.
What happens now is that when we add the point p_{12}, we obtain five triangular 2-faces, one of which is $\mathbb{C}$-planar ($(t_{23}t_{32}p_{12})$ is contained in $Fix(R_1)$), the two adjacent faces $(t_{23}s_{31}p_{12})$ and $(t_{32}s_{12}p_{12})$ are $\mathbb{R}$-planar (they are in common with the tetahedra T_1 and T_2), and the two remaining faces are not geodesic. In particular:

Lemma 3.3.3 *The pentagonal pyramid P_1 is not contained in a bisector.*

Proof. Indeed three of its faces are $\mathbb{R}$-planar, intersecting in two distinct geodesics, whereas any three (or more) $\mathbb{R}$-planes contained in a bisector intersect in a common geodesic (the real spine). □

3.4 Topology and combinatorial structure of Π

The reader can skip this section if he assumes Proposition 3.4.1. We will now show how the combinatorial structure of Π ensures that its topology is reasonable, in the following sense:

Proposition 3.4.1 *Topologically, the boundary polyhedron $\partial\Pi$ is a sphere S^3 and the whole polyhedron Π is a ball B^4.*

Proof. We show that $\partial\Pi$ is homeomorphic to S^3. The technical aspect is to show that the 3-faces as we have defined them intersect only where we expect them to, i.e. in common 2-faces or unions of 1-faces; this will be seen below and follows from the structure of the bisector faces and the special position of our cone point p_{12}. Assuming this, the fact that every 2-face belongs exactly to two 3-faces ensures that $\partial\Pi$ is a 3-manifold; in fact we have a realization of $\partial\Pi$ in S^3 by considering the core part $H \cup H'$ (a topological B^3) in $\mathbb{R}^3$ and setting the point p_{12} at infinity. $\partial\Pi$ is then the union of $H \cup H'$ with the cone from p_{12} over $\partial(H \cup H')$, which is the exterior of this ball; the verifications below ensure that this is an embedding.

□

We now want to check that the different 3-faces that we have defined intersect pairwise as expected (in 2-faces or unions of 1-faces), that is, that there is no unwanted extra intersection. A real difficulty resides in the fact that bisectors are not geodesically convex and that, more precisely, the generic intersection between a geodesic and a bisector is empty or a pair of points. This is a problem for us as we have defined our polyhedron as a geodesic cone over certain objects living in bisectors. For instance, it is possible that a geodesic between p_{12} and a point $q \in H$ meets H' before reaching q. We will see that this does not happen, the key point being that p_{12} is on the complex spines of both B_1 and B'_1.

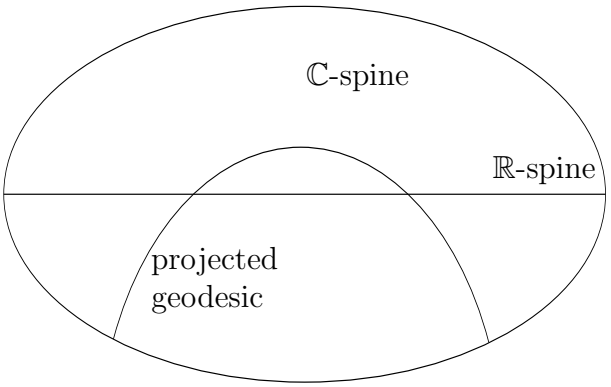

Figure 3.8: Generic intersection of a geodesic and a bisector

Lemma 3.4.1 *Let C be a complex line and π_C be the orthogonal projection onto it. If γ is a geodesic intersecting C then $\pi_C(\gamma)$ is a geodesic in C.*

Note that this is not true in general, $\pi_C(\gamma)$ being an arc of Euclidean circle (see Figure 3.8).

Proof. Normalize the coordinates in the ball model so that $C = \{(z_1, 0) \in \mathbf{B}^2_{\mathbb{C}}\}$ and $C \cap \gamma = \{(0, 0)\}$. Then the projection is simply $(z_1, z_2) \mapsto (z_1, 0)$ and the result is obvious knowing that the geodesics through the origin are the Euclidean segments. □

We apply this simple fact to the context of bisectors. Recall the slice decomposition of a bisector: if B is a bisector with (real) spine g and complex spine C, and if as above π_C is the orthogonal projection onto C, then $B = \pi_C^{-1}(g)$ where the fibers $\pi_C^{-1}(\{p\})$ for $p \in g$ are the slices of B. The above lemma implies:

Lemma 3.4.2 *Let B be a bisector with (real) spine g and complex spine C, and let $p \in C$. Then the geodesics through p:*

- *intersect B in $\{p\}$ or are contained in B if $p \in g$*
- *intersect B in at most a point if $p \notin g$.*

Proof. The first part comes from the fact that the (real) spine is contained in all meridians. For the second part, the preceding lemma shows that if γ is a geodesic through p, then $\pi_C(\gamma)$ intersects g in at most a point q. Then $B \cap \gamma$ is contained in the slice $\pi_C^{-1}(\{q\})$. The slice being totally geodesic, this shows that $B \cap \gamma$ contains only one point. □

We are now ready to analyze the different intersections of 3-faces.

Intersection of the pentagonal pyramids with H and H'

There are two types of intersection between a pentagonal pyramid and a core face H or H', as follows:

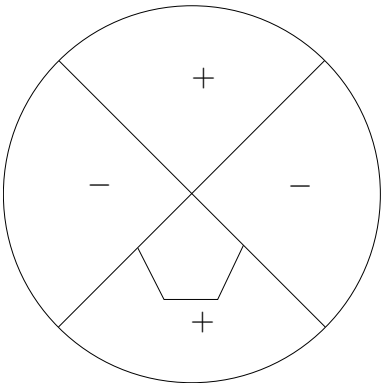

Figure 3.9: The trace of B'_1 on the $\mathbb{R}$-plane L_τ

Proposition 3.4.2 • *P_1 intersects H in the pentagon π_1*

- *P_1 intersects H' in two geodesic segments, $[\tilde{s}_{32}s_{31}]$ and $[\tilde{s}_{32}s_{12}]$.*

Proof. We prove the stronger statement that $P_1 \cap B_1 = \pi_1$ and $P_1 \cap B'_1 = [\tilde{s}_{32}s_{31}] \cup [\tilde{s}_{32}s_{12}]$, by projecting to the $\mathbb{C}$-spine of the appropriate bisector and using the above lemma. Let π_{C_1}, $\pi_{C'_1}$ denote the orthogonal projection to the $\mathbb{C}$-spine of B_1 (resp. B'_1).

For the first point: since $\pi_1 \subset B_1$, $\pi_{C_1}(\pi_1)$ is contained in the (real) spine of B_1, so that the preceding lemma implies that each geodesic from p_{12} to a point q of π_1 intersects B_1 only in q.

It remains to see how P_1 intersects H'. We start off by showing that the pentagon π_1 is entirely contained in the half-space bounded by B'_1 and containing p_{12}. Recall that π_1 is contained in the $\mathbb{R}$-plane L_τ (see Proposition 3.2.10). Now L_τ has singular intersection with B'_1, consisting in the two orthogonal geodesics $(\tilde{s}_{32}s_{31})$ and $(\tilde{s}_{32}s_{12})$ which separate L_τ into 4 regions as in Figure 3.9 (where $+$ and $-$ indicate the half-spaces bounded by B'_1). Thus π_1 (which is convex) is entirely contained in one of these half-spaces, which contains the vertices t_{23} and t_{32}. Now we can check, using two points from which B'_1 is equidistant, such as p_{12} and p_{23}, that t_{23} and t_{32} are on the same side of B'_1 as the point p_{12}. (Figure 3.10 illustrates the difference $cosh(\rho(t_{23}, p_{23})) - cosh(\rho(t_{23}, p_{12}))$ as a function of the phase shift t, the point being that it remains positive for $|t| < \frac{1}{2} - \frac{1}{p}$). We can then conclude, by projecting to the $\mathbb{C}$-spine of B'_1 and using the lemma, that the whole cone P_1 is on the same side of B'_1 as p_{12}, which implies that P_1 and B'_1 have the desired intersection which is the pair of edges $[\tilde{s}_{32}s_{31}]$ and $[\tilde{s}_{32}s_{12}]$.

□

The same argument applies to the other pentagonal pyramids, knowing that t_{13} and t_{31} are on the same side of B_1 as the point p_{12}.

Intersection of the tetrahedra with H and H'

These intersections are exactly as above, replacing the pentagons with triangles. We have in this case:

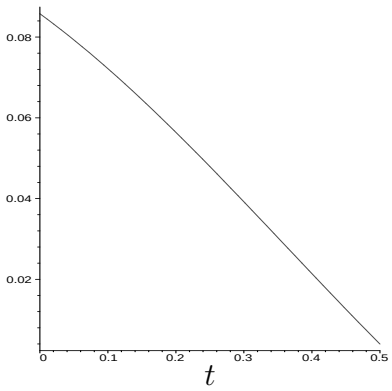

Figure 3.10: t_{23} is on the same side of B'_1 as p_{12}

Proposition 3.4.3

- T_1 *intersects* H *in the triangle* τ_{11}
- T_1 *intersects* H' *in the geodesic segment* $[\tilde{s}_{21}s_{31}]$.

Intersection of two cone faces

The intersection of two faces which are unions of geodesics from p_{12} is not much of a problem.

Lemma 3.4.3 *If* α, β *are subsets of* $\partial(H \cup H')$, *then:*

$$Cone(\alpha) \cap Cone(\beta) = Cone(\alpha \cap \beta)$$

Proof. It is obvious that: $Cone(\alpha \cap \beta) \subset Cone(\alpha) \cap Cone(\beta)$. That there is no extra intersection follows from what we have seen on the other faces. □

Intersection of the two core faces H and H'

This is the easiest case because we have defined the 2-face η so that: $H \cap H' = \eta$. Note that H (resp. H') lies entirely on one side of bisector B'_1 (resp. B_1), which is the same side as p_{12} as we have seen by testing the vertices.

3.5 Using Poincaré's polyhedron theorem

In this section we review Poincaré's polyhedron theorem. We will follow the general formulation of the theorem given in Mostow [M1], section 6 pg. 197, and we refer to it for a proof (see also [FP, Mas]). We define a polyhedron as a cellular space homeomorphic to a compact polytope. In particular, each codimension two cell is contained in exactly two codimension one cells. Its realization as a cell complex in a manifold X is also referred to as a polyhedron. We will say a polyhedron is smooth if its faces are smooth.

Definition 3.5.1 *A Poincaré polyhedron is a smooth polyhedron* D *in* X *with codimension one faces* T_i *such that*

1. *The codimension one faces are paired by a set Δ of homeomorphisms of X which respect the cell structure (the side pairing transformations). We assume that if $\gamma \in \Delta$ then $\gamma^{-1} \in \Delta$.*

2. *For every $\gamma_{ij} \in \Delta$ such that $T_i = \gamma_{ij} T_j$ then $\gamma_{ij} D \cap D = T_i$.*

Remark 3.5.1 If $T_i = T_j$, that is if a side pairing maps one side to itself then we impose, moreover, that γ_{ij} be of order two and call it a reflection. We refer to the relation $\gamma_{ij}^2 = 1$ as a reflection relation.

Let T_1 be an $(n-1)$-face and F_1 be an $(n-2)$-face contained in T_1. Let T_1' be the other $(n-1)$-face containing F_1. Let T_2 be the $(n-1)$-face paired to T_1' by $g_1 \in \Delta$ and $F_2 = g_1(F_1)$. Again, there exists only one $(n-1)$-face containing F_2 which we call T_2'. We define recursively g_i and F_i, so that $g_{i-1} \circ \cdots \circ g_1(F_1) = F_i$.

Definition 3.5.2 (Cyclic) Cyclic *is the condition that for each pair (F_1, T_1)(an $(n-2)$-face contained in an $(n-1)$-face), there exists $r \geq 1$ such that, in the construction above, $g_r \circ \cdots g_1(T_1) = T_1$ and $g_r \circ \cdots g_1$ restricted to F_1 is the identity. Moreover, calling $g = g_r \circ \cdots \circ g_1$, there exists a positive integer m such that $g_1^{-1}(P) \cup (g_2 \circ g_1)^{-1}(P) \cup \cdots \cup g^{-1}(P) \cup (g_1 \circ g)^{-1}(P) \cup (g_2 \circ g_1 \circ g)^{-1}(P) \cup \cdots \cup (g^m)^{-1}(P)$ is a cover of a closed neighborhood of the interior of F_1 by polyhedra with disjoint interiors.*

The relation $g^m = (g_r \circ \cdots g_1)^m = Id$ is called a *cycle relation*.

Theorem 3.5.2 *Let D be a compact Poincaré polyhedron with side-pairing transformations $\Delta \subset Isom(H^2_{\mathbb{C}})$ in $H^2_{\mathbb{C}}$ satisfying condition* **Cyclic**. *Let Γ be the group generated by Δ. Then Γ is a discrete subgroup of $Isom(H^2_{\mathbb{C}})$ and D a fundamental domain. A presentation is given by*

$$\Gamma = \langle \Delta \mid \textit{cycle relations, reflection relations} \rangle$$

3.5.1 Side-pairings

The side-pairings of our polyhedron Π are, writing $R_2 = J R_1 J^{-1}$:

$$H \xrightarrow{J} H'$$

$$P_1 \xrightarrow{R_1} P_2 \qquad\qquad P_1' \xrightarrow{R_2} P_2'$$

$$T_1 \xrightarrow{(R_2 R_1)^{-1}} T_1' \qquad\qquad T_2 \xrightarrow{R_1 R_2} T_2'$$

3.5.2 Cycles and orbits of faces

We now write the cycles of 2-faces induced by the side-pairings, according to type of 2-face.

- The hexagon cycle:

$$\eta \xrightarrow{J} \eta \xrightarrow{J} \eta \xrightarrow{J} \eta$$

- The pentagon cycle:

$$\pi_1 \xrightarrow{R_1} \pi_2 \xrightarrow{J} \pi_2' \xrightarrow{R_2^{-1}} \pi_1' \xrightarrow{J^{-1}} \pi_1$$

- The $\mathbb{C}$-planar triangle cycles:

$$\tau_{11} \xrightarrow{(R_2R_1)^{-1}} \tau_{11}' \xrightarrow{J^{-1}} \tau_{11}$$

$$\tau_{21} \xrightarrow{R_1R_2} \tau_{21}' \xrightarrow{J^{-1}} \tau_{21}$$

$$\tau_{c1} \xrightarrow{R_1} \tau_{c1}$$

$$\tau_{c2} \xrightarrow{R_2} \tau_{c2}$$

- The $\mathbb{R}$-planar triangle cycles:

$$\tau_{12} \xrightarrow{R_1} \tau_{13} \xrightarrow{(R_2R_1)^{-1}} \tau_{13}' \xrightarrow{R_2^{-1}} \tau_{12}' \xrightarrow{R_2R_1} \tau_{12}$$

$$\tau_{22} \xrightarrow{R_1} \tau_{23} \xrightarrow{R_1R_2} \tau_{23}' \xrightarrow{R_2^{-1}} \tau_{22}' \xrightarrow{(R_1R_2)^{-1}} \tau_{22}$$

- The generic triangle cycles:

$$\tau_{14} \xrightarrow{(R_2R_1)^{-1}} \tau_{14}' \xrightarrow{R_1} \tau_{g2} \xrightarrow{R_2} \tau_{14}$$

$$\tau_{24} \xrightarrow{R_1R_2} \tau_{24}' \xrightarrow{R_1^{-1}} \tau_{g1} \xrightarrow{R_2^{-1}} \tau_{24}$$

3.5.3 Verifying the tessellation conditions

First step: the side-pairings send Π off itself

We show in this section that each side-pairing g of Π satisfies:

$$\overset{\circ}{\Pi} \cap g(\overset{\circ}{\Pi}) = \emptyset$$

This is more easily seen in the case where the faces corresponding to the side-pairing live in a bisector, because the bisector in question separates Π and its image, hence the intersection of these polyhedra has dimension at most 3, and their interiors are disjoint. We now verify this claim.

- Side-pairing J

  J maps H to H', which lives in the bisector B'_1. We have:

  Proposition 3.5.1 *B'_1 separates Π and $J(\Pi)$.*

  Proof. We first see this for the core parts $H \cup H'$ and $J(H \cup H') = H' \cup H''$. Now H' is in B'_1 so we only need to check that H is on one side of B'_1 and H'' on the other. We already know that H is on the same side of B'_1 as p_{12} (see section 3.4), and the second part follows, knowing that the $\mathbb{R}$-reflection σ_{13} (in the meridian L_{13} of B'_1) exchanges H and H'', as can be checked on the vertices.

  The cone parts are then easily seen to be on the appropriate sides of B'_1, because the cone points p_{12} and $p_{23} = J(p_{12})$ are in the $\mathbb{C}$-spine of B'_1, each on the same side as the base of its cone. □

- Side-pairings R_1R_2 and R_2R_1:

  We treat the case of R_1R_2, the other being completely analogous. R_1R_2 maps T_2 to T'_2 which is contained in the bisector $B_{T'_2}$, having as real spine the geodesic $(t_{13}p_{12})$. We have:

  Proposition 3.5.2 *$B_{T'_2}$ separates Π and $R_1R_2(\Pi)$.*

  Proof. It suffices to show that Π is entirely on one side of $B_{T'_2}$. Indeed, Π is then analogously entirely on one side of B_{T_2}, so that by the side-pairing R_1R_2, $R_1R_2(\Pi)$ is entirely on one side of $B_{T'_2} = R_1R_2(B_{T_2})$. We then check one point in each polyhedron to see that they are indeed on opposite sides.

  The fact that Π is entirely on one side of $B_{T'_2}$ can be seen by projecting to the $\mathbb{C}$-spine of $B_{T'_2}$ (the mirror of R_2), which contains the points p_{12}, t_{13}, t_{31}.

  - Position of H': H' lives in the bisector B'_1, which has the same $\mathbb{C}$-spine as $B_{T'_2}$; its projection is thus contained in the geodesic $(t_{13}t_{31})$ (the real spine of B'_1), and in light of the foliation of H' by complex triangles it is in fact inside the segment $[t_{13}t_{31}]$.

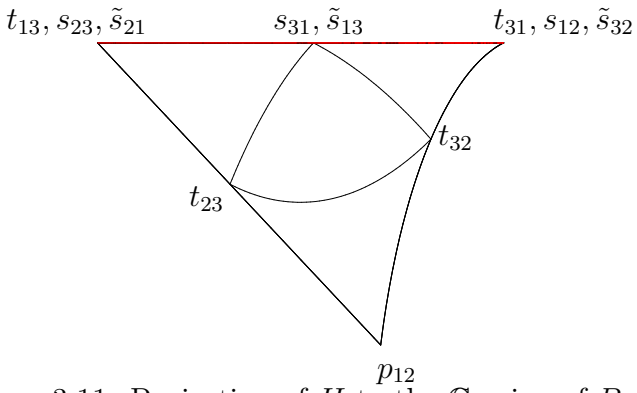

Figure 3.11: Projection of H to the $\mathbb{C}$-spine of $B_{T_2'}$

– Position of H: Recall that the 2-skeleton of H consists in η, π_1, π_2, τ_{11} and τ_{21}.
η is also in H' so it projects in the segment $[t_{13}t_{31}]$. For the pentagons we need the following lemma:

Lemma 3.5.1 *The four points p_{12}, $\tilde{s}_{21}$, t_{13}, t_{23} (respectively, p_{12}, s_{12}, t_{31}, t_{32}) lie in a common $\mathbb{R}$-plane.*

Proof. Indeed, as we have seen earlier, the triples $(p_{12}, \tilde{s}_{21}, t_{13})$, $(p_{12}, \tilde{s}_{21}, t_{23})$ and $(\tilde{s}_{21}, t_{13}, t_{23})$ each lie in an $\mathbb{R}$-plane because the pairs of geodesics $(p_{12}t_{13})$ and $(\tilde{s}_{21}t_{13})$, $(p_{12}t_{23})$ and $(\tilde{s}_{21}t_{23})$, $(\tilde{s}_{21}t_{13})$ and $(\tilde{s}_{21}t_{23})$ lie in pairwise orthogonal complex lines. Thus we have a tetrahedron of which 3 faces are $\mathbb{R}$-planar: by Proposition 3.2.9 this is possible only if the four points lie in the same $\mathbb{R}$-plane. □

We can now analyze the position of π_2. As we have just seen, the geodesic $(\tilde{s}_{21}t_{23})$ is contained in (a meridian of) $B_{T_2'}$, which also contains $(\tilde{s}_{21}s_{23})$ in a complex slice. Thus the intersection of the $\mathbb{R}$-plane containing π_2 with $B_{T_2'}$ is exactly a pair of geodesics, which are two sides of π_2, so that π_2 lies entirely on one side of $B_{T_2'}$, as in Figure 3.9.
We now use the other quadruple of points of the lemma: these lie on an $\mathbb{R}$- plane which is for instance a meridian of the bisector $B_{T_1'}$ having $(p_{12}t_{31})$ as real spine (and having the same $\mathbb{C}$-spine as $B_{T_2'}$). Thus the entire quadrilateral projects into the segment $[p_{12}t_{31}]$. We now know that the 1-skeleton of H projects to the appropriate side of $B_{T_2'}$, except maybe for the edge $[s_{31}t_{23}]$. This is the third side of the $\mathbb{C}$-planar triangle τ_{11}, whose two other sides, $[\tilde{s}_{21}t_{23}]$ and $(\tilde{s}_{21}s_{31})$, project as we have seen into the segments $[t_{13}p_{12}]$ and $[t_{13}t_{31}]$ respectively (see Figure 3.11). This gives us sufficient control over the third side. Indeed, the projection restricted to a complex face is holomorphic, thus an open and angle-preserving map. This rules out the possibility that the image of the edge $[s_{31}t_{23}]$ (which is an arc of hypercycle in the $\mathbb{C}$-spine of $B_{T_2'}$) pass through the real spine $(t_{13}p_{12})$ (see Figure 3.12; the first case is ruled out by "angle-preserving" and the second by "open"). We then conclude by saying that the image of H is bounded by the image of its boundary, using for instance the foliation of H by complex triangles.

– Position of the cone faces: As earlier the geodesics through p_{12} project to geodesics because p_{12} is in the complex line onto which we are projecting; moreover p_{12} is in

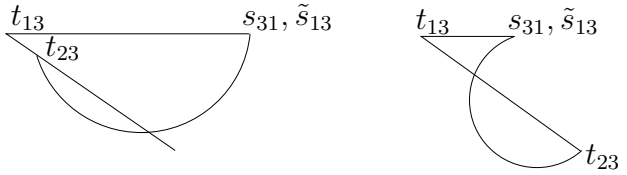

Figure 3.12: Non-admissible projections of a complex triangle

the real spine of $B_{T_2'}$, so that the cone on an object is entirely on the same side of $B_{T_2'}$ as that object.

□

- Side-pairings R_1 and R_2:

  This is the most delicate case because Π and its image cannot be separated by a bisector (or else this bisector would contain one of the pentagonal pyramids, which we have seen to be impossible).

  To prove that $R_1(\Pi)$ and Π have disjoint interiors, a possible approach would be to show that Π is contained in a fundamental domain for R_1 (as suggested to us by the referee). In fact R_1 acts on complex lines orthogonal to its mirror as a rotation. Therefore, the choice of a wedge (of angle $2\pi/p$) in each of these lines defines a fundamental domain for R_1. Unfortunately, there does not seem to be a simple global choice of such wedges.

  Instead we have to consider separately the core faces and the cone faces, and use the fact that if the interiors of the polyhedra were to meet, then so would the interiors of some of their 3-faces.

  Proposition 3.5.3

  $$\overset{\circ}{\Pi} \cap \overset{\circ}{R_1(\Pi)} = \emptyset$$

  Proof. We follow the lines given above, first separating the core faces (H and H', $R_1(H)$ and $R_1(H')$). The only obvious intersection between these faces is that of H and $R_1(H)$ (namely P_2), which live in the same bisector B_1.

  We first prove the following

  Lemma 3.5.2 *There exists a bisector B_{R_1} which separates $H \cup H'$ and $R_1(H \cup H')$. In particular, these two objects have disjoint interiors.*

  Observe that the four faces in question all have the edges $[\tilde{s}_{13}s_{23}]$ and $[s_{23}\tilde{s}_{21}]$ in common, so that a suitable bisector must contain these edges. In fact our bisector will contain the whole $\mathbb{R}$-plane $R_1(L_\tau)$ as a meridian.

  The most natural idea is to use one of the complex slices of B_1 as a $\mathbb{C}$-spine for our bisector (the $\mathbb{C}$-plane onto which we will project). For practical reasons we use the slice containing s_{23} and $\tilde{s}_{32}$ (this is the slice containing the largest section of H). We thus

define B_{R_1} by its real spine which is the geodesic joining s_{23} and its projection to the vertical axis $(t_{23}t_{32})$. The first thing to say is:

Lemma 3.5.3 *The bisectors B_1 and B_{R_1} intersect only along the common meridian $R_1(L_\tau)$.*

Proof. It is clear that B_1 and B_{R_1} share this meridian, because it contains both real spines. One can then invoke [Go] pg. 174, or use Proposition 3.2.9 on $\mathbb{R}$-planar tetrahedra to conclude. □

This shows that H is entirely on one side of B_{R_1} (and $R_1(H)$ on the other). Consider now H'; we examine each 2-face separately.

- The most obvious is the hexagon η, which also belongs to H.
- The $\mathbb{C}$-planar triangle τ'_{21} has an edge, $[s_{23}\tilde{s}_{21}]$, which is in B_{R_1}. That geodesic can be the only intersection between B_{R_1} and the $\mathbb{C}$-plane containing τ'_{21}, so that τ'_{21} is entirely on one side of B_{R_1}.
- The $\mathbb{R}$-planar pentagon π'_1 also has an edge which is in B_{R_1}, namely $[s_{23}\tilde{s}_{13}]$. Now this geodesic meets the $\mathbb{R}$-spine of B_{R_1}, in s_{23}, so that by Proposition 3.2.8 it can be the only intersection between the $\mathbb{R}$-plane $R_1(L_\tau)$ and B_{R_1}. Thus the whole pentagon is on one side of B_{R_1}.

So far, we know that the entire 1-skeleton of H' is on one side of B_{R_1}, except maybe for the edge $[\tilde{s}_{32}t_{31}]$. Now this edge meets the $\mathbb{C}$-spine of B_{R_1} (in $\tilde{s}_{32}$) so it projects to a geodesic and stays on the same side of B_{R_1} as its endpoints. Having the 1-skeleton, we extend the result to the 2-skeleton: the only non-obvious faces are a $\mathbb{C}$-planar triangle and an $\mathbb{R}$-planar pentagon of H', which are handled by Lemma 3.2.1. Finally, we get the corresponding result for all of H' by using the foliation of H' into $\mathbb{C}$-planar triangles.

Thus $H \cup H'$ is entirely on one side of B_{R_1}; the same arguments (replacing the $\mathbb{R}$-plane $R_1(L_\tau)$ by L_τ) prove that $H \cup H'$ is entirely on one side of $B_{R_1^{-1}}$ (the bisector analogous to B_{R_1}, but containing L_τ), so that in fact $H \cup H'$ is entirely in the "wedge" of angle $\frac{2\pi}{p}$ between B_{R_1} and $B_{R_1^{-1}}$ (see Figure 3.13).

We conclude by noting that R_1 rotates the $\mathbb{C}$-spine of B_{R_1} by an angle $\frac{2\pi}{p}$ (around the point image of t_{23}, t_{32}, p_{12}), sending the wedge off itself. □

To conclude the proof of the proposition, it remains to see what happens with the cone faces: we have already seen, when describing the self-intersection of Π, that the cones from p_{12} on H and H' have no other intersection than the cone on their intersection. There remain three intersecting pairs to analyze:

Lemma 3.5.4 *1.* $Cone(H') \cap Cone(R_1(H)) = Cone(H' \cap R_1(H))$

2. $Cone(H) \cap Cone(R_1(H')) = Cone(H \cap R_1(H'))$

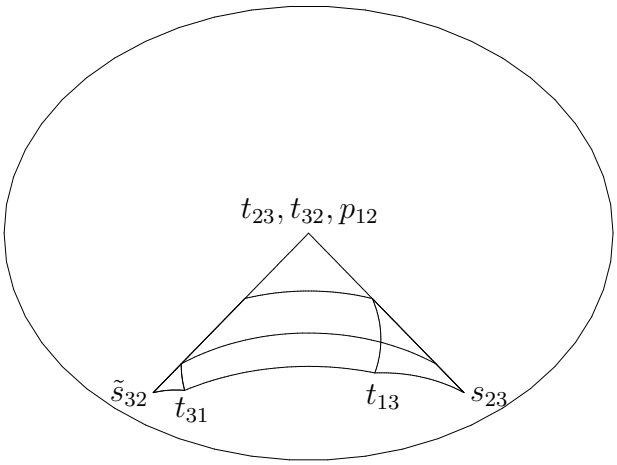

Figure 3.13: Projection of H and H' to the $\mathbb{C}$-spine of B_{R_1}

Proof. We start with the first item. We project the cones to both complex spines of B_1 and B_1'. If a geodesic containing p_{12} is in the intersection of the cones it projects onto a geodesic under both projections by Lemma 3.4.1. Such a geodesic will meet either H' or $R_1(H)$ first. The lemma is proven if we show that the geodesic meets H' and $R_1(H)$ at the same time. To see this, recall from section 3.4 that the projection of H' in the complex spine of B_1 is on the same side as p_{12} with respect to the real spine (which contains the projection of $R_1(H)$).

This shows that the geodesic meets H' first. Projecting to the complex spine of B_1' shows analogously that the same geodesic meets $R_1(H)$ first. Indeed, $R_1(H)$ is contained in B_1, on the same side of the surface S_η as H as can be seen slice by slice (if C is a slice of B_1, $S_\eta \cap C$ is a hypercycle, i.e. an arc of a Euclidean circle meeting twice the boundary circle, bounding $C \cap H$ and $C \cap R_1(H)$ is on the same side of this arc as that of $C \cap H$, see Figure 3.14); thus $R_1(H)$ is on the same side of B_1' as H and p_{12}.

The second item is proved analogously, noting that in a slice C of B_1, $C \cap H$ is on the same side of the hypercycle $C \cap R_1(S_\eta)$ as $C \cap R_1(H)$. □

Lemma 3.5.5 $Cone(H') \cap Cone(R_1(H')) = Cone(H' \cap R_1(H'))$

Proof. We project the cones on the complex spines of B_1' (which contains H') and $R_1(B_1')$ (which contains $R_1(H')$). Since p_{12} is in both complex spines, as in the previous lemma, the projections of the cones are cones over the projection by Lemma 3.4.1. The same argument as above will hold if we show that each projection is on the same side as p_{12} with respect to the corresponding real spine; we will refer to that side as the *good* side.

To show this, let us first consider the projection of $R_1(H')$ on the complex spine of B_1'. We check that the vertices of $R_1(H')$ are all in the same side of B_1' as p_{12}. That gives a hint that the whole 3-face $R_1(H')$ is in the good side. More precisely, we divide the proof in several steps:

1. We check numerically that $R_1(t_{13})$ and $R_1(t_{31})$ are in the good side of B_1'.

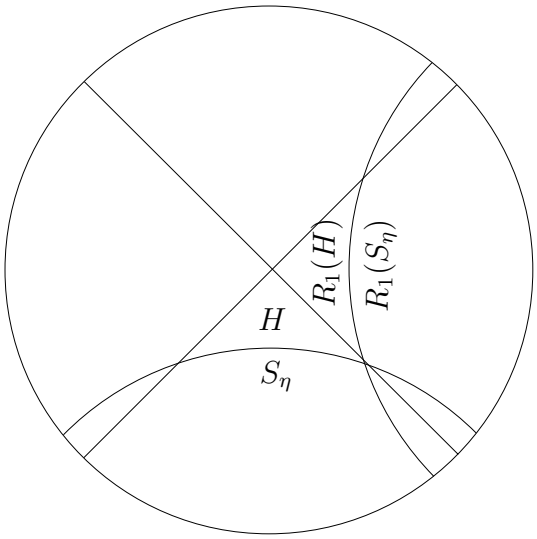

Figure 3.14: View of a complex slice of B_1 (for $p = 4$)

2. From the knowledge of $S_\eta = B_1 \cap B'_1$, which is a union of hypercycles, one in each slice of B_1, we obtain that $R_1(\eta)$ intersects S_η in precisely two geodesic segments $[\tilde{s}_{21}, s_{23}]$ and $[s_{23}, \tilde{s}_{13}]$ and, moreover, is contained in the good side of B'_1.

3. As the intersection of $R_1(\tau'_{11})$ (a slice of $R_1(H')$) with B'_1 is a hypercycle and contains the geodesic segment $[s_{23}, \tilde{s}_{13}]$, we conclude that $R_1(\tau'_{11})$ is in the good side.

4. We have to check that the pentagonal faces $R_1(\pi'_i)$, $i = 1, 2$, project on the good side. Observe that the Lagrangian pentagon $R_1(\pi'_2)$ has a geodesic in common with the bisector B'_1, namely $[\tilde{s}_{21}, s_{23}]$. Now the intersection of the whole Lagrangian with the bisector could contain at most one more geodesic, orthogonal to the first (see Proposition 3.2.8). However, if such a second geodesic existed and met the pentagon $R_1(\pi'_2)$, the vertices of $R_1(\pi'_2)$ would lie on both sides of this geodesic (because the pentagon has only right angles) and thus on both sides of B'_1. This is impossible since we have verified that all points are on the same side of B'_1. We conclude that the whole pentagon is on the good side.

   Concerning the other pentagon $R_1(\pi'_1)$, the same argument does not apply (because a priori it has no intersection with B'_1), and it remains to check that one of its edges is in the good side, namely the edge $[R_1(t_{13}), R_1(s_{23})]$. This is done in the next item.

5. We need to prove the following statement, which seems quite obvious on Figure 3.15: the geodesic segment between $R_1(t_{13})$ and $R_1(s_{23})$ does not intersect the bisector B'_1. Computer investigation shows that a stronger statement is true, namely that the entire geodesic (and not only the segment) does not intersect the relevant bisector. We shall explain how this can be done for the first case only, the second one being completely analogous.

   Let γ be the geodesic segment between $p = R_1 t_{13}$ and $q = R_1 s_{23}$. We claim that it never intersects the bisector B'_1 equidistant from p_{12} and p_{23}.

   We write $\gamma(x) = (1-x)p + xq/\langle q, p\rangle = v + xw$ (note the geodesic is not parameterized

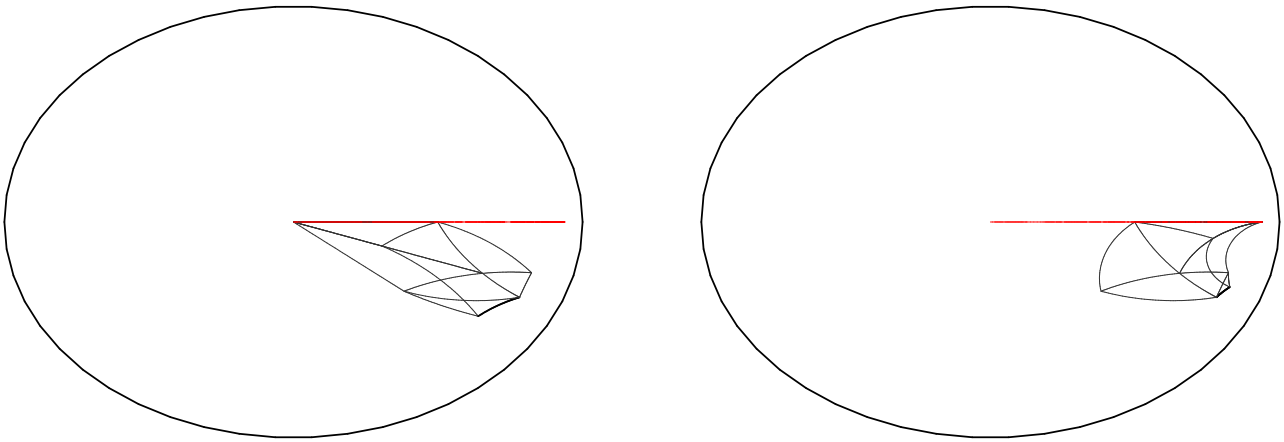

(a) $Cone(R_1(H'))$ projected onto $e_2^\perp$ (b) $Cone(H')$ projected onto $R_1(e_2^\perp)$

Figure 3.15: The straight line segments represent the spine of the relevant bisector, which we need to separate H' and $R_1(H')$. The thick segment is the only one that we need to check numerically. The pictures are drawn for $p = 3$ and $t = 1/18$.

with constant speed, so the parameter x should range through some interval, whose endpoints are irrelevant to our computation).

Any possible intersection of γ with B_1' would be found by solving the equation

$$|\langle v + xw, p_{12}\rangle| = |\langle v + xw, p_{23}\rangle| \tag{3.5.1}$$

Using the linearity of the Hermitian product and squaring both sides of the equation, we can rewrite it in the form of a quadratic equation

$$ax^2 + bx + c = 0 \tag{3.5.2}$$

where

$$a = |\langle w, p_{12}\rangle|^2 - |\langle w, p_{23}\rangle|^2 \tag{3.5.3}$$
$$b = 2\mathfrak{Re}\left(\langle v, p_{12}\rangle\langle p_{12}, w\rangle - \langle v, p_{23}\rangle\langle p_{23}, w\rangle\right) \tag{3.5.4}$$
$$c = |\langle v, p_{12}\rangle|^2 - |\langle v, p_{23}\rangle|^2 \tag{3.5.5}$$

It can easily be checked that the discriminant of this quadratic equation is negative for small phase shift. The values of $\Delta = b^2 - 4ac$ for the values of t corresponding to discrete groups with $p = 3$ are given in the following table:

t	Δ
0	$-0.2369\ldots$
1/30	$-0.2465\ldots$
1/18	$-0.2472\ldots$
5/42	$-0.2236\ldots$

6. The projection of the face $R_1(H')$ in the complex spine of B_1' is bounded by the image of its 2-skeleton because $R_1(H')$ is foliated by triangles in slices and the image

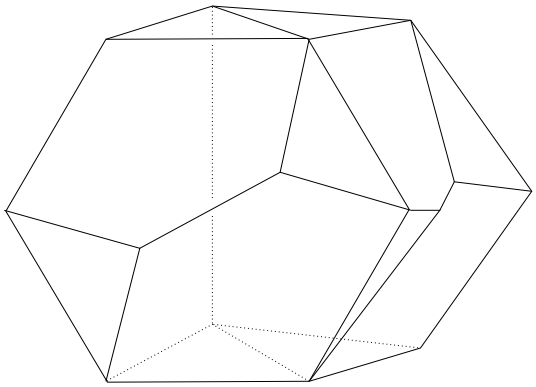

Figure 3.16: The 3-faces H' and $R_1(H')$ and H and $R_1(H)$. Note that H and $R_1(H)$ are contained in the bisector B_1.

by the projection (a holomorphic map) of each triangle is a triangle in the complex spine of B_1'. In fact it is also bounded by the projection of the 1-skeleton by Lemma 3.2.1. Using the items above we then conclude the proof that the projection of the face $R_1(H')$ in the complex spine of B_1' is in the good side.

The same argument shows that H' is in the good side of $R_1(B_1')$. In particular a key step is to show that the geodesic segment between t_{31} and $\tilde{s}_{32}$ does not intersect the bisector $R_1(B_1')$ (see again Figure 3.15).

To conclude the proof of the lemma we show as above, by projecting to both $\mathbb{C}$-spines, that the intersection on the cones over the bases has to contain a point of the intersection of the bases. □

The proposition follows from the three main lemmas. □

Second step: further along the cycles

In this section we verify condition **Cyclic** of the Poincaré theorem. Recall that for a cycle of codimension-2-faces ϕ_i:

$$\phi_1 \xrightarrow{g_1} \phi_2 \xrightarrow{g_2} \ldots \phi_k \xrightarrow{g_k} \phi_1$$

the cycle transformation $g_k \circ g_{k-1} \ldots \circ g_1$ has a certain finite order m (this is one of the hypotheses we have to check; the side-pairings g_i are explicit in matrix form which allows us to find m). We will call k the *length* of the cycle, and $m \cdot k$ its *total length*. Condition **Cyclic** ensures that the $m \cdot k$ images of Π:

$$g_1^{-1}(\Pi), (g_2 \circ g_1)^{-1}(\Pi), \ldots, ((g_k \circ g_{k-1} \ldots \circ g_1)^m)^{-1}(\Pi) = \Pi$$

tile a neighborhood of the face ϕ_1. In fact, each of these polyhedra shares a codimension-1-face with its two closest neighbors, so that we only need to check that all of these polyhedra have

pairwise disjoint interiors.

We have shown in the preceding section that this is true for all pairs of adjacent polyhedra (those differing by a side-pairing). This settles the case of all cycles of maximum total length 3; for greater total length we must check that Π and its non-adjacent images have disjoint interiors. We will start with the 3 cycles of total length 4, where we only need to compare Π with its "diagonal" image (see diagrams below). The cycles of total length 4 are:

- the pentagon cycle:

$$\pi_1 \xrightarrow{R_1} \pi_2 \xrightarrow{J} \pi_2' \xrightarrow{R_2^{-1}} \pi_1' \xrightarrow{J^{-1}} \pi_1$$

A schematic picture of the tiling of a neighborhood of the 2-face π_1 (represented by the central vertex) is:

$J^{-1}(\Pi) =$ $R_1^{-1}.J^{-1}.R_2(\Pi)$	Π
$J^{-1}.R_2^{-1}(\Pi)$ $= R_1^{-1}.J^{-1}(\Pi)$	$R_1^{-1}(\Pi)$

The fact that Π and its "diagonal" image $J^{-1}.R_2^{-1}(\Pi) = R_1^{-1}.J^{-1}(\Pi)$ have disjoint interiors follows easily from what we have already seen. Indeed, we know that the bisector B_1 separates Π and $J^{-1}(\Pi)$. Now R_1 fixes pointwise the $\mathbb{C}$-spine of B_1 (which is its mirror) and commutes with the orthogonal projection onto it, so that it preserves each of the half-spaces bounded by B_1.

Thus, applying R_1^{-1} to $J^{-1}(\Pi)$, we see that B_1 separates Π from $R_1^{-1}.J^{-1}(\Pi)$.

- the $\mathbb{R}$-planar triangle cycles:

$$\tau_{12} \xrightarrow{R_1} \tau_{13} \xrightarrow{(R_2R_1)^{-1}} \tau_{13}' \xrightarrow{R_2^{-1}} \tau_{12}' \xrightarrow{R_2R_1} \tau_{12}$$

$$\tau_{22} \xrightarrow{R_1} \tau_{23} \xrightarrow{R_1R_2} \tau_{23}' \xrightarrow{R_2^{-1}} \tau_{22}' \xrightarrow{(R_1R_2)^{-1}} \tau_{22}$$

A diagram for the first cycle is:

$R_2.R_1(\Pi) =$ $R_1^{-1}.R_2.R_1.R_2(\Pi)$	Π
$R_1^{-1}.R_2.R_1(\Pi)$ $= R_2.R_1.R_2^{-1}(\Pi)$	$R_1^{-1}(\Pi)$

As above, we can easily separate Π and its diagonal image $R_1^{-1}.R_2.R_1(\Pi) = R_2.R_1.R_2^{-1}(\Pi)$, this time by the bisector B_{T_1}. Indeed, B_{T_1} separates Π and $R_2.R_1(\Pi)$, as we have already seen, and as above R_1 preserves the half-spaces bounded by B_{T_1} (whose $\mathbb{C}$-spine is again the mirror of R_1), so that B_{T_1} separates Π and $R_1^{-1}.R_2.R_1(\Pi)$.

The second cycle is analogous.

Now the only other cycles with total length greater than 3 are the $\mathbb{C}$-planar triangle cycles:

$$\tau_{11} \xrightarrow{(R_2R_1)^{-1}} \tau'_{11} \xrightarrow{J^{-1}} \tau_{11}$$

$$\tau_{21} \xrightarrow{R_1R_2} \tau'_{21} \xrightarrow{J^{-1}} \tau_{21}$$

on one hand, which has length 2 but arbitrarily large total length, and:

$$\tau_{c1} \xrightarrow{R_1} \tau_{c1}$$

$$\tau_{c2} \xrightarrow{R_2} \tau_{c2}$$

on the other, of length 1 and of total length p (in our cases, $p = 3, 4$ or 5).

- We start with the first pair of cycles. The cycle transformations are respectively $(R_2R_1J)^{-1}$ and $J^{-1}R_1R_2$; they both fix pointwise a $\mathbb{C}$-plane, namely the one containing the triangle τ_{11} (resp. τ_{21}). Computing the eigenvalues of these two elements tells us that they act on $\mathbb{C}$-planes orthogonal to their mirror by multiplication by $\overline{\eta}i\overline{\varphi}^3$ (resp. $-\eta i\overline{\varphi}^3$), corresponding to rotations of angle $\pi(\frac{1}{2} - \frac{1}{p} \pm t)$. If the group is discrete, these elliptic elements are to have finite order. In fact, imposing the angles to be of the form $\frac{2\pi}{k}$, $\frac{2\pi}{l}$ with $k, l \in \mathbb{Z} \cup \{\infty\}$ is sufficient to obtain the cyclic condition for these two cycles, and thus discreteness of our group. Precisely:

Proposition 3.5.4 – *If $k = (\frac{1}{4} - \frac{1}{2p} + \frac{t}{2})^{-1} \in \mathbb{Z}$, the polyhedra*

$$\Pi,\ R_2R_1(\Pi),\ R_2R_1J(\Pi),\ ...,\ (R_2R_1J)^k(\Pi),\ (R_2R_1J)^kR_2R_1(\Pi)$$

have disjoint interiors. In fact, two of these share a common 3-face if they are adjacent, or else they only have the 2-face τ_{11} in common.

– *Analogously, if $l = (\frac{1}{4} - \frac{1}{2p} - \frac{t}{2})^{-1} \in \mathbb{Z}$,the polyhedra*

$$\Pi,\ (R_1R_2)^{-1}(\Pi),\ (R_1R_2)^{-1}J(\Pi),\ ...,\ ((R_1R_2)^{-1}J)^l(\Pi),\ ((R_1R_2)^{-1}J)^l(R_1R_2)^{-1}(\Pi)$$

have disjoint interiors, and two of them share a common 3-face if they are adjacent, or else they only have the 2-face τ_{21} in common.

Proof. We have just seen that the elements $(R_2R_1J)^{-1}$ and $J^{-1}R_1R_2$ act on $\mathbb{C}$-planes orthogonal to their mirror by certain rotations, the two integral conditions saying that these are of angle $\frac{2\pi}{k}$ and $\frac{2\pi}{l}$. Now we know that the $\mathbb{C}$-plane containing the points t_{23}, t_{32}, p_{12} (which is the common spine of bisectors B_1, B_{T_1}, B_{T_2}) is orthogonal to the mirrors of $(R_2R_1J)^{-1}$ and $J^{-1}R_1R_2$, at points t_{23} and t_{32} respectively. We project to this $\mathbb{C}$-plane, which contains the geodesic triangle (t_{23}, t_{32}, p_{12}), each of the sides being the real spine of one of the bisectors B_1, B_{T_1}, B_{T_2}. We have shown that the polyhedron Π is

entirely on one side of each of these bisectors, which means that its projection is entirely inside of the triangle (t_{23}, t_{32}, p_{12}). This proves the proposition. □

Remark 3.5.3 There are finitely many values of t for which the two numbers $(\frac{1}{4} - \frac{1}{2p} \pm \frac{t}{2})^{-1}$ are integers, listed in the following table:

p	$\lvert t\rvert < \frac{1}{2} - \frac{1}{p}$	$\lvert t\rvert = \frac{1}{2} - \frac{1}{p}$	$\lvert t\rvert > \frac{1}{2} - \frac{1}{p}$
3	$0, \frac{1}{30}, \frac{1}{18}, \frac{1}{12}, \frac{5}{42}$	$\frac{1}{6}$	$\frac{7}{30}, \frac{1}{3}$
4	$0, \frac{1}{12}, \frac{3}{20}$	$\frac{1}{4}$	$\frac{5}{12}$
5	$\frac{1}{10}, \frac{1}{5}$		$\frac{11}{30}, \frac{7}{10}$

Remark 3.5.4 It follows from what we have done that the group generated by $A = (R_2 R_1 J)^{-1}$ and $B = J^{-1} R_1 R_2$ is a $\mathbb{C}$-Fuchsian triangle goup, preserving the mirror of R_1. Indeed, one checks that the product AB acts on this complex geodesic as a rotation by an angle $2\pi/N$, where $N = \frac{2p}{6-p}$, fixing p_{12} (a geometric reason for this value can be found in [M1], p.243). In particular, a fundamental domain for its action is given by the union of the triangle τ_{c1} and its reflection about the geodesic $(t_{23}t_{32})$.

- Now consider the last cycles, where the cycle transformations are R_1 and R_2, of order $p = 3, 4$ or 5. For $p = 3$ there is nothing to add, but for $p = 4$ or 5 we must ensure that the non-adjacent polyhedra Π and $R_i^2(\Pi)$ have disjoint interiors. We do this by following the lines of the analogous verification for Π and $R_i(\Pi)$ (proof of proposition 3.5.3); in principlethe two non-adjacent polyhedra are easier to separate because they have a smaller intersection, however we lose some control over this intersection. Rather, we handle this by using the computer to check the position of the 16 core edges (as opposed to just 1 previously).

  The core faces are easily separated using the bisector B_{R_1} which was introduced in the proof of proposition 3.5.3:

  Lemma 3.5.6 *For $p = 4$ and 5, B_{R_1} separates $H \cup H'$ and $R_1^2(H \cup H')$.*

  Proof. This follows from what we have seen: we know that $H \cup H'$ projects to the $\mathbb{C}$-spine of B_{R_1} inside a wedge of angle $\frac{2\pi}{p}$ (see Figure 3.13) whose images under R_1^k $(k = 0, ..., p-1)$ tile this $\mathbb{C}$-plane. □

  As before, two of the three cases of intersections of cones are easily described (using arguments of elementary plane geometry on hypercycles). However the bases of the cones are now disjoint, so that the cones intersect only at the common apex p_{12}, as follows:

  Lemma 3.5.7 *1. $Cone(H') \cap Cone(R_1^2(H)) = \{p_{12}\}$*

  2. $Cone(H) \cap Cone(R_1^2(H')) = \{p_{12}\}$

  The last case, which requires some numerical verifications, is the following:

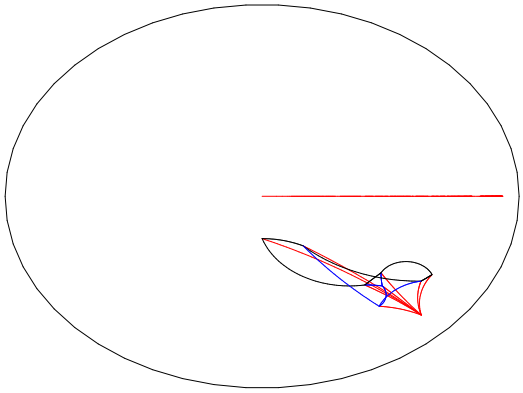

(a) $Cone(R_1^2(H'))$ projected onto $e_2^\perp$

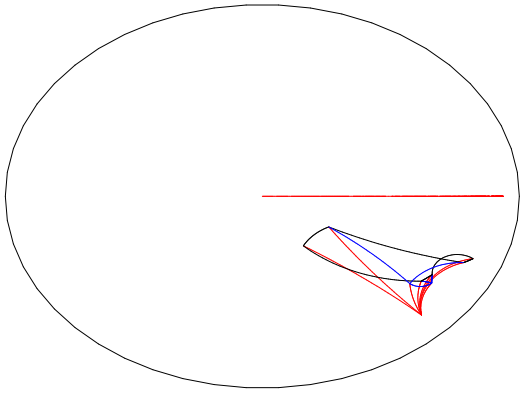

(b) $Cone(H')$ projected onto $R_1^2(e_2)^\perp$

Figure 3.17: $Cone(H')$ and $Cone(R_1^2(H'))$ intersect only in the point p_{12}, as can be seen by projecting each one onto the complex spine of the other. The pictures are drawn for $p = 5$ and $t = 1/5$.

Lemma 3.5.8 $Cone(H') \cap Cone(R_1^2(H')) = \{p_{12}\}$

Proof. As before, we consider simultaneously the projections to both complex spines of the bisectors containing the bases of the cones, namely B'_1 and $R_1^2(B'_1)$. Both complex spines contain the cone point p_{12}, so that the cones will behave well provided that the bases H' and $R_1^2(H')$ are on the appropriate side of these bisectors. Using the same arguments as earlier, we reduce this to a verification on the 1-skeleton of these 3-faces. It then remains to check the position of 16 edges for each face (32 in all), for every value of t where the integrality condition holds, listed in Remark 3.5.3. One way to do this is to plot the projection of these edges using a computer, as done in Figure 3.17. Note that the picture is fairly unambiguous in the sense that all edges are "very far" from the real spine, i.e. at a distance much larger than the implied precision. In principle, a detailed verification could also be written along the lines of part 5 of the proof of Lemma 3.5.5. □

3.6 Beyond the critical phase shift

In this section we describe the modification of the combinatorics of our polyhedron for $|t| \geq \frac{1}{2} - \frac{1}{p}$.

For small phase shift, the starting point of our construction is the hexagon η contained in the intersection of the two natural bisectors $B_1 = B(p_{12}, p_{13})$ and $B'_1 = J(B_1)$. Recall that the sides of the hexagon are contained in the complex geodesics polar to the points v_{ijk} (see section 3.2.4).

As already observed by Mostow, when $|t| = t_c := \frac{1}{2} - \frac{1}{p}$, the hexagon degenerates, three of its sides collapsing to points on the boundary (three of the v_{ijk}). After this critical value, the corresponding v_{ijk} are inside the ball (see Figure 3.18), and they replace their polar triangles in the construction of our polyhedron. More precisely, for $t > t_c$, the 3-face H simplifies to a tetrahedron with vertices v_{132}, v_{213}, v_{321} and t_{32}, having one $\mathbb{C}$-planar and two $\mathbb{R}$-planar faces

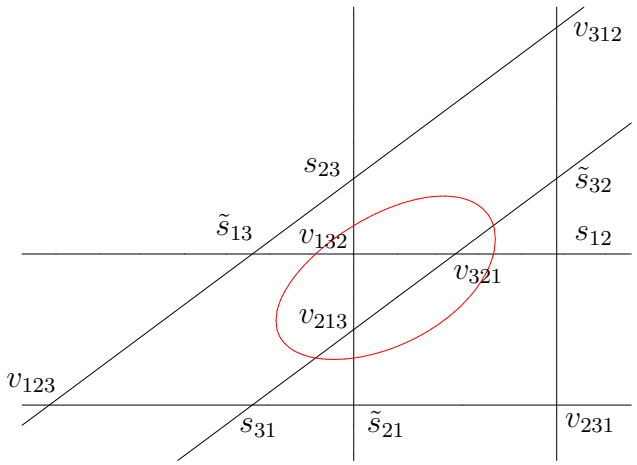

Figure 3.18: For large phase shift, some edges of the hexagon η are outside complex hyperbolic space. The corresponding face is a triangle, with vertices v_{132}, v_{213}, v_{321}, if $t > 0$.

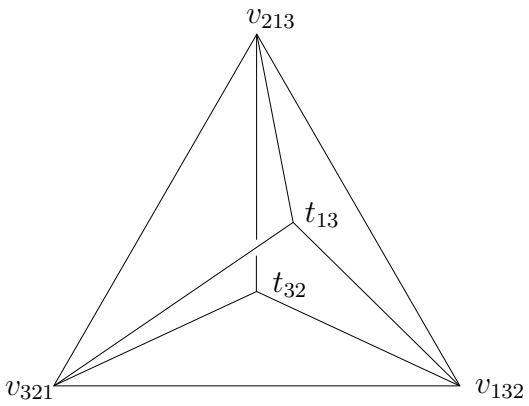

Figure 3.19: The core part $H \cup H'$ for large phase shift.

(see Figure 3.19). The whole polyhedron Π is then a cone over a union of two such tetrahedra, H and $J(H)$. Note that Π is non compact only for the critical values where $|t| = t_c$.

The side-pairings and cycles remain the same as earlier, removing those involving the 3-faces which have disappeared (namely T_1 and T_1' for $t > t_c$ and T_2 and T_2' for $t < -t_c$). In particular, there remains only one of the two integrality conditions from proposition 3.5.4.

Keeping these changes in mind, the arguments given above for small phase shift go through without any major modification. The main difference occurs for critical phase shift, since the hypotheses of the Poincaré polyhedron theorem include an extra verification at the cusps (see [FP]).

3.7 Comparison with Mostow's domains

In this section we comment on Mostow's fundamental domains for the groups $\Gamma(p,t)$ generated by R_1, R_2 and R_3 (for more details see [De]). The goal of his construction is to describe the Dirichlet fundamental domain centered at p_0. Mostow gives an explicit set of points in the orbit of p_0 that are supposed to describe all the faces of F, namely $R_i^{\pm 1}p_0$,$(R_iR_j)^{\pm 1}p_0$,$(R_iR_jR_i)^{\pm 1}p_0$

(a total of 24 points).

One then needs to prove that the corresponding 24 inequalities suffice. As explained in [M1], this can be done by using the appropriate version of the Poincaré polyhedron theorem, by verifying that the polyhedron bounded by the above 24 hypersurfaces has side pairings, compatible along the codimension two faces.

To explain what goes wrong in his agument, we observe that Mostow describes a polyhedron by giving each face of his k-skeleton, $0 \leq k \leq 3$, as the intersection of a number of bisectors (perhaps more than $4-k$ of them, some intersections not being transverse). Most of this skeleton is not geodesic, and in particular there are several instances of bigons, i.e. two different 1-faces with the same endpoints.

Mostow's verification that there are side pairings between the 3-faces is correct, but it is relatively easy to check numerically that, for some specific values of the parameters p and t, he missed some of the intersections between the 3-faces. This means that the polyhedron he uses is not simple, which makes it doubtful that it could be used in the context of a Poincaré polyhedron theorem.

Moreover, some of the verifications on the cycles of non totally geodesic 2-faces are incorrect, some of his 3-faces having (very tiny) extra intersections, that are easy to miss at first glance with coarse numerical experiments.

It turns out that for two of the groups (the ones with $p = 5$ and large phase shift, namely $\Gamma(5, 11/30)$ and $\Gamma(5, 7/10)$), there are more faces in the Dirichlet domain than expected, corresponding to $(R_i R_j)^{\pm 2} p_0$ (see [De]). Although this might seem only like a minor correction, it illustrates the difficulty in using Dirichlet domains in complex hyperbolic geometry. Even though the construction is quite canonical (it depends only on the choice of the point p_0), bisector intersections are too complicated to be practical.

The complexity of Dirichlet domains is explained in part by the fact that none of its codimension two faces can ever be in a Lagrangian plane. Indeed, any two bisectors bounding faces of a Dirichlet domain are coequidistant, since their complex spines all contain p_0 (see section 3.2.5). If their intersection were to contain a Lagrangian plane L, the real reflection fixing L would preserve both complex spines, hence fix their intersection point, which is a contradiction.

In Mostow's Dirichlet domains, certain pairs of 2-faces are close to a Lagrangian plane, in the sense that their vertices are all contained in such an $\mathbb{R}$-plane. These two non totally geodesic faces wrap around a certain Lagrangian quadrilateral contained in the Dirichlet domain, forming some kind of droplet contained in a bisector having the Lagrangian as a meridian (see the pictures in [M1], Figure 14.4 in pg. 239, and [De]). One expects this phenomenon to be due to the rigid nature of Dirichlet domains, and indeed we get rid of such faces in our fundamental domains.

3.8 Appendix: list of faces and combinatorial structure of Π

We will now list the (proper) faces of Π; the inclusions are obvious because the 1- and 2-faces are determined by their vertices. The 1-faces are all geodesic segments, and the 2-faces are either $\mathbb{R}$- or $\mathbb{C}$-planar or unions of geodesics from p_{12} to a segment (the hexagon η is apart).

This contrasts strongly with Mostow's Dirichlet domain, where faces shaped like "bubbles" occur, in the form of distinct 1-faces having the same endpoints and of distinct 2-faces having the same boundary.

- The ten 3-faces:
  These are of three types (and five isometry classes): the core faces H and H', the tetrahedra T_1, T_1', T_2, T_2' (where $T_i^{(\prime)}$ is the cone based on the triangle $\tau_{i1}^{(\prime)}$) and the pentagonal pyramids P_1, P_1', P_2, P_2' (where $P_i^{(\prime)}$ is the cone based on the pentagon $\pi_i^{(\prime)}$).

- The twenty-five 2-faces:
  These are of three types (and ten isometry classes):

  - The right-angled hexagon $\eta = (s_{12}, \tilde{s}_{13}, s_{23}, \tilde{s}_{21}, s_{31}, \tilde{s}_{32})$ living in the intersection of bisectors B_1 and B_1'
  - Four $\mathbb{R}$-planar right-angled pentagons:

$$\pi_1 = (t_{23}, s_{31}, \tilde{s}_{32}, s_{12}, t_{32})$$

$$\pi_2 = R_1(\pi_1) = (t_{23}, \tilde{s}_{21}, s_{23}, \tilde{s}_{13}, t_{32})$$

$$\pi_1' = J(\pi_1) = (t_{31}, s_{12}, \tilde{s}_{13}, s_{23}, t_{13})$$

$$\pi_2' = J(\pi_2) = (t_{31}, \tilde{s}_{32}, s_{31}, \tilde{s}_{21}, t_{13})$$

  - Twenty triangles:

    The faces of T_1:
    $\tau_{11} = (t_{23}, s_{31}, \tilde{s}_{21})$ ($\mathbb{C}$-planar)
    $\tau_{12} = (t_{23}, s_{31}, p_{12})$ ($\mathbb{R}$-planar)
    $\tau_{13} = (t_{23}, \tilde{s}_{21}, p_{12})$ ($\mathbb{R}$-planar)
    $\tau_{14} = (p_{12}, s_{31}, \tilde{s}_{21})$ (generic)

    The faces of T_2:
    $\tau_{21} = (t_{32}, s_{12}, \tilde{s}_{13})$ ($\mathbb{C}$-planar)
    $\tau_{22} = (t_{32}, s_{12}, p_{12})$ ($\mathbb{R}$-planar)
    $\tau_{23} = (t_{32}, \tilde{s}_{13}, p_{12})$ ($\mathbb{R}$-planar)
    $\tau_{24} = (p_{12}, s_{12}, \tilde{s}_{13})$ (generic)

    The faces of T_1':
    $\tau_{11}' = (t_{31}, s_{12}, \tilde{s}_{32})$ ($\mathbb{C}$-planar)
    $\tau_{12}' = (t_{31}, s_{12}, p_{12})$ ($\mathbb{R}$-planar)
    $\tau_{13}' = (t_{31}, \tilde{s}_{32}, p_{12})$ ($\mathbb{R}$-planar)
    $\tau_{14}' = (p_{12}, s_{12}, \tilde{s}_{32})$ (generic)

    The faces of T_2':
    $\tau_{21}' = (t_{13}, s_{23}, \tilde{s}_{21})$ ($\mathbb{C}$-planar)

$\tau'_{22} = (t_{13}, s_{23}, p_{12})$ ($\mathbb{R}$-planar)
$\tau'_{23} = (t_{13}, \tilde{s}_{21}, p_{12})$ ($\mathbb{R}$-planar)
$\tau'_{24} = (p_{12}, s_{23}, \tilde{s}_{21})$ (generic)

And four triangles belonging to two pentagonal pyramids:
$\tau_{c1} = (t_{23}, t_{32}, p_{12})$ ($\mathbb{C}$-planar)
$\tau_{c2} = (t_{13}, t_{31}, p_{12})$ ($\mathbb{C}$-planar)
$\tau_{g1} = (s_{31}, \tilde{s}_{32}, p_{12})$ (generic)
$\tau_{g2} = (s_{23}, \tilde{s}_{13}, p_{12})$ (generic)

- The twenty-six edges (1-faces):

  These are the sixteen edges of the core part (6 for the hexagon, adding 5 for each of H and H') together with the ten edges joining the ten vertices of the core part to the cone point p_{12}.

- The eleven vertices (0-faces):

  These are the vertices of the hexagon: $s_{12}, \tilde{s}_{13}, s_{23}, \tilde{s}_{21}, s_{31}, \tilde{s}_{32}$ together with vertices t_{23}, t_{32} of H, t_{13}, t_{31} of H' and the cone point p_{12}.

Bibliography

[C] H. S. M. Coxeter; Regular Complex Polytopes. Cambridge University Press (1991).

[DM] P. Deligne, G. D. Mostow; *Monodromy of hypergeometric functions and non-lattice integral monodromy*. Publ. Math. IHES **63** (1986), 5–89.

[De] M. Deraux; *Dirichlet domains for the Mostow lattices*. To appear in Experimental Math..

[FK] E. Falbel, P.-V. Koseleff; *Rigidity and flexibility of triangle groups in complex hyperbolic geometry*. Topology **41**, no. 4 (2002), 767–786.

[FPa] E. Falbel, J. Paupert; *Fundamental domains for finite subgroups in $U(2)$ and configurations of Lagrangians*. Geom. Ded. **109** (2004), 221–238.

[FP] E. Falbel, J.R. Parker; *The Geometry of the Eisenstein-Picard modular group*. To appear in Duke Math. Journal.

[Gi] G. Giraud; *Sur certaines fonctions automorphes de deux variables*. Ann. ENS **38** (1921), 43–164.

[Go] W.M. Goldman; Complex Hyperbolic Geometry. Oxford Mathematical Monographs. Oxford Science Publications (1999).

[Mas] B. Maskit; Kleinian Groups. Springer-Verlag (1988).

[M1] G. D. Mostow; *On a remarkable class of polyhedra in complex hyperbolic space*. Pacific J. Mathematics **86** (1980), 171–276.

[M2] G. D. Mostow; *Generalized Picard lattices arising from half-integral conditions*. Inst. Hautes Études Sci. Publ. Math. **63** (1986), 91–106.

[Pi] E. Picard; *Sur les fonctions hyperfuchsiennes provenant des séries hypergéométriques de deux variables*. Ann. ENS III, **2** (1885), 357–384.

[Sz1] R. E. Schwartz; *Real hyperbolic on the outside, complex hyperbolic on the inside*. Invent. Math. **151** (2003), no. 2, 221–295.

[Sz2] R. E. Schwartz; *Complex hyperbolic triangle groups*. Proceedings of the International Congress of Mathematicians, Vol. II (Beijing, 2002), 339–349, Higher Ed. Press, Beijing, 2002.

Chapter 4

Elliptic triangle groups in $PU(2,1)$, Lagrangian triples and momentum maps

4.1 Introduction

What we call an *elliptic triangle group* in $PU(2,1)$ is a subgroup generated by two elliptic elements A and B such that the product AB is elliptic. We address here the following question: in such a group, what are the possible conjugacy classes for the product AB when A and B are each in a fixed conjugacy class?

It is a classical problem in a linear group to characterize the possible eigenvalues of matrices $A_1, ..., A_n$ satisfying $A_1...A_n = 1$. In the group $GL(n, \mathbb{C})$, this question, known as the Deligne-Simpson problem, has arisen from the study of so-called Fuchsian differential systems on Riemann's sphere $\mathbb{C}P^1$ and is closely related to the Riemann-Hilbert problem (Hilbert's 21^{st} problem); see [Ko] for a survey of these questions and the partial answers which are known so far. The antipodal case of the compact group $U(n)$ has also been extensively studied and essentially solved in [AW], [Be], [Bi2], [Kl1]; it is related to many surprising branches of mathematics as is pointed out in the surveys [F] and [Kl2]. The case of $U(n)$ is also studied in relation with Lagrangian subspaces and reflections of $\mathbb{C}^n$ in [FW], from which we have adapted some ideas to the setting of the non-compact group $PU(2,1)$.

Recall that an elliptic conjugacy class in $PU(2,1)$ is characterized by an unordered pair of angles (see chapter 1); our question amounts to determining the image in the surface $\mathbb{T}^2/\mathfrak{S}_2$ of the group product map restricted to a product $C_1 \times C_2$ of two conjugacy classes. This map is an example of a momentum map on the quasi-Hamiltonian space $C_1 \times C_2$, as defined in [AMM], which is a group-valued generalization of classical (Lie algebra-valued) momentum maps associated to Hamiltonian group actions on a symplectic manifold.

In the classical case there are general theorems which ensure that the image is convex, the most famous of which is the Atiyah-Guillemin-Sternberg theorem (see [A], [GS1], [GS2]), which states, in the case of a torus action on a compact connected symplectic manifold, that the image is a convex polytope, the convex hull of the image of fixed points under the group action. In the case of non-compact group actions, some conditions on the target are required (see [W1]) to obtain such a convexity theorem. Note also that all results in the non-compact case require the momentum map to be proper, which is not the case here (the conjugacy classes are not compact, and the product may remain bounded when each factor goes off to infinity).

In another direction, [AMM] contains an analogous convexity theorem for group-valued momentum maps, but only in the case of a compact group (see also [Sf]). In the present case, when the group is non-compact and the target is the group itself, there is presently no such convexity result. In fact we have examples where the image is a non-convex union of segments, but these arise in cases where both conjugacy classes are degenerate in the sense that their elements have large centralizers, in which case they are not "strongly stable" as defined by Weinstein in [W1] (although he imposes this condition at the target).

The first part of this chapter is devoted to the determination of the image of the momentum map, a polygon in the surface $\mathbb{T}^2/\mathfrak{S}_2$. We will use a direct approach based on a careful explicit description of the reducible groups (in the sense of linear representations, in our case those groups fixing a point in $\mathbb{C}P^2$), the main idea (inspired by the analogous question in $U(n)$ studied in [FW]) being that points corresponding to irreducible groups project to interior points of the image, because the momentum map is of maximal rank at such a point. The main result is theorem 4.2.1 which is a convexity result reminiscent of that of Atiyah-Guillemin-Sternberg.

The second part of the chapter is devoted to a related question (in fact, a question con-

tained in the preceding one), namely that of the classification of triples of pairwise intersecting Lagrangian subspaces of $H^2_{\mathbb{C}}$ (or $\mathbb{R}$-planes). These two questions are related through the group generated by the corresponding $\mathbb{R}$-reflections (antiholomorphic involutions fixing pointwise an $\mathbb{R}$-plane) as follows. If L_1, L_2, L_3 are three $\mathbb{R}$-planes intersecting inside $H^2_{\mathbb{C}}$, with associated $\mathbb{R}$-reflections σ_1, σ_2, σ_3 then the holomorphic subgroup generated by $A = \sigma_2\sigma_1$ and $B = \sigma_3\sigma_2$ is an elliptic triangle group as defined above. The converse relation, going from an elliptic subgroup to a Lagrangian decomposition, is not obvious. The dimension count tells us that in general, a given pair of elliptic transformations A and B is not simultaneously decomposable into $\mathbb{R}$-reflections as above (for instance, a generic elliptic conjugacy class in $PU(2,1)$ has dimension 6, whereas Lagrangians possibly decomposing a pair A, B, fixing A and letting B vary inside this class have dimension 3). However it seems as in the case of $U(n)$ (see the main result of [FW]), that with fixed conjugacy classes for A and B the image polygon should be the same; we have strong evidence in favor of this but lack a complete proof. We also compute at the end of the section a parametrization of triples of $\mathbb{R}$-planes for two given angle pairs, which allows us to draw some experimental pictures (thanks to which most of the phenomena we describe were discovered) and mostly to parametrize possible generators for candidates of discrete groups.

The last two sections are devoted to a detailed study of examples, the main example, which motivated this work, being that where the generators A and B have angle pairs $\{0, 2\pi/3\}$ and $\{2\pi/3, -2\pi/3\}$. This corresponds to generators for Mostow's lattices $\Gamma(3,t)$ defined in [M1]. The image is in that case a triangle, inside of which the family considered by Mostow is a segment going from one side to the other, see figures 4.13 and 4.22 (the lattices comprise 8 points inside this segment). The geometric impression is clear: it would be very surprising not to find other discrete groups (hopefully some nonarithmetic lattices) inside this picture. We finish by describing how we intend to approach this question in practice, and give some of the candidates which we have (only) started to investigate.

4.2 Elliptic triangle groups, a polygon of configurations

4.2.1 Introduction

In this section we describe the image of our momentum map $\tilde{\mu}$ in the surface $\mathbb{T}^2/\mathfrak{S}_2$ (see section 4.2.2 for a precise definition of $\tilde{\mu}$). We first describe in detail the collection of reducible points (in the sense that these are the images of pairs (A,B) which generate a reducible linear group), the main idea being that irreducible points project to interior points of the image, so that the image will be a union of the *chambers* bounded by the *reducible walls* (we will make these terms precise later on).

Reducible groups are here of two types, according to whether the fixed point of the action is inside or outside of complex hyperbolic space (it cannot be on the boundary if the generators are elliptic). When the fixed point is inside complex hyperbolic space, the group $\Gamma = \langle A, B\rangle$ is conjugate to a subgroup of $U(2)$ which is the stabilizer of a point in $PU(2,1)$; in that case we will say that Γ is *spherical reducible*. When the fixed point is outside complex hyperbolic space, the group $\Gamma = \langle A, B\rangle$ is conjugate to a subgroup of $P(U(1)\times U(1,1))$ which is the stabilizer of a complex geodesic, or $\mathbb{C}$-plane; in that case we will say that Γ is *hyperbolic reducible*. There are two special points which are both spherical reducible and hyperbolic reducible: these are

Figure 4.1: A configuration of reducibles

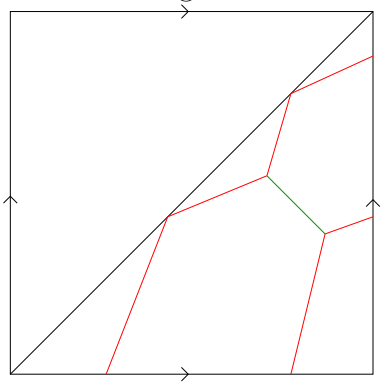

the points where Γ is Abelian (in other words the two matrix generators have a common basis of eigenvectors). We will call these two groups *totally reducible*.

The image of all these reducible groups in $\mathbb{T}^2/\mathfrak{S}_2$ is then a trivalent graph with two vertices, with the following properties (which we will prove in section 4.2.3). The two vertices are the images of the two totally reducible groups. They are joined by a line segment of slope -1 which is the image of the spherical reducible groups. Two other segments emanate from each vertex, one of slope 2 and the other of slope $1/2$ corresponding to the two hyperbolic reducible families containing the vertex. Note that the slope of a line is well defined in the torus, but is only defined up to inversion in the quotient $\mathbb{T}^2/\mathfrak{S}_2$. Here we will use once and for all the same affine chart for $\mathbb{T}^2/\mathfrak{S}_2$, namely the lower half of the square, as in figure 4.1. Note that the sides of the square in this chart have a geometric meaning (in other words, the torus is not homogeneous) because they correspond to special conjugacy classes. In fact there is a subtlety because a point on one of these sides can represent two distinct conjugacy classes, one comprising $\mathbb{C}$-reflections (i.e. elliptic elements fixing a $\mathbb{C}$-plane) and the other parabolic transformations; these two classes are indistinguishable from the point of view of angles or trace (compare with Goldman's triangle in the complex plane of traces on pp. 204–205 of [G]; see also chapter 1). This ambiguity is greater at the three vertices of the triangle (all identified in the quotient) which represent the identity and all unipotent isometries (these are the Heisenberg translations on the boundary $\partial H^2_{\mathbb{C}} = H^3$).

We will denote by $W_{red} \subset \mathbb{T}^2/\mathfrak{S}_2$ the image of all reducible groups; each linear segment of W_{red} will be called a *wall*. The complete description of this reducible framework, including a justification of the above facts and a classification of admissible types, occupies section 4.2.3. Now W_{red} **together with the two axes** $\{0\} \times S^1$ **and** $S^1 \times \{0\}$ disconnect $\mathbb{T}^2/\mathfrak{S}_2$ into a union of open convex polygons which we will call *chambers* (see section 4.2.5 for the appropriate notion of convexity). A detailed analysis shows that there are at most 9 of these chambers. We will call *closed chamber* the union of a chamber, its bounding reducible walls and the eventual points of the axes which are on the boundary of the chamber and correspond to an elliptic product.

The fact that the momentum map is of maximal rank at irreducible groups shows that its image is a union of chambers (together with their bounding walls), see section 4.2.4. The main question that remains, and which we haven't been able to answer in full generality for the time being, is to know exactly which chambers are in the image (we lack general arguments to exclude all superfluous chambers). The most we can say is the following result; the map $\tilde{\mu}$ is

the momentum (product) map, appropriately restricted, followed by projection to $\mathbb{T}^2/\mathfrak{S}_2$ (see section 4.2.2).

Theorem 4.2.1 *Let C_1 and C_2 be two elliptic conjugacy classes in $PU(2,1)$, at least one of which is not a class of complex reflections. Then the image of the map $\tilde{\mu}$ in $\mathbb{T}^2/\mathfrak{S}_2$ is a union of closed chambers, containing in a neighborhood of each totally reducible vertex the convex hull of the reducible walls containing that vertex.*

This is reminiscent of the result of Atiyah-Guillemin-Sternberg, knowing that in this case reducible groups are what come closest to fixed points under the action of $PU(2,1)$ by conjugation (they have the smallest orbits).

Concerning the hypothesis on C_1 and C_2, it is easily seen that two complex reflections always generate a reducible group because their mirrors (fixed $\mathbb{C}$-planes) intersect in $\mathbb{C}P^2$, so in that case the image is a non-convex union of segments; see section 4.4.3.

4.2.2 The group product: a group-valued momentum map

The setting is that of the group $G = PU(2,1)$ which is a real semisimple Lie group, connected but not simply-connected, and non compact (more precisely, with real rank one). Each of these characteristics has its importance in the study of the momentum map which we now introduce. The most basic feature of this Lie group is its group product; in our setting, we are interested in the behavior (principally, the image) of this map restricted to a product of two fixed conjugacy classes. More precisely, let C_1 and C_2 be two conjugacy classes of elliptic elements in $PU(2,1)$; we consider the map:

$$\begin{array}{rccc} \mu: & C_1 \times C_2 & \longrightarrow & G \\ & (A,B) & \longmapsto & AB \end{array}$$

$C_1 \times C_2$ is a typical example of a quasi-Hamiltonian G-space (the G-action being by conjugation on each factor), as defined in [AMM] (see also chapter 4 of [Sf] for more details) with an associated group-valued momentum map which is simply the product μ. The classical notion of a momentum map associated with a Hamiltonian group action on a symplectic manifold can be found for instance in [W2], with a survey of different directions of generalization.

In fact, we are only concerned here with the conjugacy class of the product and we restrict ourselves to the case when this product is elliptic, so that we consider the map:

$$\tilde{\mu} : (C_1 \times C_2) \cap \mu^{-1}(\{\text{elliptics}\}) \xrightarrow{\mu} G \xrightarrow{\pi} \mathbb{T}^2/\mathfrak{S}_2$$

where π denotes the projection from G to the set of its conjugacy classes (recall that an elliptic conjugacy class in $PU(2,1)$ is characterized by, and identified to, an unordered pair of angles, see chapter 1). Note that we might have lost the quasi-Hamiltonian structure by restricting μ to $\mu^{-1}(\{\text{elliptics}\})$; however when this structure is needed we can restrict a bit more, to $\mu^{-1}(\{\text{regular elliptics}\})$ which is an open subset of $C_1 \times C_2$ and thus inherits the quasi-Hamiltonian structure (recall that a regular elliptic element is one whose angles are distinct and non-zero, see [G] p. 203).

We will analyze in more detail the differential properties of this map in sections 4.2.4 and 4.2.5.

4.2.3 Walls and reducible groups

In this section we describe in detail the collection W_{red} of reducible walls. The two elliptic conjugacy classes C_1 and C_2 are given by two angle pairs $\{\theta_1, \theta_2\}$ and $\{\theta_3, \theta_4\}$ normalized so that $\theta_i \in [0; 2\pi[$. We will look at the image of $\tilde{\mu}$ in the affine chart $\{(\theta_5, \theta_6) | \, \theta_i \in [0; 2\pi[, \theta_5 \geqslant \theta_6\}$ of $\mathbb{T}^2/\mathfrak{S}_2$ (we will use unordered pairs as long as we don't know which coordinate is larger).

As we have said, W_{red} is a trivalent graph with two vertices $D_1 = \{\theta_1 + \theta_3, \theta_2 + \theta_4\}$ and $D_2 = \{\theta_2 + \theta_3, \theta_1 + \theta_4\}$; these vertices are joined by the segment U of spherical reducible groups which has slope -1. If the two vertices have same index as defined in [FW] (this means that they are on the same antidiagonal line in the affine chart), then U is simply the line segment joining them. If they have distinct indices (meaning that they are on two parallel antidiagonal lines in the affine chart), then U is the segment (disconnected in the affine chart) joining them by going through the sides of the square. Note that in both cases U is the shortest geodesic segment joining the vertices.

Each vertex is also the endpoint of two segments of hyperbolic reducible groups which go to the boundary of the square (and may even sometimes wrap once around the torus, see below), one of slope 2 and the other of slope 1/2. We will label these segments C_{13} and C_{24} through D_1, and C_{23} and C_{14} through D_2 (the notation will become clear below).

Totally reducible groups: the two vertices

These two points are the angle pairs of the product AB when A and B are simultaneously in diagonal form. Write these as $A = Diag(e^{i\theta_1}, e^{i\theta_2}, 1)$ and $B = Diag(e^{i\theta_3}, e^{i\theta_4}, 1)$ and we obtain $D_1 = \{\theta_1 + \theta_3, \theta_2 + \theta_4\}$; using $B = Diag(e^{i\theta_4}, e^{i\theta_3}, 1)$, we obtain $D_2 = \{\theta_1 + \theta_4, \theta_2 + \theta_3\}$.

Groups fixing a point

The question of eigenvalues of the product of matrices with fixed conjugacy classes in $U(2)$ has been studied in [Bi1] from the point of view of holomorphic bundles over the projective line, and in [FMS] from the point of view of the geometry of Lagrangian triples in $\mathbb{C}^2$. We will begin by quoting from [FW] the following description of the allowed region for these eigenvalues, which they obtain by following the Biswas' method.

Their notation is a bit different from ours because they consider representations in $U(2)$ of the fundamental group of the thrice-punctured sphere with presentation

$$\langle A, B, C \mid A.B.C = 1 \rangle$$

The conditions involve the notion of *index* I of a representation which is an integer; in the notation of [FW], I is the sum of angles of all six eigenvalues of the generators, each normalized in $[0, 1[$. In the case of Lagrangian representations (see next section), this index is in one-to-one correpondence with the Maslov index (or inertia index) of the Lagrangian triple. In our notation, the index of the representation (given by A, B and $(AB)^{-1}$) is written:

$$I = 2 + \frac{1}{2\pi}(\theta_1 + \theta_2 + \theta_3 + \theta_4 - \theta_5 - \theta_6)$$

The result is then that the allowable region for the sextuples of angles is a union of convex polyhedra in parallel hyperplanes corresponding to admissible integer values of the index I. The explicit inequalities involve the following quantities:

- $MM := \mathrm{Max}\{\theta_1, \theta_2\} + \mathrm{Max}\{\theta_3, \theta_4\}$
- $mm := \min\{\theta_1, \theta_2\} + \min\{\theta_3, \theta_4\}$
- $Mm := \mathrm{Max}\{\min\{\theta_1, \theta_2\} + \mathrm{Max}\{\theta_3, \theta_4\}, \mathrm{Max}\{\theta_1, \theta_2\} + \min\{\theta_3, \theta_4\}\}$

Proposition 4.2.1 (see [Bi1], [FW]) *Let $A, B \in U(2)$ with respective angles $\{\theta_1, \theta_2\}$ and $\{\theta_3, \theta_4\}$, with $\theta_i \in [0; 2\pi[$. Then the possible angle pairs for the product AB are (θ_5, θ_6) (with $\theta_i \in [0; 2\pi[$ and $\theta_5 \geqslant \theta_6$) satisfying one of the following conditions:*

- *$I = 2$ (i.e. $\theta_5 + \theta_6 = \theta_1 + \theta_2 + \theta_3 + \theta_4$) and:*

$$\begin{cases} \theta_5 & \geqslant & Mm \\ \theta_6 & \geqslant & mm \end{cases}$$

- *$I = 3$ (i.e. $\theta_5 + \theta_6 = \theta_1 + \theta_2 + \theta_3 + \theta_4 - 2\pi$) and:*

$$\begin{cases} \theta_5 & \geqslant & MM - 2\pi \\ \theta_6 & \geqslant & Mm - 2\pi \\ \theta_6 & \leqslant & MM - 2\pi \end{cases}$$

- *$I = 4$ (i.e. $\theta_5 + \theta_6 = \theta_1 + \theta_2 + \theta_3 + \theta_4 - 4\pi$) and:*

$$\begin{cases} \theta_5 & \geqslant & Mm - 2\pi \\ \theta_6 & \geqslant & mm - 2\pi \end{cases}$$

The geometric picture is not obvious from these inequalities; in fact, for fixed pairs $\{\theta_1, \theta_2\}$ and $\{\theta_3, \theta_4\}$, one of the three cases above is empty, if not two. We now translate this result in our setting. The image is then simply the convex segment joining the vertices D_1 and D_2, i.e. the shortest geodesic segment between them, see section 4.2.5. Note that this shortest segment is always included in a -1-sloped line of the torus, even when the segment is disconnected in the affine chart.

Proposition 4.2.2 *Let $A, B \in U(2)$ with respective angles $\{\theta_1, \theta_2\}$ and $\{\theta_3, \theta_4\}$, with $\theta_i \in \mathbb{R}/2\pi\mathbb{Z}$. Then the angles of the product AB are any pair $\{\theta_5, \theta_6\}$ lying in the convex segment of $\mathbb{T}^2/\mathfrak{S}_2$ joining the two totally reducible vertices $D_1 = \{\theta_1+\theta_3, \theta_2+\theta_4\}$ and $D_2 = \{\theta_2+\theta_3, \theta_1+\theta_4\}$.*

Concretely, in the affine chart $\{(\theta_5, \theta_6) |\, \theta_i \in [0; 2\pi[, \theta_5 \geqslant \theta_6\}$ of $\mathbb{T}^2/\mathfrak{S}_2$, this segment is:

- *the usual Euclidian segment (of slope -1) joining D_1 and D_2 if these two vertices have same index.*
- *the union of two Euclidian segments of slope -1, each going from a vertex to the horizontal or vertical boundary of the chart, if the vertices have different index .*

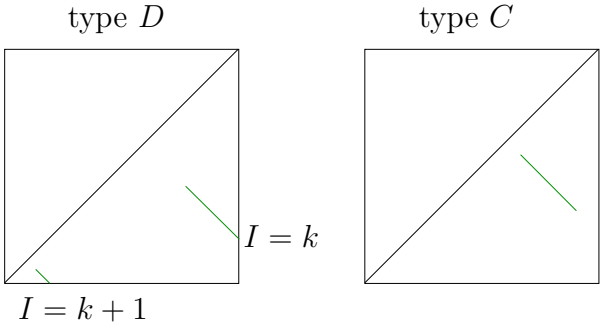

Figure 4.2: Configurations of spherical reducible groups

We will call such a configuration of *type C* (connected) in the first case, and of *type D* (disconnected) in the second case, see figure 4.2. Note that the fact that all these points lie on a common line of slope -1 of the torus simply expresses that the determinant of the product is the product of determinants.

Hyperbolic reducible groups

We now focus on the hyperbolic reducible groups, those which stabilize a $\mathbb{C}$-plane (or complex geodesic), that is a copy of $H^1_{\mathbb{C}}$ in $H^2_{\mathbb{C}}$. The decription simply comes from analyzing the product of matrices in block-diagonal form in $U(2,1)$, together with a characterization of the (oriented) angles of a triangle in the hyperbolic plane.

The totally reducible groups each stabilize two $\mathbb{C}$-planes intersecting at the common fixed point, so we expect that, by deformation, the corresponding vertex will be contained in two distinct hyperbolic reducible families. This is indeed the case, except in the degenerate cases when one generator (or both) is a $\mathbb{C}$-reflection (one angle is 0) or a complex reflection in a point (two equal angles). For instance, in matrix form, one hyperbolic reducible family containing the vertex D_1, which we will denote by C_{24}, is given by the following generators:

$$A = \begin{pmatrix} e^{i\theta_1} & 0 & 0 \\ 0 & e^{i\theta_2} & 0 \\ 0 & 0 & 1 \end{pmatrix} \quad \text{and} \quad B = \begin{pmatrix} e^{i\theta_3} & 0 & 0 \\ 0 & b_1 & b_2 \\ 0 & b_3 & b_4 \end{pmatrix}$$

where the conjugacy class of:

$$\widetilde{B} = \begin{pmatrix} b_1 & b_2 \\ b_3 & b_4 \end{pmatrix} \in U(1,1)$$

is given by its eigenvalues: $e^{i\theta_4}$ of positive type and 1 of negative type (this simply means that $\widetilde{B}$ acts on $H^1_{\mathbb{C}}$ by a rotation of θ_4). Recall that the type of an eigenvalue refers to the position of its associated eigenspace relative to the null cone of the Hermitian form (here, in $\mathbb{C}^{1,1}$). The other three hyperbolic reducible families C_{23}, C_{14}, and C_{13} are defined in the same way, exchanging the roles via $\theta_1 \leftrightarrow \theta_2$ and $\theta_3 \leftrightarrow \theta_4$.

In each family the product AB, as long as it is elliptic, has two angles θ_F and θ_N. We denote θ_C the angle of rotation in the stable $\mathbb{C}$-plane; θ_N is then the angle of rotation in the normal $\mathbb{C}$-planes. The result is then the following:

Proposition 4.2.3 *Let A, B be two elliptic elements in $PU(2,1)$ with respective angles $\{\theta_1, \theta_2\}$ and $\{\theta_3, \theta_4\}$ (with $\theta_i \in [0, 2\pi[$), such that the product AB is elliptic. If the group generated by A and B is hyperbolic reducible, then the angle pair $\{\theta_C, \theta_N\}$ of AB is in one of the four following segments:*

$$C_{24} : \begin{cases} \theta_C = 2\theta_N + \theta_2 + \theta_4 - 2\theta_1 - 2\theta_3 \ [2\pi] \quad \textit{and} \\ \theta_2 + \theta_4 < \theta_C < 2\pi \quad (\textit{if} \ \ \theta_2 + \theta_4 < 2\pi) \\ 0 < \theta_C < \theta_2 + \theta_4 - 2\pi \quad (\textit{if} \ \ \theta_2 + \theta_4 > 2\pi). \end{cases}$$

$$C_{13} : \begin{cases} \theta_C = 2\theta_N + \theta_1 + \theta_3 - 2\theta_2 - 2\theta_4 \ [2\pi] \quad \textit{and} \\ \theta_1 + \theta_3 < \theta_C < 2\pi \quad (\textit{if} \ \ \theta_1 + \theta_3 < 2\pi) \\ 0 < \theta_C < \theta_1 + \theta_3 - 2\pi \quad (\textit{if} \ \ \theta_1 + \theta_3 > 2\pi). \end{cases}$$

$$C_{23} : \begin{cases} \theta_C = 2\theta_N + \theta_2 + \theta_3 - 2\theta_1 - 2\theta_4 \ [2\pi] \quad \textit{and} \\ \theta_2 + \theta_3 < \theta_C < 2\pi \quad (\textit{if} \ \ \theta_2 + \theta_3 < 2\pi) \\ 0 < \theta_C < \theta_2 + \theta_3 - 2\pi \quad (\textit{if} \ \ \theta_2 + \theta_3 > 2\pi). \end{cases}$$

$$C_{14} : \begin{cases} \theta_C = 2\theta_N + \theta_1 + \theta_4 - 2\theta_2 - 2\theta_3 \ [2\pi] \quad \textit{and} \\ \theta_1 + \theta_4 < \theta_C < 2\pi \quad (\textit{if} \ \ \theta_1 + \theta_4 < 2\pi) \\ 0 < \theta_C < \theta_1 + \theta_4 - 2\pi \quad (\textit{if} \ \ \theta_1 + \theta_4 > 2\pi). \end{cases}$$

Note that each of these four segments has an endpoint which is a totally reducible vertex, the other endpoint being on one of the sides of the square; it is however possible that the segment wrap once around the torus before reaching its endpoint (see the examples section). We leave the inequalities in this form, which don't make apparent which segments have slope 2 and 1/2, because typically this can change inside the same family (in the case when the segment bounces off the diagonal of the square). For instance, if $\theta_1 + \theta_3 < \theta_2 + \theta_4 < 2\pi$, the segment C_{24} has slope 2 (at least, close to D_1) and C_{13} has slope 1/2 (also, close to D_1).

Proof. We treat the case of the family C_{24} whose generators are written above, A in diagonal form and B in block-diagonal form. Then the product $C = AB$ is also in block-diagonal form:

$$C = \begin{pmatrix} e^{i(\theta_1+\theta_3)} & 0 & 0 \\ 0 & c_1 & c_2 \\ 0 & c_3 & c_4 \end{pmatrix} \quad \text{with} \quad \widetilde{C} = \begin{pmatrix} c_1 & c_2 \\ c_3 & c_4 \end{pmatrix} \in U(1,1)$$

$\widetilde{C}$ has two eigenvalues of norm 1, say $e^{i\psi_1}$ and $e^{i\psi_2}$ with the latter of negative type. Then the angles of rotation of C are given by dividing the two eigenvalues of positive type by that of negative type. This is written:

$$\begin{cases} \theta_C = \psi_1 - \psi_2 \\ \theta_N = \theta_1 + \theta_3 - \psi_2 \end{cases}$$

Now we have again a condition coming from the determinant, which says here that $\psi_1 + \psi_2 = \theta_2 + \theta_4 \ [2\pi]$. Combining these equations, we obtain the condition: $\theta_C = 2\theta_N + \theta_2 + \theta_4 - 2\theta_1 - 2\theta_3 \ [2\pi]$.

The exact range of θ_C inside this line is given by the geometric condition which says what the possible third angle is for a triangle in the hyperbolic plane having two prescribed angles. The following lemma is just an oriented version of the fact that triangles exist in the hyperbolic plane if and only if their angle sum is less than π:

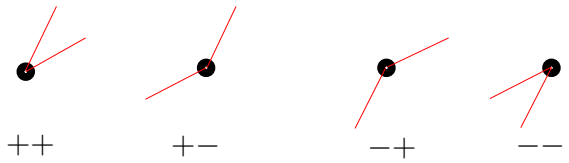

Figure 4.3: Local hyperbolic reducible types

Lemma 4.2.1 *Let $\tilde{A}$ and $\tilde{B}$ be two elliptic isometries of $H^1_{\mathbb{C}}$, with respective rotation angles θ_2 and θ_4 ($\theta_i \in [0, 2\pi[$). As the fixed points of $\tilde{A}$ and $\tilde{B}$ vary, the rotation angle θ_C of the product $\tilde{C} = \tilde{A}\tilde{B}$ (when it is elliptic) ranges over the interval $[\theta_2 + \theta_4, 2\pi[$ if $\theta_2 + \theta_4 < 2\pi$, and $[0, \theta_2 + \theta_4 - 2\pi[$ if $\theta_2 + \theta_4 > 2\pi$.*

This completes the proof. □

Classifying the configurations of reducibles

We start by concentrating on the local configuration at each vertex. We have seen that the spherical reducible configurations are of two types, connected (type C) or disconnected (type D) in the half-square affine chart. As for the hyperbolic reducible configurations, we have just seen that two segments emanate from each vertex, one of slope 2 and the other of slope 1/2. The direction of each segment, upward or downward from the vertex, is determined by the following data (see Prop. 4.2.3). We denote, for $i = 1, 2$ and $j = 3, 4$:

$$\sigma_{ij} := \theta_i + \theta_j$$

(where we have again normalized with $\theta_i \in [0, 2\pi[$). Then, at the vertex $\{\sigma_{ij}, \sigma_{kl}\}$ (see section 4.2.3), the segment C_{ij} goes upward if and only if $\sigma_{ij} < 2\pi$ (and C_{kl} goes upward if and only if $\sigma_{kl} < 2\pi$).

We will then assign a symbol to each configuration of reducibles, consisting in a letter (C or D) for the spherical reducible type and four $+$ or $-$ signs, arbitrarily ordered as follows. There are two pairs of signs, each corresponding to a vertex. The top pair corresponds to the "top" vertex (that with larger θ_6 in the affine chart $\{(\theta_5, \theta_6) | \, \theta_i \in [0; 2\pi[, \theta_5 \geqslant \theta_6\}$), and in each pair we have put the segment with slope 2 first. A $+$ sign means that the corresponding segment goes upward; see Figure 4.3 and examples in Figures 4.4 and 4.5. There are a priori 32 possibilities of such symbols, but in fact only 4 of type C and 4 of type D correspond to configurations of reducibles which actually occur. They are listed in the following result.

Proposition 4.2.4 *The possible local types of reducible configurations are, with the above notation, C^{++}_{++}, C^{--}_{--}, C^{-+}_{-+}, C^{+-}_{+-} and D^{++}_{-+}, D^{++}_{+-}, D^{-+}_{--}, D^{+-}_{--} (see Figures 4.4 and 4.5).*

Proof. We use three different criteria to discard the non-admissible configurations, then give examples of the remaining types. This is made easier by the fact that there is a symmetry among types which we will make explicit, after introducing some useful notation.

The hyperbolic reducible configurations are determined by the position of each $\sigma_{ij} = \theta_i + \theta_j$ (with $\theta_i \in [0, 2\pi[$ and $i = 1, 2$, $j = 3, 4$) relatively to 2π. This is nicely expressed in terms of

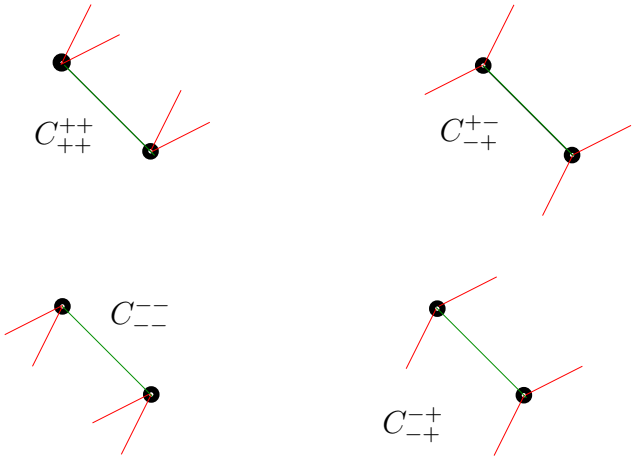

Figure 4.4: Local configurations of type C

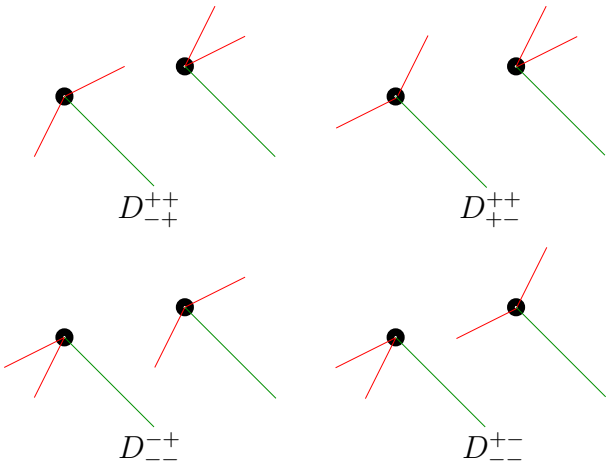

Figure 4.5: Local configurations of type D

the integer parts k_{ij} of $\frac{\sigma_{ij}}{2\pi}$, whose value is accordingly 0 or 1. These integers also appear when we normalize the cooordinates of the vertices in the affine chart, as we will see.

The symmetry is then as follows. Recall that each configuration is defined by the choice of two unordered pairs of angles, $\{\theta_1, \theta_2\}$ and $\{\theta_3, \theta_4\}$, with $\theta_i \in [0, 2\pi[$. The transformation S which we consider is simply taking each θ_i to its complementary (or symmetric) angle $2\pi - \theta_i$. This is interesting because obviously:

$$\theta_i + \theta_j < 2\pi \iff S(\theta_i) + S(\theta_j) > 2\pi$$

(in other words: $S(k_{ij}) = 1 - k_{ij}$) so that all the signs of the hyperbolic reducible segments are exchanged. However we have to be a bit careful to see the effect on the whole configuration, because this also mixes up the vertices and their coordinates. First of all, the spherical reducible types C and D are stable under this transformation, because of the following characterization of type D (with as above $k_{ij} = Int(\frac{\sigma_{ij}}{2\pi})$):

Lemma 4.2.2 *The two vertices have a different index* $\iff$ $k_{13} + k_{24} \neq k_{14} + k_{23}$.

Proof of lemma. This follows simply by writing the indices in question. The only thing to note is that the vertices have coordinates σ_{ij}, appropriately normalized in $[0, 2\pi[$ as $\sigma_{ij} - 2\pi k_{ij}$. Then, denoting I_i the index of the vertex D_i, we have:

$$\begin{cases} 2\pi I_1 = \theta_1 + \theta_2 + \theta_3 + \theta_4 + (2\pi - (\sigma_{13} - 2\pi k_{13})) + (2\pi - (\sigma_{24} - 2\pi k_{24})) \\ 2\pi I_2 = \theta_1 + \theta_2 + \theta_3 + \theta_4 + (2\pi - (\sigma_{14} - 2\pi k_{14})) + (2\pi - (\sigma_{23} - 2\pi k_{23})) \end{cases}$$

so that:

$$I_2 - I_1 = k_{14} + k_{23} - (k_{13} + k_{24})$$

□

Now we note what happens to the vertices when we apply the transformation S. In type D, the two vertices have different indices and S sends the vertex with lower index to the vertex with higher index, so that the "top" and "bottom" vertices are exchanged by S. In type C, the two vertices have same index but for instance the "top" vertex is closer to the diagonal, and this remains unchanged by S so that the "top" and "bottom" vertices are not exchanged.

Last, at each vertex the two hyperbolic reducible segments are exchanged (because the larger coordinate of a vertex becomes the smaller one of its image) and, as we have said, the signs are changed. The following examples will be of particular interest to us:

$$\begin{array}{ll} S(C^{+-}_{++}) = C^{+-}_{--} & S(C^{+-}_{+-}) = C^{+-}_{+-} \\ S(D^{++}_{+-}) = D^{+-}_{--} & S(D^{-+}_{--}) = D^{++}_{-+} \\ S(D^{--}_{+-}) = D^{+-}_{++} & S(D^{--}_{-+}) = D^{-+}_{++} \end{array}$$

Now that we have reduced the number of cases (except for those which are unfortunately stable under S), we exclude the unwanted configurations. The first thing to notice is that $\sigma_{13} + \sigma_{24} = \sigma_{14} + \sigma_{23}$; this discards the four types C^{++}_{--}, C^{--}_{++}, D^{++}_{--} and D^{--}_{++}. The next criterion follows from the above lemma which characterizes type D, knowing that $k_{ij} = 1$ corresponds to a + sign. Thus, in type C the sum of the two top signs must be equal to that of the bottom

signs (where "adding signs" is meant like 0 and 1 with $0 \neq 2$), whereas in type D the sums must be different.

This gets rid of half of the cases; now, using the symmetry we have described, we are only left with the announced admissible types along with four ambiguous cases: C^{+-}_{+-} and C^{-+}_{+-} which are symmetric under S, D^{--}_{+-} (with its image D^{+-}_{++}), and D^{--}_{-+} (with its image D^{-+}_{++}).

The four latter, of type D, are easily discarded by the observation that in that type, the only vertex which can have a double $-$ sign is the vertex of larger index.

As for the last cases, suppose that we have a configuration of type C with a $+$ and a $-$ sign at each vertex. We can suppose by reordering that $\theta_1 > \theta_2, \theta_3$ and $\theta_3 > \theta_4$. The assumption on the signs says that we have one of the two situations:

$$\sigma_{13} > \sigma_{23} > 2\pi > \sigma_{14} > \sigma_{24}$$
$$\sigma_{13} > \sigma_{14} > 2\pi > \sigma_{23} > \sigma_{24}$$

We use the following lemma, which follows from reducing the σ_{ij} in $[0, 2\pi[$:

Lemma 4.2.3 *A vertex $\{\sigma_{ij}, \sigma_{kl}\}$ with $\sigma_{ij} > 2\pi > \sigma_{kl}$ is of type:*

- $(-,+)$ *if* $\sigma_{kl} > \sigma_{ij} - 2\pi$
- $(+,-)$ *if* $\sigma_{kl} < \sigma_{ij} - 2\pi$.

Now two σ_{ij} which share a subscript are certainly in the first case (because $\sigma_{ij} - \sigma_{jk} = \theta_i - \theta_k$), so that a $(+,-)$ couple cannot occur twice in any of the two above situations. This discards type C^{+-}_{+-}. As for type C^{-+}_{+-}, if we have one vertex of type $(-,+)$ and one of type $(+,-)$, the lemma implies that the top vertex must be of type $(+,-)$ (indeed the top vertice is the one with the smaller difference of coordinates).

We finish the proof by giving examples of the remaining possible cases (see section 4.4 for details). We give here only the corresponding values of the pairs $\{\theta_1, \theta_2\}$ and $\{\theta_3, \theta_4\}$.

The configuration for $\{\frac{2\pi}{3}, \frac{2\pi}{4}\}$,$\{\frac{2\pi}{5}, \frac{2\pi}{6}\}$ is of type C^{++}_{++}, and its image under S is of type C^{--}_{--}. The configuration for $\{\frac{2\pi}{3}, -\frac{2\pi}{4}\}$,$\{\frac{2\pi}{5}, -\frac{2\pi}{6}\}$ is of type C^{+-}_{-+} (stable under S). Type C^{-+}_{-+} (stable under S) is obtained for instance with pairs $\{2\pi - \varepsilon, \varepsilon\}$,$\{2\varepsilon, 3\varepsilon\}$, provided that $5\varepsilon < 2\pi$.

As for types D: D^{-+}_{--} is obtained with $\{\frac{2\pi}{4}, \frac{2\pi}{6}\}$, $\{-\frac{2\pi}{5}, -\frac{2\pi}{7}\}$ and its image under S is D^{++}_{-+}. Finally, type D^{+-}_{--} is obtained with $\{\frac{2\pi}{4}, -\frac{2\pi}{6}\}$, $\{\frac{2\pi}{5}, -\frac{2\pi}{7}\}$ and its image under S is D^{++}_{+-}. □

4.2.4 Chambers and irreducible groups

In this section we focus on the claim that pairs (A, B) such that the group generated by A and B is irreducible are sent to interior points of the image. This follows from the fact that the map $\tilde{\mu}$ is a submersion at such a point; in order to ensure that the source is a manifold (and identify its tangent space) we consider $\tilde{\mu}$ restricted to those elements whose product is regular elliptic (in the half-square affine chart, this means that we consider only the interior points of the triangle):

$$\tilde{\mu}_r : \left\{ \begin{array}{rcccc} (C_1 \times C_2) \cap \mu^{-1}(\{\text{regular elliptics}\}) & \xrightarrow{\mu} & G & \xrightarrow{\pi} & \mathbb{T}^2/\mathfrak{S}_2 \\ (A, B) & \longmapsto & AB & \longmapsto & \text{Angles}(AB) \end{array} \right.$$

Since the regular elliptic elements of $G = PU(2,1)$ form an open set (see [G] p. 203), the source is now an open subset of $C_1 \times C_2$ and thus is a manifold with the same tangent space. Before going into the details, we give the result:

Proposition 4.2.5 *Let $(A,B) \in C_1 \times C_2$ such that AB is regular elliptic and the group generated by A and B is irreducible. Then the differential of $\tilde{\mu}_r$ at (A,B) is surjective and thus $\tilde{\mu}_r$ is locally surjective at that point.*

This phenomenon was brought to our attention by the analog in the compact group $U(n)$, described in [FW] (see lemma 4.2.4 below). Thus $\tilde{\mu}$ is of rank 2 at an irreducible; we will see in the next section that it is of rank 1 at a generic reducible, and of rank 0 at a totally reducible.

Note also that we prove a stronger version of this statement in section 4.3.1, using only a certain class of Lagrangian deformations.

Proof. We will consider separately the product map μ and the projection π from G to its conjugacy classes, showing that each is a submersion at an irreducible. We begin by recalling a few facts about the Lie group structure of $G = PU(2,1)$ and its conjugacy classes. Consider a conjugacy class with a preferred representative A (in our case, the conjugacy class being elliptic, we can choose A to be a diagonal matrix):

$$C_1 = \{P.A.P^{-1} \mid P \in PU(2,1)\}$$

This is a submanifold of G of dimension $dim(PU(2,1)) - dim(Z(A))$ where the centralizer $Z(A)$ is of dimension 2 if A is regular elliptic (as can be seen on the diagonal form with 3 distinct eigenvalues) and of dimension 4 if A has two equal eigenvalues. Recall that $PU(2,1)$ has dimension 8; we thus obtain dimension 6 for the regular elliptic classes, and 4 for the special elliptic classes (note that in all cases the submanifold consisting of Lagrangian decompositions has half of this dimension, see section 4.3). The tangent space to this conjugacy class at A is then:

$$T_A C_1 = \{XA - AX \mid X \in \mathfrak{g}\} = \{(X - AXA^{-1})A \mid X \in \mathfrak{g}\}$$

the latter expression identifying this subspace of $T_A G$ to the subspace $Im(Id - Ad_A)$ of $\mathfrak{g} = T_1 G$ by right translation by A^{-1} (or right Maurer-Cartan form). This is the point of view taken in [FW], where the following result is derived, denoting by $\mathfrak{z}(A,B)$ the Lie algebra of the centralizer of the group generated by A and B (and taking the orthogonal subspace with respect to the Killing form):

Lemma 4.2.4 $Im(d_{(A,B)}\mu) = \mathfrak{z}(A,B)^{\perp}.AB$.

In the notation of [FW], our μ is $\pi^{(1)}$; this result can be found in the proof of Prop. 4.2 on p. 23. We include a short proof for the reader's convenience. Write, for $h_1 \in T_A C_1$ and $h_2 \in T_B C_2$: $\mu(A + h_1, B + h_2) = AB + Ah_2 + h_1 B + h_1 h_2$. This gives the expression of the differential of μ at (A,B): $d_{(A,B)}\mu(h_1, h_2) = Ah_2 + h_1 B$. If we translate as before these tangent vectors into $\mathfrak{g} = T_1 G$ by writing $h_1 = X_1.A$, $h_2 = X_2.B$ (with $X_1 \in Im(Id - Ad_A)$ and $X_2 \in Im(Id - Ad_B)$) and $d_{(A,B)}\mu(h_1, h_2) = X_3.AB$, we obtain the cocycle relation:

$$X_3 = X_1 + Ad_A(X_2)$$

Using an Ad-invariant non-degenerate bilinear form on $\mathfrak{g}$ such as the Killing form, the lemma follows by noting that:

$$[Im(Id-Ad_A)+Ad_A(Im(Id-Ad_B)]^{\perp} = Ker(Id-Ad_A)\cap Ad_A(Ker(Id-Ad_B)) = \mathfrak{z}(A)\cap\mathfrak{z}(B)$$

Now if A and B generate an irreducible group, then $\mathfrak{z}(A,B) = \{0\}$ (because $PU(2,1)$ has trivial center), so that μ is indeed a submersion at such a point.

Finally, the projection π restricted to elliptic elements is in coordinates the map which to a matrix associates its eigenvalues (rather, two linear combinations of its eigenvalues), so that it is classically differentiable and a submersion at those points which yield distinct eigenvalues: these are the regular elliptic elements. □

4.2.5 Which chambers are full ?

It follows from the previous section that a chamber is either entirely in the image of $\tilde{\mu}$ ("full") or entirely in its complement ("empty"). We have two types of arguments to determine which chambers are full and which are empty: constructive arguments such as local convexity tell us that some chambers must be full, and obstructions which force other chambers to be empty.

Convexity, local convexity

There is a natural notion of convexity in the surface $\mathbb{T}^2/\mathfrak{S}_2$ as in any Riemannian manifold, that of geodesic convexity. The only subtlety arises from the fact that there are (as in the torus) many geodesic segments joining two points, and sometimes there is not a unique shortest path among them. However, such pairs of points are isolated so we don't really need to worry about them in the definition of convexity. We justify this briefly before writing a possible definition.

Consider a torus $\mathbb{T}^2$, quotient of the Euclidian plane E^2 by the group of isometries generated by two translations of (linearly independant) vectors e_1 and e_2. Given two points p_1 and p_2 in $\mathbb{T}^2$, any line of E^2 passing through a preimage of each projects to a geodesic containing p_1 and p_2. Suppose for instance that (e_1, e_2) is an orthonormal basis of E^2 and fix a preimage of p_1, say $\tilde{p_1} \in p_1 + \mathbb{Z}e_1 + \mathbb{Z}e_2$. If the slope of the line $(\tilde{p_1}, \tilde{p_2})$ is irrational for one representative $\tilde{p_2} \in p_2+\mathbb{Z}e_1+\mathbb{Z}e_2$, then it is irrational for all representatives; in that case all of the lines $(\tilde{p_1}, \tilde{p_2})$ project to distinct geodesics in $\mathbb{T}^2$. If on the other hand the slopes are rational, then each of these lines contains a countable family of $\tilde{p_2} \in p_2 + \mathbb{Z}e_1 + \mathbb{Z}e_2$, but there is still a countable family of distinct lines which project to distinct geodesics. As for uniqueness of the shortest geodesic segment, the only problematic case is when more than one point of $p_2 + \mathbb{Z}e_1 + \mathbb{Z}e_2$ is at shortest distance from p_1. This only happens when the grid $p_2 + \mathbb{Z}e_1 + \mathbb{Z}e_2$ contains the midpoints of certain edges of the grid $p_1 + \mathbb{Z}e_1 + \mathbb{Z}e_2$ (there are then two closest points) or the centers of its squares (there are then four closest points). The situation in $\mathbb{T}^2/\mathfrak{S}_2$ is analogous via the projection which is a double cover outside of the diagonal. The ambiguous cases are thus sufficiently isolated that we can overlook them in the following definition (and choose the appropriate segment by considering neighboring points).

Definition 4.2.1 *A subset C of $\mathbb{T}^2/\mathfrak{S}_2$ will be called* **convex** *if for all pairs of points $(x,y) \in C^2$ which are joined by a unique shortest geodesic segment, this segment is contained in C.*

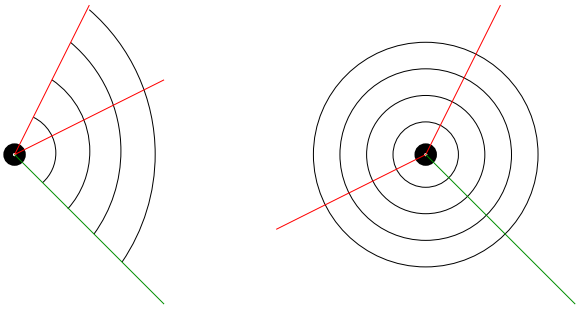

Figure 4.6: Local convexity around a totally reducible vertex

In fact we only need here the notion of local convexity in the neighborhood of a vertex; this notion is clear because the surface $\mathbb{T}^2/\mathfrak{S}_2$ has an affine structure (as a quotient of $\mathbb{R}^2$ by a group of affine transformations). There are two types of vertices which appear in the present case: the two totally reducible vertices which we have already seen and some "accidental" vertices which occur when two hyperbolic reducible families meet (of course only their images meet). The local structure around the totally reducible vertices is of fundamental importance and we conjecture that it determines the whole image; as for the other vertices, they seem to project to interior points of the image, although we lack a complete proof for the time being (for instance, it would follow if we knew that the fibers were connected as in the classical case). Our main argument of local convexity at a totally reducible vertex relies on the differential properties of $\tilde{\mu}$ at such a point; namely we show that the first differential is null, but that **if one of** A **or** B **is not a complex reflection** the second differential is non-null along the reducible segments, so that the image is locally a convex cone bounded by the reducible walls. The main result is the following:

Proposition 4.2.6 *If one of A or B is not a complex reflection, then the image of $\tilde{\mu}$ contains all chambers which touch a totally reducible vertex and meet the local convex hull of the three reducible walls containing that vertex. In particular, if these three walls meet with obtuse angles, then the vertex is an interior point of the image (see Figure 4.6).*

Proof. We begin with the following lemma which completes what we have seen before, namely that $\tilde{\mu}$ is of rank 2 at an irreducible:

Lemma 4.2.5

- *If A and B generate a totally reducible group, then $d_{(A,B)}\tilde{\mu}$ is null.*
- *If A and B generate a generic reducible group (i.e. whose image is an interior point of a wall), then $d_{(A,B)}\tilde{\mu}$ is of rank 1.*

Proof of lemma. We have seen during the study of irreducible points (lemma 4.2.4) that :

$$Im(d_{(A,B)}\mu) = \mathfrak{z}(A,B)^{\perp}.AB$$

We have also seen that the centralizer of a regular elliptic element is of dimension 2 (that of a special elliptic being 4), so that if A or B is regular elliptic, the dimension of $\mathfrak{z}(A,B)$ is 2 for a totally reducible group and 1 for a generic reducible group. It only remains to see that the subspace $Im(d_{(A,B)}\mu)$ is tangent to the fiber of π at a totally reducible (respectively contains

the tangent space of the fiber at a generic reducible). But this is clear because $Im(d_{(A,B)}\mu) = \mathfrak{z}(A,B)^{\perp}.AB$ always contains the tangent space to the fiber which is $T_{AB}C_3 = \mathfrak{z}(AB)^{\perp}.AB$ (where C_3 denotes the conjugacy class of AB). □

We then focus on a totally reducible vertex where the image will be locally described by the second differential.

Lemma 4.2.6 *The image of the quadratic differential $Q : v \longmapsto d^2_{(A,B)}\tilde{\mu}(v,v)$ is a convex cone in $\mathbb{R}^2$.*

Proof of lemma. This is a general fact about quadratic maps; we include a short proof in the case where the image is of dimension 2. Denote $B(v,w) = d^2_{(A,B)}\tilde{\mu}(v,w)$ the associated symmetric bilinear map and $Q(v) = B(v,v)$. The image of Q is clearly a cone (because $Q(\lambda v) = \lambda^2 Q(v)$ for $\lambda \in \mathbb{R}$). To show that it is convex, consider two vectors $w_1 = Q(v_1)$ and $w_2 = Q(v_2)$ in the image; we show that the whole segment $[w_1, w_2]$ is in the image of the plane spanned by v_1 and v_2. Indeed, suppose that w_1 and w_2 are linearly independant and write, for $\lambda, \mu \in \mathbb{R}$:

$$Q(\lambda v_1 + \mu v_2) = \lambda^2 w_1 + \mu^2 w_2 + 2\lambda\mu B(v_1, v_2) = (\lambda^2 + 2\lambda\mu x_1)w_1 + (\mu^2 + 2\lambda\mu x_2)w_2$$

where we have expressed $B(v_1, v_2) = x_1 w_1 + x_2 w_2$ in the basis (w_1, w_2). It suffices to prove that the ratio of the two coordinates $f(\lambda,\mu) = \frac{\mu^2+2\lambda\mu x_2}{\lambda^2+2\lambda\mu x_1}$ surjects $\mathbb{R}^+$. But this is clear because the map f is continuous outside of the two lines $\{\lambda = 0\}, \{\lambda + 2\mu x_1 = 0\}$ and for instance on a line $\{\mu = p\lambda\}$ it takes the value $\frac{p^2+2px_2}{1+2px_1}$ which takes all values between 0 and $+\infty$ (in two of the four quadrants where f is defined). □

It remains to find non-null vectors in the image of Q tangent to the reducible segments.

Lemma 4.2.7

- *If neither A nor B is a complex reflection in a point (i.e. if $\theta_1 \neq \theta_2$ and $\theta_3 \neq \theta_4$), then at each totally reducible vertex the spherical reducible family contains paths with a non-null second derivative.*
- *If neither A nor B is a complex reflection (i.e. if $\theta_i \neq 0$ for $i = 1...4$) then at its totally reducible vertex each hyperbolic reducible family contains paths with a non-null second derivative.*

Proof of lemma. We show this by an explicit computation of deformations in the neighborhood of a totally reducible vertex, along the Lie algebra of $U(2)$ on one hand and of $U(1,1)$ on the other. In fact, we compute the second derivative not of the map $\tilde{\mu}$ itself (the angle pair) but of the trace of the product matrix, which is equivalent (at least locally, see chapter 1) and simplifies the computation greatly. Note that we don't normalize the determinant of the product matrix, but this doesn't matter because it only depends on $\theta_1, \theta_2, \theta_3, \theta_4$ so it is invariant by deformation.

We thus consider A and B in diagonal form (a totally reducible point) and write deformations of B inside its conjugacy class as a path $h(t).B.h(t)^{-1}$ where $h(t)$ is a path in $U(2,1)$ with $h(0) = 1$. We will then specialize to the cases where $\dot{h}(0)$ is in $\mathfrak{u}(2)$ or $\mathfrak{u}(1,1)$ (with the notation $\dot{h} = \frac{dh}{dt}$). We begin by computing the second derivative, noting that $\frac{d(h^{-1})}{dt} = -h^{-1}\dot{h}h^{-1}$:

$$\begin{aligned}\tfrac{d^2}{dt^2}Tr(A.hBh^{-1})(0) &= \tfrac{d}{dt}Tr(A\dot{h}Bh^{-1} - AhBh^{-1}\dot{h}h^{-1})(0)\\ &= Tr(A\ddot{h}B - 2A\dot{h}B\dot{h} - AB(-\dot{h})\dot{h} - AB\ddot{h} - AB\dot{h}(-\dot{h}))(0)\\ &= 2Tr(AB\dot{h}^2 - A\dot{h}B\dot{h})(0)\end{aligned}$$

where we have simplified repeatedly by $h(0) = h^{-1}(0) = 1$ and used the fact that A and B commute. We compute this last expression for $\dot{h}(0) \in \mathfrak{u}(2)$ then $\mathfrak{u}(1,1)$. Recall that:

$$U(2) = \{A \ \in \ GL(2,\mathbb{C}) \mid A.A^* \ = \ 1\} \text{ so that}$$

$$\mathfrak{u}(2) = \{A \ \in \ M(2,\mathbb{C}) \mid A + A^* \ = \ 0\} = \left\{ \begin{pmatrix} ri & b \\ -\overline{b} & si \end{pmatrix} \mid r,s \in \mathbb{R},\ b \in \mathbb{C} \right\}$$

With this latter expression for $\dot{h}$, writing A and B as diagonal matrices in $U(2)$ (here $A = Diag(e^{i\theta_1}, e^{i\theta_2})$ and $B = Diag(e^{i\theta_3}, e^{i\theta_4})$), we obtain:

$$AB\dot{h}(0)^2 = \begin{pmatrix} -(r^2+|b|^2)e^{i(\theta_1+\theta_3)} & (r+s)ibe^{i(\theta_1+\theta_3)} \\ -(r+s)i\overline{b}e^{i(\theta_2+\theta_4)} & -(s^2+|b|^2)e^{i(\theta_2+\theta_4)} \end{pmatrix}$$

$$A\dot{h}(0)B\dot{h}(0) = \begin{pmatrix} -r^2e^{i(\theta_1+\theta_3)} - |b|^2e^{i(\theta_1+\theta_4)} & bi(re^{i(\theta_1+\theta_3)} + se^{i(\theta_1+\theta_4)}) \\ -\overline{b}i(re^{i(\theta_2+\theta_3)} + se^{i(\theta_2+\theta_4)}) & -s^2e^{i(\theta_2+\theta_4)} - |b|^2e^{i(\theta_2+\theta_3)} \end{pmatrix}$$

so that:

$$Tr(AB\dot{h}^2 - A\dot{h}B\dot{h})(0) = |b|^2(e^{i(\theta_1+\theta_4)} + e^{i(\theta_2+\theta_3)} - e^{i(\theta_1+\theta_3)} - e^{i(\theta_2+\theta_4)})$$

This gives us the result for $U(2)$ because this complex number, sum of four terms of equal norm, is non-zero as long as ($b \neq 0$ and) the terms are not pairwise equal (as in a rhombus), that is if $\theta_1 \neq \theta_2$ and $\theta_3 \neq \theta_4$. Note that the second derivative is always in the same half-line of the complex plane.

Now we do the same thing for $\dot{h}(0) \in \mathfrak{u}(1,1)$. Recall that, denoting $J = Diag(1,-1)$:

$$U(1,1) = \{A \ \in \ GL(2,\mathbb{C}) \mid A.J.A^* \ = \ J\} \text{ so that}$$

$$\mathfrak{u}(1,1) = \{A \ \in \ M(2,\mathbb{C}) \mid AJ + JA^* \ = \ 0\} = \left\{ \begin{pmatrix} ri & b \\ \overline{b} & si \end{pmatrix} \mid r,s \in \mathbb{R},\ b \in \mathbb{C} \right\}$$

We use this latter expression for $\dot{h}(0)$, and write only the block of A and B corresponding to the stable $\mathbb{C}$-plane as a diagonal matrix in $U(1,1)$ (for instance, $A = Diag(e^{i\theta_2}, 1)$ and $B = Diag(e^{i\theta_4}, 1)$ correspond to the family C_{24} of Prop. 4.2.3). We obtain:

$$AB\dot{h}(0)^2 = \begin{pmatrix} (|b|^2 - r^2)e^{i(\theta_2+\theta_4)} & (r+s)ibe^{i(\theta_2+\theta_4)} \\ (r+s)i\overline{b} & |b|^2 - s^2 \end{pmatrix}$$

$$A\dot{h}(0)B\dot{h}(0) = \begin{pmatrix} -r^2e^{i(\theta_2+\theta_4)} + |b|^2e^{i\theta_2} & bi(re^{i(\theta_2+\theta_4)} + se^{i\theta_2}) \\ \overline{b}i(re^{i\theta_4} + s) & |b|^2e^{i\theta_4} - s^2 \end{pmatrix}$$

so that:

$$Tr(AB\dot{h}^2 - A\dot{h}B\dot{h})(0) = |b|^2(e^{i(\theta_2+\theta_4)} + 1 - e^{i\theta_2} - e^{i\theta_4}).$$

As above, this number is non-zero for ($b \neq 0$ and) $\theta_2 \neq 0$ and $\theta_4 \neq 0$. We obtain the analogous condition for the three other hyperbolic reducible segments. □

This completes the proof of the proposition, except maybe for the cases where one of A or B is a complex reflection (resp. complex reflection in a point), and where A and B are complex reflections in a point, which the preceding lemma excluded. But this is only normal, because in each case the vanishing second derivative corresponds to a reducible family which is in fact reduced to a point. Precisely, if one of the generators has two equal angles then the two reducible vertices are equal and the spherical reducible segment is reduced to this point; if one of the angles is zero then the two corresponding hyperbolic reducible families collapse to a point (for instance, if $\theta_1 = 0$ then C_{13} and C_{14} collapse). □

We now come to the study of the image near a crossing of reducible families. For this purpose we examine deformations of a regular hyperbolic reducible or spherical reducible point, transversally to the reducible family. The main result is that there is at least one side of the reducible segment in the surface (defined by the configuration near a totally reducible vertice) which stays full along the whole segment. Note that the sides defined by a segment change when this segment bounces off the diagonal of the square (the orientation changes in the affine chart).

Proposition 4.2.7 *If one side of a reducible segment is locally full near a totally reducible vertice, then this side is full along the whole segment, even after possible intersection with other reducible segments.*

Proof. We write as before deformations of the product AB near the pair (A, B) with each in a fixed conjugacy class as paths $Ah(t)Bh(t)^{-1}$ with $h(t) \in PU(2,1)$ and $h(0) = 1$. But now (A, B) is a regular reducible point and we deform in directions transverse to the reducible family to which (A, B) belongs. We first show that there are always such deformations locally around a regular hyperbolic reducible point; we have already seen that the differential $d_{(A,B)}\tilde{\mu}$ is of rank one at such a point (see lemma 4.2.5), its image being tangent to the reducible segment.

Lemma 4.2.8 *Let $(A, B) \in C_1 \times C_2$ be a regular hyperbolic reducible point (i.e. A and B generate a hyperbolic reducible group without fixed point). Then the image of the quadratic second differential $Q : v \longmapsto d^2_{(A,B)}\tilde{\mu}(v, v)$ contains directions transverse to the image of $d_{(A,B)}\tilde{\mu}$.*

Proof of lemma. Consider for instance a point in the hyperbolic reducible family C_{24}, of the form:

$$A = \begin{pmatrix} e^{i\theta_1} & 0 & 0 \\ 0 & e^{i\theta_2} & 0 \\ 0 & 0 & 1 \end{pmatrix} \quad \text{and} \quad B = \begin{pmatrix} e^{i\theta_3} & 0 & 0 \\ 0 & b_1 & b_2 \\ 0 & b_3 & b_4 \end{pmatrix}$$

where $\widetilde{B} = \begin{pmatrix} b_1 & b_2 \\ b_3 & b_4 \end{pmatrix} \in U(1,1)$ has eigenvalues $e^{i\theta_4}$ of positive type and 1 of negative type.

We compute as earlier the trace along the path, which we take transverse to the hyperbolic reducible family by taking $\dot{h}(0)$ in the orthogonal complement of the corresponding Lie algebra $\mathfrak{u}(1,1)$, namely:

$$\dot{h}(0) = \begin{pmatrix} 0 & h_1 & h_2 \\ \overline{h_1} & 0 & 0 \\ \overline{h_2} & 0 & 0 \end{pmatrix} \text{ with } h_1, h_2 \in \mathbb{C}$$

We have seen that at a regular reducible point the differential of $\tilde{\mu}$ (or equivalently, of the trace of the product) is of rank one (its image is tangent to the reducible segment). We are now looking for vectors in the image of the quadratic second differential which are transverse to this line, and compute the corresponding complex numbers. A vector tangent to the reducible line is given by:

$$\frac{d}{dt} Tr(Ah(t)Bh(t)^{-1})(0) = Tr(A\dot{h}B - AB\dot{h})(0) \text{ with } \dot{h}(0) \in \mathfrak{u}(1,1)$$

For instance, taking $\dot{h}(0) = \begin{pmatrix} 0 & 1 \\ 1 & 0 \end{pmatrix}$ gives us:

$$Tr(A\dot{h}B - AB\dot{h})(0) = (b_3 - b_2)(e^{i\theta_2} - 1)$$

which is non-zero provided that $\theta_2 \neq 0$ (if not, the hyperbolic reducible family is reduced to a point) and $b_2 \neq b_3$; if the latter condition is not satisfied we use another $\dot{h}(0) \in \mathfrak{u}(1,1)$.

Now that we have a vector tangent to the reducible segment, we compute the image of the quadratic second differential:

$$\begin{aligned} \tfrac{d^2}{dt^2} Tr(A.hBh^{-1})(0) &= \tfrac{d}{dt} Tr(A\dot{h}Bh^{-1} - AhBh^{-1}\dot{h}h^{-1})(0) \\ &= Tr(A\ddot{h}B - 2A\dot{h}B\dot{h} - AB(-\dot{h})\dot{h} - AB\ddot{h} - AB\dot{h}(-\dot{h}))(0) \\ &= 2Tr(AB\dot{h}^2 - A\dot{h}B\dot{h})(0) \end{aligned}$$

which is the same result as before; only now the second order terms vanish not because A and B commute but because $Tr([A,B]\ddot{h})(0) = 0$ due to the special form of $\dot{h}(0)$. We thus obtain:

$$\begin{aligned} Tr(AB\dot{h}^2 - A\dot{h}B\dot{h})(0) &= |h_1|^2(e^{i(\theta_1+\theta_3)} + b_1(e^{i\theta_2} - e^{i\theta_1}) - e^{i(\theta_2+\theta_3)}) \\ &\quad -h_1\overline{h_2}(e^{i\theta_1}b_2 + e^{-i\theta_1}\overline{b_3}) \\ &\quad +|h_2|^2(e^{i(\theta_1+\theta_3)} + b_4(1 - e^{i\theta_1}) - e^{i\theta_3}) \end{aligned}$$

This expression is a Hermitian form in (h_1, h_2); our claim is equivalent to saying that this form is non-degenerate, which we prove by computing its discriminant Δ:

$$\begin{aligned} \Delta &= [e^{i(\theta_1+\theta_3)} + b_1(e^{i\theta_2} - e^{i\theta_1}) - e^{i(\theta_2+\theta_3)}] \cdot [e^{i(\theta_1+\theta_3)} + b_4(1 - e^{i\theta_1}) - e^{i\theta_3}] \\ &+ \tfrac{1}{4}\left[|b_1|^2 + |b_4|^2 + 2Re(e^{2i\theta_1}(b_1b_4 - 1)) - 2\right] \end{aligned}$$

where we have eliminated b_2 and b_3 by the relations saying that $\tilde{B}$ is in $U(1,1)$. In fact we can simplify even more by supposing that $\tilde{B}$ is in $SU(1,1)$; in that case its trace is determined by its angle: $Tr(\tilde{B}) = b_1 + b_4 = 2\cos(\frac{\theta_4}{2})$ which we will denote c_4. This gives us for Δ, after simplifying and gathering terms:

$$\begin{aligned} \Delta &= \tfrac{|b_1|^2 + |c_4 - b_1|^2}{4} + (e^{i\theta_2} - e^{i\theta_1})(1 - e^{i\theta_1})[(e^{i\theta_3} - c_4/2)^2 - (b_1 - c_4/2)^2] \\ &+ 1/2 \cdot \left[Re[e^{2i\theta_1}(b_1c_4 - b_1^2)] + \cos 2\theta_1 - 1\right] \end{aligned}$$

which has for instance non-null imaginary part (note that $|b_1| \geqslant 1$ because $|b_1|^2 - |b_2|^2 = 1$, $\tilde{B}$ being in $U(1,1)$). □

We then show the analogous result for regular spherical reducible points.

Lemma 4.2.9 *Let $(A,B) \in C_1 \times C_2$ be a regular spherical reducible point (i.e. A and B generate a group which fixes a point in $H^2_{\mathbb{C}}$ but is not hyperbolic reducible). Then the image of the quadratic second differential $Q : v \longmapsto d^2_{(A,B)}\tilde{\mu}(v,v)$ contains directions transverse to the image of $d_{(A,B)}\tilde{\mu}$.*

Proof. This goes exactly as in the above case, but the block matrices are not in the same place. The computation yields:

$$\begin{aligned} Tr(AB\dot{h}^2 - A\dot{h}B\dot{h})(0) &= |h_1|^2(e^{i\theta_1}b_1 + 1 - e^{i\theta_1} - b_1) \\ &\quad -h_1\overline{h_2}(\overline{b_2} + b_3) \\ &\quad +|h_2|^2(e^{i\theta_2}b_4 + 1 - e^{i\theta_2} - b_4) \end{aligned}$$

which is as above a non-degenerate Hermitian form in (h_1, h_2). □

Obstructions

We would like to state here obstructions for some specific chambers to be full. The main obstruction that we have seen in all examples, but for which we lack a complete proof, is the following. We conjecture that, given angle pairs $\{\theta_1, \theta_2\}$ and $\{\theta_3, \theta_4\}$ without restriction, the momentum polygon cannot contain both chambers touching the two "diagonal" corners of the half-square. In other words, the product cannot have angle pairs of the form $\{\varepsilon, \varepsilon\}$ and $\{-\varepsilon, -\varepsilon\}$ for ε arbitrarily small. Note however that the lower right corner of the half-square can be attained, as in figures 4.16 and 4.17 (this means that the product can have angle pairs of the form $\{\varepsilon, -\varepsilon\}$ for ε arbitrarily small).

The problem in trying to prove this is the subtleties that arise near the border, mostly near the three (identified) vertices of the square which represent not only the identity but also all unipotent (parabolic) isometries (which are the Heisenberg translations of the border). In general we can rule out the identity from the image (unless the conjugacy class of B contains the inverse of A, if the angles are $\{\theta_1, \theta_2\}$ and $\{-\theta_1, -\theta_2\}$) and with it a whole (non-uniform) neighborhood of the identity, but this does not forbid any of the unipotent isometries or elliptics which accumulate near them. There are some results of a related flavor in [Sz2] (see section 13, pp. 111–122), but they do not apply to our case, mainly because they all suppose ordinary convergence in $PU(2,1)$ and derive a more subtle notion of convergence. What seems to us the main feature that we could use is the study of accumulation points of complex reflections in a point with arbitrarily small rotation angle (these are the angle pairs $\{\varepsilon, \varepsilon\}$ or $\{-\varepsilon, -\varepsilon\}$).

4.3 Configurations of Lagrangian triples

We consider in this section a more restricted class of elliptic triangle groups, which we will call *Lagrangian* or *decomposable*. Namely these groups are of index 2 in a group generated by three

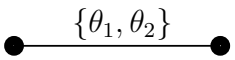

Figure 4.7: Coxeter diagram for a pair of $\mathbb{R}$-reflections

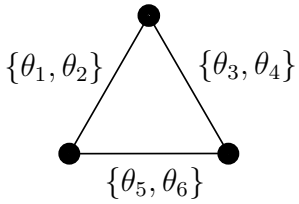

Figure 4.8: Coxeter diagram for a triple of $\mathbb{R}$-reflections

$\mathbb{R}$-reflections (or antiholomorphic involutions) in $\mathbb{R}$-planes intersecting pairwise inside complex hyperbolic space; more pecisely, the two generators of the triangle group are products of two $\mathbb{R}$-reflections, one of these being common to both generators. This is analogous to the classical idea of considering (orientation-preserving) triangle groups of the plane (Euclidian, spherical, or hyperbolic) inside of a group generated by reflections in the sides of a triangle, which is how their geometric properties are usually analyzed.

Recall that an intersecting pair of Lagrangians is characterized up to isometry by a pair of (reflection) angles which are half of the (rotation) angles of the elliptic isometry obtained by composing the two associated $\mathbb{R}$-reflections. This produces an angle pair $\{\theta_1, \theta_2\}$ with $\theta_i \in \mathbb{R}/\pi\mathbb{Z}$, which we write in a Coxeter-type diagram (see figure 4.7). The question of the possible configurations of pairwise intersecting triples of $\mathbb{R}$-planes then translates into that of possible angle pairs as labels for the triangle graph of figure 4.8.

As in the classical case of planar groups, we gain some geometric information by introducing these $\mathbb{R}$-reflections; in fact we obtain a geometric obstruction which is completely analogous to the planar case in the sense that it expresses the admissible Riemannian angles in a geodesic triangle (see section 4.3.1). However, we have not found a way to express this condition on the three angle pairs in an elliptic triangle group which is not Lagrangian, although we conjecture that the image polygon must be the same (which in the case of the compact group $U(n)$ is the main theorem of [FW]).

Apart from this specific obstruction, everything we have done for elliptic triangle groups carries over to the Lagrangian setting: on one hand, the restricted momentum map is also of maximal rank at an irreducible, and on the other, the reducible groups are exactly the same in both cases. We gain a lot for practical reasons though, mostly from the smaller dimension count at the source: the dimension of $\mathbb{R}$-reflections decomposing a given elliptic conjugacy class is 3 (see section 4.3.2 for an explicit parametrization), half of that of the conjugacy class itself. This fits in with Schaffhauser's description of the space of decomposable groups as a Lagrangian submanifold of the symplectic representation manifold of a surface group (that of the punctured sphere inside $U(n)$, see [Sf]). From the practical viewpoint, $\mathbb{R}$-reflections give us a way of paramatrizing a given conjugacy class tranversally to the fibers of our momentum map (with half as many parameters); most notable is the fact that we obtain (generic) fibers of dimension 1, which is the starting point of our search for discrete groups in this setting (see last section).

4.3.1 Lagrangian triples vs. elliptic triangles

We consider here the map $\tilde{\mu}_L$ which is the restriction of the map $\tilde{\mu}$ of the preceding section (taking a pair of elliptic elements (A, B) in fixed conjugacy classes to the angle pair of their product) to pairs (A, B) which are *simultaneously decomposable* (into $\mathbb{R}$-reflections). This means that there exist $\mathbb{R}$-reflections σ_1, σ_2 and σ_3 such that $A = \sigma_2\sigma_1$ and $B = \sigma_3\sigma_2$ (it corresponds to Lagrangian representations in the terms of [FW] and [Sf]). The angles of the product $BA = \sigma_3\sigma_1$ are then (double of) those of the corresponding $\mathbb{R}$-planes L_1 and L_3, which shows that the problems of the image of the Lagrangian momentum map $\tilde{\mu}_L$ and of possible configurations of triples of $\mathbb{R}$-planes are equivalent.

It is obvious that the image of $\tilde{\mu}_L$ is contained in that of $\tilde{\mu}$; we conjecture that, as in the case of $U(n)$ investigated in [FW], these images must be equal. Evidence in favor of this is provided by the fact that all our constructive arguments from the preceding section (local surjectivity at an irreducible, description of reducibles and local convexity) carry over to the case of decomposable groups (see also the experimental pictures in section 4.4 which we have obtained by the Lagrangian parametrization). However, the obstruction on Lagrangian configurations of section 4.3.1 does not seem to carry over to the general unitary case, but it is possible that the corresponding chambers be eliminated in that case for different reasons. Or maybe we have just missed the right way to transcribe this condition in the unitary case.

Irreducible groups project to interior points

We begin by showing that the submanifold of decomposable pairs in $C_1 \times C_2$ is tranverse to the fibers of the momentum map, so that the restricted map remains locally surjective.

Proposition 4.3.1 *Let $(A, B) \in C_1 \times C_2$ be a simultaneously decomposable pair which generates an irreducible group with BA regular elliptic. Then the differential of $\tilde{\mu}_L$ at (A, B) is surjective so that $\tilde{\mu}_L$ is locally surjective at that point.*

Proof. We prove this in a manner analogous to that of the corresponding result when the source is all of $C_1 \times C_2$, but the result is more subtle which makes the proof more difficult. We use again the Lie-algebra formalism developed in [FW] for the Lagrangian setting. Our starting point is a triple of $\mathbb{R}$-planes L_1, L_2, L_3 with associated $\mathbb{R}$-reflections σ_1, σ_2, σ_3 such that: $A = \sigma_2\sigma_1$ and $B = \sigma_3\sigma_2$ and we study deformations of the conjugacy class of the product $BA = \sigma_3\sigma_1$. We could write down explicitly the tangent space of decomposable pairs inside the product $C_1 \times C_2$, but this is not easy to do. Instead, we will follow the method of [FW] and investigate an explicit subclass of deformations around a decomposable pair such that these deformations remain decomposable and they sweep all directions in the image. To do this, Falbel and Wentworth introduced two classes of Lagrangian deformations in $U(n)$, which they called *twisting* and *real bending*. The twist deformations are obtained by rotating each Lagrangian plane by a (central) $U(1)$ factor, while the bending deformations are defined by rotating a certain number of the planes by an element which stabilizes one of them (an orthogonal transformation). The twist deformations don't have an obvious analog in the complex hyperbolic setting, whereas the bending deformations can be directly transposed to this case. In fact, the bending deformations will suffice for our purposes; we will focus on those around the $\mathbb{R}$-plane L_2. Precisely, a *real bending about L_2* is a deformation which replaces σ_1, σ_2, σ_3 with σ_1, σ_2,

$O\sigma_3 O^{-1}$ where O is in the stabilizer O_2 of L_2 in $PU(2,1)$ (a subgroup conjugate to $PO(2,1)$). We will prove the following lemma which implies the statement of the proposition:

Lemma 4.3.1 *The real bendings about L_2 sweep all possible deformations of the conjugacy class of $BA = \sigma_3\sigma_1$.*

This can be seen by computing the relative positions of the tangent space to the fiber of π and the image of the bending deformations by the differential of μ in the composite map:

$$C_1 \times C_2 \xrightarrow{\mu} G \xrightarrow{\pi} \mathbb{T}^2/\mathfrak{S}_2$$

These subspaces of the tangent space $T_{BA}G$ can be seen in the Lie algebra $\mathfrak{g} = \mathfrak{su}(2,1)$ by right translation by $(BA)^{-1}$.

We will need the following important result (see Prop. 3.1 of [FW]):

Lemma 4.3.2 *Let L_i and L_j be two $\mathbb{R}$-planes in $H^2_{\mathbb{C}}$, σ_i and σ_j their associated $\mathbb{R}$-reflections with product $g = \sigma_i\sigma_j$. If O_i, O_j denote the stabilizers of L_i and L_j, $Z(g)$ the centralizer of g in $PU(2,1)$, and $\mathfrak{o}_i$, $\mathfrak{o}_j$, $\mathfrak{z}(g)$ the corresponding Lie algebras, then:*

- *there is an orthogonal decomposition: $\mathfrak{z}(g) = (\mathfrak{o}_i + \mathfrak{o}_j)^{\perp} \oplus (\mathfrak{o}_i \cap \mathfrak{o}_j)$*
- *if g is regular elliptic: $\mathfrak{su}(2,1) = \mathfrak{o}_i \oplus \mathfrak{o}_j \oplus \mathfrak{z}(g)$*

The first claim is Prop. 3.1 of [FW]. We derive the second claim (analogous to their Cor. 3.1) by noting that if g is regular elliptic the intersection $\mathfrak{o}_i \cap \mathfrak{o}_j$ is trivial, and that the Killing form is non-degenrate.

Now we can write the deformations of $BA = \sigma_3\sigma_1$ by a real bending around L_2 as paths $O(t)\sigma_3 O(t)^{-1}\sigma_1$ with $O(t) \in O_2$ and $O(1) = Id$. We differentiate this expression and obtain, translating back into $\mathfrak{g}$ by $(BA)^{-1}$ and writing $o = \dot{O}(0)$:

$$(o\sigma_3\sigma_1 - \sigma_3 o\sigma_1)\sigma_1\sigma_3 = (Id - Ad_{\sigma_3})o$$

with $o \in \mathfrak{o}_2$. Thus the image of the vectors tangent to the bending deformations span the subspace $(Id - Ad_{\sigma_3})(\mathfrak{o}_2)$ of $\mathfrak{g}$. Now recall that the tangent space to the fiber of π at the point BA is $Im(Id - Ad_{BA})$. We will have shown the surjectivity of the differential of $\tilde{\mu}_L = \pi \circ \mu_L$ if we prove that the sum of these two subspaces fills the whole tangent space $T_{BA}G$; equivalently we show that their orthogonal complements intersect trivially:

$$((Id - Ad_{\sigma_3})(\mathfrak{o}_2))^{\perp} \cap Im(Id - Ad_{BA})^{\perp} = (Id - Ad_{\sigma_3})(\mathfrak{o}_2)^{\perp} \cap \mathfrak{z}(BA) = \{0\}$$

Indeed, we show successively:

- $z \in (Id - Ad_{\sigma_3})(\mathfrak{o}_2)^{\perp} \iff (Id - Ad_{\sigma_3})z \in \mathfrak{o}_2^{\perp}$
- $z \in \mathfrak{z}(BA) \implies (Id - Ad_{\sigma_3})z \in \mathfrak{z}(BA)$
- $\mathfrak{o}_2^{\perp} \cap \mathfrak{z}(BA) = \{0\}$
- $(Id - Ad_{\sigma_3})z \in \mathfrak{o}_2^{\perp} \cap \mathfrak{z}(BA)$ and $z \in \mathfrak{z}(BA) \iff z = 0$

The first item is obtained by a computation:

$$\begin{array}{rcl} z \in (Id - Ad_{\sigma_3})(\mathfrak{o}_2)^\perp & \iff & (\forall o \in \mathfrak{o}_2)\ \langle o - Ad_{\sigma_3} o, z\rangle = 0 \\ & \iff & (\forall o \in \mathfrak{o}_2)\ \langle o, z\rangle - \langle Ad_{\sigma_3} o, z\rangle = 0 \\ & \iff & (\forall o \in \mathfrak{o}_2)\ \langle o, z\rangle - \langle o, Ad_{\sigma_3} z\rangle = 0 \\ & \iff & (\forall o \in \mathfrak{o}_2)\ \langle o, z - Ad_{\sigma_3} z\rangle = 0 \end{array}$$

For the second item we compute, for $z \in \mathfrak{z}(BA)$:

$$(Id - Ad_{BA})(z - Ad_{\sigma_3} z) = -(Id - Ad_{BA}) Ad_{\sigma_3} z = Ad_{\sigma_3\sigma_1\sigma_3} z - Ad_{\sigma_3} z = Ad_{\sigma_3}(Ad_{(BA)^{-1}} z - z) = 0$$

The third item follows from the above lemma, noting that:

$$\mathfrak{o}_2^\perp \cap \mathfrak{z}(BA) = \mathfrak{o}_2^\perp \cap (\mathfrak{o}_1 \oplus \mathfrak{o}_3)^\perp = (\mathfrak{o}_1 \oplus \mathfrak{o}_2 \oplus \mathfrak{o}_3)^\perp = \{0\}$$

The fourth item is obtained by noting that a $z \in \mathfrak{g}$ which satisfies the left-hand side is both in $\mathfrak{o}_3 = \mathfrak{z}(\sigma_3)$ and in $\mathfrak{o}_1$ which have trivial intersection if BA is regular elliptic. This concludes the proof of the proposition. □

Reducible groups are decomposable

We have just seen that decomposable groups have locally the same image as all elliptic groups near an irreducible. The situation is simpler in the case of reducible groups, which are all decomposable (so that the image is obviously the same).

Proposition 4.3.2 *Let A and B be two elliptic transformations with a common fixed point in $H^2_{\mathbb{C}}$. Then A and B are simultaneously decomposable.*

This was proven in chapter 2 (see [FP], theorem 2.1 on p. 224). The result is also valid for hyperbolic reducible groups (generated by two elliptic elements), which fix a point outside of $H^2_{\mathbb{C}}$.

Proposition 4.3.3 *Let A and B be two elliptic transformations which stabilize a common $\mathbb{C}$-plane. Then A and B are simultaneously decomposable.*

Proof. This is easily seen once we recall the characterization of which $\mathbb{R}$-reflections can appear in a decomposition of an elliptic transformation. Given $g \in PU(2,1)$, we say that an $\mathbb{R}$-plane L *decomposes* g if there is a decomposition $g = \sigma\sigma'$ where σ is the $\mathbb{R}$-reflection in L and σ' is another $\mathbb{R}$-reflection. We have proven in chapter 2 (see Proposition 4 on p. 223 of [FP]) that:

- if g is a complex reflection in a point, then any $\mathbb{R}$-plane through its fixed point decomposes g.
- if g is a $\mathbb{C}$-reflection then any $\mathbb{R}$-plane intersecting its mirror in a geodesic decomposes g.
- if g is regular elliptic, it stabilizes exactly two $\mathbb{C}$-planes (which contain its fixed point). Then an $\mathbb{R}$-plane decomposes g if and only if it passes through its fixed point and interects each of these $\mathbb{C}$-planes in a geodesic.

Now the proposition is obvious because if A and B stabilize a common $\mathbb{C}$-plane it suffices to consider an $\mathbb{R}$-plane containing the geodesic in this $\mathbb{C}$-plane joining the fixed points of A and B if they are both regular elliptic (the other cases are even easier) to see that A and B are simultaneously decomposable. $\square$

Local convexity

All the results of the analogous section on elliptic triangle groups remain valid, because all of our arguments (and computations) were based on reducible groups.

A Lagrangian obstruction

There is a condition on the pairs of angles of a triple of $\mathbb{R}$-planes which intersect pairwise inside $H^2_{\mathbb{C}}$ coming from the fact that the Riemannian angle between two geodesics, each in an $\mathbb{R}$-plane, is bounded by the angle pair as follows (see proposition 1.2.2 in chapter 1):

Proposition 4.3.4 *Let L_1 and L_2 be two intersecting $\mathbb{R}$-planes with angle pair $\{\theta_1, \theta_2\}$ ($\theta_i \in [0, \pi[$) and let $g_1 \subset L_1$, $g_2 \subset L_2$ be two intersecting geodesics, with Riemannian angle $\lambda \in [0, \pi[$. Then the following inequality holds:*

$$\text{Min}\{\theta_1, \theta_2, \pi - \theta_1, \pi - \theta_2\} \leqslant \lambda \leqslant Max\{\theta_1, \theta_2, \pi - \theta_1, \pi - \theta_2\}$$

Recall that a characteristic feature of non-positive curvature (not necessarily constant, see [BGS] p. 6) is that the sum of Riemannian angles in a geodesic triangle is less than π. This fact, combined with the above proposition, gives us the following condition in a Lagrangian triangle:

Proposition 4.3.5 *Let L_1, L_2, L_3 be three pairwise intersecting $\mathbb{R}$-planes with angle pairs $\{\theta_1, \theta_2\}$, $\{\theta_3, \theta_4\}$, $\{\theta_5, \theta_6\}$ ($\theta_i \in [0, \pi[$). Then the following inequality holds:*

$$\sum_{i=1,3,5} \text{Min}\{\theta_i, \theta_{i+1}, \pi - \theta_i, \pi - \theta_{i+1}\} < \pi$$

Now if as before we fix the two first angle pairs $\{\theta_1, \theta_2\}$, $\{\theta_3, \theta_4\}$ and look at the possible values for $\{\theta_5, \theta_6\}$, two possibilities can occur, according to the values of

$$\alpha = \text{Min}\{\theta_1, \theta_2, \pi - \theta_1, \pi - \theta_2\} \text{ and } \beta = \text{Min}\{\theta_3, \theta_4, \pi - \theta_3, \pi - \theta_4\} :$$

- If $\alpha + \beta > \frac{\pi}{2}$ there is no constraint on $\{\theta_5, \theta_6\}$, because we always have:

$$\text{Min}\{\theta_5, \theta_6, \pi - \theta_5, \pi - \theta_6\} \leqslant \frac{\pi}{2}.$$

- If $\alpha + \beta \leqslant \frac{\pi}{2}$ then $\{\theta_5, \theta_6\}$ must satisfy the inequality:

$$\text{Min} = \{\theta_5, \theta_6, \pi - \theta_5, \pi - \theta_6\} < \pi - \alpha - \beta$$

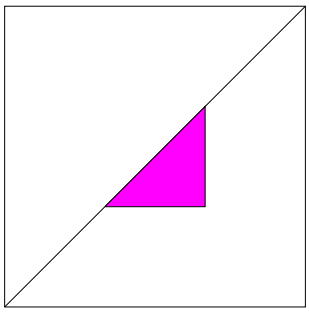

Figure 4.9: Obstruction in a Lagrangian triangle

This condition forbids a triangular region of $\mathbb{T}^2/\mathfrak{S}_2$ near the middle of the diagonal, as in figure 4.9. Unfortunately, we have not found a way to express this obstruction for elliptic triangle groups which are not decomposable, although we conjecture that the image must be the same.

4.3.2 Parametrizing the configurations

In this section we compute explicit parameters for three Lagrangian planes L_0, L_1 and L_2 intersecting pairwise inside complex hyperbolic space, with two prescribed angle pairs

$$\text{Angle}(L_0, L_1) = \{\theta_1, \theta_2\} \quad \text{and} \quad \text{Angle}(L_1, L_2) = \{\theta_3, \theta_4\}.$$

To begin with, we normalize the triple in such a way that L_0 is the standard $\mathbb{R}$-plane (the projection in $\mathbb{C}P^2$ of $\mathbb{R}^3 \subset \mathbb{C}^3$), the intersection point of L_0 and L_1 is O (the center of the ball, projection of the negative vector $[0,0,1]^T \in \mathbb{C}^{2,1}$), and L_1 is the (projection of) the diagonal image:

$$L_1 = \begin{pmatrix} e^{i\theta_1} & 0 & 0 \\ 0 & e^{i\theta_2} & 0 \\ 0 & 0 & 1 \end{pmatrix} \cdot L_0$$

This is the most we can impose, because in general this configuration of two Lagrangians has no isotropy (unless one of the angles is 0, i.e. the Lagrangians have a common geodesic, in which case there is still one parameter of isotropy, namely translation along that geodesic). We are thus left with three parameters: two for the (disk) coordinates x, y inside L_1 of the intersection point $p_1 = L_1 \cap L_2$, and an angle parameter φ for the one-parameter family of Lagrangians L_2 meeting L_1 at p_1 with prescribed angle pair $\{\theta_3, \theta_4\}$ (see next section on pairs of Lagrangians).

For the latter family, the idea is to first parametrize the family of Lagrangians $L_v(\varphi)$ passing through O and having prescribed angle pair $\{\theta_3, \theta_4\}$ with the standard Lagrangian L_0 (this is a linear problem in $\mathbb{C}^2$). We then compute a transformation $U_{01} \in U(2,1)$ which sends L_0 with its marked point O to L_1 with its marked point p_1; this is done by means of a somewhat tedious calculation which is analogous to a Gram-Schmidt orthonormalization procedure. The third Lagrangian $L_2(\varphi)$ is then simply the image $U_{01}(L_v(\varphi))$.

In fact our principal object of interest is a matrix associated to the $\mathbb{R}$-reflection σ_2 in $L_2(\varphi)$, i.e. a matrix $A_2 \in U(2,1)$ such that, in ball coordinates z, $\sigma_2(z) = A_2.\overline{z}$. Another way to write

this is that A_2 is the matrix of the unitary transformation $\sigma_2 \circ \sigma_0$, which makes it clear that it encodes the configuration of the two $\mathbb{R}$-planes L_0 and L_2 (A_2 was called a *Souriau matrix* of the pair (L_0, L_2) in [N],[FP]). In fact, the type of this isometry (elliptic, parabolic, or loxodromic) tells us if the two $\mathbb{R}$-planes intersect inside, on the boundary of, or outside the complex ball; and its precise conjugacy class (in the case we are interested in, namely the elliptic case) gives us the angle pair of the $\mathbb{R}$-planes. More precisely (see [CG] p. 64 for details), an elliptic transformation g of $H^2_{\mathbb{C}}$ is represented in $U(2,1)$ by matrices which are semisimple with eigenvalues of norm 1. One of the eigenvalues is of *negative type*, in the sense that the corresponding eigenspace is contained in the negative cone of the Hermitian form on $\mathbb{C}^{2,1}$ (and thus projects to the fixed point of g in $H^2_{\mathbb{C}}$). If the eigenvalues are $e^{i\phi_1}$,$e^{i\phi_2}$ and $e^{i\phi_3}$, with the latter of negative type, then the conjugacy class of g is characterized by the (rotation) angle pair $\{\phi_1 - \phi_3, \phi_2 - \phi_3\}$, and the (reflection) angle pair of $\mathbb{R}$-planes L_0 and L_2 is simply $\{\frac{\phi_1-\phi_3}{2}, \frac{\phi_2-\phi_3}{2}\}$.

This is very easy to describe in terms of eigenvalues and eigenvectors, but for concrete purposes, our matrix $A_2(\theta_1, \theta_2, \theta_3, \theta_4, \varphi, x, y)$ being rather complicated, it is hopeless to write explicit formulae for these angles in terms of our parameters (however, this direct approach works very well for numerical experiments). We can circumvent this difficulty by only computing the trace of A_2 (suitably normalized in $SU(2,1)$), which is in principle enough to characterize the conjugacy class of g (see [G] p. 204), in fact up to a threefold indetermination, see chapter 1.

Pairs of Lagrangians

We describe here the family of Lagrangians of $\mathbb{C}^2$ meeting the standard Lagrangian $L_0 = \mathbb{R}^2 \subset \mathbb{C}^2$ with prescribed angle pair $\{\theta_3, \theta_4\}$.

Proposition 4.3.6 *Let $\theta_3, \theta_4 \in \mathbb{R}/\pi\mathbb{Z}$. If $\theta_3 \neq \theta_4$, there is a one-parameter family $L_v(\varphi)$ ($\varphi \in \mathbb{R}/\pi\mathbb{Z}$) of Lagrangians of $\mathbb{C}^2$ meeting the standard Lagrangian L_0 with angle pair $\{\theta_3, \theta_4\}$, given by:*

$$L_v(\varphi) = \begin{pmatrix} e^{i\theta_3}\cos\varphi & -e^{i\theta_4}\sin\varphi \\ e^{i\theta_3}\sin\varphi & e^{i\theta_4}\cos\varphi \end{pmatrix} \cdot L_0$$

If $\theta_3 = \theta_4$, this family is reduced to a point.

Proof. This follows directly from Nicas' diagonalization lemma (see [N] p. 74), which states that there exists an orthonormal basis (v_1, v_2) of L_0 such that $(e^{i\theta_3}v_1, e^{i\theta_4}v_2)$ is a basis of $L_v(\varphi)$. □

A unitary map $U_{01} : (L_0, O) \longmapsto (L_1, p_1)$

In this section we compute a matrix $U_{01} \in U(2,1)$ which sends the $\mathbb{R}$-plane L_0 with the marked point O to L_1 with a marked point p_1 corresponding to the vector (which we also denote p_1):

$$p_1(x,y) = \begin{bmatrix} e^{i\theta_1}x \\ e^{i\theta_2}y \\ 1 \end{bmatrix} \text{ with } (x,y) \text{ in the unit disc of } \mathbb{R}^2.$$

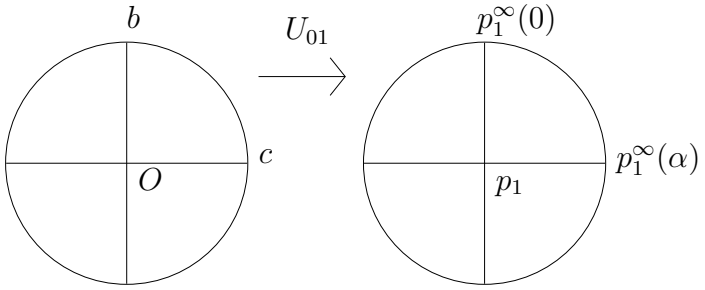

The idea is to complete each of these vectors into an ($\mathbb{R}$-) basis of the corresponding Lagrangian, suitably normalized as to obtain a unitary transformation. A simple way to do this is to choose the two remaining points on the boundary of each Lagrangian (the corresponding vectors will then have null norm, so that we can rescale them at leisure). We do this in the following manner, choosing two points b and c in L_0 corresponding to orthogonal geodesics through O, and parametrizing the points on the boundary of L_1 by:

$$p_1^\infty(\alpha) = \begin{bmatrix} e^{i\theta_1}\cos\alpha \\ e^{i\theta_2}\sin\alpha \\ 1 \end{bmatrix} \text{ with } \alpha \in \mathbb{R}/2\pi\mathbb{Z}.$$

We then want to send:

$$\begin{aligned} a = O = [0,0,1]^T &\longmapsto a' = p_1(x,y) \\ b = [1,0,1]^T &\longmapsto b' = p_1^\infty(0) \\ c = [0,1,1]^T &\longmapsto c' = p_1^\infty(\alpha) \end{aligned}$$

with the following compatibility conditions which ensure that the map is unitary:

$$\begin{cases} \langle a', a'\rangle = \langle a, a\rangle = -1 \\ \langle a', b'\rangle = \langle a, b\rangle = -1 \\ \langle a', c'\rangle = \langle a, c\rangle = -1 \\ \langle b', c'\rangle = \langle b, c\rangle = -1 \end{cases}$$

We begin by normalizing a': $\langle a', a'\rangle = x^2 + y^2 - 1$, so that we set:

$$a' := \frac{1}{r}\begin{bmatrix} e^{i\theta_1}x \\ e^{i\theta_2}y \\ 1 \end{bmatrix} \text{ with } r = \sqrt{1 - x^2 - y^2}.$$

We then force the second condition; $\langle a', b'\rangle = \frac{x-1}{r}$, so that we set:

$$b' := \frac{1}{s}\begin{bmatrix} e^{i\theta_1} \\ 0 \\ 1 \end{bmatrix} \text{ with } s = \frac{1-x}{r}.$$

Now the last two conditions are more delicate because they must be handled simultaneously. We still have the free parameter α (which has a clear geometric meaning), as well as a normalization parameter for c'. Explicitly, if we dilate c' by a real factor $-1/t$, then we must solve the following system:

$$\begin{cases} x\cos\alpha + y\sin\alpha - 1 &= rt \\ \cos\alpha - 1 &= st \\ \cos^2\alpha + \sin^2\alpha &= 1 \end{cases}$$

where we have used that $\langle a', c'\rangle = -\frac{1}{rt}(x\cos\alpha + y\sin\alpha - 1)$ and $\langle b', c'\rangle = -\frac{1}{st}(\cos\alpha - 1)$.

This system is equivalent, by some linear substitutions, to a certain quadratic equation in $\cos\alpha$, namely:

$$\cos^2\alpha(y^2 + (x - r/s)^2) + 2(x - r/s)(r/s - 1)\cos\alpha + (r/s - 1)^2 - y^2 = 0$$

The explicit solutions of this equation are quite ugly, but as it turns out they will simplify, so we keep $\cos\alpha$ and $\sin\alpha$ in this form for now. We thus have:

$$c' := -\frac{1}{t}\begin{bmatrix} e^{i\theta_1}\cos\alpha \\ e^{i\theta_2}\sin\alpha \\ 1 \end{bmatrix} \text{ with } t = \frac{\cos\alpha - 1}{s}.$$

It remains to form the matrix U_{01}; this is easy with what we have done: if M (resp. M') is the matrix whose column-vectors are a, b, c (resp. a', b', c'), then $U_{01} = M'.M^{-1}$. This gives us:

$$U_{01} = \begin{pmatrix} e^{i\theta_1}(1/s - x/r) & e^{i\theta_1}(-(\cos\alpha)/t - x/r) & e^{i\theta_1}x/r \\ -e^{i\theta_2}y/r & e^{i\theta_2}(-(\sin\alpha)/t - y/r) & e^{i\theta_2}y/r \\ 1/s - 1/r & -1/t - 1/r & 1/r \end{pmatrix}$$

with r, s, t as above.

This is where the expressions involving $\cos\alpha$ and $\sin\alpha$ simplify, because:

$$-(\cos\alpha)/t - x/r = y/(1 - x) \text{ and } -(\sin\alpha)/t - y/r = 1$$

as can be seen by rewriting the above quadratic equation in terms exclusively of x and y. This gives us the final form of U_{01}:

$$U_{01} = \begin{pmatrix} e^{i\theta_1}(1/s - x/r) & e^{i\theta_1}(y/(1 - x)) & e^{i\theta_1}x/r \\ -e^{i\theta_2}y/r & e^{i\theta_2} & e^{i\theta_2}y/r \\ 1/s - 1/r & y/(1 - x) & 1/r \end{pmatrix}$$

where, as before, $r = \sqrt{1 - x^2 - y^2}$ and $s = \frac{1-x}{r}$.

The unitary matrix $A_2(\theta_1, \theta_2, \theta_3, \theta_4, \varphi, x, y)$

The map U_{01} gives us then a parametrization of the family of $\mathbb{R}$-planes L_2 meeting L_1 at the point p_1 with prescribed angle pair $\{\theta_3, \theta_4\}$, by simply transporting the previous family $L_v(\varphi)$ via U_{01}. We denote $U_{\{\theta_3,\theta_4\}}(\varphi) \in U(2,1)$ the following matrix, which is obtained by the embedding of $U(2)$ in $U(2,1)$ as the stabilizer of the origin O:

$$U_{\{\theta_3,\theta_4\}}(\varphi) = \begin{pmatrix} e^{i\theta_3}\cos\varphi & -e^{i\theta_4}\sin\varphi & 0 \\ e^{i\theta_3}\sin\varphi & e^{i\theta_4}\cos\varphi & 0 \\ 0 & 0 & 1 \end{pmatrix}$$

Then our family of $\mathbb{R}$-planes L_2 is:

$$L_2(\varphi) := U_{01} \cdot L_v(\varphi) = U_{01} U_{\{\theta_3,\theta_4\}}(\varphi) \cdot L_0$$

so that the matrix A_2 which we are interested in (such that $\sigma_2(z) = A_2.\overline{z}$) can be written, knowing that the $\mathbb{R}$-reflection in L_0 is simply $z \mapsto \overline{z}$:

$$A_2 = U_{01}.U_{\{\theta_3,\theta_4\}}(\varphi).\overline{U_{\{\theta_3,\theta_4\}}(\varphi)^{-1}}.\overline{U_{01}^{-1}}$$

We can simplify his expression a bit, by setting for instance:

$$\tilde{U}_{\{\theta_3,\theta_4\}}(\varphi) := U_{\{\theta_3,\theta_4\}}(\varphi).\overline{U_{\{\theta_3,\theta_4\}}(\varphi)^{-1}}$$

$$= \begin{pmatrix} e^{2i\theta_3}\cos^2\varphi + e^{2i\theta_4}\sin^2\varphi & (e^{2i\theta_3} - e^{2i\theta_4})\cos\varphi\sin\varphi & 0 \\ (e^{2i\theta_3} - e^{2i\theta_4})\cos\varphi\sin\varphi & e^{2i\theta_3}\sin^2\varphi + e^{2i\theta_4}\cos^2\varphi & 0 \\ 0 & 0 & 1 \end{pmatrix}$$

$$= \begin{pmatrix} k & l & 0 \\ l & m & 0 \\ 0 & 0 & 1 \end{pmatrix}$$

Moreover, the coefficients of $\overline{U_{01}^{-1}}$ are simply obtained from those of $U_{01} \in U(2,1)$ (see [P] p. 9) in the following way. Write U_{01} as:

$$U_{01} = \begin{pmatrix} a & b & c \\ d & e & f \\ g & h & j \end{pmatrix}$$

Then:

$$\overline{U_{01}^{-1}} = \begin{pmatrix} a & d & -g \\ b & e & -h \\ -c & -f & j \end{pmatrix}$$

In the end, this gives us the following expression of A_2:

$$\begin{pmatrix} a^2k + 2abl + b^2m - c^2 & adk + ael + bdl + bem - cf & -agk - ahl - bgl - bhm + cj \\ adk + ael + bdl + bem - cf & d^2k + 2del + e^2m - f^2 & -dgk - dhl - egl - ehm + fj \\ agk + ahl + bgl + bhm - cj & dgk + dhl + egl + ehm - fj & -g^2k - 2ghl - h^2m + j^2 \end{pmatrix}$$

where:

$$
\begin{aligned}
a &= e^{i\theta_1}(1/s - x/r)\\
b &= e^{i\theta_1}(y/(1-x))\\
c &= e^{i\theta_1}x/r\\
d &= -e^{i\theta_2}y/r\\
e &= e^{i\theta_2}\\
f &= e^{i\theta_2}y/r\\
g &= 1/s - 1/r\\
h &= y/(1-x)\\
j &= 1/r\\
k &= e^{2i\theta_3}\cos^2\varphi + e^{2i\theta_4}\sin^2\varphi\\
l &= (e^{2i\theta_3} - e^{2i\theta_4})\cos\varphi\sin\varphi\\
m &= e^{2i\theta_3}\sin^2\varphi + e^{2i\theta_4}\cos^2\varphi
\end{aligned}
$$

Trace, determinant and angles

As we have said above, this expression of A_2 is quite indigest, and in particular it is not reasonable to compute formally its eigenvalues; however we can compute its trace. Note that, for this trace to have any meaning in $PU(2,1)$, we should normalize A_2 (for instance in $SU(2,1)$), or at least keep track of its determinant. This determinant is easily obtained, knowing that by the multiplicative expression:

$$A_2 = U_{01}.\tilde{U}_{\{\theta_3,\theta_4\}}(\varphi).\overline{U_{01}^{-1}}$$

we will have:

$$\det A_2 = e^{2i\psi}.\det\tilde{U}_{\{\theta_3,\theta_4\}}(\varphi) \text{ if } \det U_{01} = r.e^{i\psi} \text{ in polar coordinates.}$$

Then, noting that $\det\tilde{U}_{\{\theta_3,\theta_4\}}(\varphi) = e^{2i(\theta_3+\theta_4)}$, we have the nice expression:

$$\det A_2 = e^{2i(\theta_1+\theta_2+\theta_3+\theta_4)}.$$

The trace of A_2 is obtained from the explicit form of A_2 by a simple but tedious computation. We obtain:

$$
\begin{aligned}
TrA_2 &= (a^2+d^2-g^2)k + 2(ab+de-gh)l + (b^2+e^2-h^2)m + j^2 - c^2 - f^2\\
&= e^{2i(\theta_1+\theta_3)}[(1/s - x/r)\cos\varphi + y/(1-x)\sin\varphi]^2\\
&+ e^{2i(\theta_1+\theta_4)}[(1/s - x/r)\sin\varphi - y/(1-x)\cos\varphi]^2\\
&+ e^{2i(\theta_2+\theta_3)}[y/r\cos\varphi - \sin\varphi]^2\\
&+ e^{2i(\theta_2+\theta_4)}[y/r\sin\varphi + \cos\varphi]^2\\
&- e^{2i\theta_1}x^2/r^2\\
&- e^{2i\theta_2}y^2/r^2\\
&- e^{2i\theta_3}[(1/s - 1/r)\cos\varphi + y/(1-x)\sin\varphi]^2\\
&- e^{2i\theta_4}[(1/s - 1/r)\sin\varphi - y/(1-x)\cos\varphi]^2\\
&+ 1/r^2
\end{aligned}
$$

We will use this explicit formula to determine the fibers in certain cases where it simplifies a bit, see section 4.5.

4.4 Examples and experimental pictures

In this section we investigate specific examples of the polygonal image of $\tilde{\mu}$ which we have described. Each such example is given by fixing two pairs of angles $\{\theta_1, \theta_2\}$ and $\{\theta_3, \theta_4\}$, corresponding to the elliptic conjugacy classes of the two generators A and B. Recall that the map $\tilde{\mu}$ sends a pair (A, B) of elliptic isometries (each in a fixed conjugacy class) to the angle pair of the product AB (if it is elliptic). Note that these are rotation angles; they are the double of the angles in the Lagrangian triple (or reflection angles). We try to emphasize the experimental manner in which the structure of these polygons was discovered by giving two pictures for each example. The first, in the spirit of section 4.2, shows the collection of reducible walls in the half-square affine chart of $\mathbb{T}^2/\mathfrak{S}_2$; we have added crosshatching in the region which is proved to be contained in the image (see theorem 4.2.1). The second is an experimental picture obtained (via Maple) by the parametrization of Lagrangian triples of section 4.3 (which depends on the 3 above real parameters x, y and φ), using a grid-like partition of the parameters (with circle coordinates for the angle and polar coordinates for the two disk parameters). Typically each picture has between 1000 and 20000 points, each of these taking approximately 0.1 seconds to compute using an ordinary machine, so that the whole picture takes between a minute and a half hour to compute.

We start with the degenerate cases where at least one of the generators is a complex reflection (one angle is zero) or a complex reflection in a point (two equal angles); these cases do not exactly fit in the generic description which we have given, so that we describe them here in detail. In fact in all these cases (except the non-convex case of two $\mathbb{C}$-reflections) we can prove that the image is exactly the convex hull of the reducibles. The result is the following:

Proposition 4.4.1 *If one of the generators A or B is a complex reflection (resp. in a point) then the momentum polygon is exactly the convex hull of the reducible walls. Moreover, for each point on the boundary of the square which is in the image but not reducible, the product AB is parabolic.*

Recall that in general we do not know whether the latter points (with angles $\{0, \theta\}$) represent parabolic elements or complex reflections.

Proof. The argument is the same for both claims; it is simply the fact that if A or B is special elliptic (a complex reflection or a complex reflection in a point) and if AB is also special elliptic, then the group is reducible. Indeed, these two motions then each fix pointwise a complex line of $\mathbb{C}P^2$, and these lines must intersect in $\mathbb{C}P^2$. Thus all chambers touching the diagonal at more than a reducible point are excluded. □

A case of particular interest is the case of one complex reflection, since it contains the case which originally motivated this work, that of Mostow's lattices $\Gamma(p, t)$ (see [M1], [M2] and figures 4.13 and 4.14). We will go into this example in more detail in the last section, in the hope of finding new discrete groups in those pictures.

The generic examples which we have included after that span the different types of reducible configurations described in section 4.2.3 and complete the proof of the classification. We also hope that they will provide the reader with some insight as to the possible behavior of these objects: inner and outer walls, self-intersection...

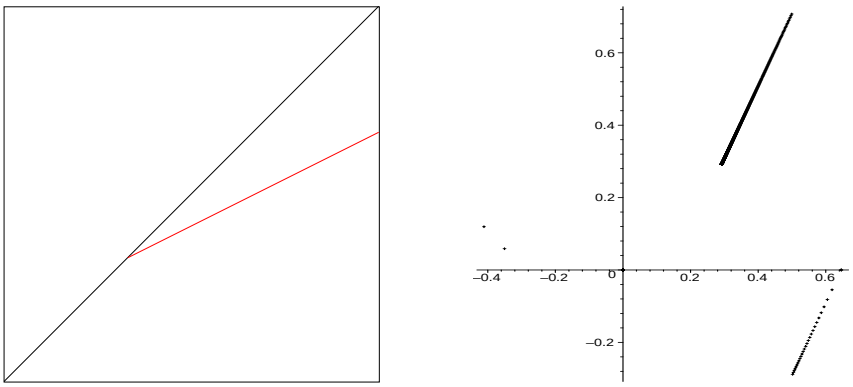

Figure 4.10: The picture for angle pairs $\{\frac{2\pi}{6}, \frac{2\pi}{6}\}$, $\{\frac{2\pi}{8}, \frac{2\pi}{8}\}$

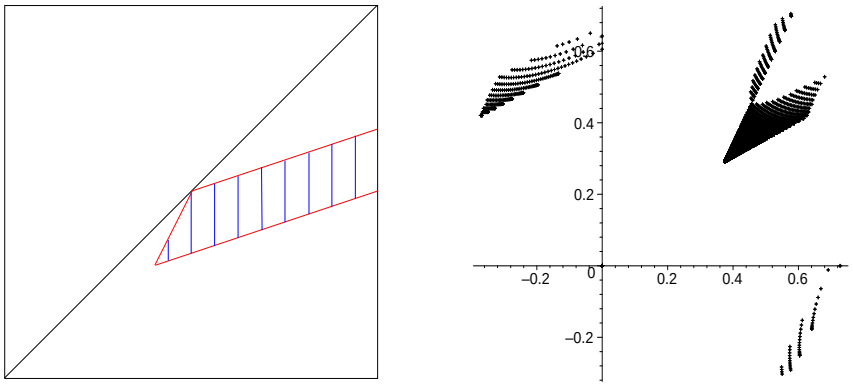

Figure 4.11: The picture for angle pairs $\{\frac{2\pi}{4}, \frac{2\pi}{6}\}$, $\{\frac{2\pi}{8}, \frac{2\pi}{8}\}$

4.4.1 The two generators are complex reflections in a point

This is the most degenerate case because the reducibles consist in a single totally reducible vertex (on the diagonal) with a single hyperbolic reducible segment, so that the whole image is this segment (see figure 4.10). Indeed, a complex reflection in a point stabilizes all $\mathbb{C}$-planes containing its fixed point (in $U(2)$ such an element is a central $e^{i\theta}.Id$), so that two of these transformations always generate a hyperbolic reducible group: they both stabilize the $\mathbb{C}$-plane containing the two fixed points.

4.4.2 One generator is a complex reflection in a point

As above there is only one totally reducible vertex, but now it gives rise to two hyperbolic reducible segments, which enclose a convex hull with non-empty interior (see figure 4.11). The image is exactly this convex hull because of the above argument (if a point of the image is on the diagonal then it must be reducible).

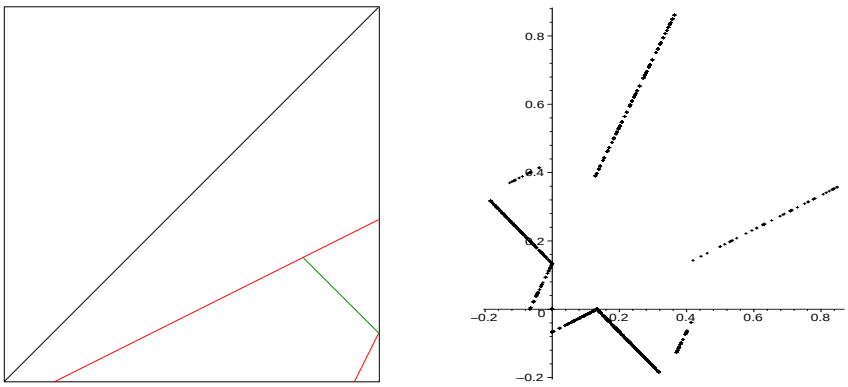

Figure 4.12: The picture for angle pairs $\{0, \frac{2\pi}{3}\}$, $\{0, \frac{8\pi}{5}\}$ (non-convex)

4.4.3 The two generators are complex reflections: a non-convex example

This is the case where our argument of local convexity at a totally reducible vertex fails, and it fails for the good reason that the result is not true in this case. There are now two distinct reducible vertices joined by a spherical reducible segment, as well as one hyperbolic reducible segment (the others collapse to a point) which contains both vertices (see figure 4.12). The whole image is the non-convex union of these two segments, because two complex reflections always generate a reducible group (their mirrors, or fixed-point loci, intersect in $\mathbb{C}P^2$).

4.4.4 One generator is a complex reflection: families containing Mostow's lattices $\Gamma(p, t)$

The reducible configuration now consists in the spherical reducible segment together with two non-degenerate hyperbolic reducible segments (one at each vertex); as before we know that the whole image is exactly the convex hull of the reducibles (see figures 4.13, 4.14). In these figures we have also featured a segment inside the polygon which represents Mostow's one-parameter family of lattices $\Gamma(p, t)$ (here, each integer value of p corresponds to a different picture). We will focus on the case of $\Gamma(3, t)$ in the last section (in our notation, this is a segment inside the image for pairs $\{\frac{2\pi}{3}, \frac{4\pi}{3}\}$, $\{0, \frac{2\pi}{3}\}$).

4.4.5 Generic examples

We now come to generic cases which illustrate more faithfully our description of reducible configurations. As we have said, the values we have chosen here are meant to show different cases of our classification of reducible types. We will just mention some remarkable features of these pictures. The case of pairs $\{\frac{2\pi}{3}, \frac{2\pi}{4}\}$, $\{\frac{2\pi}{5}, \frac{2\pi}{6}\}$ (figure 4.15) shows self-intersection of the reducibles, namely different hyperbolic reducible segments meeting. Also, it is worth noting that the same hyperbolic reducible segment can have a part which is an outer wall of the image, and another which is an inner wall (before or after bouncing off the diagonal). Moreover the image contains a segment of the diagonal. The next pictures also feature some inner vertices

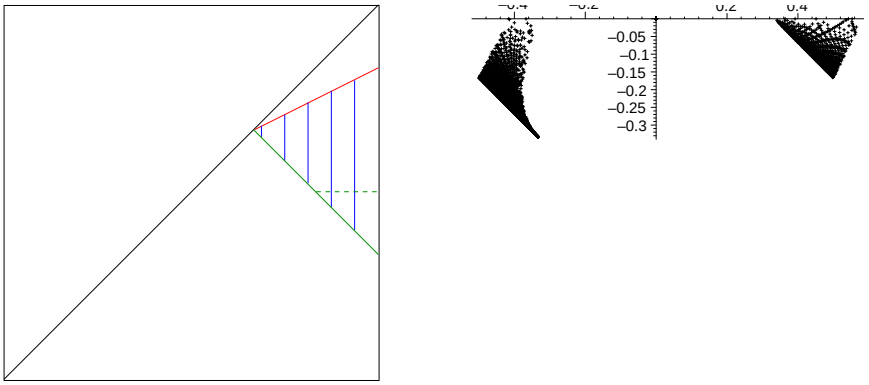

Figure 4.13: The picture for angle pairs $\{\frac{2\pi}{3}, \frac{4\pi}{3}\}$, $\{0, \frac{2\pi}{3}\}$; the dotted line represents Mostow's family $\Gamma(3, t)$ (see also enlargement in figure 4.22).

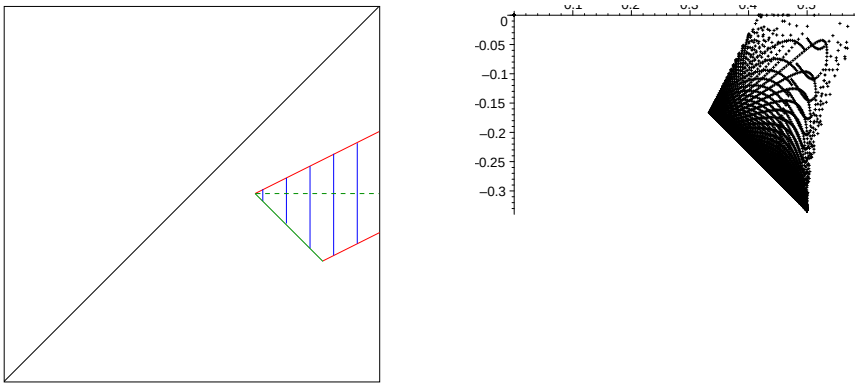

Figure 4.14: The picture for angle pairs $\{\frac{2\pi}{3}, \frac{4\pi}{3}\}$, $\{0, \frac{2\pi}{6}\}$; the dotted line represents Mostow's family $\Gamma(6, t)$.

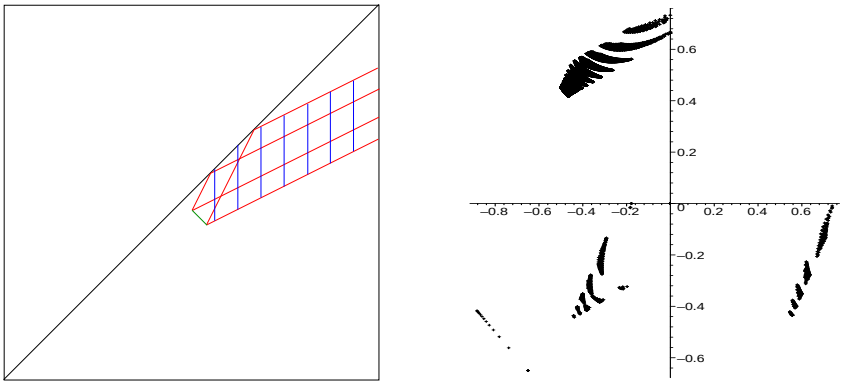

Figure 4.15: The picture for angle pairs $\{\frac{2\pi}{3}, \frac{2\pi}{4}\}$, $\{\frac{2\pi}{5}, \frac{2\pi}{6}\}$ (type C^{++}_{++})

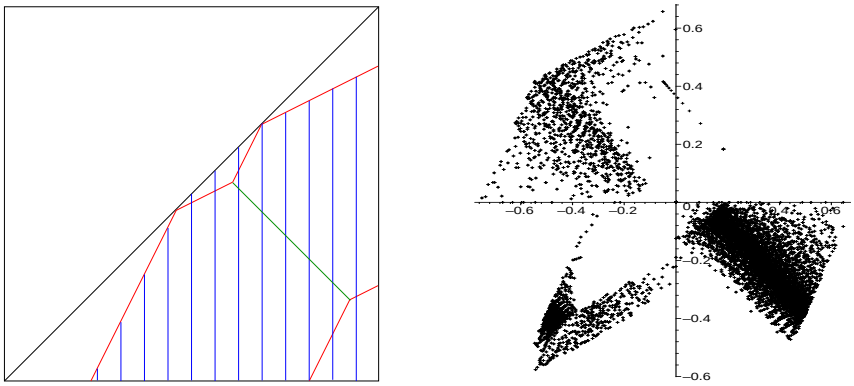

Figure 4.16: The picture for angle pairs $\{\frac{2\pi}{3}, -\frac{2\pi}{4}\}$, $\{\frac{2\pi}{5}, -\frac{2\pi}{6}\}$ (type C^{+-}_{-+})

(totally reducible vertices which are interior points of the image), which are easily spotted on the experimental picture.

4.5 The search for discrete groups: experimental aspects

There is an obvious condition that a subgroup of $PU(2,1)$ must satisfy in order to be discrete (as in any Lie group acting on a space with compact point stabilizers), namely that elements in this subgroup which fix a point must be of finite order. For an elliptic element in $PU(2,1)$, this means that both of its angles are rational multiples of π; in fact it is often safer to ask for integer fractions of 2π (or for pairs of the type $\{\frac{2\pi}{n}, \frac{2k\pi}{n}\}$) for some generators if we hope for Poincaré-type tessellation conditions.

Our setting is well adapted to this simple idea because we can simultaneously control the angles of the generators A, B and of their product. Moreover the parametrization we have given using Lagrangian planes (3 parameters once the angles of A and B are given) leaves us in general with a one-dimensional fiber of non-conjugate groups where the angles of the product remain unchanged. One-dimensional objects are very nice because you can wander through them without getting lost, and mostly without missing any points (in a connected component). If you are looking for something rare and precious like a lattice (which is an isolated point by

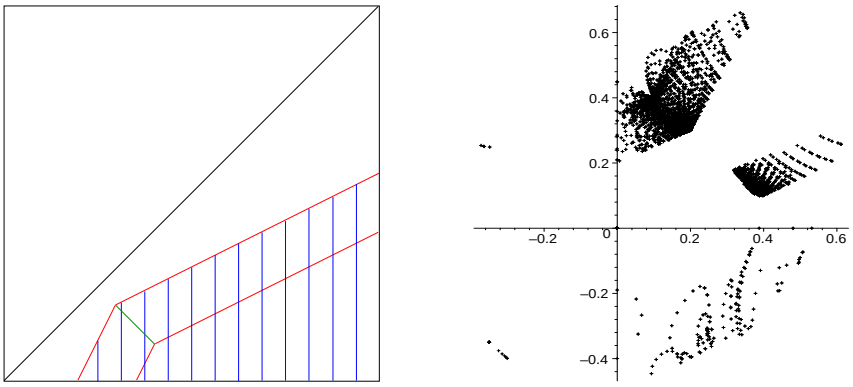

Figure 4.17: The picture for angle pairs $\{-\frac{2\pi}{10}, \frac{2\pi}{10}\}$, $\{\frac{4\pi}{10}, \frac{6\pi}{10}\}$ (type C_{-+}^{-+})

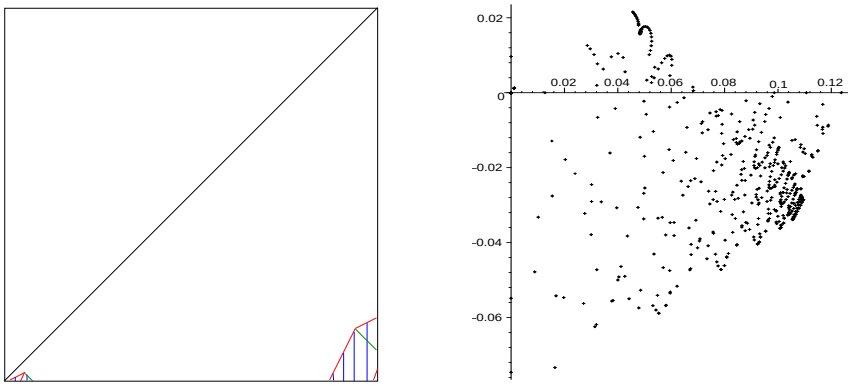

Figure 4.18: The picture for angle pairs $\{\frac{2\pi}{4}, \frac{2\pi}{6}\}$, $\{-\frac{2\pi}{5}, -\frac{2\pi}{7}\}$ (type D_{--}^{-+})

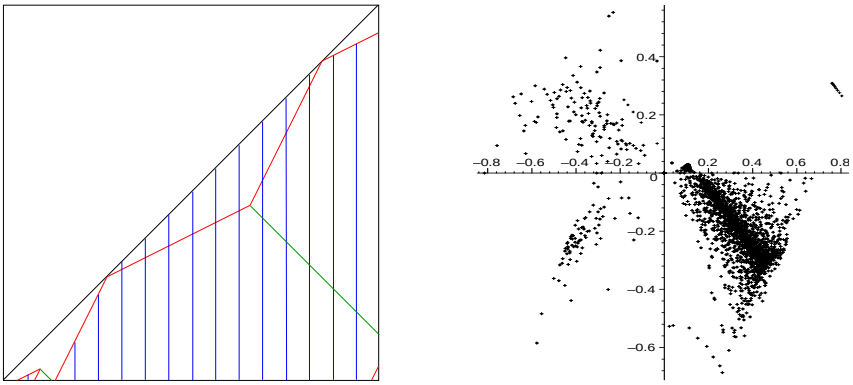

Figure 4.19: The picture for angle pairs $\{\frac{2\pi}{4}, -\frac{2\pi}{6}\}$, $\{\frac{2\pi}{5}, -\frac{2\pi}{7}\}$ (type D_{--}^{+-})

Mostow's rigidity theorem), staying on such a path will spare you the unpleasant impression of looking for a needle in a haystack, provided that the path in question has any good reason to contain one. All previous families of examples were found according to this guiding principle: Mostow's lattices (see [M1], [M2] and below), the ideal triangle groups of Goldman and Parker along with other triangle groups investigated by Falbel-Koseleff, Gusevskii-Parker, Schwartz, Falbel-Parker, Deraux... (see [Sz1] for an overview of these groups).

A first difficulty is then to choose a place to start looking; we have chosen as a first step to further investigate some cases where lattices or discrete groups were previously known to exist. For the time being, we have only begun the search in the case of Mostow's lattices $\Gamma(3,t)$. This case is not typical because one of the generators is a $\mathbb{C}$-reflection, so that there are no fibers: each point of the image of $\tilde{\mu}$ (a triangle) corresponds to a single group generated by $\mathbb{R}$-reflections. For this reason we also include here an apparently less interesting example containing $\mathbb{R}$-Fuchsian groups to illustrate deformations inside a fiber.

What we have seen so far only indicates what might be some interesting candidates for discrete groups or lattices, but there remains the difficult question of deciding whether or not a given group (defined by two matrix generators) is discrete. There are several ways to do this; a basic idea (which is mostly useful to discard indiscrete groups) is to test all words of a given maximal length, first sorting out which of them are elliptic, then computing their angles. The strategy here is to stop at the first word which "doesn't work", and see what happens to this word by deformation in the fiber. In the case of triangle groups generated by three complex involutions, Schwartz conjectures that two words (namely $ACBC$ and ABC) govern the behavior of the whole group (see again [Sz1]). We hope for a similar phenomenon to make our strategy reasonable: in the worst case, the first word for which you need to deform leaves you only with isolated points in the fiber, so that you are quickly left with nothing if there are many problematic conjugacy classes.

There is also a notable difference between being convinced that a group is discrete and proving it. In fact, if there is no arithmetic reason for the group to be discrete, there are very few methods to do this, the most widely used being to construct a fundamental domain for the action of the group on $H^2_{\mathbb{C}}$. There are many beautiful and exotic constructions of such objects, but it is no easy task and should only be undertaken for good reasons. There are other experimental methods which can provide a good compromise, such as Deraux's use of the Dirichlet method (see [D1], [D2]) which we apply to some of our groups using his java applets ([D3]), modified according to the generators.

Before going into the details, we point out the fact that the process is only at its beginning, so that at this point we describe more a research project than factual results.

4.5.1 Families containing Mostow's lattices $\Gamma(p,t)$

We will focus on the groups introduced by Mostow in his 1980 paper ([M1]), which he denoted $\Gamma(p,t)$ (where $p = 3,4,5$ and t is a real parameter); note however that this description also includes, for larger integer values of p, 22 of the 27 Picard lattices (also known as the Deligne-Mostow lattices of dimension 2), as described in detail in his subsequent paper [M2].

We will only decribe briefly the construction of these groups, for which we refer to (the original paper or) chapter 3 (see [DFP]). The group $\Gamma(p,t)$ is generated by three braiding complex reflections of order p (R_1,R_2, and R_3) which are permuted by a cyclic element J. We

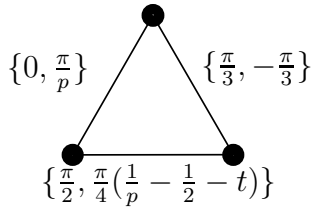

Figure 4.20: Diagram of $\mathbb{R}$-reflections for $\tilde{\Gamma}(p,t)$

consider as in [DFP] not exactly $\Gamma(p,t)$ but the sometimes bigger group $\tilde{\Gamma}(p,t)$ generated by R_1 and J (it contains $\Gamma(p,t)$ with index 1 or 3). We have noticed that these two generators are decomposed into $\mathbb{R}$-reflections in the following way (with the notation from [DFP]):

$$\begin{cases} J &= \sigma_{12}\sigma_{23} \\ R_1 &= \sigma_{23}\tau \end{cases}$$

The elliptic transformations R_1 and J have respective angle pairs $\{0, \frac{2\pi}{p}\}$ and $\{\frac{2\pi}{3}, -\frac{2\pi}{3}\}$. A computation using the explicit form for these matrices tells us that the product $JR_1 = \sigma_{12}\tau$ is semisimple with eigenvalues $-\eta i\overline{\phi} = e^{i\pi(1+1/p+1/2-t/3)}$ and $\pm\sqrt{-\eta i\phi} = \pm e^{i\pi(1+1/p+1/2+t/3)/2}$ where $\eta = e^{i\pi/p}$ and $\phi = e^{i\pi t/3}$. Thus it is elliptic and its angles are given by dividing the two eigenvalues of positive type by that of negative type, which is here (by a tedious computation) $-e^{i\pi(1+1/p+1/2+t/3)/2}$. We obtain for JR_1 the angle pair $\{\pi, \frac{\pi}{2}(\frac{1}{p} - \frac{1}{2} - t)\}$ (note that $(JR_1)^2$ is a complex reflection). The angles in the Lagrangian triple are obtained by dividing all of these by two; this gives us the diagram of figure 4.20.

We now consider the case $p = 3$ and see how the family $\tilde{\Gamma}(p,t)$ fits into the picture of the momentum polygon associated to angle pairs $\{0, \frac{2\pi}{p}\}$ and $\{\frac{2\pi}{3}, -\frac{2\pi}{3}\}$. This gives us the segment of figure 4.13, which we will now enlarge in order to see the points corresponding to lattices (see figure 4.22). Note that this segment is characterized by the fact that R_1 and its two conjugates R_2 and R_3 satisfy a braiding relation of order 3 (namely, $R_iR_jR_i = R_jR_iR_j$). There are 8 values of the parameter t which yield lattices, listed in the table of figure 4.21 along with the corresponding values of the (non-trivial) rotation angle of JR_1.

An important thing to note is that this angle is closely related to one of the two conditions (the Picard integrality conditions, see [DFP]) which ensure the discreteness of the group. Recall that these conditions come from the analysis of only two conjugacy classes of $\mathbb{C}$-reflections in the group, namely those of R_2R_1J and $J^{-1}R_1R_2$; their rotation angle must be an integer fraction of 2π if the group is to be discrete, and it turns out that these two conditions suffice. Now the former of these conjugacy classes contains $(R_1J^{-1})^2$ and the latter contains $(JR_1)^2$, because $R_2 = JR_1J^{-1}$ so that:

$$R_2R_1J = JR_1J^{-1}R_1J = J(R_1J^{-1}R_1J^{-1})J^{-1} \text{ and } J^{-1}R_1R_2 = J^{-1}R_1JR_1J^{-1} = J(JR_1JR_1)J^{-1}$$

This means that one of the two discreteness conditions is immediately visible on our picture: the angle of JR_1 which depends on the parameters must be an even integer fraction of 2π. In fact the second condition also fits in the same picture, because it so happens that J^{-1} is conjugate to J, so that the angles of R_1J^{-1} are contained in the same picture (but correspond to different points). The value of the (non-trivial) rotation angle of R_1J^{-1} in the 8 discrete groups is also listed in table 4.21; the corresponding points of the picture are in the same segment as the

t	0	$\frac{1}{30}$	$\frac{1}{18}$	$\frac{1}{12}$	$\frac{5}{42}$	$\frac{1}{6}$	$\frac{7}{30}$	$\frac{1}{3}$
$-\frac{1}{\pi}\cdot$Angle of JR_1	$\frac{1}{12}$	$\frac{1}{10}$	$\frac{1}{9}$	$\frac{1}{8}$	$\frac{1}{7}$	$\frac{1}{6}$	$\frac{1}{5}$	$\frac{1}{4}$
$-\frac{1}{\pi}\cdot$Angle of R_1J^{-1}	$\frac{1}{12}$	$\frac{1}{15}$	$\frac{1}{18}$	$\frac{1}{24}$	$\frac{1}{42}$	0	$-\frac{1}{30}$	$-\frac{1}{12}$

Figure 4.21: The discrete groups $\Gamma(3,t)$

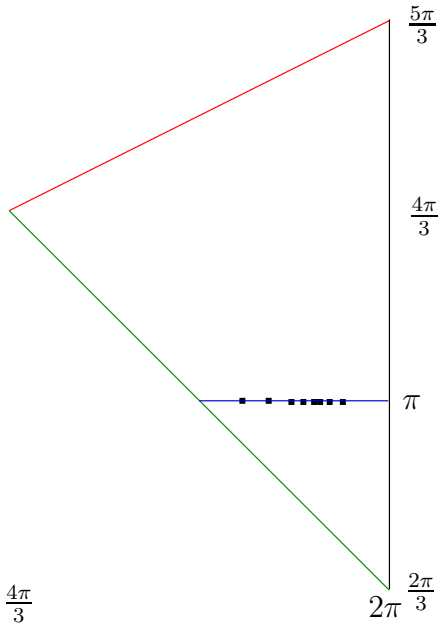

Figure 4.22: Mostow's groups $\tilde{\Gamma}(p,t)$ inside the momentum polygon

previous ones, but to their right. This is an example of different points in the same picture which yield conjugate subgroups of $PU(2,1)$; this situation only becomes worse if we worry about commensurability classes of subgroups. In fact this simple idea of exchanging two among the four fundamental classes of $\mathbb{C}$-reflections is behind the isomorphisms and commensurabilities among lattices discovered by Sauter (see [Sa]) and further investigated in the book of Deligne and Mostow (see [DM]).

Before going into the experimental aspects, we recall a complete description of the momentum polygon (see proposition 4.4.1).

In the present case (angles $\{0, \frac{2\pi}{3}\}$ and $\{\frac{2\pi}{3}, -\frac{2\pi}{3}\}$) the polygon is the triangle of figures 4.13 and 4.22, bounded by a spherical reducible segment, a hyperbolic reducible segment, and the "boundary segment" $[2\pi, \theta]$ for $\theta \in [\frac{2\pi}{3}, \frac{5\pi}{3}]$ which comprises parabolic conjugacy classes (except at its endpoints).

To investigate explicitly other points of the image, we use our parametrisation from section 4.3 in tandem with the trace formula at the end of the same section. Here this formula becomes particularly simple because of the values of the angles. We obtain after various simplifications, with the notation from section 4.3, and denoting τ the trace of A_2:

$$\left\{\begin{array}{rcl} \frac{2}{3}Re(\tau) & = & 1+2\frac{y^2}{r^2}-(\frac{y}{r}\cos\varphi-\sin\varphi)^2 \\ \frac{2}{\sqrt{3}}Im(\tau) & = & (\cos^2\varphi-\sin^2\varphi)(1-\frac{y^2}{r^2})+6\cos\varphi\sin\varphi\frac{y}{r} \end{array}\right.$$

This allows in principle an explicit parametrization of points of the image, which we do not need immediately (of course we will need algebraic expressions to know the arithmetic properties of each group). We have chosen as a test point a point near the center of the triangle with simple coordinates, namely $(\frac{5\pi}{3}, \frac{4\pi}{3})$. We have tested in this group words up to length 5; no new elliptic classes have appeared. We have also run Deraux's Dirichlet procedure on the generators; after 5 steps (a few days of computation) this procedure has yielded two cospinal bisectors, namely those defined by the pairs of words $\{433121, 434421\}$ and $\{434433434, 343443121\}$ (using the digit notation $1 = A$, $2 = B$, $3 = B^{-1}$, $4 = A^{-1}$). The occurrence of cospinal bisectors in the Dirichlet construction is special. The two words themselves have no reason to be of particular interest (here we check that three of these words are in the basic elliptic conjugacy classes of A, B, and AB and the fourth is loxodromic). However the intersection of the two bisectors (a part of a $\mathbb{C}$-plane) leads to a cycle transformation in the Poincaré setting, and this cycle transformation (a complex reflection) could be very interesting; in Mostow's examples two such transformations yield the discreteness conditions. Unfortunately for the time being we have not yet written the corresponding cycles, but it seems to be a promising path.

4.5.2 Families containing $\mathbb{R}$-Fuchsian groups

Recall that an elliptic transformation of $H^2_{\mathbb{C}}$ preserves an $\mathbb{R}$-plane if and only if its angle pair is of the form $\{\theta, -\theta\}$ (or $\{0, \pi\}$, see chapter 1). We choose a simple example, given by the angle pairs $\{\frac{\pi}{2}, -\frac{\pi}{2}\}$ and $\{\frac{\pi}{2}, -\frac{\pi}{2}\}$; the momentum polygon, depicted in figure 4.23 is then large enough to allow many possibilities. The first idea is to consider products which are also of the form $\{\theta, -\theta\}$: this seems to yield $\mathbb{R}$-Fuchsian groups (in the examples we have considered). The more surprising feature is that such angle pairs appear as well if we try to avoid them. We have tried two other examples, considering the fibers over the points $\{\pi, \frac{\pi}{2}\}$ and $\{\frac{2\pi}{5}, \frac{6\pi}{5}\}$. In both cases the same phenomenon appears as we investigate elliptic words in the group: we encounter a conjugacy class (that of 122422 in the first case and 1243 in the second) which has angles $\{\theta, -\theta\}$ with $\theta \notin \pi\mathbb{Q}$ (which is normal because we start at an arbitrary point of the fiber). The striking thing is that as we move inside the fiber, the angles stay of this form (until they go to 0 and the product becomes loxodromic). We have checked that none of these groups is itself $\mathbb{R}$-Fuchsian, however the specific form of the angles indicates that there must be a subgroup which is $\mathbb{R}$-Fuchsian. As we go along the fiber, θ ranges over a certain interval; another striking feature is that in our first example the maximum is $\frac{\pi}{4}$, so that there must be more to say about the configuration which realizes this maximum.

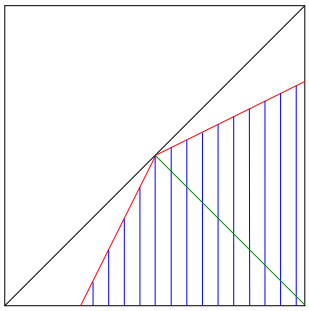

Figure 4.23: The momentum polygon for $\{\frac{\pi}{2}, -\frac{\pi}{2}\}$,$\{\frac{\pi}{2}, -\frac{\pi}{2}\}$: $\mathbb{R}$-Fuchsian families

Bibliography

[A] M. F. Atiyah; *Convexity and commuting Hamiltonians*. Bull. London Math. Soc. **14(1)** (1982), 1–15.

[AMM] A. Alekseev, A. Malkin, E. Meinrenken; *Lie group valued moment maps*. J. Diff. Geom. **48(3)** (1998), 445–495.

[AW] S. Agnihotri, C. Woodward; *Eigenvalues of products of unitary matrices and quantum Schubert calculus*. Math. Res. Lett. **5(6)** (1998), 817–836.

[BGS] W. Ballmann, M. Gromov, V. Schroeder; Manifolds of Nonpositive Curvature. Birkhaüser Progress in Math. vol. 61, 1985.

[Be] P. Belkale; *Local systems on $P^1 - S$ for S a finite set*. Compositio Math. **129(1)** (2001), 67–86.

[Bi1] I. Biswas; *A criterion for the existence of a parabolic stable bundle of rank two over the projective line*. Internat. J. Math. **9(5)** (1998), 523–533.

[Bi2] I. Biswas; *On the existence of unitary flat connections over the punctured sphere with given local monodromy around the punctures*. Asian J. Math. **3(2)** (1999), 333–344.

[CG] S. Chen, L. Greenberg; *Hyperbolic spaces*. In Contributions to Analysis. Academic Press, New York (1974), 49–87.

[D1] M. Deraux; *Dirichlet domains for the Mostow lattices*. To appear in Experimental Math..

[D2] M. Deraux; *Deforming the $\mathbb{R}$-Fuchsian $(4,4,4)$-triangle group into a lattice*. Preprint, 2005.

[D3] M. Deraux; *Dirichlet domains in complex hyperbolic space*, java applets, `http://www-fourier.ujf-grenoble.fr/~deraux/java`.

[DFP] M. Deraux, E. Falbel, J. Paupert; *New constructions of fundamental polyhedra in complex hyperbolic space*. Acta Math. **194** (2005), 155–201.

[DM] P. Deligne, G. D. Mostow; Commensurabilities among lattices in $PU(1,n)$. Annals of Mathematics Studies **132**. Princeton University Press (1993).

[FMS] E. Falbel, J.-P. Marco, F. Schaffhauser; *Classifying triples of Lagrangians in a Hermitian vector space*. Topology Appl. **144** (2004), 1–27.

[FP] E. Falbel, J. Paupert; *Fundamental domains for finite subgroups in $U(2)$ and configurations of Lagrangians*. Geom. Dedicata **109** (2004), 221–238.

[FW] E. Falbel, R. Wentworth; *Eigenvalues of products of unitary matrices and Lagrangian involutions*. To appear in Topology.

[F] W. Fulton; *Eigenvalues, invariant factors, highest weights, and Schubert calculus*. Bull. Amer. Math. Soc. **37(3)** (2000), 209–249.

[G] W.M. Goldman; Complex Hyperbolic Geometry. Oxford Mathematical Monographs. Oxford Science Publications (1999).

[GS1] V. Guillemin, S. Sternberg; *Convexity properties of the moment mapping*. Invent. Math. **67(3)** (1982), 491–513.

[GS2] V. Guillemin, S. Sternberg; *Convexity properties of the moment mapping II*. Invent. Math. **77(3)** (1984), 533–546.

[Kl1] A. Klyachko; *Stable bundles, representation theory and Hermitian operators*. Selecta Math. (NS) **4(3)** (1998), 419–445.

[Kl2] A. Klyachko; *Vector bundles, linear representations, and spectral problems*. Proceedings of the International Congress of Mathematicians, Vol. II (Beijing, 2002), 599–613, Higher Ed. Press, Beijing (2002).

[Ko] V. P. Kostov; *The Deligne-Simpson problem–a survey*. J. Algebra **281** (2004), 83–108.

[M1] G. D. Mostow; *On a remarkable class of polyhedra in complex hyperbolic space*. Pacific J. Math. **86** (1980), 171–276.

[M2] G. D. Mostow; *Generalized Picard lattices arising from half-integral conditions*. Publ. Math. IHES **63** (1986), 91–106.

[N] A. J. Nicas; *Classifying pairs of Lagrangians in a Hermitian vector space*. Topology Appl. **42** (1991), 71–81.

[P] J. R. Parker; Notes on complex hyperbolic geometry, preliminary version (2003).

[Sa] J. K. Sauter; *Isomorphisms among monodromy groups and applications to lattices in $PU(1,2)$*. Pacific J. Math. **146(2)** (1990), 331–384.

[Sf] F. Schaffhauser; Decomposable representations and Lagrangian submanifolds of moduli spaces associated to surface groups. Thesis, Université Paris 6, 2005.

[Sz1] R. E. Schwartz; *Complex hyperbolic triangle groups*. Proceedings of the International Congress of Mathematicians, Vol. II (Beijing, 2002), 339–349, Higher Ed. Press, Beijing, 2002.

[Sz2] R. E. Schwartz; Spherical CR geometry and Dehn surgery. Research monograph, 2004.

[W1] A. Weinstein; *Poisson geometry of discrete series orbits, and momentum convexity for noncompact group actions*. Lett. Math. Phys. **56(1)** (2001), 17-30.

[W2] A. Weinstein; *The geometry of momentum*. Preprint, arXiv:math.SG/0208108 (2002).

Chapter 5

Groupes triangulaires elliptiques dans $PU(2,1)$, triplets de lagrangiens et applications moment

5.1 Introduction

On appellera ici *groupe triangulaire elliptique* dans $PU(2,1)$ tout sous-groupe engendré par deux transformations elliptiques A et B dont le produit AB est aussi elliptique. La question que l'on se pose dans ce chapitre est alors la suivante: dans un tel groupe, quelles sont les classes de conjugaison possibles pour le produit AB lorsque A et B sont chacun dans une classe de conjugaison fixée?

C'est un problème classique dans un groupe linéaire de caractériser les valeurs propres possibles de matrices $A_1, ..., A_n$ vérifiant $A_1...A_n = 1$. Dans le groupe $GL(n, \mathbb{C})$, cette question est connue sous le nom de problème de Deligne-Simpson et provient de l'étude des systèmes différentiels dits fuchsiens sur la sphère de Riemann $\mathbb{C}P^1$. Ce problème est intimement lié au problème de Riemann-Hilbert (ou 21^{eme} problème de Hilbert) et a fait l'objet de beaucoup de travaux; on pourra se reporter à [Ko] pour un panorama de ces questions et des réponses partielles dont on dispose à ce jour. Le cas opposé du groupe compact $U(n)$ a aussi été très étudié, et essentiellement résolu dans [AW], [Be], [Bi2], [Kl1]; il est lié de façon surprenante à plusieurs branches des mathématiques, voir les panoramas [F] et [Kl2]. Ce cas du groupe $U(n)$ a aussi été étudié du point de vue des sous-espaces lagrangiens et des réflexions associées de $\mathbb{C}^n$ dans [FW], dont on a adapté quelques idées au cadre du groupe non compact $PU(2,1)$.

Rappelons qu'une classe de conjugaison de transformations elliptiques dans $PU(2,1)$ est caractérisée par une paire d'angles non ordonnée (voir le chapitre 1); notre question revient alors à déterminer l'image dans la surface $\mathbb{T}^2/\mathfrak{S}_2$ de l'application produit du groupe, restreinte à un produit $C_1 \times C_2$ de classes de conjugaison. Cette application est un exemple d'application moment associée à l'espace quasi-hamiltonien $C_1 \times C_2$, notion définie dans [AMM] comme généralisation à valeurs dans le groupe de la notion classique (à valeurs dans l'algèbre de Lie) d'application moment associée à l'action hamiltonnienne d'un groupe sur une variété symplectique.

On dispose dans ce cas classique de théorèmes généraux de convexité de l'image, le plus célèbre étant celui d'Atiyah et Guillemin-Sternberg (voir [A], [GS1], [GS2]), qui stipule dans les cas d'action d'un tore sur une variété symplectique connexe et compacte que l'image de l'application moment est un polytope convexe, l'enveloppe convexe des images des points fixes de l'action. Dans le cas d'actions de groupes non compacts, certaines conditions au but sont requises pour obtenir de tels énoncés de convexité de l'image (voir [W1]). Notons également que les résultats dans le cas non compact supposent que l'application moment soit propre, ce qui n'est pas le cas ici (les classes de conjugaison ne sont pas compactes, et le produit peut rester borné alors que chaque facteur part à l'infini).

Dans une autre direction, on trouve dans [AMM] un théorème analogue de convexité de l'image pour l'application moment à valeurs dans le groupe, mais seulement lorsque le groupe est compact (voir aussi [Sf]). Dans le cas présent, où le groupe est non compact et le but est le groupe lui-même, on ne dispose pas pour l'instant d'un tel résultat de convexité. Il y a d'ailleurs dans notre cas des exemples où l'image de l'application moment est une union non convexe de segments; mais ceux-ci ne proviennent que de cas dégénérés au sens où les deux classes de conjugaisons fixées à la source ont des gros centralisateurs (ce sont des classes de réflexions complexes), auquel cas elles ne sont pas "fortement stables" au sens de Weinstein dans [W1] (où cette condition est imposée au but).

La première partie du chapitre est consacrée à la détermination de l'image de l'application

moment, qui est un polygone dans la surface $\mathbb{T}^2/\mathfrak{S}_2$. On utilise une approche directe, reposant sur une decription explicite soigneuse de l'image des groupes réductibles (au sens des représentations, à savoir ici les groupes qui fixent un point de $\mathbb{C}P^2$); l'idée principale (inspirée de la question analogue dans $U(n)$ étudiée dans [FW]) étant que les points correspondant aux groupes irréductibles se projettent sur des points intérieurs de l'image, parce que l'application moment est de rang maximal en un tel point. Le résultat principal est le théorème 4, qui est un résultat de convexité évoquant celui d'Atiyah et Guillemin-Sternberg.

La deuxième partie du chapitre est consacrée à une question liée (en fait contenue dans la précédente), à savoir celle de la classification des configurations de triplets de sous-espaces lagrangiens de $H^2_{\mathbb{C}}$ (ou $\mathbb{R}$-plans) s'intersectant deux à deux. Le lien entre ces deux questions se fait via le groupe engendré par les $\mathbb{R}$-réflexions associées aux trois $\mathbb{R}$-plans (ce sont des involutions antiholomorphes fixant le $\mathbb{R}$-plan en question), de la façon suivante. Si L_1, L_2, L_3 sont trois $\mathbb{R}$-plans s'intersectant deux à deux dans $H^2_{\mathbb{C}}$, avec $\mathbb{R}$-réflexions associées σ_1, σ_2, σ_3, alors le sous-groupe holomorphe engendré par $A = \sigma_2\sigma_1$ et $B = \sigma_3\sigma_2$ est un groupe triangulaire elliptique au sens où on l'a défini. Le lien réciproque, allant du sous groupe elliptique à une décomposition en $\mathbb{R}$-réflexions, est moins évident. Le compte des dimensions nous dit qu'en général, deux transformations fixées A et B ne sont pas comme ci-dessus simultanément décomposables en $\mathbb{R}$-réflexions (par exemple, une classe de conjugaison elliptique générique dans $PU(2,1)$ est de dimension 6, alors que l'espace des lagrangiens décomposant une paire A, B avec A fixé et B variant dans cette classe est de dimension 3). Cependant il semblerait que, comme dans le cas de $U(n)$ (voir le résultat principal de [FW]), avec deux classes fixées pour A et B, le polygone image devrait être le même; on dispose de forts indices dans ce sens, mais pas pour l'instant d'une démonstration complète. On calcule à la fin de cette section un paramétrage des configurations de triplets de $\mathbb{R}$-plans réalisant deux paires d'angles fixées; ceci nous permet d'une part d'étudier des dessins expérimenatux (grâce auxquels la plupart des phénomènes que l'on décrit ont été découverts), mais surtout de paramétrer des générateurs possibles pour des groupes candidats à la discrétude.

Les deux dernières sections sont consacrées à l'étude détaillée d'exemples, l'exemple principal (qui a motivé ce travil) étant celui où les générateurs ont pour paires d'angles $\{0, 2\pi/3\}$ et $\{2\pi/3, -2\pi/3\}$. Ceci correspond à des générateurs pour les réseaux $\Gamma(3,t)$ de Mostow construits dans [M1]. L'image dans ce cas est un triangle, à l'intérieur duquel la famille considérée par Mostow est un segment traversant le triangle de part en part, voir figures 5.13 et 5.22 (les réseaux forment huit points isolés dans ce segment). L'impression géométrique est très nette: il serait très surprenant de ne pas trouver d'autres groupes discrets (éventuellement des réseaux non arithmétiques) dans ce dessin. On termine en indiquant une approche pratique possible, et en explicitant des candidats que l'on a commencé à étudier.

5.2 Groupes triangulaires elliptiques, un polygone de configurations

5.2.1 Introduction

On décrit dans cette partie l'image de notre application moment $\tilde{\mu}$ dans la surface $\mathbb{T}^2/\mathfrak{S}_2$ (voir la partie 5.2.2 pour la définition précise de $\tilde{\mu}$). On commence par décrire en détail la configuration

des points réductibles (au sens où ce sont les images des paires (A, B) qui engendrent un groupe linéaire réductible), l'idée principale étant comme on l'a dit que les points irréductibles se projettent sur des points intérieurs de l'image, laquelle sera donc une réunion de *chambres* délimitées par les *murs réductibles* (on précisera ces termes plus tard).

Les groupes réductibles sont ici de deux types, selon que le point fixe de l'action sur $\mathbb{C}P^2$ est à l'intérieur ou à l'extérieur de l'espace hyperbolique complexe $H^2_{\mathbb{C}}$ (il ne peut pas être au bord si les générateurs sont elliptiques). Lorsque ce point fixe est dans $H^2_{\mathbb{C}}$, le groupe $\Gamma = \langle A, B\rangle$ est conjugué à un sous-groupe de $U(2)$ (le stabilisateur d'un point dans $PU(2,1)$); on dira alors que Γ est *réductible sphérique*. Lorsque le point fixe est à l'extérieur de $H^2_{\mathbb{C}}$, le groupe $\Gamma = \langle A, B\rangle$ est conjugué à un sous-groupe de $P(U(1)\times U(1,1))$ (le stabilisateur d'une géodésique complexe, ou $\mathbb{C}$-plan); on dira alors que Γ est *réductible hyperbolique*. Il y a alors deux points spéciaux, qui sont à la fois réductibles sphériques et réductibles hyperboliques: ce sont les points où Γ est abélien (autrement dit, les deux générateurs ont sous forme matricielle une base commune de vecteurs propres). On dira que ces deux groupes sont *totalement réductibles*.

L'image dans $\mathbb{T}^2/\mathfrak{S}_2$ de tous ces groupes réductibles est alors un graphe trivalent à deux sommets, jouissant des propriétés suivantes (que l'on démontrera dans la partie 4.2.3). Les deux sommets sont les images des deux groupes totalement réductibles. Ils sont joints par un segment de droite de pente -1 qui est l'image des groupes réductibles sphériques. Deux autres segments sont issus de chaque sommet, l'un de pente 2 et l'autre de pente $1/2$, correspondant aux deux familles réductibles hyperboliques contenant le sommet. Notons que la pente d'une droite est bien définie dans le tore, mais qu'elle n'est définie qu'à inversion près dans le quotient $\mathbb{T}^2/\mathfrak{S}_2$. On fixe ici une fois pour toutes une carte affine donnée pour $\mathbb{T}^2/\mathfrak{S}_2$, à savoir le demi-carré inférieur comme dans la figure 5.1. Il est important de noter que les bords du carré en question ont un sens géométrique (autrement dit, le tore n'est pas homogène) parce qu'ils correspondent à des classes de conjugaison spéciales. Il y a en fait une subtilité, parce que ces points du bord représentent chacun deux classes de conjugaison distinctes, l'une composée de $\mathbb{C}$-réflexions (i.e. des transformations elliptiques qui fixent un $\mathbb{C}$-plan) et l'autre de transformations paraboliques; ces deux classes sont indiscernables du point de vue des angles ou de la trace (à comparer avec le "triangle" de Goldman dans le plan complexe des traces, pp. 204–205 de [G]; voir aussi le chapitre 1).

Cette ambiguïté est encore plus grande aux trois sommets du demi-carré (qui ne font qu'un dans le quotient) qui représentent l'identité ainsi que toutes les classes de conjugaison d'unipotents (ce sont les translations de Heisenberg du bord $\partial H^2_{\mathbb{C}} = H^3$).

On notera $W_{red} \subset \mathbb{T}^2/\mathfrak{S}_2$ l'image de tous les groupes réductibles, et on appellera chaque segment de droite de W_{red} un *mur*. La description complète de cette charpente réductible, comprenant une justification des faits évoqués ainsi qu'une classification des types possibles, fait l'objet de la partie 5.2.3. Alors W_{red} **avec les deux axes** $\{0\}\times S^1$ **et** $S^1\times\{0\}$ sépare $\mathbb{T}^2/\mathfrak{S}_2$ en une union de polygones convexes ouverts que l'on appelera des *chambres* (voir la partie 5.2.5 pour la notion appropriée de convexité). Une analyse détaillée montre qu'il y a au plus 9 de ces chambres. On appellera également *chambre fermée* la réunion d'une chambre, des segments de murs réductibles qui la bordent, ainsi que des éventuels points des axes qui sont à la frontière de la chambre et qui correspondent à un produit elliptique.

Le fait que l'application moment soit de rang maximal aux points irréductibles montre que l'image est une réunion de ces chambres (avec les murs qui les bordent), voir la partie 5.2.4. La question principale qui reste à étudier, et que nous n'avons pas encore résolue en toute

Figure 5.1: Une configuration de réductibles

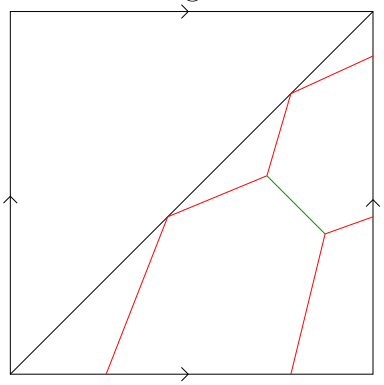

généralité, est de savoir exactement quelles chambres sont dans l'image (il nous manque des arguments pour exclure systématiquement les chambres superflues). Le plus que l'on puisse dire pour l'instant est le résultat suivant; l'application $\tilde{\mu}$ est l'application moment (produit) restreinte de façon adéquate, suivie de la projection sur $\mathbb{T}^2/\mathfrak{S}_2$ (voir section 5.2.2).

Théorème 4 *Soient C_1 et C_2 deux classes de conjugaison elliptiques dans $PU(2,1)$, dont une au moins n'est pas une classe de réflexions complexes. Alors l'image de l'application $\tilde{\mu}$ dans $\mathbb{T}^2/\mathfrak{S}_2$ est une réunion de chambres fermées, contenant au voisinage de chaque sommet totalement réductible l'enveloppe convexe des murs réductibles qui contiennent ce sommet.*

Ceci évoque le résultat d'Atiyah-Guillemin-Sternberg, sachant que dans notre cas les groupes réductibles sont ce qui s'approche le plus de points fixes sous l'action de $PU(2,1)$ par conjugaison (ce sont eux qui ont les plus petites orbites).

En ce qui concerne l'hypothèse faite sur C_1 et C_2, il est facile de voir que deux réflexions complexes engendrent toujours un groupe réductible, parce que leurs miroirs ($\mathbb{C}$-plans fixes) s'intersectent toujours dans $\mathbb{C}P^2$, et que l'image est donc dans ce cas une réunion non convexe de segments; voir section 5.4.3.

5.2.2 Le produit de groupe: une application moment à valeurs dans le groupe

Le cadre est celui du groupe $G = PU(2,1)$ qui est un groupe de Lie réel semisimple, connexe mais non simplement connexe et non compact (plus précisément, de rang réel 1). Chacune de ces caractéristiques a son importance pour l'étude de l'application moment que l'on va introduire. Le produit du groupe est une donnée de base dans ce groupe de Lie; on s'intéresse ici au comportement (principalement, l'image) de cette application restreinte au produit de deux classes de conjugaison fixées. Plus précisément, soient C_1 et C_2 deux classes de conjugaison d'éléments elliptiques dans $PU(2,1)$; on considère l'application:

$$\begin{array}{rccc} \mu: & C_1 \times C_2 & \longrightarrow & G \\ & (A,B) & \longmapsto & AB \end{array}$$

$C_1 \times C_2$ est un exemple typique de G-espace quasi-hamiltonien (l'action de G étant par conjugaison sur chaque facteur) tel qu'il est défini dans [AMM] (voir aussi le chapitre 4 de [Sf] pour

plus de détails), l'application moment associée à cette structure étant simplement le produit μ. On pourra trouver dans le panorama [W2] une genèse de la notion classique d'application moment associée à l'action hamiltonnienne d'un groupe sur une variété symplectique, avec différentes directions possibles de généralisation.

En fait, on ne s'intéresse ici qu'à la classe de conjugaison du produit, et au cas où celui-ci est elliptique, ce qui fait que notre objet principal d'étude sera l'application suivante:

$$\tilde{\mu} : (C_1 \times C_2) \cap \mu^{-1}(\{\text{elliptiques}\}) \xrightarrow{\mu} G \xrightarrow{\pi} \mathbb{T}^2/\mathfrak{S}_2$$

où l'on a noté π pour la projection de G vers l'ensemble de ses classes de conjugaison (on rappelle qu'une classe de conjugaison elliptique dans $PU(2,1)$ est caractérisée par, et donc identifiée à, une paire d'angles non ordonnée, voir le chapitre 1). Notons qu'on a pu perdre la structure quasi-hamiltonienne en restreignant μ à $\mu^{-1}(\{\text{elliptiques}\})$; mais quand cela sera nécessaire, on pourra restreindre légèrement plus à $\mu^{-1}(\{\text{elliptiques réguliers}\})$ qui est un ouvert de $C_1 \times C_2$ et qui hérite donc de la structure quasi-hamiltonienne (on rappelle qu'une transformation elliptique est dite régulière si ses angles sont distincts et non nuls, voir [G] p. 203).

On analysera les propriétés différentielles de cette application dans les sections 5.2.4 et 5.2.5.

5.2.3 Murs et groupes réductibles

Dans cette section, on décrit en détail la configuration W_{red} des murs réductibles. Les deux classes de conjugaison elliptiques fixées sont données par deux paires d'angles $\{\theta_1, \theta_2\}$ et $\{\theta_3, \theta_4\}$ normalisées de façon que $\theta_i \in [0; 2\pi[$. On regardera l'image de $\tilde{\mu}$ dans la carte affine $\{(\theta_5, \theta_6) |\, \theta_i \in [0; 2\pi[, \theta_5 \geqslant \theta_6\}$ de $\mathbb{T}^2/\mathfrak{S}_2$ (et on gardera des paires sans ordre tant qu'on ne sait pas quelle coordonnée est plus grande).

Comme on l'a dit, W_{red} est un graphe trivalent avec deux sommets $D_1 = \{\theta_1 + \theta_3, \theta_2 + \theta_4\}$ et $D_2 = \{\theta_2 + \theta_3, \theta_1 + \theta_4\}$; ces sommets sont joints par un segment U de pente -1 correspondant aux groupes réductibles sphériques. Si les deux sommets ont le même indice (au sens de [FW], voir ci-dessous; ceci signifie qu'ils sont sur une même droite antidiagonale dans la carte affine), alors U est simplement le segment affine qui les joint. S'ils ont des indices distincts, ils sont sur deux droites antidiagonales parallèles de la carte affine, et U est le segment, disconnecté dans la carte affine, qui les joint via les bords du carré. Notons que dans tous les cas U est le segment géodésique le plus court joignant ces deux sommets.

Chaque sommet est également l'extrémité de deux segments de groupes réductibles hyperboliques qui vont jusqu'aux bords du carré (et qui peuvent même parfois s'enrouler une fois autour du tore), l'un de pente 2 et l'autre de pente 1/2. On notera C_{13} et C_{24} ces segments issus de D_1, et C_{23} et C_{14} ceux issus de D_2 (avec des notations qui deviendront claires plus bas).

Groupes totalement réductibles: les deux sommets

Ces deux points sont les paires d'angles du produit AB lorsque A et B sont simultanément sous forme diagonale. En écrivant ceux-ci comme $A = Diag(e^{i\theta_1}, e^{i\theta_2}, 1)$ et $B = Diag(e^{i\theta_3}, e^{i\theta_4}, 1)$, on obtient $D_1 = \{\theta_1 + \theta_3, \theta_2 + \theta_4\}$; utilisant $B = Diag(e^{i\theta_4}, e^{i\theta_3}, 1)$, on obtient $D_2 = \{\theta_1 + \theta_4, \theta_2 + \theta_3\}$.

Groupes avec point fixe

La question des valeurs propres possibles d'un produit de matrices, chacune dans une classe de conjugaison fixée de $U(2)$, a été étudiée dans [Bi1] du point de vue des fibrés holomorphes sur la droite projective, et dans [FMS] du point de vue de la géométrie des triplets de lagrangiens dans $\mathbb{C}^2$. On commencera par citer la description suivante de la région autorisée pour ces valeurs propres, obtenue dans [FW] par la méthode de Biswas. Leurs notations diffèrent légèrement des notres en ce qu'ils considèrent les représentations dans $U(2)$ du groupe fondamental de la sphère privée de trois points, avec la présentation suivante:

$$\langle A, B, C \mid A.B.C = 1 \rangle$$

Les conditions que l'on va expliciter font intervenir la notion d'*indice* I d'une représentation qui est un entier; dans les notations de [FW], I est la somme des angles des six valeurs propres des générateurs normalisés dans $[0, 1[$. Dans le cas des représentations lagrangiennes (voir section suivante), cet indice est en bijection avec l'indice de Maslov (ou indice d'inertie) du triplet de lagrangiens. Dans nos notations, l'indice de la représentation (définie par A, B et $(AB)^{-1}$) s'écrit:

$$I = 2 + \frac{1}{2\pi}(\theta_1 + \theta_2 + \theta_3 + \theta_4 - \theta_5 - \theta_6)$$

Le résultat est alors que la région autorisée pour les sextuplets d'angles est une réunion de polyèdres convexes dans des hyperplans parallèles correspondant aux valeurs entières admissibles de l'indice I. Les inégalités explicites font intervenir les quantités suivantes:

- $MM := \mathrm{Max}\{\theta_1, \theta_2\} + \mathrm{Max}\{\theta_3, \theta_4\}$
- $mm := \min\{\theta_1, \theta_2\} + \min\{\theta_3, \theta_4\}$
- $Mm := \mathrm{Max}\{\min\{\theta_1, \theta_2\} + \mathrm{Max}\{\theta_3, \theta_4\}, \mathrm{Max}\{\theta_1, \theta_2\} + \min\{\theta_3, \theta_4\}\}$

Proposition 5.2.1 (voir [Bi1], [FW]) *Soit $A, B \in U(2)$ avec angles respectifs $\{\theta_1, \theta_2\}$ et $\{\theta_3, \theta_4\}$, où $\theta_i \in [0; 2\pi[$. Alors les paires d'angles possibles pour le produit AB sont les (θ_5, θ_6) (avec $\theta_i \in [0; 2\pi[$ et $\theta_5 \geqslant \theta_6$) satisfaisant l'une des conditions suivantes:*

- *$I = 2$ (i.e. $\theta_5 + \theta_6 = \theta_1 + \theta_2 + \theta_3 + \theta_4$) et:*

$$\begin{cases} \theta_5 & \geqslant & Mm \\ \theta_6 & \geqslant & mm \end{cases}$$

- *$I = 3$ (i.e. $\theta_5 + \theta_6 = \theta_1 + \theta_2 + \theta_3 + \theta_4 - 2\pi$) et:*

$$\begin{cases} \theta_5 & \geqslant & MM - 2\pi \\ \theta_6 & \geqslant & Mm - 2\pi \\ \theta_6 & \leqslant & MM - 2\pi \end{cases}$$

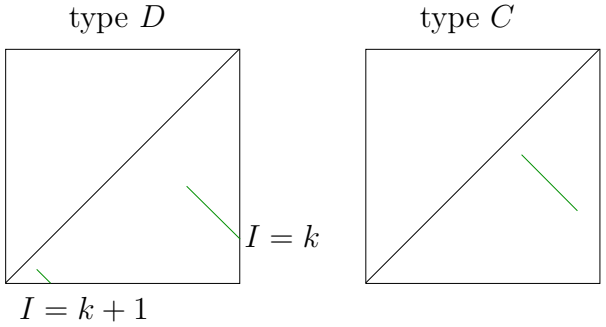

Figure 5.2: Configurations de groupes réductibles sphériques

- $I = 4$ *(i.e.* $\theta_5 + \theta_6 = \theta_1 + \theta_2 + \theta_3 + \theta_4 - 4\pi$*) et:*

$$\begin{cases} \theta_5 & \geqslant & Mm - 2\pi \\ \theta_6 & \geqslant & mm - 2\pi. \end{cases}$$

L'image géométrique ne saute pas aux yeux sur ces inégalités; à vrai dire, pour des paires $\{\theta_1, \theta_2\}$ et $\{\theta_3, \theta_4\}$ fixées, au moins l'un des trois cas ci-dessus est vide. Traduisons donc ce résultat dans notre cadre. L'image est alors simplement le segment convexe joignant les deux sommets D_1 et D_2, c'est-à-dire le segment géodésique le plus court entre eux, voir la partie 5.2.5. Notons que ce segment est toujours contenu dans une droite de pente -1 du tore, même quand il n'est pas connexe dans la carte affine.

Proposition 5.2.2 *Soit $A, B \in U(2)$ avec angles respectifs $\{\theta_1, \theta_2\}$ et $\{\theta_3, \theta_4\}$, où $\theta_i \in \mathbb{R}/2\pi\mathbb{Z}$. Alors le produit AB a pour angles toute paire $\{\theta_5, \theta_6\}$ appartenant au segment convexe de $\mathbb{T}^2/\mathfrak{S}_2$ joignant les deux sommets totalement réductibles $D_1 = \{\theta_1+\theta_3, \theta_2+\theta_4\}$ et $D_2 = \{\theta_2+\theta_3, \theta_1+\theta_4\}$.*

Concrètement, dans la carte affine $\{(\theta_5, \theta_6) | \, \theta_i \in [0; 2\pi[, \theta_5 \geqslant \theta_6\}$ de $\mathbb{T}^2/\mathfrak{S}_2$, ce segment est:

- *le segment euclidien usuel (de pente -1) joignant D_1 et D_2 si ces deux sommets ont même indice.*
- *la réunion de deux segments euclidiens de pente -1, allant chacun d'un sommet à un bord horizontal ou vertical de la carte, si ces sommets ont des indices différents.*

On dira qu'une telle configuration est de *type C* (connexe) dans le premier cas, et de *type D* dans le second, voir figure 5.2. Notons que le fait que tous ces points soient sur une même droite de pente -1 exprime simplement le fait que le déterminant du produit est le produit des déterminants.

Groupes réductibles hyperboliques

On s'intéresse maintenant aux groupes réductibles hyperboliques, ceux qui stabilisent un $\mathbb{C}$-plan (ou géodésique complexe), c'est-à-dire une copie de $H^1_{\mathbb{C}}$ dans $H^2_{\mathbb{C}}$. La description provient simplement de l'analyse du produit de matrices diagonales par blocs dans $U(2,1)$, et de la caractérisation des angles (orientés) d'un triangle dans le plan hyperbolique.

Les groupes totalement réductibles stabilisent chacun deux $\mathbb{C}$-plans s'intersectant au point fixe commun, donc on s'attend à ce que par déformation chaque sommet soit contenu dans deux

familles réductibles hyperboliques distinctes. Ceci est bien le cas, sauf dans les cas dégénérés où l'un des deux générateurs au moins est une $\mathbb{C}$-réflexion (un angle nul) ou une réflexion complexe par rapport à un point (deux angles égaux). L'une de ces familles, que l'on va noter C_{24} et qui contient le sommet D_1, est donnée par les générateurs suivants sous forme matricielle:

$$A = \begin{pmatrix} e^{i\theta_1} & 0 & 0 \\ 0 & e^{i\theta_2} & 0 \\ 0 & 0 & 1 \end{pmatrix} \quad \text{et} \quad B = \begin{pmatrix} e^{i\theta_3} & 0 & 0 \\ 0 & b_1 & b_2 \\ 0 & b_3 & b_4 \end{pmatrix}$$

où la classe de conjugaison de:

$$\widetilde{B} = \begin{pmatrix} b_1 & b_2 \\ b_3 & b_4 \end{pmatrix} \in U(1,1)$$

est donnée par ses valeurs propres: $e^{i\theta_4}$ de type positif et 1 de type négatif (ceci signifie simplement que $\widetilde{B}$ agit sur $H^1_{\mathbb{C}}$ par une rotation d'angle θ_4). Rappelons que le type d'une valeur propre désigne la position de son espace propre par rapport au cône isotrope de la forme hermitienne (ici dans $\mathbb{C}^{1,1}$).

Les trois autres familles réductibles hyperboliques C_{23}, C_{14}, et C_{13} sont définies de la même manière, échangeant les rôles par $\theta_1 \leftrightarrow \theta_2$ et $\theta_3 \leftrightarrow \theta_4$.

Dans chaque famille le produit AB, tant qu'il est elliptique, a deux angles θ_C et θ_N. On note θ_C l'angle de rotation dans le $\mathbb{C}$-plan stable; θ_N est alors l'angle de rotation dans le $\mathbb{C}$-plan normal. Le résultat est alors le suivant:

Proposition 5.2.3 *Soient A, B deux éléments elliptiques dans $PU(2,1)$ avec angles respectifs $\{\theta_1, \theta_2\}$ et $\{\theta_3, \theta_4\}$ (où $\theta_i \in [0, 2\pi[$), tels que le produit AB soit elliptique. Si le groupe engendré par A et B est réductible hyperbolique, alors la paire d'angles $\{\theta_C, \theta_N\}$ de AB est sur l'un des quatre segments suivants:*

$$C_{24} : \begin{cases} \theta_C = 2\theta_N + \theta_2 + \theta_4 - 2\theta_1 - 2\theta_3 \ [2\pi] \quad et \\ \theta_2 + \theta_4 < \theta_C < 2\pi \quad (si \ \ \theta_2 + \theta_4 < 2\pi) \\ 0 < \theta_C < \theta_2 + \theta_4 - 2\pi \quad (si \ \ \theta_2 + \theta_4 > 2\pi). \end{cases}$$

$$C_{13} : \begin{cases} \theta_C = 2\theta_N + \theta_1 + \theta_3 - 2\theta_2 - 2\theta_4 \ [2\pi] \quad et \\ \theta_1 + \theta_3 < \theta_C < 2\pi \quad (si \ \ \theta_1 + \theta_3 < 2\pi) \\ 0 < \theta_C < \theta_1 + \theta_3 - 2\pi \quad (si \ \ \theta_1 + \theta_3 > 2\pi). \end{cases}$$

$$C_{23} : \begin{cases} \theta_C = 2\theta_N + \theta_2 + \theta_3 - 2\theta_1 - 2\theta_4 \ [2\pi] \quad et \\ \theta_2 + \theta_3 < \theta_C < 2\pi \quad (si \ \ \theta_2 + \theta_3 < 2\pi) \\ 0 < \theta_C < \theta_2 + \theta_3 - 2\pi \quad (si \ \ \theta_2 + \theta_3 > 2\pi). \end{cases}$$

$$C_{14} : \begin{cases} \theta_C = 2\theta_N + \theta_1 + \theta_4 - 2\theta_2 - 2\theta_3 \ [2\pi] \quad et \\ \theta_1 + \theta_4 < \theta_C < 2\pi \quad (si \ \ \theta_1 + \theta_4 < 2\pi) \\ 0 < \theta_C < \theta_1 + \theta_4 - 2\pi \quad (si \ \ \theta_1 + \theta_4 > 2\pi). \end{cases}$$

Notons que chacun de ces segments a une extrémité qui est un sommet totalement réductible, l'autre étant sur un des côtés du carré; il est cependant possible que le segment s'enroule une fois autour du tore avant d'atteindre cette extrémité (voir la section d'exemples). On a laissé

les inégalités sous cette forme, qui ne précise pas quel segment a pente 2 ou 1/2, parce que ceci peut changer à l'intérieur d'une même famille, lorsque le segment rebondit sur la diagonale du carré. Par exemple, si $\theta_1 + \theta_3 < \theta_2 + \theta_4 < 2\pi$, le segment C_{24} a pente 2 (au moins, près de D_1) et C_{13} a pente 1/2 (aussi, près de D_1).

Démonstration. On traite le cas de la famille C_{24} dont les générateurs sont écrits ci-dessus, A sous forme diagonale et B diagonale par blocs. Alors le produit $C = AB$ est aussi par blocs:

$$C = \begin{pmatrix} e^{i(\theta_1+\theta_3)} & 0 & 0 \\ 0 & c_1 & c_2 \\ 0 & c_3 & c_4 \end{pmatrix} \quad \text{avec} \quad \widetilde{C} = \begin{pmatrix} c_1 & c_2 \\ c_3 & c_4 \end{pmatrix} \in U(1,1)$$

$\widetilde{C}$ a deux valeurs propres, de norme 1, mettons $e^{i\psi_1}$ et $e^{i\psi_2}$, cette dernière étant de type négatif. Alors les angles de rotation de C sont obtenus en divisant ses deux valeurs propres de type positif par celle de type négatif. Ceci s'écrit:

$$\begin{cases} \theta_C = \psi_1 - \psi_2 \\ \theta_N = \theta_1 + \theta_3 - \psi_2 \end{cases}$$

On a également une condition de déterminant, qui nous dit ici que $\psi_1 + \psi_2 = \theta_2 + \theta_4$ $[2\pi]$. En combinant ces équations, on obtient la condition: $\theta_C = 2\theta_N + \theta_2 + \theta_4 - 2\theta_1 - 2\theta_3$ $[2\pi]$.

L'intervalle précis parcouru par θ_C à l'intérieur de cette droite provient de la condition géométrique sur le troisième angle d'un triangle du plan hyperbolique ayant deux angles prescrits. Le lemme suivant est simplement une version orientée du fait qu'un triangle se réalise dans le plan hyperbolique si et seulement si la somme de ses angles est strictement inférieure à π:

Lemme 5.2.1 *Soient $\tilde{A}$ et $\tilde{B}$ deux isométries elliptiques de $H^1_{\mathbb{C}}$, avec angles de rotation respectifs θ_2 et θ_4 ($\theta_i \in [0, 2\pi[$). Lorsque les points fixes de $\tilde{A}$ et $\tilde{B}$ varient, l'angle de rotation θ_C du produit $\tilde{C} = \tilde{A}\tilde{B}$ (quand il est elliptique) parcourt l'intervalle $[\theta_2 + \theta_4, 2\pi[$ si $\theta_2 + \theta_4 < 2\pi$, et $[0, \theta_2 + \theta_4 - 2\pi[$ si $\theta_2 + \theta_4 > 2\pi$.*

Ceci complète la démonstration. □

Une classification des configurations réductibles

On commence par se concentrer sur la configuration locale au voisinage de chaque sommet. On a vu que les configurations réductibles sphériques sont de deux types, connexe (type C) ou non (type D) dans la carte affine du demi-carré. Quant aux configurations réductibles hyperboliques, on vient de voir que deux segments sont issus de chaque sommet, l'un de pente 2 et l'autre 1/2. La direction de chaque segment, vers le haut ou vers le bas, est déterminée par les données suivantes, d'après la proposition 5.2.3. On note, pour $i = 1, 2$ et $j = 3, 4$:

$$\sigma_{ij} := \theta_i + \theta_j$$

(où l'on a normalisé de façon que $\theta_i \in [0, 2\pi[$). Alors, au sommet $\{\sigma_{ij}, \sigma_{kl}\}$ (voir section 5.2.3), le segment C_{ij} part vers le haut si et seulement si $\sigma_{ij} < 2\pi$ (et C_{kl} part vers le haut si et seulement si $\sigma_{kl} < 2\pi$).

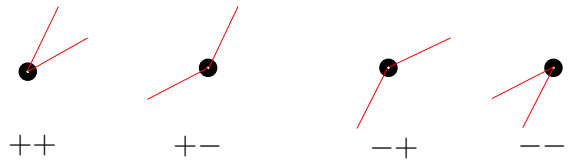

Figure 5.3: Types réductibles hyperboliques locaux

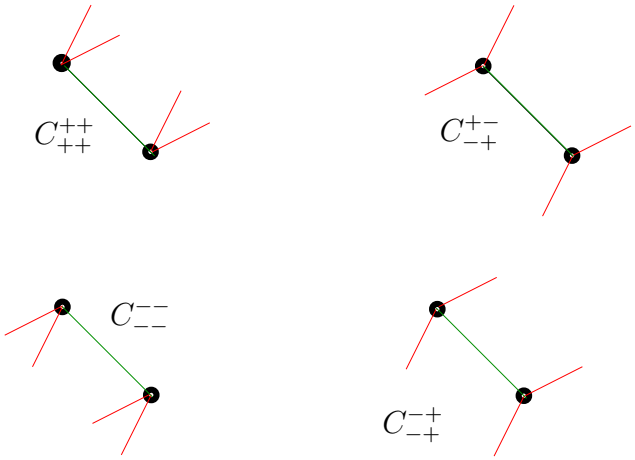

Figure 5.4: Configurations locales de type C

On va alors assigner un symbole à chaque configuration de réductibles, composé d'une lettre (C ou D) pour le type réductible sphérique et de quatre signes $+$ ou $-$, ordonnés de la façon arbitraire suivante. Il y a deux paires de signes, correspondant chacune à un sommet. La paire du haut correspond au sommet "le plus haut" (celui avec plus grand θ_6 dans la carte affine $\{(\theta_5, \theta_6) | \, \theta_i \in [0; 2\pi[, \theta_5 \geqslant \theta_6\}$), et à l'intérieur de chaque paire on met le segment de pente 2 d'abord. Enfin, un signe $+$ correspond à un segment qui monte; voir Figure 5.3 et les exemples dans les Figures 5.4 et 5.5). Il y a a priori 32 tels symboles possibles, mais seulement 4 du type C et 4 du type D correspondent à des configurations admissibles; ils sont énumérés dans l'énoncé suivant:

Proposition 5.2.4 *Les types locaux possibles de configurations réductibles sont, avec les notations précédentes,* C^{++}_{++}, C^{--}_{--}, C^{-+}_{-+}, C^{+-}_{-+} *et* D^{++}_{-+}, D^{++}_{+-}, D^{-+}_{--}, D^{+-}_{--} *(voir Figures 5.4 et 5.5).*

Démonstration. On utilise trois critères différents pour éliminer les types non admissibles, puis on donne des exemples des types restants. Ceci est facilité par le fait qu'il y a une symétrie dans les types que l'on va expliciter après avoir introduit quelques notations utiles.

Les configurations réductibles hyperboliques sont déterminées par la position de chaque $\sigma_{ij} = \theta_i + \theta_j$ (avec $\theta_i \in [0, 2\pi[$ et $i = 1, 2$, $j = 3, 4$) relativement à 2π. Ceci s'exprime de façon simple en fonction de la partie entière k_{ij} de $\frac{\sigma_{ij}}{2\pi}$, dont la valeur est en conséquence 0 ou 1. Ces entiers apparaissent aussi lorsqu'on normalise les coordonnées des sommets dans la carte affine, comme on va le voir.

La symétrie est alors la suivante. Rappelons que chaque configuration est définie par le choix de deux paires d'angles $\{\theta_1, \theta_2\}$ et $\{\theta_3, \theta_4\}$, avec $\theta_i \in [0, 2\pi[$. La transformation S que

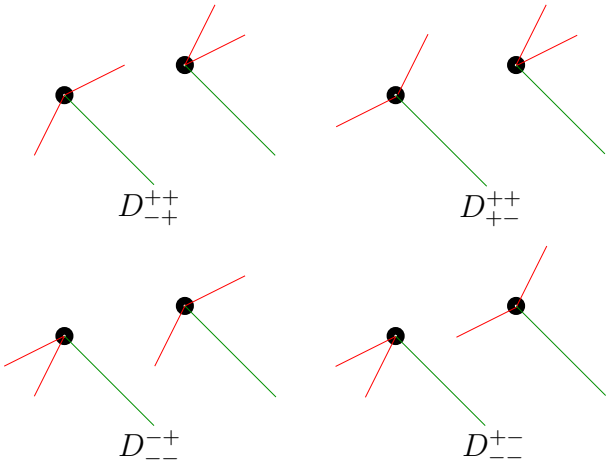

Figure 5.5: Configurations locales de type D

l'on considère est celle qui envoie chaque angle θ_i sur son angle opposé (ou symétrique) $2\pi - \theta_i$. Ceci nous intéresse parce que manifestement:

$$\theta_i + \theta_j < 2\pi \iff S(\theta_i) + S(\theta_j) > 2\pi$$

(autrement dit: $S(k_{ij}) = 1 - k_{ij}$) ce qui fait que tous les signes des segments réductibles hyperboliques sont changés par S. Par contre, il faut faire un peu attention à l'effet global sur la configuration parce que les sommets et leurs coordonnées peuvent aussi être échangés. Remarquons déjà que les types réductibles sphériques C et D sont stables sous l'action de S, comme on peut le voir par la caractérisation suivante du type D (avec comme ci-dessus $k_{ij} = E(\frac{\sigma_{ij}}{2\pi})$):

Lemme 5.2.2 *Les deux sommets ont des indices différents* $\iff$ $k_{13} + k_{24} \neq k_{14} + k_{23}$.

Démonstration du lemme. Ceci peut se voir en écrivant simplement les indices en question, une fois qu'on a remarqué que les coordonnées σ_{ij} des sommets se normalisent dans $[0, 2\pi[$ sous la forme $\sigma_{ij} - 2\pi k_{ij}$. On a alors, notant I_i l'indice du sommet D_i:

$$\begin{cases} 2\pi I_1 = \theta_1 + \theta_2 + \theta_3 + \theta_4 + (2\pi - (\sigma_{13} - 2\pi k_{13})) + (2\pi - (\sigma_{24} - 2\pi k_{24})) \\ 2\pi I_2 = \theta_1 + \theta_2 + \theta_3 + \theta_4 + (2\pi - (\sigma_{14} - 2\pi k_{14})) + (2\pi - (\sigma_{23} - 2\pi k_{23})) \end{cases}$$

et ainsi:

$$I_2 - I_1 = k_{14} + k_{23} - (k_{13} + k_{24})$$

□

Regardons maintenant de plus près ce qui se passe avec les sommets lorsqu'on applique S aux paires d'angles des générateurs. En type D, les deux sommets ont des indices différents et S envoie le sommet qui a l'indice le plus haut sur celui qui a l'indice le plus bas; les sommets du haut et du bas sont donc échangés par S. En type C les deux sommets ont même indice, mais on peut par exemple caractériser le sommet du haut par le fait qu'il est plus proche de la diagonale; ceci reste inchangé par S, donc dans ce type les sommets ne sont pas échangés.

Enfin, à chaque sommet les deux segments réductibles hyperboliques sont échangés (parce que la coordonnée la plus grande du sommet est envoyée sur la plus petite de son image) et comme on l'a dit tous les signes sont changés. On utilisera en particulier les exemples suivants:

$$\begin{array}{ll} S(C_{++}^{+-}) = C_{--}^{+-} & S(C_{+-}^{+-}) = C_{+-}^{+-} \\ S(D_{+-}^{++}) = D_{--}^{+-} & S(D_{--}^{-+}) = D_{-+}^{++} \\ S(D_{+-}^{--}) = D_{++}^{+-} & S(D_{-+}^{--}) = D_{++}^{-+} \end{array}$$

Maintenant que l'on a un peu réduit le nombre de cas, on peut exclure les types non admissibles. La première chose à remarquer est que $\sigma_{13} + \sigma_{24} = \sigma_{14} + \sigma_{23}$; ceci élimine les quatre types C_{--}^{++}, C_{++}^{--}, D_{--}^{++} et D_{++}^{--}. Le critère suivant repose sur le lemme ci-dessus qui caractérise le type D, sachant que $k_{ij} = 1$ correspond à un signe $+$. Ainsi en type C la somme des signes du haut doit être égale à celle du bas, alors qu'en type D elles doivent être différentes (où "additionner les signes" se fait comme 0 et 1, avec $0 \neq 2$).

Ceci nous débarrasse de la moitié des cas; utilisant la symétrie que l'on a décrite, il ne nous reste que les cas annoncés et quatre cas ambigus: C_{+-}^{+-} et C_{+-}^{-+} qui sont symétriques par S, D_{+-}^{--} (avec son image D_{++}^{+-}), et D_{-+}^{--} (avec son image D_{++}^{-+}).

Les deux derniers cas, de type D, sont facilement éliminés en remarquant que pour ce type le seul sommet qui puisse avoir deux signes $-$ est celui d'indice plus élevé (donc le sommet "du bas").

Quant aux deux derniers cas, supposons que l'on ait une configuration de type C avec un signe $+$ et un signe $-$ à chaque sommet. On peut supposer, quitte à réordonner, que $\theta_1 > \theta_2, \theta_3$ et $\theta_3 > \theta_4$. L'hypothèse sur les signes nous dit qu'on est dans une des deux situations suivantes:

$$\sigma_{13} > \sigma_{23} > 2\pi > \sigma_{14} > \sigma_{24}$$

$$\sigma_{13} > \sigma_{14} > 2\pi > \sigma_{23} > \sigma_{24}$$

On utilise alors le lemme suivant, qui découle de la normalisation de σ_{ij} dans $[0, 2\pi[$:

Lemme 5.2.3 *Un sommet $\{\sigma_{ij}, \sigma_{kl}\}$ avec $\sigma_{ij} > 2\pi > \sigma_{kl}$ est de type:*

- $(-,+)$ *si* $\sigma_{kl} > \sigma_{ij} - 2\pi$
- $(+,-)$ *si* $\sigma_{kl} < \sigma_{ij} - 2\pi$.

Or deux σ_{ij} ayant un indice commun sont certainement dans le premier cas (puisque $\sigma_{ij} - \sigma_{jk} = \theta_i - \theta_k$), donc un couple $(+,-)$ ne peut pas apparaître deux fois dans les situations ci-dessus. Ceci élimine le type C_{+-}^{+-}. Quant au type C_{+-}^{-+}, si on a un sommet de type $(-,+)$ et un de type $(+,-)$, le lemme implique que celui du haut doit être de type $(+,-)$ (en effet, le sommet du haut est celui qui a la plus petite différence de coordonnées).

On termine la démonstration en donnant des exemples des types qui restent (voir la section 5.4 pour les détails). On donne ici seulement les valeurs correspondantes des paires $\{\theta_1, \theta_2\}$ et $\{\theta_3, \theta_4\}$.

La configuration pour $\{\frac{2\pi}{3}, \frac{2\pi}{4}\}$,$\{\frac{2\pi}{5}, \frac{2\pi}{6}\}$ est de type C_{++}^{++}, et son image par S est de type C_{--}^{--}. La configuration pour $\{\frac{2\pi}{3}, -\frac{2\pi}{4}\}$,$\{\frac{2\pi}{5}, -\frac{2\pi}{6}\}$ est de type C_{-+}^{+-} (stable par S). Le type C_{-+}^{-+} (stable par S) est obtenu par exemple avec les paires $\{2\pi - \varepsilon, \varepsilon\}$,$\{2\varepsilon, 3\varepsilon\}$, pourvu que $5\varepsilon < 2\pi$.

Quant aux types D: D^{-+}_{--} est obtenu avec $\{\frac{2\pi}{4}, \frac{2\pi}{6}\}$, $\{-\frac{2\pi}{5}, -\frac{2\pi}{7}\}$ et son image par S est D^{++}_{-+}. Enfin, le type D^{+-}_{--} est obtenu avec $\{\frac{2\pi}{4}, -\frac{2\pi}{6}\}$, $\{\frac{2\pi}{5}, -\frac{2\pi}{7}\}$ et son image par S est D^{++}_{+-}. □

5.2.4 Chambres et groupes irréductibles

On se concentre dans cette section sur l'affirmation que les paires (A, B) qui engendrent un groupe irréductible sont envoyées sur des points intérieurs de l'image. Ceci découle du fait que l'application $\tilde{\mu}$ est une submersion en un tel point; pour s'assurer que la source est bien lisse (et identifier son espace tangent), on restreint $\tilde{\mu}$ aux paires dont le produit est elliptique régulier (dans la carte affine du demi-carré, ceux-ci correspondent aux points intérieurs au triangle):

$$\tilde{\mu}_r : \left\{ \begin{array}{rcccc} (C_1 \times C_2) \cap \mu^{-1}(\{\text{elliptiques réguliers}\}) & \xrightarrow{\mu} & G & \xrightarrow{\pi} & \mathbb{T}^2/\mathfrak{S}_2 \\ (A, B) & \longmapsto & AB & \longmapsto & \text{Angles}(AB) \end{array} \right.$$

Comme les elliptiques réguliers forment un ouvert de $G = PU(2,1)$ (voir [G] p. 203), la source est maintenant un ouvert de $C_1 \times C_2$ et a en particulier même espace tangent. Avant d'entrer dans les détails, énonçons le résultat:

Proposition 5.2.5 *Soit $(A, B) \in C_1 \times C_2$ tel que AB soit elliptique régulier et tel que le groupe engendré par A et B soit irréductible. Alors la différentielle de $\tilde{\mu}_r$ en (A, B) est surjective et donc $\tilde{\mu}_r$ est localement surjective en ce point.*

On a remarqué ce phénomène par analogie avec le cas du groupe compact $U(n)$ décrit dans [FW] (voir lemme 5.2.4 ci-dessous). Ainsi $\tilde{\mu}$ est de rang 2 en un irréductible; on verra dans la prochaine section qu'elle est de rang 1 en un réductible générique, et de rang 0 en un point totalement réductible.

Notons également que l'on démontre une version plus forte de ce résultat dans la section 5.3.1, en utilisant seulement une certaine classe de déformations lagrangiennes.

Démonstration. On considère séparément le produit μ et la projection π de G sur ses classes de conjugaison, et on montre que chacune est une submersion aux points irréductibles. Commençons par rappeler quelques faits sur la structure de groupe de Lie de $G = PU(2,1)$ et sur ses classes de conjugaison. Considérons une classe de conjugaison avec un représentant particulier A (dans notre cas, la classe étant elliptique, on peut prendre une matrice diagonale):

$$C_1 = \{P.A.P^{-1} \mid P \in PU(2,1)\}$$

Ceci est une sous-variété de G de dimension $dim(PU(2,1)) - dim(Z(A))$, où le centralisateur $Z(A)$ est de dimension 2 si A est elliptique régulier (comme on peut le voir sur la forme diagonale avec trois valeurs propres distinctes) et de dimension 4 si A a une valeur propre double. Rappelons que $PU(2,1)$ est de dimension 8; on obtient ainsi une dimension 6 pour les classes de conjugaison elliptiques régulières, et 4 pour les classes elliptiques spéciales (notons que dans tous les cas le sous-espace formé des décompositions lagrangiennes est de dimension moitié, voir section 5.3). L'espace tangent en A à sa classe de conjugaison est alors:

$$T_A C_1 = \{XA - AX \mid X \in \mathfrak{g}\} = \{(X - AXA^{-1})A \mid X \in \mathfrak{g}\}$$

où la dernière expression identifie ce sous-espace de T_AG au sous-espace $Im(Id - Ad_A)$ de $\mathfrak{g} = T_1G$ par translation à droite par A^{-1} (ou forme de Maurer-Cartan à droite). Ceci est le point de vue développé dans [FW], où le résultat suivant est obtenu, notant $\mathfrak{z}(A, B)$ l'algèbre de Lie du centralisateur du groupe engendré par A et B (et l'orthogonal étant pris par rapport à la forme de Killing):

Lemme 5.2.4 $Im(d_{(A,B)}\mu) = \mathfrak{z}(A, B)^{\perp}.AB$.

Dans les notations de [FW], notre μ est $\pi^{(1)}$; ce résultat se trouve dans la démonstration de la Prop. 4.2 en p. 23. On donne ici une démonstration rapide pour la commodité du lecteur. Ecrivons, pour $h_1 \in T_AC_1$ et $h_2 \in T_BC_2$: $\mu(A+h_1, B+h_2) = AB+Ah_2+h_1B+h_1h_2$. Ceci donne l'expression de la différentielle de μ en (A, B): $d_{(A,B)}\mu(h_1, h_2) = Ah_2 + h_1B$. Si l'on translate comme ci-dessus ces vecteurs tangents dans $\mathfrak{g} = T_1G$ en écrivant $h_1 = X_1.A$, $h_2 = X_2.B$ (avec $X_1 \in Im(Id - Ad_A)$ et $X_2 \in Im(Id - Ad_B)$) et $d_{(A,B)}\mu(h_1, h_2) = X_3.AB$, on obtient la relation de cocycle :

$$X_3 = X_1 + Ad_A(X_2)$$

Utilisant alors une forme bilinéaire non-dégénérée Ad-invariante sur $\mathfrak{g}$ telle que la forme de Killing, le lemme découle de l'observation suivante:

$$[Im(Id - Ad_A) + Ad_A(Im(Id - Ad_B)]^{\perp} = Ker(Id - Ad_A) \cap Ad_A(Ker(Id - Ad_B)) = \mathfrak{z}(A) \cap \mathfrak{z}(B)$$

Or si A et B engendrent un groupe irréductible, alors $\mathfrak{z}(A, B) = \{0\}$ (parce que le centre de $PU(2, 1)$ est trivial), donc μ est bien une submersion en un tel point.

Enfin, la projection π restreinte aux éléments elliptiques est en coordonnées l'application qui associe à une matrice ses valeurs propres (ou plutôt, deux combinaisons linéaires de ses valeurs propres); ceci est de façon classique différentiable et une submersion en une matrice à valeurs propres distinctes, ce qui est le cas des éléments elliptiques réguliers. □

5.2.5 Quelles chambres sont pleines ?

Il découle de la section précédente qu'une chambre est soit entièrement dans l'image de $\tilde{\mu}$ ("pleine"), soit entièrement dans son complémentaire ("vide"). On dispose de deux types d'arguments pour déterminer exactement quelles chambres sont vides et lesquelles sont pleines: des arguments constructifs, comme la convexité locale au voisinage d'un sommet, qui nous disent que certaines chambres sont pleines, et des obstructions qui forcent d'autres chambres à être vides.

Convexité, convexité locale

Il y a une notion naturelle de convexité dans la surface $\mathbb{T}^2/\mathfrak{S}_2$ comme dans toute variété riemannienne, celle de convexité géodésique. La seule subtilité provient du fait qu'il y a (comme dans le tore) beaucoup de segments géodésiques entre deux points, et qu'il n'y a pas toujours unicité du plus court. Ce qui compte est que de telles paires de points sont isolées et qu'on

peut donc les négliger dans la définition de la convexité. On va justifier ceci rapidement avant d'écrire une définition possible.

Considérons un tore $\mathbb{T}^2$, quotient du plan euclidien E^2 par le groupe d'isométries engendré par deux translations de vecteurs (linéairement indépendants) e_1 et e_2. Etant donnés deux points p_1 et p_2 de T^2, toute droite de E^2 passant par un antécédent de chacun se projette sur une géodésique contenant p_1 et p_2. Supposons par example que la base (e_1, e_2) est orthonormée et fixons un antécédent de p_1, disons $\tilde{p_1} \in p_1 + \mathbb{Z}e_1 + \mathbb{Z}e_2$. Alors, pour $\tilde{p_2} \in p_2 + \mathbb{Z}e_1 + \mathbb{Z}e_2$, la pente de la droite $(\tilde{p_1}, \tilde{p_2})$ est irrationnelle si et seulement elle l'est pour tout choix d'un tel $\tilde{p_2}$; dans ce cas toutes les droites $(\tilde{p_1}, \tilde{p_2})$ se projettent sur des géodésiques distinctes de $\mathbb{T}^2$. Si par contre les pentes sont rationnelles, alors chacune de ces droites contient une famille dénombrable de $\tilde{p_2} \in p_2 + \mathbb{Z}e_1 + \mathbb{Z}e_2$, mais il y a encore une famille dénombrable de droites qui se projettent sur des géodésiques distinctes. Quant à l'unicité du plus court segment géodésique, le seul cas problématique se pose quand il y a plus d'un point de $p_2 + \mathbb{Z}e_1 + \mathbb{Z}e_2$ qui est à la plus courte distance de p_1. Mais ce cas se produit seulement lorsque le réseau $p_2 + \mathbb{Z}e_1 + \mathbb{Z}e_2$ contient les milieux de certaines arêtes de $p_1 + \mathbb{Z}e_1 + \mathbb{Z}e_2$ (il y a alors deux points les plus proches) ou les centres de ses carrés (il y a alors quatre points les plus proches). La situation dans $\mathbb{T}^2/\mathfrak{S}_2$ est analogue via la projection qui est un revêtement double hors de la diagonale. Les cas ambigus sont donc suffisament isolés pour qu'on les néglige dans la définition suivante (on peut alors choisir le segment approprié en considérant des points voisins).

Definition 5.2.1 *On dira qu'une partie C de $\mathbb{T}^2/\mathfrak{S}_2$ est* **convexe** *si pour toutes paires de points $(x, y) \in C^2$ qui sont joints par un unique plus court segment géodésique dans $\mathbb{T}^2/\mathfrak{S}_2$, ce segment est contenu dans C.*

A vrai dire on n'a besoin ici que de la notion de convexité locale au voisinage d'un sommet; cette notion est claire par la structure affine de $\mathbb{T}^2/\mathfrak{S}_2$ (comme quotient de $\mathbb{R}^2$ par un groupe de transformations affines). On obtient dans le cas présent deux types de sommets: les deux sommets totalement réductibles que l'on a déjà vus, et des sommets "accidentels" qui apparaissent quand deux segments réductibles hyperboliques se croisent. La structure locale autour des sommets totalement réductibles est d'importance fondamentale et on conjecture qu'elle détermine l'image toute entière; quant aux autres sommets, ils semblent se projeter sur des points intérieurs de l'image, bien qu'on n'en ait pas une preuve complète pour le moment (par exemple, si les fibres étaient connexes comme dans le cas classique, cela suivrait). Notre argument principal de convexité locale autour d'un sommet totalement réductible s'appuie sur les propriétés différentielles de $\tilde{\mu}$ en un tel point; on montre qu'en un tel point la différentielle de μ est nulle, mais que **si A ou B n'est pas une réflexion complexe** la différentielle seconde est non nulle au long des segments réductibles, et que l'image est donc localement un cône convexe bordé par les segments réductibles. Le résultat principal est le suivant:

Proposition 5.2.6 *Si A ou B n'est pas une réflexion complexe, l'image de $\tilde{\mu}$ contient toutes les chambres qui touchent un sommet totalement réductible et rencontrent l'enveloppe localement convexe des trois murs réductibles contenant ce sommet. En particulier, si ces trois murs se rencontrent avec des angles obtus, alors le sommet est un point intérieur de l'image (voir Figure 5.6).*

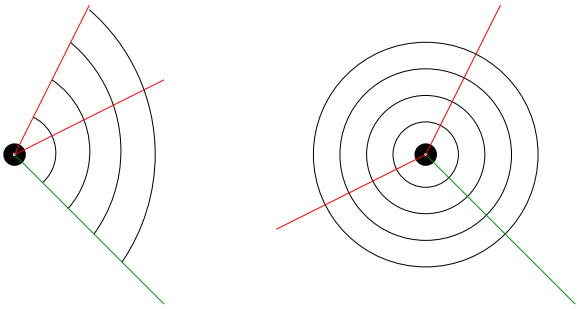

Figure 5.6: Convexité locale autour d'un sommet totalement réductible

Démonstration. On commence par le lemme suivant qui complète ce que l'on a vu, à savoir que $\tilde{\mu}$ est de rang 2 aux irréductibles:

Lemme 5.2.5
- *Si A et B engendrent un groupe totalement réductible, alors $d_{(A,B)}\tilde{\mu}$ est nulle.*
- *Si A et B engendrent un groupe réductible générique (i.e. dont l'image est un point intérieur d'un mur), alors $d_{(A,B)}\tilde{\mu}$ est de rang 1.*

Démonstration du lemme. On a vu au cours de l'étude des points irréductibles (lemme 5.2.4) que:

$$Im(d_{(A,B)}\mu) = \mathfrak{z}(A,B)^{\perp}.AB$$

On a aussi vu que le centralisateur d'un élément elliptique régulier est de dimension 2 (celle pour un elliptique spécial étant 4), et donc que si A ou B est elliptique régulier, la dimension de $\mathfrak{z}(A,B)$ est 2 pour un groupe totalement réductible et 1 pour un réductible générique. Il reste seulement à voir que le sous-espace $Im(d_{(A,B)}\mu)$ est tangent à la fibre de π en un totalement réductible (respectivement, contient l'espace tangent à la fibre en un réductible générique). Mais ceci est clair parce que $Im(d_{(A,B)}\mu) = \mathfrak{z}(A,B)^{\perp}.AB$ contient toujours l'espace tangent à la fibre qui est $T_{AB}C_3 = \mathfrak{z}(AB)^{\perp}.AB$ (où l'on a noté C_3 la classe de conjugaison de AB). □

On se concentre alors sur le cas d'un sommet totalement réductible où l'image va être localement décrite par la différentielle seconde.

Lemme 5.2.6 *L'image de la différentielle quadratique $Q : v \longmapsto d^2_{(A,B)}\tilde{\mu}(v,v)$ est un cône convexe dans $\mathbb{R}^2$.*

Démonstration du lemme. Ceci est une propriété générale des applications quadratiques; on donne ici une preuve rapide dans le cas où le but est de dimension 2. Notons $B(v,w) = d^2_{(A,B)}\tilde{\mu}(v,w)$ l'application bilinéaire symétrique associée et $Q(v) = B(v,v)$. L'image de Q est clairement un cône (parce que $Q(\lambda v) = \lambda^2 Q(v)$ pour $\lambda \in \mathbb{R}$). Pour montrer qu'elle est convexe, considérons deux vecteurs $w_1 = Q(v_1)$ et $w_2 = Q(v_2)$ dans l'image; on montre que tout le segment $[w_1, w_2]$ est contenu dans l'image du plan engendré par v_1 et v_2. En effet, supposons que w_1 et w_2 soient linéairement indépendants et écrivons, pour $\lambda, \mu \in \mathbb{R}$:

$$Q(\lambda v_1 + \mu v_2) = \lambda^2 w_1 + \mu^2 w_2 + 2\lambda\mu B(v_1, v_2) = (\lambda^2 + 2\lambda\mu x_1)w_1 + (\mu^2 + 2\lambda\mu x_2)w_2$$

où l'on a exprimé $B(v_1, v_2) = x_1 w_1 + x_2 w_2$ dans la base (w_1, w_2). Il suffit de montrer que le rapport des deux coordonnées $f(\lambda, \mu) = \frac{\mu^2 + 2\lambda\mu x_2}{\lambda^2 + 2\lambda\mu x_1}$ surjecte $\mathbb{R}^+$. Mais ceci est clair parce que l'application f est continue hors des deux droites $\{\lambda = 0\}, \{\lambda + 2\mu x_1 = 0\}$ et que par exemple sur une droite $\{\mu = p\lambda\}$, elle vaut $\frac{p^2 + 2px_2}{1 + 2px_1}$ qui prend toutes les valeurs entre 0 et $+\infty$ (dans deux des quarts de plan où elle est définie). □

Il reste alors à trouver des vecteurs non nuls dans l'image de Q qui soient tangents aux segments réductibles.

Lemme 5.2.7
- *Si ni A ni B n'est une réflexion complexe par rapport à un point (i.e. si $\theta_1 \neq \theta_2$ et $\theta_3 \neq \theta_4$), alors la famille réductible sphérique contient à chaque sommet totalement réductible des chemins ayant une dérivée seconde non nulle.*
- *Si ni A ni B n'est une réflexion complexe (i.e. si $\theta_i \neq 0$ pour $i = 1...4$), alors chaque famille réductible hyperbolique contient à son sommet totalement réductible des chemins ayant une dérivée seconde non nulle.*

Démonstration du lemme. On va montrer ce résultat en calculant explicitement des déformations au voisinage d'un sommet totalement réductible, le long de l'algèbre de Lie de $U(2)$ d'une part et de $U(1,1)$ de l'autre. En fait, on va calculer la dérivée seconde non pas de $\tilde{\mu}$ elle-même (la paire d'angles), mais de la trace de la matrice produit, ce qui est équivalent (au moins localement, voir le chapitre 1) et simplifie beaucoup les calculs. Notons que l'on n'a pas normalisé le déterminant de la matrice produit, mais cela n'importe pas parce que celui-ci ne dépend que de $\theta_1, \theta_2, \theta_3, \theta_4$ et est donc invariant par la déformation.

On considère donc A et B sous forme diagonale (un point totalement réductible), et on écrit les déformations de B à l'intérieur de sa classe de conjugaison comme des chemins $h(t).B.h(t)^{-1}$ où $h(t)$ est un chemin dans $U(2,1)$ avec $h(0) = 1$. On va alors se restreindre au cas où $\dot{h}(0)$ est dans $\mathfrak{u}(2)$ ou $\mathfrak{u}(1,1)$ (avec la notation $\dot{h} = \frac{dh}{dt}$). On commence par calculer la dérivée seconde, notant que $\frac{d(h^{-1})}{dt} = -h^{-1}\dot{h}h^{-1}$:

$$\begin{aligned}
\tfrac{d^2}{dt^2} Tr(A.hBh^{-1})(0) &= \tfrac{d}{dt} Tr(A\dot{h}Bh^{-1} - AhBh^{-1}\dot{h}h^{-1})(0) \\
&= Tr(A\ddot{h}B - 2A\dot{h}B\dot{h} - AB(-\dot{h})\dot{h} - AB\ddot{h} - AB\dot{h}(-\dot{h}))(0) \\
&= 2Tr(AB\dot{h}^2 - A\dot{h}B\dot{h})(0)
\end{aligned}$$

où l'on a simplifié plusieurs fois par $h(0) = h^{-1}(0) = 1$ et utilisé le fait que A et B commutent. On calcule cette dernière expression pour $\dot{h}(0) \in \mathfrak{u}(2)$ puis $\mathfrak{u}(1,1)$. On rappelle que:

$$U(2) = \{A \in GL(2,\mathbb{C}) \mid A.A^* = 1\} \text{ et donc}$$

$$\mathfrak{u}(2) = \{A \in M(2,\mathbb{C}) \mid A + A^* = 0\} = \left\{ \begin{pmatrix} ri & b \\ -\overline{b} & si \end{pmatrix} \mid r, s \in \mathbb{R},\ b \in \mathbb{C} \right\}$$

Avec cette dernière expression pour $\dot{h}(0)$, écrivant A et B comme des matrices diagonales dans $U(2)$ (ici $A = Diag(e^{i\theta_1}, e^{i\theta_2})$ et $B = Diag(e^{i\theta_3}, e^{i\theta_4})$), on obtient:

$$AB\dot{h}(0)^2 = \begin{pmatrix} -(r^2 + |b|^2)e^{i(\theta_1+\theta_3)} & (r+s)ibe^{i(\theta_1+\theta_3)} \\ -(r+s)i\overline{b}e^{i(\theta_2+\theta_4)} & -(s^2+|b|^2)e^{i(\theta_2+\theta_4)} \end{pmatrix}$$

$$A\dot{h}(0)B\dot{h}(0) = \begin{pmatrix} -r^2e^{i(\theta_1+\theta_3)} - |b|^2e^{i(\theta_1+\theta_4)} & bi(re^{i(\theta_1+\theta_3)} + se^{i(\theta_1+\theta_4)}) \\ -\overline{b}i(re^{i(\theta_2+\theta_3)} + se^{i(\theta_2+\theta_4)}) & -s^2e^{i(\theta_2+\theta_4)} - |b|^2e^{i(\theta_2+\theta_3)} \end{pmatrix}$$

de façon que:

$$Tr(AB\dot{h}^2 - A\dot{h}B\dot{h})(0) = |b|^2(e^{i(\theta_1+\theta_4)} + e^{i(\theta_2+\theta_3)} - e^{i(\theta_1+\theta_3)} - e^{i(\theta_2+\theta_4)})$$

Ceci nous donne le résultat pour $U(2)$ puisque ce nombre complexe, somme de quatre termes de normes égales, ne peut être nul que s'ils sont deux à deux opposés (ou si $b = 0$) (comme dans un losange), c'est-à-dire si $\theta_1 = \theta_2$ ou $\theta_3 = \theta_4$. Notons que la dérivée seconde est toujours dans une même demi-droite du plan complexe.

On fait maintenant la même chose pour $\dot{h}(0) \in \mathfrak{u}(1,1)$. Rappelons que, notant $J = Diag(1,-1)$:

$$U(1,1) = \{A \in GL(2,\mathbb{C}) \mid A.J.A^* = J\} \text{ et donc}$$

$$\mathfrak{u}(1,1) = \{A \in M(2,\mathbb{C}) \mid AJ + JA^* = 0\} = \left\{ \begin{pmatrix} ri & b \\ \overline{b} & si \end{pmatrix} \mid r,s \in \mathbb{R},\ b \in \mathbb{C} \right\}$$

On utilise cette dernière expression pour $\dot{h}$, et on écrit seulement le bloc de A et B correspondant au $\mathbb{C}$-plan stable comme une matrice diagonale dans $U(1,1)$ (par exemple, $A = Diag(e^{i\theta_2}, 1)$ et $B = Diag(e^{i\theta_4}, 1)$ correspondent à la famille C_{24} de la proposition 5.2.3). On obtient:

$$AB\dot{h}(0)^2 = \begin{pmatrix} (|b|^2 - r^2)e^{i(\theta_2+\theta_4)} & (r+s)ibe^{i(\theta_2+\theta_4)} \\ (r+s)i\overline{b} & |b|^2 - s^2 \end{pmatrix}$$

$$A\dot{h}(0)B\dot{h}(0) = \begin{pmatrix} -r^2e^{i(\theta_2+\theta_4)} + |b|^2e^{i\theta_2} & bi(re^{i(\theta_2+\theta_4)} + se^{i\theta_2}) \\ \overline{b}i(re^{i\theta_4} + s) & |b|^2e^{i\theta_4} - s^2 \end{pmatrix}$$

et donc:

$$Tr(AB\dot{h}^2 - A\dot{h}B\dot{h})(0) = |b|^2(e^{i(\theta_2+\theta_4)} + 1 - e^{i\theta_2} - e^{i\theta_4}).$$

Comme ci-dessus, ce nombre est non nul pour ($b \neq 0$ et) $\theta_2 \neq 0$ et $\theta_4 \neq 0$. On obtient la condition analogue pour les trois autres segments réductibles hyperboliques. □

Ceci achève la démonstration de la proposition, sauf dans les cas où A ou B est une réflexion complexe (respectivement, une réflexion complexe par rapport à un point) qui sont exclus du lemme précédent. Mais ceci est tout à fait normal, parce que dans ces cas la dérivée seconde qui s'annule correspond à une famille réductible réduite à un point. Plus précisément, si l'un des générateurs a deux angles égaux alors les deux sommets totalement réductibles sont confondus et le segment réductible sphérique est réduit à ce point; si l'un des angles est nul alors les deux familles réductibles hyperboliques correspondantes sont réduites à un point (par exemple, si $\theta_1 = 0$ alors C_{13} et C_{14} sont réduites à un point). □

On en vient maintenant à l'étude de l'image au voisinage d'un croisement de familles réductibles. A cette fin, on examine les déformations d'un point réductible régulier (réductible hyperbolique ou réductible sphérique) qui sont transverses à la famille réductible en question. Le résultat principal est qu'il y a au moins un côté du segment réductible (défini par la configuration locale au sommet) dans la surface qui reste plein tout au long du segment. Notons que les

deux côtés du segment sont échangés lorsque ce segment rebondit sur la diagonale (l'orientation change dans la carte affine).

Proposition 5.2.7 *Si un côté d'un segment réductible est plein au voisinage d'un sommet totalement réductible, alors ce même côté reste plein tout au long du segment, même après éventuelle intersection avec d'autres segments réductibles.*

Démonstration. On écrit comme précédemment des déformations du produit AB autour de la paire (A, B) comme des chemins $Ah(t)Bh(t)^{-1}$ avec $h(t) \in PU(2,1)$ et $h(0) = 1$. Mais maintenant (A, B) est un point réductible régulier et on déforme dans des directions transverses à la famille réductible à laquelle appartient (A, B). On commence par montrer qu'il y a toujours de telles déformations localement autour d'un point réductible hyperbolique régulier; on a déjà vu que la différentielle $d_{(A,B)}\tilde{\mu}$ est de rang un en un tel point (voir lemme 5.2.5), son image étant tangente au segment réductible.

Lemme 5.2.8 *Soit $(A, B) \in C_1 \times C_2$ un point réductible hyperbolique régulier (i.e. A et B engendrent un groupe réductible hyperbolique sans point fixe). Alors l'image de la differentielle seconde quadratique $Q : v \longmapsto d^2_{(A,B)}\tilde{\mu}(v, v)$ contient des directions transverses à l'image de $d_{(A,B)}\tilde{\mu}$.*

Démonstration du lemme. Considérons par exemple un point de la famille réductible hyperbolique C_{24}, de la forme:

$$A = \begin{pmatrix} e^{i\theta_1} & 0 & 0 \\ 0 & e^{i\theta_2} & 0 \\ 0 & 0 & 1 \end{pmatrix} \quad \text{et} \quad B = \begin{pmatrix} e^{i\theta_3} & 0 & 0 \\ 0 & b_1 & b_2 \\ 0 & b_3 & b_4 \end{pmatrix}$$

où $\widetilde{B} = \begin{pmatrix} b_1 & b_2 \\ b_3 & b_4 \end{pmatrix} \in U(1,1)$ a comme valeurs propres $e^{i\theta_4}$ de type positif et 1 de type négatif.

On calcule comme précédemment la trace le long du chemin, que l'on choisit transverse à la famille réductible hyperbolique en prenant $\dot{h}(0)$ dans l'orthogonal de l'algèbre de Lie $\mathfrak{u}(1,1)$ correspondante, à savoir:

$$\dot{h}(0) = \begin{pmatrix} 0 & h_1 & h_2 \\ \overline{h_1} & 0 & 0 \\ \overline{h_2} & 0 & 0 \end{pmatrix} \text{ avec } h_1, h_2 \in \mathbb{C}$$

On a vu qu'en un point réductible régulier la différentielle de $\tilde{\mu}$ (ou, de façon équivalente, de la trace du produit) est de rang un (son image est tangente au segment réductible). On cherche maintenant des vecteurs dans l'image de la différentielle quadratique qui soient transverses à cette droite, et on calcule les nombres complexes correspondants. Un vecteur tangent au segment réductible est donné par:

$$\frac{d}{dt}Tr(Ah(t)Bh(t)^{-1})(0) = Tr(A\dot{h}B - AB\dot{h})(0) \text{ avec } \dot{h}(0) \in \mathfrak{u}(1,1)$$

Par exemple, en prenant $\dot{h}(0) = \begin{pmatrix} 0 & 1 \\ 1 & 0 \end{pmatrix}$, on obtient:

$$Tr(A\dot{h}B - AB\dot{h})(0) = (b_3 - b_2)(e^{i\theta_2} - 1)$$

qui est non nul pourvu que $\theta_2 \neq 0$ (si ce n'est pas le cas, la famille réductible hyperbolique est réduite à un point) et $b_2 \neq b_3$; si cette dernière condition n'est pas satisfaite on peut utiliser un autre $\dot{h}(0) \in \mathfrak{u}(1,1)$.

Maintenant qu'on a un vecteur tangent au segment réductible, on calcule l'image de la différentielle seconde:

$$\begin{aligned}
\tfrac{d^2}{dt^2}Tr(A.hBh^{-1})(0) &= \tfrac{d}{dt}Tr(A\dot{h}Bh^{-1} - AhBh^{-1}\dot{h}h^{-1})(0) \\
&= Tr(A\ddot{h}B - 2A\dot{h}B\dot{h} - AB(-\dot{h})\dot{h} - AB\ddot{h} - AB\dot{h}(-\dot{h}))(0) \\
&= 2Tr(AB\dot{h}^2 - A\dot{h}B\dot{h})(0)
\end{aligned}$$

ce qui est le même résultat qu'avant; mais ici les termes de deuxième ordre ne s'annulent plus parce que A et B commutent, mais parce que $Tr([A,B]\ddot{h})(0) = 0$, grâce à la forme particulière de $\dot{h}(0)$. On obtient ainsi:

$$\begin{aligned}
Tr(AB\dot{h}^2 - A\dot{h}B\dot{h})(0) &= |h_1|^2(e^{i(\theta_1+\theta_3)} + b_1(e^{i\theta_2} - e^{i\theta_1}) - e^{i(\theta_2+\theta_3)}) \\
&\quad -h_1\overline{h_2}(e^{i\theta_1}b_2 + e^{-i\theta_1}\overline{b_3}) \\
&\quad +|h_2|^2(e^{i(\theta_1+\theta_3)} + b_4(1 - e^{i\theta_1}) - e^{i\theta_3})
\end{aligned}$$

Cette expression est une forme hermitienne en (h_1, h_2); notre assertion revient à dire que cette forme est non dégénérée, ce que l'on montre en calculant son discriminant Δ:

$$\begin{aligned}
\Delta &= [e^{i(\theta_1+\theta_3)} + b_1(e^{i\theta_2} - e^{i\theta_1}) - e^{i(\theta_2+\theta_3)}] \cdot [e^{i(\theta_1+\theta_3)} + b_4(1 - e^{i\theta_1}) - e^{i\theta_3}] \\
&+ \tfrac{1}{4}\left[|b_1|^2 + |b_4|^2 + 2Re(e^{2i\theta_1}(b_1b_4 - 1)) - 2\right]
\end{aligned}$$

où l'on a éliminé b_2 et b_3 par les relations exprimant le fait que $\tilde{B}$ soit dans $U(1,1)$. On peut même simplifier un peu plus en supposant que $\tilde{B} \in SU(1,1)$, et dans ce cas sa trace est entièrement déterminée par son angle: $Tr(\tilde{B}) = b_1 + b_4 = 2\cos(\frac{\theta_4}{2})$, que l'on note c_4. On obtient donc pour Δ, en simplifiant et regroupant des termes:

$$\begin{aligned}
\Delta &= \tfrac{|b_1|^2 + |c_4 - b_1|^2}{4} + (e^{i\theta_2} - e^{i\theta_1})(1 - e^{i\theta_1})[(e^{i\theta_3} - c_4/2)^2 - (b_1 - c_4/2)^2] \\
&+ 1/2 \cdot \left[Re[e^{2i\theta_1}(b_1c_4 - b_1^2)] + \cos 2\theta_1 - 1\right]
\end{aligned}$$

qui a par exemple une partie imaginaire non nulle (notons que $|b_1| \geqslant 1$ parce que $|b_1|^2 - |b_2|^2 = 1$, $\tilde{B}$ étant dans $U(1,1)$). □

On montre maintenant le résultat analogue pour les points réductibles sphériques réguliers:

Lemme 5.2.9 *Soit $(A,B) \in C_1 \times C_2$ un point réductible sphérique régulier (i.e. A et B engendrent un groupe qui fixe un point mais n'est pas réductible hyperbolique). Alors l'image de la differentielle seconde quadratique $Q : v \longmapsto d^2_{(A,B)}\tilde{\mu}(v,v)$ contient des directions transverses à l'image de $d_{(A,B)}\tilde{\mu}$.*

Démonstration. Ceci se montre exactement comme le cas précédent, mais les blocs ne sont plus au même endroit. Le calcul donne:

$$\begin{aligned} Tr(AB\dot{h}^2 - A\dot{h}B\dot{h})(0) &= |h_1|^2(e^{i\theta_1}b_1 + 1 - e^{i\theta_1} - b_1) \\ &\quad -h_1\overline{h_2}(\overline{b_2} + b_3) \\ &\quad +|h_2|^2(e^{i\theta_2}b_4 + 1 - e^{i\theta_2} - b_4) \end{aligned}$$

qui est comme ci-dessus une forme hermitienne non dégénérée en (h_1, h_2). □

Obstructions

On voudrait donner ici des obstructions à ce que certaines chambres spécifiques soient pleines. L'obstruction principale que l'on a remarquée dans tous les exemples, mais dont on n'a pas encore de démonstration complète, est la suivante. On conjecture qu'étant données deux paires d'angles $\{\theta_1, \theta_2\}$ et $\{\theta_3, \theta_4\}$ sans restriction, le polygone du moment ne peut pas contenir simultanément les deux chambres qui touchent les coins "diagonaux" du demi-carré. Autrement dit, le produit ne peut pas avoir des angles de la forme $\{\varepsilon, \varepsilon\}$ et $\{-\varepsilon, -\varepsilon\}$ pour ε arbitrairement petit. Notons cependant que le coin inférieur droit du demi-carré peut être atteint, comme dans les figures 5.16 et 5.17 (ceci signifie que le produit peut avoir des angles de la forme $\{\varepsilon, -\varepsilon\}$ avec ε arbitrairement petit).

Les problèmes que l'on rencontre lorsqu'on essaie de démontrer ceci proviennent des subtilités au bord, surtout près des trois sommets (identifiés) du carré qui représentent l'identité mais aussi toutes les isométries paraboliques unipotentes (qui sont les translations de Heisenberg du bord). On peut en général éliminer l'identité de l'image (sauf lorsque la classe de conjugaison de B contient l'inverse de A, si les angles sont $\{\theta_1, \theta_2\}$ et $\{-\theta_1, -\theta_2\}$) et avec elle tout un voisinage (non uniforme) de l'identité, mais ceci n'interdit pas les unipotents ni les elliptiques qui s'accumulent sur eux. Il existe des résultats de ce type dans [Sz2] (voir section 13, pp. 111–122), mais ils ne s'appliquent pas ici, surtout parce qu'ils supposent tous la convergence ordinaire dans $PU(2,1)$ pour démontrer une forme de convergence plus fine. Ce qui nous semble être ici une approche raisonnable est d'étudier les points d'accumulation de réflexions complexes par rapport à des points ayant un angle de rotation arbitrairement petit (ce sont les paires d'angles $\{\varepsilon, \varepsilon\}$ et $\{-\varepsilon, -\varepsilon\}$).

5.3 Configurations de triplets lagrangiens

On s'intéresse dans cette section à une classe plus restreinte de groupes triangulaires elliptiques, que l'on appellera *lagrangiens* ou *décomposables*, à savoir ceux qui sont sous-groupe d'indice 2 d'un groupe engendré par trois $\mathbb{R}$-réflexions (ou involutions antiholomorphes) par rapport à des $\mathbb{R}$-plans qui s'intersectent deux à deux dans l'espace hyperbolique complexe. Plus précisément, les deux générateurs du groupe triangulaire sont des produits de deux $\mathbb{R}$-réflexions dont une est commune aux deux. Ceci est analogue au cas classique où l'on considère un groupe engendré par deux rotations du plan (euclidien, sphérique ou hyperbolique) à l'intérieur d'un groupe engendré par les réflexions par rapport aux côtés d'un triangle, de façon à en comprendre les propriétés géométriques.

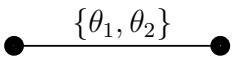

Figure 5.7: Diagramme de Coxeter pour une paire de $\mathbb{R}$-réflexions

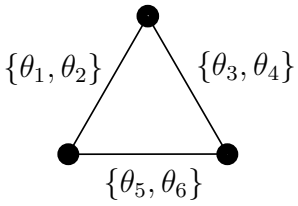

Figure 5.8: Diagramme de Coxeter pour un triplet de $\mathbb{R}$-réflexions

Rappelons qu'une paire de lagrangiens sécants est caractérisée à isométrie près par une paire d'angles (de réflexion) qui sont la moitié des angles (de rotation) de l'isométrie elliptique obtenue en composant les deux $\mathbb{R}$-réflexions associées. Ceci produit une paire d'angles $\{\theta_1, \theta_2\}$ avec $\theta_i \in \mathbb{R}/\pi\mathbb{Z}$, que l'on écrit dans un diagramme à la Coxeter (voir figure 5.7). La question des configurations possibles de triplets de $\mathbb{R}$-plans deux à deux sécants se traduit alors en celle de savoir quelles sont les paires d'angles possibles comme étiquettes pour le diagramme triangulaire de la figure 5.8.

Comme dans le cas classique des groupes plans, on gagne de l'information géométrique en introduisant ces $\mathbb{R}$-réflexions; on obtient ici une obstruction géométrique qui est complètement analogue au cas plan au sens où elle exprime quels sont les angles riemanniens admissibles dans un triangle géodésique (voir section 5.3.1). Remarquons qu'on n'a pas trouvé de façon d'exprimer cette condition sur les trois paires d'angles dans un groupe qui n'est pas décomposable, bien qu'on conjecture que le polygone image soit le même (ce qui dans le cas du groupe compact $U(n)$ est le résultat principal de [FW]).

Cette obstruction mise à part, tout ce que l'on a fait pour les groupes triangulaires elliptiques se transpose au cadre lagrangien: d'une part, l'application moment restreinte est aussi de rang maximal aux points irréductibles, et d'autre part les groupes réductibles sont exactement les mêmes dans les deux cas. On gagne par contre beaucoup au niveau pratique, surtout grâce à la dimension plus petite à la source: la dimension de l'espace des $\mathbb{R}$-réflexions décomposant une classe de conjugaison elliptique régulière donnée est 3 (voir la section 5.3.2 pour une paramétrisation explicite), soit la moitié de celle de la classe de conjugaison elle-même. Ceci cadre bien avec la description par Schaffhauser de l'espace des représentations décomposables comme variété lagrangienne de la variété des représentations d'un groupe de surface (celui de la sphère épointée dans $U(n)$, voir [Sf]). Du point de vue pratique, les $\mathbb{R}$-réflexions nous donnent un moyen de paramétrer une classe de conjugaison donnée transversalement aux fibres de notre application moment (avec deux fois moins de paramètres); il est surtout remarquable que l'on obtient alors génériquement des fibres de dimension 1, ce qui est le point de départ de notre recherche de groupes discrets dans ce cadre (voir la dernière section).

5.3.1 Triplets lagrangiens vs. triangles elliptiques

On considère ici l'application $\tilde{\mu}_L$ qui est la restriction de l'application $\tilde{\mu}$ de la section précédente (qui associait à une paire de transformations elliptiques (A, B) dans des classes de conjugaison

fixées la paire d'angles de leur produit) aux paires (A, B) qui sont *simultanément décomposables* (en $\mathbb{R}$-réflexions). Ceci signifie qu'il existe des $\mathbb{R}$-réflexions σ_1, σ_2 et σ_3 telles que $A = \sigma_2\sigma_1$ et $B = \sigma_3\sigma_2$ (ceci correspond aux représentations lagrangiennes au sens de [FW] et [Sf]). Les angles du produit $BA = \sigma_3\sigma_1$ sont alors (le double de) ceux des $\mathbb{R}$-plans correspondants L_1 et L_3, ce qui montre que les problèmes de l'image de l'application moment lagrangienne $\tilde{\mu}_L$ et des configurations possibles de triplets de $\mathbb{R}$-plans sont équivalents.

Il est évident que l'image de $\tilde{\mu}_L$ est incluse dans celle de $\tilde{\mu}$; on conjecture que, comme dans le cas de $U(n)$ étudié dans [FW], ces images sont les mêmes. Un indice dans ce sens est le fait que tous nos arguments constructifs de la section précédente (surjectivité locale aux irréductibles, description des réductibles et convexité locale) se transposent au cas décomposable; voir aussi les dessins expérimentaux de la section 5.4 que l'on obtient par la paramétrisation lagrangienne. Il semblerait cependant que l'obstruction de la section 5.3.1 ne se transpose pas au cas unitaire, mais il est possible que les chambres correspondantes soient éliminées pour d'autres raisons. Ou alors on n'a juste pas vu comment traduire cette condition dans le cas unitaire.

Les groupes irréductibles se projettent sur des points intérieurs

On commence par montrer que la sous-variété formée des paires décomposables est transverse aux fibres de l'application moment, dont la restriction à cette sous-variété reste donc localement surjective.

Proposition 5.3.1 *Soit $(A, B) \in C_1 \times C_2$ une paire simultanément décomposable qui engendre un groupe irréductible avec BA elliptique régulier. Alors la différentielle de $\tilde{\mu}_L$ en (A, B) est surjective et donc $\tilde{\mu}_L$ est localement surjective en ce point.*

Démonstration. On montre ceci de façon analogue à celle pour le résultat correspondant quand la source est $C_1 \times C_2$ tout entier, mais le résultat est plus subtil ce qui rend la preuve plus délicate. On utilise encore le formalisme d'algèbre de Lie développé dans [FW] pour le cadre lagrangien. Notre point de départ est un triplet de $\mathbb{R}$-plans L_1, L_2, L_3 avec $\mathbb{R}$-réflexions associées σ_1, σ_2, σ_3 (telles que: $A = \sigma_2\sigma_1$ et $B = \sigma_3\sigma_2$) et on étudie les déformations de la classe de conjugaison du produit $BA = \sigma_3\sigma_1$. On pourrait écrire explicitement l'espace tangent à l'espace des paires décomposables dans $C_1 \times C_2$, mais ce n'est pas facile à faire. On va plutôt suivre les lignes de [FW] et étudier une sous-classe explicite de déformations autour d'une paire décomposable, telles que ces déformations restent décomposables et balaient toutes les directions dans l'image. Dans ce but, Falbel et Wentworth ont introduit deux types de déformations lagrangiennes dans $U(n)$, qu'ils appellent *twisting* ("torsion") et *real bending* ("pliage réel"). Les déformations de torsion sont obtenues en tournant chaque lagrangien d'un facteur (central) de $U(1)$, alors que celles de pliage sont obtenues en tournant un certain nombre de lagrangiens par un élément qui stabilise l'un d'entre eux (une transformation orthogonale). Les déformations de torsion n'ont pas d'analogue évident dans le cadre hyperbolique complexe, mais les pliages peuvent être transposés directement. En fait, les déformations par pliage réel suffiront à nos besoins; on se limitera à celles autour du $\mathbb{R}$-plan L_2. Précisément, on appellera *pliage réel autour de L_2* toute déformation qui remplace σ_1, σ_2, σ_3 par σ_1, σ_2, $O\sigma_3O^{-1}$ où O est dans le stabilisateur O_2 de L_2 dans $PU(2,1)$ (un sous-groupe conjugué à $PO(2,1)$). On va prouver le lemme suivant qui entraîne le résultat de la proposition:

Lemme 5.3.1 *Les pliages réels autour de L_2 balaient toutes les déformations possibles de la classe de conjugaison du produit $BA = \sigma_3\sigma_1$.*

Ceci peut se voir en évaluant les positions relatives de l'espace tangent à la fibre de π et de l'image de ces déformations par la différentielle de μ dans la composée:

$$C_1 \times C_2 \xrightarrow{\mu} G \xrightarrow{\pi} \mathbb{T}^2/\mathfrak{S}_2$$

Ces sous-espaces de l'espace tangent $T_{BA}G$ peuvent se voir dans l'algèbre de Lie $\mathfrak{g} = \mathfrak{su}(2,1)$ en translatant à droite par $(BA)^{-1}$.

On aura besoin du résultat important suivant (voir Prop. 3.1 de [FW]):

Lemme 5.3.2 *Soient L_i et L_j deux $\mathbb{R}$-plans dans $H^2_{\mathbb{C}}$, σ_i et σ_j les $\mathbb{R}$-réflexions associées, de produit $g = \sigma_i\sigma_j$. Si l'on note O_i, O_j les stabilisateurs de L_i et L_j, $Z(g)$ le centralisateur de g dans $PU(2,1)$, et $\mathfrak{o}_i$, $\mathfrak{o}_j$, $\mathfrak{z}(g)$ les algèbres de Lie correspondantes, alors:*

- *on a une décomposition orthogonale: $\mathfrak{z}(g) = (\mathfrak{o}_i + \mathfrak{o}_j)^\perp \oplus (\mathfrak{o}_i \cap \mathfrak{o}_j)$*
- *si g est elliptique régulier: $\mathfrak{su}(2,1) = \mathfrak{o}_i \oplus \mathfrak{o}_j \oplus \mathfrak{z}(g)$.*

La preemière assertion est la proposition 3.1 de [FW]. La deuxième, analogue à leur corollaire 3.1, en découle en notant que si g est elliptique régulier, alors l'intersection $\mathfrak{o}_i \cap \mathfrak{o}_j$ est triviale, et que la forme de Killing est non dégénérée. □

On peut alors écrire les déformations de $BA = \sigma_3\sigma_1$ par pliage réel autour de L_2 comme des chemins $O(t)\sigma_3 O(t)^{-1}\sigma_1$ avec $O(t) \in O_2$ et $O(1) = Id$. On différencie cette expression et on obtient, en translatant dans $\mathfrak{g}$ par $(BA)^{-1}$ et en écrivant $o = \dot{O}(0)$:

$$(o\sigma_3\sigma_1 - \sigma_3 o\sigma_1)\sigma_1\sigma_3 = (Id - Ad_{\sigma_3})o$$

avec $o \in \mathfrak{o}_2$. Ainsi l'image des vecteurs tangents aux déformations par pliage réel autour de L_2 est le sous-espace $(Id - Ad_{\sigma_3})(\mathfrak{o}_2)$ de $\mathfrak{g}$. Rappelons maintenant que l'espace tangent à la fibre de π au point BA est $Im(Id - Ad_{BA})$. On aura montré la surjectivité de la différentielle de $\tilde{\mu}_L = \pi \circ \mu_L$ si l'on prouve que la somme de ces deux sous-espaces remplit tout l'espace tangent $T_{BA}G$; de façon équivalente, on montre que leurs supplémentaires orthogonaux s'intersectent trivialement:

$$((Id - Ad_{\sigma_3})(\mathfrak{o}_2))^\perp \cap Im(Id - Ad_{BA})^\perp = (Id - Ad_{\sigma_3})(\mathfrak{o}_2)^\perp \cap \mathfrak{z}(BA) = \{0\}.$$

On va montrer successivement les points suivants:

- $z \in (Id - Ad_{\sigma_3})(\mathfrak{o}_2)^\perp \iff (Id - Ad_{\sigma_3})z \in \mathfrak{o}_2^\perp$
- $z \in \mathfrak{z}(BA) \implies (Id - Ad_{\sigma_3})z \in \mathfrak{z}(BA)$
- $\mathfrak{o}_2^\perp \cap \mathfrak{z}(BA) = \{0\}$
- $(Id - Ad_{\sigma_3})z \in \mathfrak{o}_2^\perp \cap \mathfrak{z}(BA)$ et $z \in \mathfrak{z}(BA) \iff z = 0$.

Le premier point s'obtient par un calcul:

$$\begin{aligned} z \in (Id - Ad_{\sigma_3})(\mathfrak{o}_2)^\perp &\iff (\forall o \in \mathfrak{o}_2)\ \langle o - Ad_{\sigma_3} o, z\rangle = 0 \\ &\iff (\forall o \in \mathfrak{o}_2)\ \langle o, z\rangle - \langle Ad_{\sigma_3} o, z\rangle = 0 \\ &\iff (\forall o \in \mathfrak{o}_2)\ \langle o, z\rangle - \langle o, Ad_{\sigma_3} z\rangle = 0 \\ &\iff (\forall o \in \mathfrak{o}_2)\ \langle o, z - Ad_{\sigma_3} z\rangle = 0 \end{aligned}$$

Pour le deuxième point, on calcule, pour $z \in \mathfrak{z}(BA)$:

$$(Id - Ad_{BA})(z - Ad_{\sigma_3} z) = -(Id - Ad_{BA}) Ad_{\sigma_3} z = Ad_{\sigma_3\sigma_1\sigma_3} z - Ad_{\sigma_3} z = Ad_{\sigma_3}(Ad_{(BA)^{-1}} z - z) = 0$$

Le troisième point découle du lemme précédent en notant que:

$$\mathfrak{o}_2^\perp \cap \mathfrak{z}(BA) = \mathfrak{o}_2^\perp \cap (\mathfrak{o}_1 \oplus \mathfrak{o}_3)^\perp = (\mathfrak{o}_1 \oplus \mathfrak{o}_2 \oplus \mathfrak{o}_3)^\perp = \{0\}$$

Le dernier point s'obtient en remarquant qu'un $z \in \mathfrak{g}$ qui satisfait l'assertion de gauche est à la fois dans $\mathfrak{o}_3 = \mathfrak{z}(\sigma_3)$ et dans $\mathfrak{o}_1$, qui ont une intersection triviale si BA est elliptique régulier. Ceci achève la preuve de la proposition. □

Les groupes réductibles sont décomposables

On vient de voir que les groupes décomposables ont localement la même image que tous les groupes elliptiques au voisinage d'un irréductible. La situation est plus simple pour les groupes réductibles puisqu'ils sont tous décomposables (et donc l'image est évidemment la même).

Proposition 5.3.2 *Soient A et B deux transformations elliptiques ayant un point fixe commun dans $H^2_{\mathbb{C}}$. Alors A et B sont simultanément décomposables.*

Ceci a été démontré au chapitre 2 (voir le théorème 2.1 à la p. 224 de [FP]). Le résultat reste vrai pour les groupes réductibles hyperboliques (engendrés par deux elliptiques), qui fixent un point hors de $H^2_{\mathbb{C}}$.

Proposition 5.3.3 *Soient A et B deux transformations elliptiques stabilisant un même $\mathbb{C}$-plan. Alors A et B sont simultanément décomposables.*

Démonstration. Ceci se voit facilement une fois que l'on se rappelle la caractérisation de quelles $\mathbb{R}$-réflexions peuvent apparaître dans une décomposition d'une transformation elliptique. Etant donné $g \in PU(2,1)$, on dit qu'un $\mathbb{R}$-plan L *décompose* g s'il existe une décomposition $g = \sigma\sigma'$ où σ est la $\mathbb{R}$-réflexion par rapport à L et σ' est une autre $\mathbb{R}$-réflexion. On a démontré au chapitre 2 (voir Proposition 4 à la p. 223 de [FP]) que:

- si g est une réflexion complexe par rapport à un point, alors tout $\mathbb{R}$-plan passant par son point fixe décompose g.
- si g est une réflexion complexe, alors tout $\mathbb{R}$-plan coupant son miroir en une géodésique décompose g.

- si g est elliptique régulier, il stabilise exactement deux $\mathbb{C}$-plans (qui contiennent son point fixe). Alors un $\mathbb{R}$-plan décompose g si et seulement s'il passe par son point fixe et coupe chacun de ces $\mathbb{C}$-plans en une géodésique.

Maintenant le résultat de la proposition est évident, parce que si A et B stabilisent un même $\mathbb{C}$-plan il suffit de considérer un $\mathbb{R}$-plan contenant la géodésique dans ce $\mathbb{C}$-plan qui joint les points fixes de A et B (en supposant que A et B sont elliptiques réguliers, ce qui est le cas le plus difficile) pour voir que A et B sont simultanément décomposables. □

Convexité locale

Tous les résultats de la section analogue sur les groupes triangulaires elliptiques restent valables, parce que tous les arguments (et les calculs) reposaient sur les groupes réductibles.

Une obstruction lagrangienne

Il existe une condition que doivent satisfaire les paires d'angles pour un triplet de $\mathbb{R}$-plans s'intersectant deux à deux dans $H^2_{\mathbb{C}}$, qui provient du fait que l'angle riemannien entre deux géodésiques, chacune dans un $\mathbb{R}$-plan, est borné par la paire d'angles de la façon suivante (voir la proposition 1.2.2 du chapitre 1):

Proposition 5.3.4 *Soient L_1 et L_2 deux $\mathbb{R}$-plans s'intersectant dans $H^2_{\mathbb{C}}$ avec paire d'angles $\{\theta_1, \theta_2\}$ ($\theta_i \in [0, \pi[$) et soient $g_1 \subset L_1$, $g_2 \subset L_2$ deux géodesiques se coupant avec angle riemannien $\lambda \in [0, \pi[$. On a alors l'encadrement suivant:*

$$\mathrm{Min}\{\theta_1, \theta_2, \pi - \theta_1, \pi - \theta_2\} \leqslant \lambda \leqslant \mathrm{Max}\{\theta_1, \theta_2, \pi - \theta_1, \pi - \theta_2\}$$

Rappelons qu'une des caractéristiques de la courbure négative (pas nécessairement constante, voir [BGS] p. 6) est que la somme des angles riemanniens dans un triangle géodésique est strictement inférieure à π. En combinant ceci avec l'énoncé précédent, on obtient la condition suivante dans un triangle lagrangien:

Proposition 5.3.5 *Soient L_1, L_2, L_3 trois $\mathbb{R}$-plans deux à deux sécants avec paires d'angles $\{\theta_1, \theta_2\}$, $\{\theta_3, \theta_4\}$, $\{\theta_5, \theta_6\}$ ($\theta_i \in [0, \pi[$). On a alors l'inégalité suivante:*

$$\sum_{i=1,3,5} \mathrm{Min}\{\theta_i, \theta_{i+1}, \pi - \theta_i, \pi - \theta_{i+1}\} < \pi$$

Maintenant, si l'on fixe comme précédemment les deux premières paires d'angles $\{\theta_1, \theta_2\}$, $\{\theta_3, \theta_4\}$ et que l'on regarde les valeurs possibles pour $\{\theta_5, \theta_6\}$, deux possibilités peuvent se présenter selon les valeurs de

$$\alpha = \mathrm{Min}\{\theta_1, \theta_2, \pi - \theta_1, \pi - \theta_2\} \text{ et } \beta = \mathrm{Min}\{\theta_3, \theta_4, \pi - \theta_3, \pi - \theta_4\} :$$

- Si $\alpha + \beta > \frac{\pi}{2}$ il n'y a pas de contrainte sur $\{\theta_5, \theta_6\}$, parce que l'on a toujours:

$$\mathrm{Min}\{\theta_5, \theta_6, \pi - \theta_5, \pi - \theta_6\} \leqslant \frac{\pi}{2}.$$

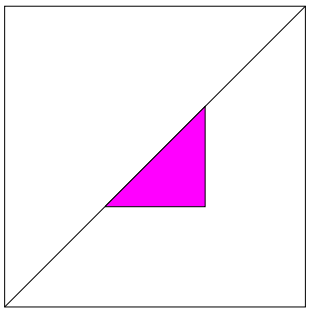

Figure 5.9: Une obstruction dans un triangle lagrangien

- Si $\alpha + \beta \leqslant \frac{\pi}{2}$ alors $\{\theta_5, \theta_6\}$ doit satisfaire l'inégalité:

$$\text{Min}\{\theta_5, \theta_6, \pi - \theta_5, \pi - \theta_6\} < \pi - \alpha - \beta$$

Cette condition interdit une zone triangulaire de $\mathbb{T}^2/\mathfrak{S}_2$ proche du milieu de la diagonale, comme sur la figure 5.9. On n'a malheureusement pas trouvé de façon d'exprimer cette condition dans un groupe triangulaire elliptique non décomposable, bien que l'on conjecture que l'image soit la même.

5.3.2 Un paramétrage des configurations

On calcule dans cette section des paramètres explicites pour trois plans lagrangiens L_0, L_1 et L_2 deux à deux sécants dans l'espace hyperbolique complexe, avec deux paires d'angles fixées

$$\text{Angle}(L_0, L_1) = \{\theta_1, \theta_2\} \quad \text{et} \quad \text{Angle}(L_1, L_2) = \{\theta_3, \theta_4\}.$$

On commence par normaliser de façon que L_0 soit le $\mathbb{R}$-plan standard (la projection dans $\mathbb{C}P^2$ de $\mathbb{R}^3 \subset \mathbb{C}^3$), le point d'intersection de L_0 et L_1 soit O (le centre de la boule, projection du vecteur négatif $[0, 0, 1]^T \in \mathbb{C}^{2,1}$), et que L_1 soit la projection de l'image diagonale:

$$L_1 = \begin{pmatrix} e^{i\theta_1} & 0 & 0 \\ 0 & e^{i\theta_2} & 0 \\ 0 & 0 & 1 \end{pmatrix} \cdot L_0$$

Ceci est le maximum que l'on puisse imposer, parce qu'en général cette configuration de deux lagrangiens n'a plus d'isotropie (sauf si l'un des angles est nul, i.e. les lagrangiens ont une géodésique commune, auquel cas on a encore un paramètre d'isotropie, à savoir la translation le long de cette géodésique). Il nous reste donc trois paramètres: deux pour les coordonnées x, y dans L_1 du point d'intersection $p_1 = L_1 \cap L_2$, et un paramètre angulaire φ pour la famille de lagrangiens L_2 rencontrant L_1 en p_1 avec angles fixés $\{\theta_3, \theta_4\}$ (voir la section suivante sur les paires de lagrangiens).

Pour cette dernière famille, l'idée est de paramétrer d'abord la famille $L_v(\varphi)$ de lagrangiens passant par O et ayant la paire d'angles fixée $\{\theta_3, \theta_4\}$ avec le lagrangien standard L_0 (ceci est un problème vectoriel dans $\mathbb{C}^2$). On trouve alors une transformation $U_{01} \in U(2, 1)$ qui envoie L_1 avec son point marqué O sur L_2 avec son point marqué p_1, au moyen d'un calcul un peu

pénible analogue au procédé d'orthonormalisation de Gram-Schmidt. Le troisième lagrangien $L_2(\varphi)$ est alors simplement l'image $U_{01}(L_v(\varphi))$.

Nous nous intéresserons principalement à une matrice asociée à la $\mathbb{R}$-réflexion σ_2 par rapport à $L_2(\varphi)$, c'est-à-dire une matrice $A_2 \in U(2,1)$ telle que, en coordonnées z de la boule, $\sigma_2(z) = A_2.\overline{z}$. Une autre manière d'exprimer ceci est de dire que A_2 est une matrice de la transformation unitaire $\sigma_2 \circ \sigma_0$, et on voit ainsi qu'elle contient toute l'information sur la configuration des deux $\mathbb{R}$-plans L_0 et L_2 (A_2 est une *matrice de Souriau* de la paire (L_0, L_1) au sens de [N],[FP]). Concrètement, le type de cette isométrie (elliptique, parabolique, ou loxodromique) nous dit si les deux $\mathbb{R}$-plans se coupent à l'intérieur, au bord, ou à l'extérieur de la boule; sa classe de conjugaison particulière (dans le cas elliptique qui nous intéresse) nous donne la paire d'angles entre les $\mathbb{R}$-plans. Plus précisément (voir [CG] p. 64 pour plus de détails), une transformation elliptique g de $H^2_{\mathbb{C}}$ est représentée par des matrices de $U(2,1)$ qui sont diagonalisables avec valeurs propres de norme 1. Une de ces valeurs propres est de *type négatif* au sens où l'espace propre associé est contenu dans le cône négatif de la forme hermitienne de $\mathbb{C}^{2,1}$ (il se projette ainsi sur le point fixe de g dans $H^2_{\mathbb{C}}$). Si les valeurs propres sont $e^{i\phi_1}$, $e^{i\phi_2}$ et $e^{i\phi_3}$, la dernière étant de type négatif, alors la classe de conjugaison de g est caractérisée par la paire d'angles (de rotation) $\{\phi_1 - \phi_3, \phi_2 - \phi_3\}$, et la paire d'angles (de réflexion) entre les $\mathbb{R}$-plans L_0 et L_2 est simplement $\{\frac{\phi_1-\phi_3}{2}, \frac{\phi_2-\phi_3}{2}\}$.

Ceci est très simple à décrire en termes de valeurs propres et de vecteurs propres, mais pour des raisons pratiques, notre matrice $A_2(\theta_1, \theta_2, \theta_3, \theta_4, \varphi, x, y)$ étant un peu compliquée, il n'est pas réaliste de vouloir écrire des formules explicites pour les angles en fonction de nos paramètres (cependant cette approche directe marche très bien pour des expériences numériques). On peut circonvenir cette difficulté en calculant seulement la trace de A_2 (convenablement normalisée dans $SU(2,1)$), ce qui est en principe suffisant pour caractériser la classe de conjugaison de g (voir [G] p. 204), en fait à une indétermination triple près, voir le chapitre 1.

Paires de lagrangiens

On décrit ici la famille de lagrangiens de $\mathbb{C}^2$ rencontrant le lagrangien standard $L_0 = \mathbb{R}^2 \subset \mathbb{C}^2$ avec une paire d'angles fixée $\{\theta_3, \theta_4\}$.

Proposition 5.3.6 *Soient $\theta_3, \theta_4 \in \mathbb{R}/\pi\mathbb{Z}$. Si $\theta_3 \neq \theta_4$, il existe une famille à un paramètre $L_v(\varphi)$ ($\varphi \in \mathbb{R}/\pi\mathbb{Z}$) de lagrangiens de $\mathbb{C}^2$ rencontrant le lagrangien standard L_0 avec la paire d'angles $\{\theta_3, \theta_4\}$, donnée par:*

$$L_v(\varphi) = \begin{pmatrix} e^{i\theta_3}\cos\varphi & -e^{i\theta_4}\sin\varphi \\ e^{i\theta_3}\sin\varphi & e^{i\theta_4}\cos\varphi \end{pmatrix} \cdot L_0$$

Si $\theta_3 = \theta_4$, cette famille est réduite à un point.

Démonstration. Ceci découle directement du lemme de diagonalisation de Nicas (voir [N] p. 74), qui dit qu'il existe une base orthonormée (v_1, v_2) de L_0 telle que $(e^{i\theta_3}v_1, e^{i\theta_4}v_2)$ soit une base de $L_v(\varphi)$. □

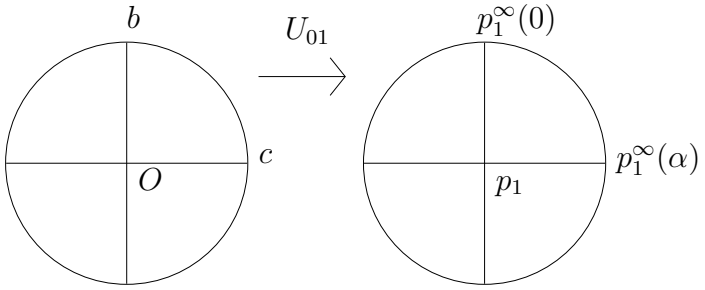

Une application unitaire $U_{01} : (L_0, O) \longmapsto (L_1, p_1)$

On cherche dans cette section une matrice $U_{01} \in U(2,1)$ qui envoie le $\mathbb{R}$-plan L_0 avec le point marqué O sur L_1 avec le point marqué p_1 correspondant au vecteur (que l'on note également p_1):

$$p_1(x,y) = \begin{bmatrix} e^{i\theta_1}x \\ e^{i\theta_2}y \\ 1 \end{bmatrix} \text{ avec } (x,y) \text{ dans le disque unité de } \mathbb{R}^2.$$

L'idée est de compléter chacun de ces vecteurs en une ($\mathbb{R}$-)base du lagrangien correspondant, normalisée de façon à obtenir une transformation unitaire. Un moyen simple de faire cela est de choisir les deux points restants au bord de chaque lagrangien (les vecteurs correspondants ont alors une norme nulle donc on peut les multiplier à loisir par des scalaires). On le fait de la manière suivante, choisissant deux points b et c au bord de L_0 correspondant à des géodésiques orthogonales passant par O, et paramétrant les points du bord de L_1 par:

$$p_1^\infty(\alpha) = \begin{bmatrix} e^{i\theta_1}\cos\alpha \\ e^{i\theta_2}\sin\alpha \\ 1 \end{bmatrix} \text{ avec } \alpha \in \mathbb{R}/2\pi\mathbb{Z}.$$

On veut alors envoyer:

$$\begin{aligned} a = O = [0,0,1]^T &\longmapsto a' = p_1(x,y) \\ b = [1,0,1]^T &\longmapsto b' = p_1^\infty(0) \\ c = [0,1,1]^T &\longmapsto c' = p_1^\infty(\alpha) \end{aligned}$$

avec les conditions de compatibilité suivantes, qui assurent que l'application est unitaire:

$$\begin{cases} \langle a', a' \rangle = \langle a, a \rangle = -1 \\ \langle a', b' \rangle = \langle a, b \rangle = -1 \\ \langle a', c' \rangle = \langle a, c \rangle = -1 \\ \langle b', c' \rangle = \langle b, c \rangle = -1. \end{cases}$$

On commence par normaliser a': $\langle a', a' \rangle = x^2 + y^2 - 1$; on pose donc:

$$a' := \frac{1}{r} \begin{bmatrix} e^{i\theta_1}x \\ e^{i\theta_2}y \\ 1 \end{bmatrix} \text{ avec } r = \sqrt{1 - x^2 - y^2}.$$

On impose alors la deuxième condition: $\langle a', b' \rangle = \frac{x-1}{r}$ et on pose donc:

$$b' := \frac{1}{s}\begin{bmatrix} e^{i\theta_1} \\ 0 \\ 1 \end{bmatrix} \text{ avec } s = \frac{1-x}{r}.$$

Les deux dernières conditions sont un peu plus délicates parce qu'il faut les traiter simultanément. On a encore le paramètre libre α (qui a un sens géométrique clair), ainsi qu'un paramètre de normalisation pour c'. Explicitement, si l'on dilate c' par un facteur réel $-1/t$, on doit résoudre le système suivant:

$$\begin{cases} x\cos\alpha + y\sin\alpha - 1 &= rt \\ \cos\alpha - 1 &= st \\ \cos^2\alpha + \sin^2\alpha &= 1 \end{cases}$$

où l'on a utilisé le fait que $\langle a', c'\rangle = -\frac{1}{rt}(x\cos\alpha + y\sin\alpha - 1)$ et $\langle b', c'\rangle = -\frac{1}{st}(\cos\alpha - 1)$.

Ce système est équivalent par des substitutions linéaires à une certaine équation quadratique en $\cos\alpha$, à savoir:

$$\cos^2\alpha(y^2 + (x - r/s)^2) + 2(x - r/s)(r/s - 1)\cos\alpha + (r/s - 1)^2 - y^2 = 0$$

Les solutions explicites de cette équation ne sont pas très jolies, mais il se trouve qu'elles vont se simplifier donc on les garde pour l'instant sous la forme $\cos\alpha$ et $\sin\alpha$. On a ainsi:

$$c' := -\frac{1}{t}\begin{bmatrix} e^{i\theta_1}\cos\alpha \\ e^{i\theta_2}\sin\alpha \\ 1 \end{bmatrix} \text{ avec } t = \frac{\cos\alpha - 1}{s}.$$

Il reste à former la matrice U_{01}, ce qui est facile avec ce que l'on a vu: si M (resp. M') est la matrice dont les vecteurs-colonnes sont a, b, c (resp. a', b', c'), alors $U_{01} = M'.M^{-1}$. On obtient ainsi:

$$U_{01} = \begin{pmatrix} e^{i\theta_1}(1/s - x/r) & e^{i\theta_1}(-(\cos\alpha)/t - x/r) & e^{i\theta_1}x/r \\ -e^{i\theta_2}y/r & e^{i\theta_2}(-(\sin\alpha)/t - y/r) & e^{i\theta_2}y/r \\ 1/s - 1/r & -1/t - 1/r & 1/r \end{pmatrix}$$

avec r, s, t comme ci-dessus.

C'est ici que se simplifient les expressions faisant intervenir $\cos\alpha$ et $\sin\alpha$ parce que:

$$-(\cos\alpha)/t - x/r = y/(1-x) \text{ et } -(\sin\alpha)/t - y/r = 1$$

comme on peut le voir en écrivant l'équation quadratique précédente uniquement en termes de x et y. On obtient ainsi la forme finale de U_{01}:

$$U_{01} = \begin{pmatrix} e^{i\theta_1}(1/s - x/r) & e^{i\theta_1}(y/(1-x)) & e^{i\theta_1}x/r \\ -e^{i\theta_2}y/r & e^{i\theta_2} & e^{i\theta_2}y/r \\ 1/s - 1/r & y/(1-x) & 1/r \end{pmatrix}$$

avec comme ci-dessus $r = \sqrt{1 - x^2 - y^2}$ et $s = \frac{1-x}{r}$.

La matrice unitaire $A_2(\theta_1, \theta_2, \theta_3, \theta_4, \varphi, x, y)$

L'application U_{01} nous permet alors de paramétrer la famille de $\mathbb{R}$-plans L_2 rencontrant L_1 au point p_1 avec les angles fixés $\{\theta_3, \theta_4\}$, en transportant simplement la famille précédente $L_v(\varphi)$ par U_{01}. On note $U_{\{\theta_3,\theta_4\}}(\varphi) \in U(2,1)$ la matrice suivante, qui est obtenue en utilisant le plongement standard de $U(2)$ dans $U(2,1)$ en tant que stabilisateur de l'origine O:

$$U_{\{\theta_3,\theta_4\}}(\varphi) = \begin{pmatrix} e^{i\theta_3}\cos\varphi & -e^{i\theta_4}\sin\varphi & 0 \\ e^{i\theta_3}\sin\varphi & e^{i\theta_4}\cos\varphi & 0 \\ 0 & 0 & 1 \end{pmatrix}$$

Notre famille de $\mathbb{R}$-plans L_2 est alors:

$$L_2(\varphi) := U_{01} \cdot L_v(\varphi) = U_{01}U_{\{\theta_3,\theta_4\}}(\varphi) \cdot L_0$$

ce qui fait que la matrice A_2 qui nous intéresse (telle que $\sigma_2(z) = A_2.\overline{z}$) peut s'écrire, sachant que la $\mathbb{R}$-réflexion par rapport à L_0 est simplement $z \mapsto \overline{z}$:

$$A_2 = U_{01}.U_{\{\theta_3,\theta_4\}}(\varphi).\overline{U_{\{\theta_3,\theta_4\}}(\varphi)^{-1}}.\overline{U_{01}^{-1}}.$$

On peut simplifier un peu cette expression, en posant par exemple:

$$\tilde{U}_{\{\theta_3,\theta_4\}}(\varphi) := U_{\{\theta_3,\theta_4\}}(\varphi).\overline{U_{\{\theta_3,\theta_4\}}(\varphi)^{-1}}$$

$$= \begin{pmatrix} e^{2i\theta_3}\cos^2\varphi + e^{2i\theta_4}\sin^2\varphi & (e^{2i\theta_3} - e^{2i\theta_4})\cos\varphi\sin\varphi & 0 \\ (e^{2i\theta_3} - e^{2i\theta_4})\cos\varphi\sin\varphi & e^{2i\theta_3}\sin^2\varphi + e^{2i\theta_4}\cos^2\varphi & 0 \\ 0 & 0 & 1 \end{pmatrix}$$

$$= \begin{pmatrix} k & l & 0 \\ l & m & 0 \\ 0 & 0 & 1 \end{pmatrix}.$$

De plus, les coefficients de $\overline{U_{01}^{-1}}$ s'obtiennent de façon simple à partir de ceux de $U_{01} \in U(2,1)$ (voir [P] p. 9). Si U_{01} s'écrit:

$$U_{01} = \begin{pmatrix} a & b & c \\ d & e & f \\ g & h & j \end{pmatrix}$$

alors:

$$\overline{U_{01}^{-1}} = \begin{pmatrix} a & d & -g \\ b & e & -h \\ -c & -f & j \end{pmatrix}$$

On obtient en fin de compte l'expression suivante pour A_2:

$$\begin{pmatrix} a^2k + 2abl + b^2m - c^2 & adk + ael + bdl + bem - cf & -agk - ahl - bgl - bhm + cj \\ adk + ael + bdl + bem - cf & d^2k + 2del + e^2m - f^2 & -dgk - dhl - egl - ehm + fj \\ agk + ahl + bgl + bhm - cj & dgk + dhl + egl + ehm - fj & -g^2k - 2ghl - h^2m + j^2 \end{pmatrix}$$

où:

$$
\begin{aligned}
a &= e^{i\theta_1}(1/s - x/r)\\
b &= e^{i\theta_1}(y/(1-x))\\
c &= e^{i\theta_1}x/r\\
d &= -e^{i\theta_2}y/r\\
e &= e^{i\theta_2}\\
f &= e^{i\theta_2}y/r\\
g &= 1/s - 1/r\\
h &= y/(1-x)\\
j &= 1/r\\
k &= e^{2i\theta_3}\cos^2\varphi + e^{2i\theta_4}\sin^2\varphi\\
l &= (e^{2i\theta_3} - e^{2i\theta_4})\cos\varphi\sin\varphi\\
m &= e^{2i\theta_3}\sin^2\varphi + e^{2i\theta_4}\cos^2\varphi.
\end{aligned}
$$

Trace, déterminant et angles

Comme on l'a évoqué précédemment, cette expression de A_2 est asez indigeste, et en particulier il ne serait pas raisonnable de calculer formellement ses valeurs propres; par contre on obtient facilement sa trace. Notons que, pour que cette trace ait un sens dans $PU(2,1)$, il faudrait normaliser A_2 (par exemple dans $SU(2,1)$), ou au moins garder en tête son déterminant. Ce déterminant s'exprime facilement à partir de l'expression multiplicative:

$$A_2 = U_{01}.\tilde{U}_{\{\theta_3,\theta_4\}}(\varphi).\overline{U_{01}^{-1}}$$

On a ainsi:

$$\det A_2 = e^{2i\psi}.\det\tilde{U}_{\{\theta_3,\theta_4\}}(\varphi) \text{ si } \det U_{01} = r.e^{i\psi} \text{ en coordonnées polaires.}$$

Notant alors que $\det\tilde{U}_{\{\theta_3,\theta_4\}}(\varphi) = e^{2i(\theta_3+\theta_4)}$, on obtient l'expression simple:

$$\det A_2 = e^{2i(\theta_1+\theta_2+\theta_3+\theta_4)}.$$

La trace de A_2 s'obtient à partir de la forme explicite de A_2 par un calcul simple mais pénible; on obtient:

$$
\begin{aligned}
TrA_2 &= (a^2+d^2-g^2)k + 2(ab+de-gh)l + (b^2+e^2-h^2)m + j^2 - c^2 - f^2\\
&= e^{2i(\theta_1+\theta_3)}[(1/s - x/r)\cos\varphi + y/(1-x)\sin\varphi]^2\\
&+ e^{2i(\theta_1+\theta_4)}[(1/s - x/r)\sin\varphi - y/(1-x)\cos\varphi]^2\\
&+ e^{2i(\theta_2+\theta_3)}[y/r\cos\varphi - \sin\varphi]^2\\
&+ e^{2i(\theta_2+\theta_4)}[y/r\sin\varphi + \cos\varphi]^2\\
&- e^{2i\theta_1}x^2/r^2\\
&- e^{2i\theta_2}y^2/r^2\\
&- e^{2i\theta_3}[(1/s - 1/r)\cos\varphi + y/(1-x)\sin\varphi]^2\\
&- e^{2i\theta_4}[(1/s - 1/r)\sin\varphi - y/(1-x)\cos\varphi]^2\\
&+ 1/r^2
\end{aligned}
$$

On utilisera cette formule explicite pour déterminer les fibres dans certains cas où elle se simplifie un peu, voir section 5.5.

5.4 Exemples et images expérimentales

On étudie dans cette section des exemples précis des polygones image de $\tilde{\mu}$ que l'on a décrits. Chacun de ces exemples est donné par deux paires d'angles $\{\theta_1, \theta_2\}$ et $\{\theta_3, \theta_4\}$, correspondant aux classes de conjugaison elliptiques des deux générateurs A et B. Rappelons que l'application $\tilde{\mu}$ associe à une paire d'isométries elliptiques (A, B) (chacune dans une classe de conjugaison fixée) la paire d'angles du produit AB lorsque celui-ci est elliptique. Notons que les angles en question sont les angles de rotation, c'est-à-dire le double des angles (de réflexion) entre les différents lagrangiens. On essaie de mettre l'accent sur la manière expérimentale dont la structure de ces polygones a été découverte, en donnant deux images pour chaque exemple. La première, dans l'esprit de la section 5.2, montre l'ensemble des murs réductibles dans la carte affine en demi-carré de $\mathbb{T}^2/\mathfrak{S}_2$; on a également hachuré la région que l'on a démontré être incluse dans l'image (voir le théorème 4). La deuxième est une image expérimentale obtenue (par Maple) en utilisant le paramétrage des triplets lagrangiens de la section 5.3 (qui dépend des 3 paramètres réels x, y et φ précédents) avec un maillage régulier des paramètres (en coordonnées circulaires pour l'angle et polaires pour le point du disque). Chaque image comporte typiquement entre 1000 et 20000 points, le temps de calcul pour chaque point étant d'environ 0,1 secondes (avec une machine universitaire ordinaire), ce qui fait que l'image entière prend entre une minute et une demi-heure à calculer.

On commence par les cas dégénérés où l'un au moins des générateurs est une réflexion complexe (un angle est nul) ou une réflexion complexe par rapport à un point (les deux angles sont égaux); ces cas ne rentrent pas dans la description générale que l'on a donnée précédemment, et on va les décrire ici en détail. On connaît en fait la réponse complète pour ces cas: l'image est exactement l'enveloppe convexe des murs réductibles (sauf dans le cas non convexe où les deux générateurs sont des réflexions complexes). Le résultat est le suivant:

Proposition 5.4.1 *Si l'un des générateurs A ou B est une réflexion complexe (resp. par rapport à un point), le polygone image de l'application moment est exactement l'enveloppe convexe des murs réductibles. De plus, en tout point du bord du carré qui est dans l'image mais qui n'est pas réductible, le produit AB est parabolique.*

Rappelons qu'on ne sait pas en général si ces derniers points (avec angles $\{0, \theta\}$) représentent des éléments paraboliques ou des réflexions complexes.

Démonstration. L'argument est le même pour les deux assertions; c'est simplement le fait que si A ou B est un elliptique spécial (une réflexion complexe ou une réflexion complexe par rapport à un point) et si AB est aussi un elliptique spécial, alors tout le groupe est réductible. En effet, ces transformations fixent alors chacune une droite complexe dans $\mathbb{C}P^2$, et celles-ci doivent se couper dans $\mathbb{C}P^2$. Ceci exclut donc toutes les chambres qui touchent la diagonale ailleurs qu'en un réductible. □

Le cas qui nous intéresse particulièrement est celui où l'un des générateurs est une réflexion complexe, puisque c'est le cas des exemples qui ont fourni la motivation d'origine de ce travail,

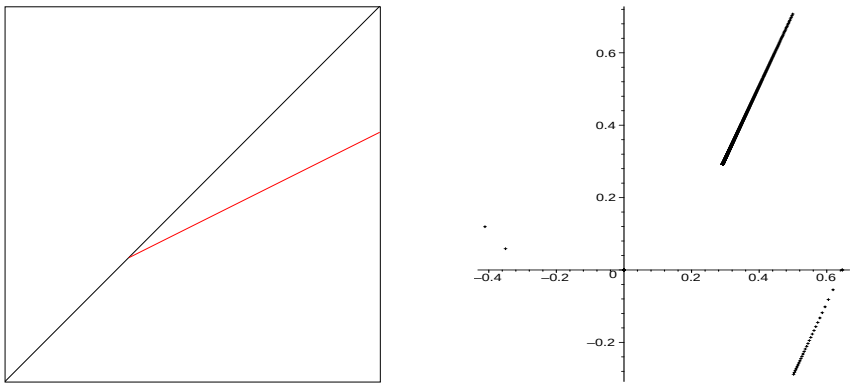

Figure 5.10: L'image pour les paires d'angles $\{\frac{2\pi}{6}, \frac{2\pi}{6}\}$, $\{\frac{2\pi}{8}, \frac{2\pi}{8}\}$

à savoir les réseaux $\Gamma(p,t)$ de Mostow (voir [M1], [M2] et les figures 5.13 et 5.14). On donnera plus de détails sur ces exemples dans la dernière section, où l'on explique pourquoi et comment on espère trouver de nouveaux groupes discrets dans ces images.

Les exemples génériques que l'on donne ensuite parcourent les différents types de configurations réductibles que l'on a décrits dans la section 5.2.3 et complètent la preuve de la classification. On espère également qu'ils donneront au lecteur une certaine intuition quant au comportement possible de ces objets: murs intérieurs et extérieurs, auto-intersection...

5.4.1 Les deux générateurs sont des réflexions complexes par rapport à un point

Ceci constitue le cas le plus dégénéré au sens où les réductibles consistent simplement en un sommet totalement réductible avec un segment réductible hyperbolique, et l'image complète est réduite à cela (voir figure 5.10). En effet, une réflexion complexe par rapport à un point stabilise tous les $\mathbb{C}$-plans passant par son point fixe (dans $U(2)$ un tel élément est un élément $e^{i\theta}.Id$ du centre); ainsi deux de ces transformations engendrent toujours un groupe réductible hyperbolique: elles stabilisent toutes deux le $\mathbb{C}$-plan passant par les deux points fixes.

5.4.2 L'un des générateurs est une réflexion complexe par rapport à un point

Il n'y a comme ci-dessus qu'un sommet totalement réductible, mais il donne maintenant lieu à deux familles réductibles hyperboliques, qui délimitent une enveloppe convexe d'intérieur non vide (voir figure 5.11). L'image est alors exactement cette enveloppe convexe par l'argument précédent (si un point de l'image est sur la diagonale alors il est réductible).

5.4.3 Les deux générateurs sont des réflexions complexes: un exemple non convexe

Ceci est le cas où notre argument de convexité locale autour d'un sommet totalement réductible est en défaut, et il l'est pour la bonne raison que le résultat est faux dans ce cas. Il y a maintenant

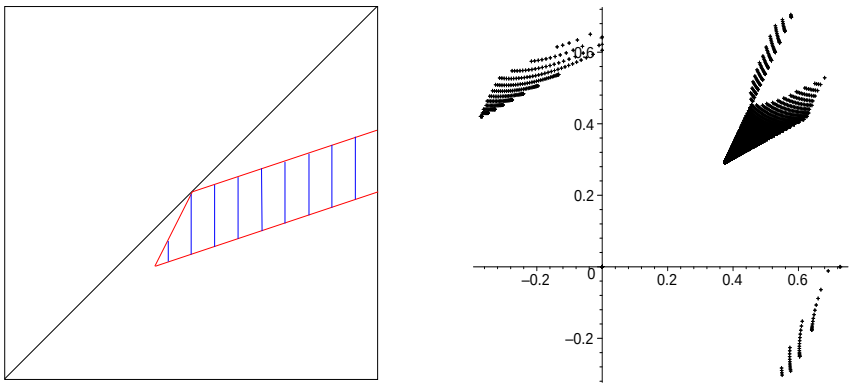

Figure 5.11: L'image pour les paires d'angles $\{\frac{2\pi}{4}, \frac{2\pi}{6}\}$, $\{\frac{2\pi}{8}, \frac{2\pi}{8}\}$

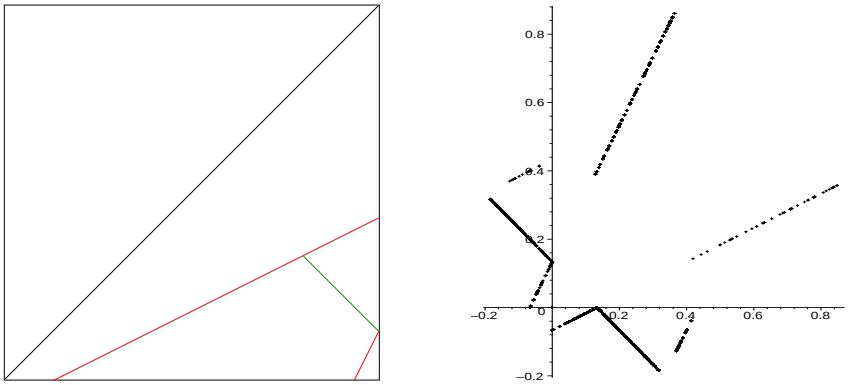

Figure 5.12: L'image pour les paires d'angles $\{0, \frac{2\pi}{3}\}$, $\{0, \frac{8\pi}{5}\}$ (non convexe)

deux sommets totalement réductibles distincts, joints par le segment réductible sphérique, ainsi qu'un segment réductible hyperbolique (les autres sont réduits à un point) qui passe par les deux sommets, voir figure 5.12. L'image complète est alors la réunion non convexe de ces deux segments, parce que deux réflexions complexes engendrent toujours un groupe réductible (leurs miroirs, ou lieux des points fixes, se coupent dans $\mathbb{C}P^2$).

5.4.4 L'un des générateurs est une réflexion complexe: familles contenant les réseaux $\Gamma(p,t)$ de Mostow

La configuration réductible est maintenant la réunion du segment réductible sphérique avec deux segments réductibles hyperboliques (un à chaque sommet); on sait comme ci-dessus que l'image complète est exactement l'envelope convexe des réductibles (voir figures 5.13, 5.14). On a également représenté sur ces images un segment en pointillés qui est la famille à un paramètre $\Gamma(p,t)$ de Mostow (chaque valeur entière de p correspond à un dessin différent). On va se concentrer dans la dernière section sur le cas de $\Gamma(3,t)$ (qui est avec nos notations un segment dans l'image pour les paires $\{\frac{2\pi}{3}, \frac{4\pi}{3}\}$, $\{0, \frac{2\pi}{3}\}$).

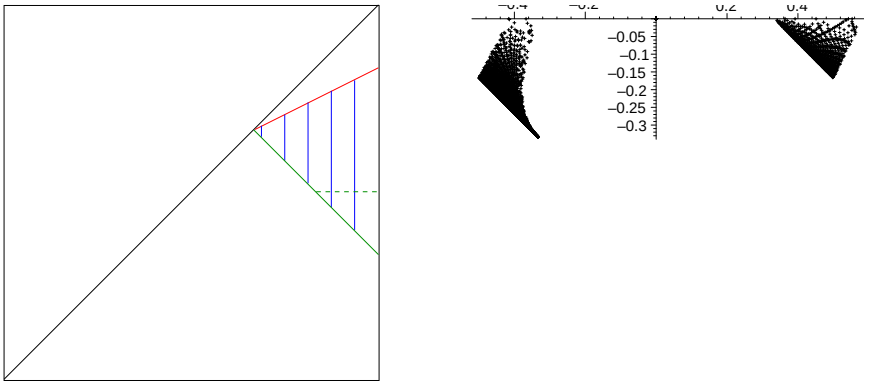

Figure 5.13: L'image pour les paires d'angles $\{\frac{2\pi}{3}, \frac{4\pi}{3}\}$, $\{0, \frac{2\pi}{3}\}$; le segment en pointillés représente la famille $\Gamma(3,t)$ de Mostow (voir aussi l'agrandissement dans la figure 5.22).

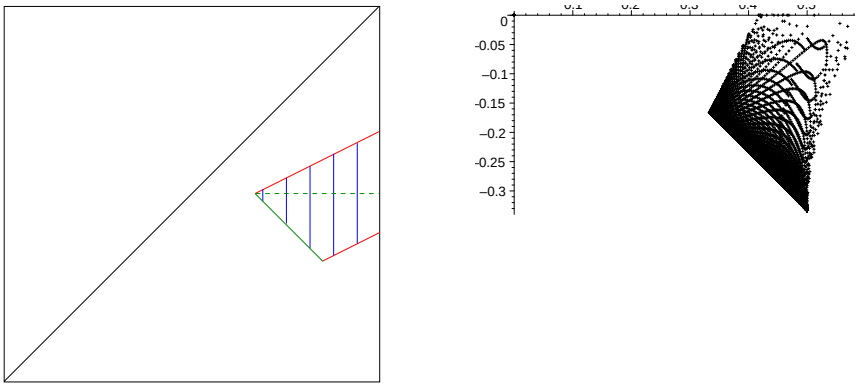

Figure 5.14: L'image pour les paires d'angles $\{\frac{2\pi}{3}, \frac{4\pi}{3}\}$, $\{0, \frac{2\pi}{6}\}$; le segment en pointillés représente la famille $\Gamma(6,t)$ de Mostow.

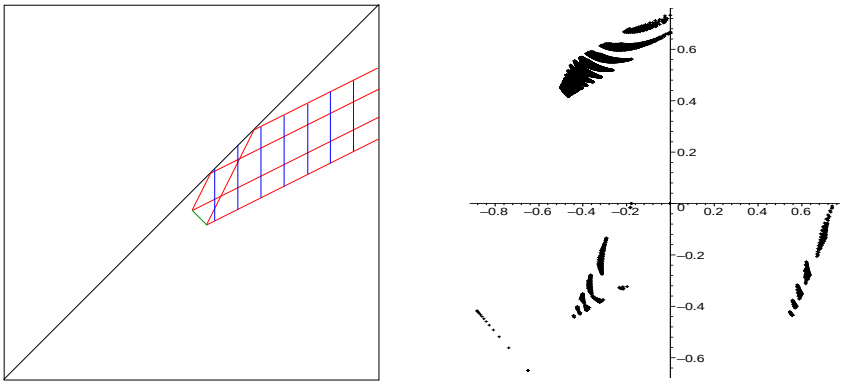

Figure 5.15: L'image pour les paires d'angles $\{\frac{2\pi}{3}, \frac{2\pi}{4}\}$, $\{\frac{2\pi}{5}, \frac{2\pi}{6}\}$ (type C^{++}_{++})

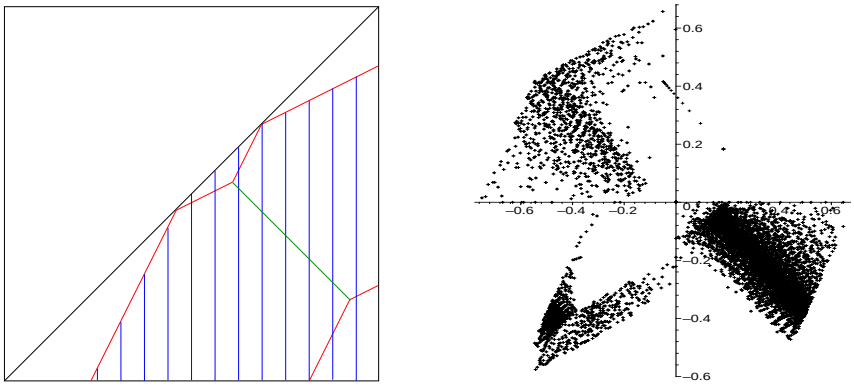

Figure 5.16: L'image pour les paires d'angles $\{\frac{2\pi}{3}, -\frac{2\pi}{4}\}$, $\{\frac{2\pi}{5}, -\frac{2\pi}{6}\}$ (type C^{+-}_{-+})

5.4.5 Exemples génériques

On en vient maintenant à des exemples génériques qui illustrent plus fidèlement notre decription des configurations réductibles. Comme on l'a dit, les valeurs ont été choisies pour montrer toute la palette des types de configurations réductibles mentionnés dans notre classification. Notons également quelques caractéristiques visibles sur ces images. Le cas des paires $\{\frac{2\pi}{3}, \frac{2\pi}{4}\}$, $\{\frac{2\pi}{5}, \frac{2\pi}{6}\}$ (figure 5.15) montre des points d'auto-intersection de la charpente réductible, entre différents segments réductibles hyperboliques. On peut également remarquer qu'un même segment réductible hyperbolique peut avoir une partie qui est un mur extérieur de l'image, et une autre qui est un mur intérieur (après avoir rebondi sur la diagonale). L'image contient également tout un segment de la diagonale. Les images suivantes fournissent des exemples de sommets intérieurs (des sommets totalement réductibles qui sont des points intérieurs de l'image), que l'on repère aisément sur les images expérimentales.

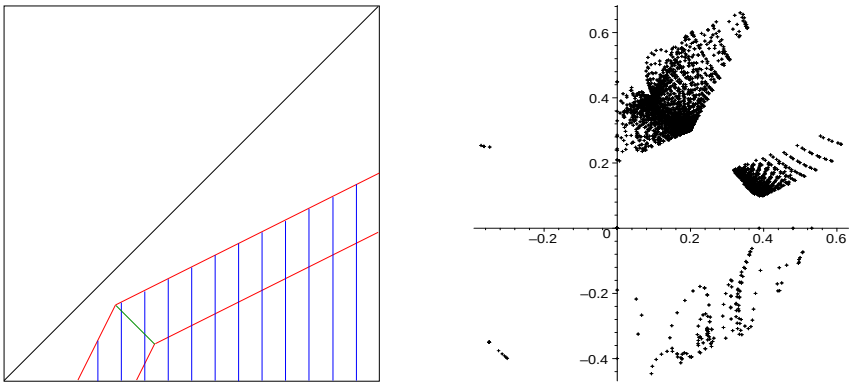

Figure 5.17: L'image pour les paires d'angles $\{-\frac{2\pi}{10}, \frac{2\pi}{10}\}$, $\{\frac{4\pi}{10}, \frac{6\pi}{10}\}$ (type C_{-+}^{-+})

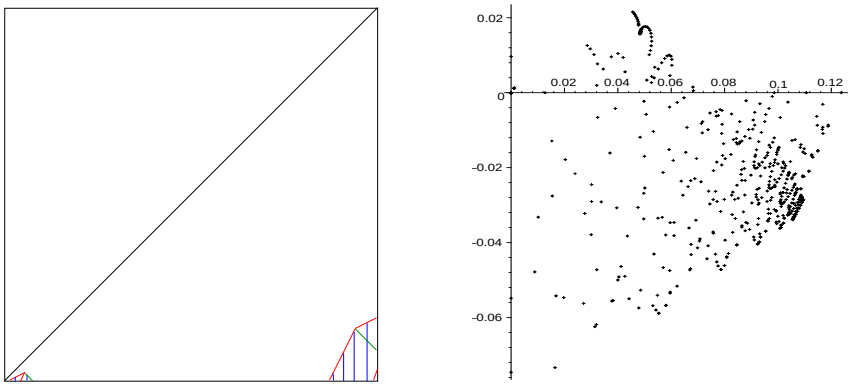

Figure 5.18: L'image pour les paires d'angles $\{\frac{2\pi}{4}, \frac{2\pi}{6}\}$, $\{-\frac{2\pi}{5}, -\frac{2\pi}{7}\}$ (type D_{--}^{-+})

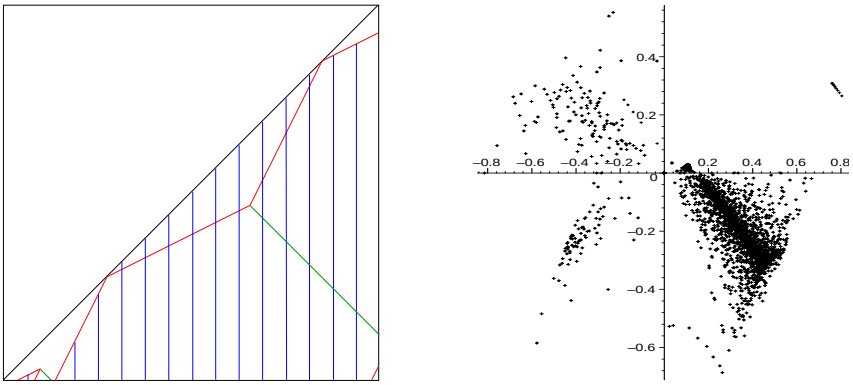

Figure 5.19: L'image pour les paires d'angles $\{\frac{2\pi}{4}, -\frac{2\pi}{6}\}$, $\{\frac{2\pi}{5}, -\frac{2\pi}{7}\}$ (type D_{--}^{+-})

5.5 A la recherche des groupes discrets: aspects expérimentaux

Il y a une condition évidente que doit satisfaire un sous-groupe de $PU(2,1)$ afin d'être discret (comme dans tout groupe de Lie agissant sur un espace avec des stabilisateurs de points compacts), à savoir que tous les éléments de ce sous-groupe qui ont un point fixe doivent être d'ordre fini. Pour un élément elliptique de $PU(2,1)$, ceci signifie que ses deux angles doivent être des multiples rationnels de π; on demandera en général des conditions plus fortes pour certains générateurs, par exemple des fractions entières de π ou des paires de la forme $\{\frac{2\pi}{n}, \frac{2k\pi}{n}\}$, dans l'espoir d'obtenir des conditions locales de pavage du type du théorème de Poincaré.

Notre cadre est bien adapté à cette idée simple parce qu'on peut contrôler simultanément les angles de A, B et de leur produit. De plus, le paramétrage que l'on a obtenu en utilisant les plans lagrangiens (3 paramètres lorsque les angles de A et B sont fixés) nous laisse une fibre à une dimension de groupes non conjugués où les angles du produit restent fixés. Les objets de dimension un sont très sympathiques parce qu'on peut s'y promener sans se perdre, et surtout sans rater de point (dans une composante connexe). Si l'on cherche quelque chose de rare et de précieux comme un réseau (qui est un point isolé par le théorème de rigidité forte de Mostow), rester sur un tel chemin vous épargne l'impression désagréable de chercher une aiguille dans une botte de foin, à condition que le chemin ait une bonne raison de contenir un tel point. Toutes les familles précédentes d'exemples ont été trouvées en suivant ce principe: les réseaux de Mostow (voir [M1], [M2] et ci-dessous), les groupes triangulaires idéaux de Goldman et Parker ainsi que les autres groupes triangulaires étudiés par Falbel-Koseleff, Gusevskii-Parker, Schwartz, Falbel-Parker, Deraux... (voir [Sz1] pour un panorama sur ces groupes).

Une première difficulté est alors de choisir où commencer à chercher: nous avons choisi dans un premier temps de pousser plus loin l'étude de cas où des réseaux ou des groupes discrets ont déjà été trouvés. On n'a fait que commencer cette recherche pour l'instant, dans le cas des réseaux $\Gamma(3,t)$ de Mostow. Ce cas n'est pas typique au sens où l'un des générateurs est une réflexion complexe, et où il n'y a donc pas de fibre: chaque point du triangle image de $\tilde{\mu}$ correspond à un seul groupe engendré par des $\mathbb{R}$-réflexions. C'est pourquoi on va présenter aussi un exemple apparemment moins intéressant, contenant des groupes $\mathbb{R}$-fuchsiens, pour illustrer les déformations dans une fibre.

Ce que l'on a fait pour l'instant ne fait qu'indiquer ce que pourraient être des candidats intéressants à la discrétude; il reste alors l'épineuse question de décider si un groupe donné (défini par deux générateurs sous forme matricielle) est discret ou non. Il y a peu de méthodes pour ce faire; une idée de base (utile surtout pour éliminer des candidats) est de tester tous les mots de longueur maximale donnée, pour trier d'abord ceux qui sont elliptiques et calculer les angles de ceux-ci. La stratégie sera alors de s'arrêter au premier mot qui "ne marche pas", et de voir ce qui arrive à ce mot par déformation dans la fibre. Dans le cas des groupes triangulaires engendrés par trois involutions complexes, Schwartz conjecture que tout est gouverné par deux mots (à savoir $ACBC$ et ABC, voir de nouveau [Sz1]). On espère qu'il se produise ici un phénomène analogue afin que notre stratégie soit raisonnable: au pire, si le premier mot pour lequel on doit déformer nous laisse seulement avec des points isolés dans la fibre, il ne reste rapidement plus rien s'il y a beaucoup de classes de conjugaison problématiques.

Il y également une grande différence entre être convaincu qu'un groupe est discret et le

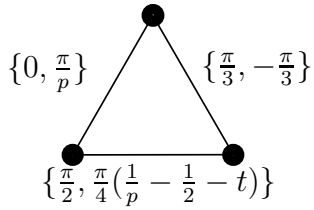

Figure 5.20: Diagramme de $\mathbb{R}$-réflexions pour $\tilde{\Gamma}(p,t)$

prouver. A vrai dire, s'il n'y a pas de raison arithmétique pour laquelle le groupe doit être discret, il y a très peu de méthodes pour le faire, la plus utilisée étant de construire un domaine fondamental pour l'action du groupe sur $H^2_{\mathbb{C}}$. Il y a des constructions très belles et exotiques de tels objets, mais ce n'est pas une tâche facile et elle ne devrait être entreprise que pour de bonnes raisons. Il y a d'autres méthodes expérimentales qui fournissent un bon compromis, comme l'utilisation que fait Deraux de la méthode de Dirichlet (voir [D1], [D2]), que nous essayons d'appliquer à nos groupes en utilisant ses applets java ([D3]), modifiés selon les générateurs.

Avant d'entrer dans les détails, soulignons qu'on n'en est qu'au début de cette démarche, et que l'on décrit plus à ce stade un projet de recherche que des résultats factuels.

5.5.1 Familles contenant les réseaux $\Gamma(p,t)$ de Mostow

On va maintenant se concentrer sur les groupes introduits par Mostow dans son article de 1980 ([M1]), groupes qu'il a notés $\Gamma(p,t)$ (où $p = 3, 4, 5$ et t est un paramètre réel); notons cependant que cette description contient aussi, pour des valeurs supérieures de p, 22 des 27 réseaux de Picard (ou réseaux de Deligne-Mostow de dimension 2), comme il est décrit en détail dans l'article ultérieur [M2].

On ne va décrire ici que très brièvement la construction de ces groupes, pour laquelle le lecteur pourra se reporter (à l'article original ou) auchapitre 3 (voir [DFP]). Le groupe $\Gamma(p,t)$ est engendré par trois réflexions complexes d'ordre p (R_1,R_2, et R_3) qui sont permutées cycliquement par un élément J et satisfont deux à deux une relation de tresse. On considère comme dans [DFP] le groupe $\tilde{\Gamma}(p,t)$ engendré par J et R_1, qui contient $\Gamma(p,t)$ avec indice 1 ou 3 selon les cas. On a remarqué que ces deux générateurs se décomposent simultanément en produit de $\mathbb{R}$-réflexions de la façon suivante, avec les notations de [DFP]:

$$\begin{cases} J &= \sigma_{12}\sigma_{23} \\ R_1 &= \sigma_{23}\tau \end{cases}$$

Les transformations elliptiques R_1 et J ont pour paire d'angle $\{0, \frac{2\pi}{p}\}$ et $\{\frac{2\pi}{3}, -\frac{2\pi}{3}\}$ respectivement. Un calcul utilisant la forme matricielle explicite nous dit alors que $JR_1 = \sigma_{12}\tau$ est diagonalisable avec valeurs propres $-\eta i\overline{\phi} = e^{i\pi(1+1/p+1/2-t/3)}$ et $\pm\sqrt{-\eta i\phi} = \pm e^{i\pi(1+1/p+1/2+t/3)/2}$, où $\eta = e^{i\pi/p}$ et $\phi = e^{i\pi t/3}$. Le produit est donc elliptique, et ses angles sont obtenus en divisant les deux valeurs propres de type positif par celle de type négatif, qui est ici par un autre calcul $-e^{i\pi(1+1/p+1/2+t/3)/2}$. On obtient ainsi la paire d'angles suivante pour JR_1: $\{\pi, \frac{\pi}{2}(\frac{1}{p} - \frac{1}{2} - t)\}$ (notons que $(JR_1)^2$ est une réflexion complexe). Les angles entre les trois lagrangiens sont obtenus en divisant les précédents par 2, ce qui nous donne le diagramme de la figure 5.20.

Considérons maintenant le cas $p = 3$ et voyons comment la famille $\tilde{\Gamma}(p,t)$ s'inscrit dans

t	0	$\frac{1}{30}$	$\frac{1}{18}$	$\frac{1}{12}$	$\frac{5}{42}$	$\frac{1}{6}$	$\frac{7}{30}$	$\frac{1}{3}$
$-\frac{1}{\pi}\cdot$Angle de JR_1	$\frac{1}{12}$	$\frac{1}{10}$	$\frac{1}{9}$	$\frac{1}{8}$	$\frac{1}{7}$	$\frac{1}{6}$	$\frac{1}{5}$	$\frac{1}{4}$
$-\frac{1}{\pi}\cdot$Angle de R_1J^{-1}	$\frac{1}{12}$	$\frac{1}{15}$	$\frac{1}{18}$	$\frac{1}{24}$	$\frac{1}{42}$	0	$-\frac{1}{30}$	$-\frac{1}{12}$

Figure 5.21: Les groupes discrets $\Gamma(3,t)$

le polygone du moment associé aux paires $\{0,\frac{2\pi}{p}\}$ et $\{\frac{2\pi}{3},-\frac{2\pi}{3}\}$. Ceci nous donne le segment de la figure 5.13, que l'on agrandit sur la figure 5.22 pour voir les points correspondant à des réseaux. Notons que ce segment est caractérisé par le fait que R_1 et ses deux conjugués R_2 et R_3 satisfont une relation de tresse d'ordre 3 (à savoir $R_iR_jR_i = R_jR_iR_j$). On obtient des réseaux pour 8 valeurs du paramètre t, dont la liste se trouve dans la figure 5.21 avec les valeurs correspondantes de l'angle de rotation (non trivial) de JR_1.

Une chose importante à noter est que cet angle est intimement lié à l'une des deux conditions suffisantes de discrétude du groupe (les conditions d'intégralité de Picard, voir [DFP]). Rappelons que ces deux conditions proviennent de l'analyse de seulement deux classes de conjugaison de $\mathbb{C}$-réflexions dans la groupe, à savoir celles de R_2R_1J et $J^{-1}R_1R_2$; il se trouve que demander que les deux angles de rotation correspondants soient des fractions entières de 2π suffit à garantir la discrétude du groupe. Or la première de ces classes de conjugaison contient $(R_1J^{-1})^2$ et la deuxième $(JR_1)^2$, parce que $R_2 = JR_1J^{-1}$ et donc:

$$R_2R_1J = JR_1J^{-1}R_1J = J(R_1J^{-1}R_1J^{-1})J^{-1} \text{ et } J^{-1}R_1R_2 = J^{-1}R_1JR_1J^{-1} = J(JR_1JR_1)J^{-1}$$

Ceci signifie qu'une des deux conditions de discrétude est immédiatement visible sur notre image: l'angle de JR_1 qui varie avec le paramètre doit être une fraction entière paire de 2π. Il se trouve que l'on peut même voir la deuxième condition sur le même dessin, parce que J^{-1} est conjugué à J, et donc les angles de R_1J^{-1} apparaissent également sur ce dessin (mais correspondent à des points différents). Les valeurs de l'angle de rotation (non trivial) de R_1J^{-1} apparaissent également dans le tableau de la figure 5.21; les points correspondants sont sur le même segment que les précédents, mais plus à droite. Ceci nous fournit un exemple de points distincts d'un même polygone image qui correspondent à des sous-groupes conjugués dans $PU(2,1)$; cette situation ne fait qu'empirer si l'on s'intéresse seulement aux classes de commensurabilité de tels sous-groupes. Cette idée simple d'échanger deux des quatre classes fondamentales de $\mathbb{C}$-réflexions est en fait derrière les isomorphismes et commensurabilités entre réseaux découverts par Sauter (voir [Sa]) et étudiées plus en détail dans le livre de Deligne et Mostow (voir [DM]).

Avant d'entrer dans les aspects expérimentaux, on rappelle la description complète du polygone image du moment (voir Proposition 5.4.1). Dans le cas présent (angles $\{0,\frac{2\pi}{3}\}$ et $\{\frac{2\pi}{3},-\frac{2\pi}{3}\}$), le polygone en question est le triangle des figures 5.13 et 5.22, borné par un segment réductible sphérique, un segment réductible hyperbolique, et le segment "au bord" $[2\pi,\theta]$ pour $\theta \in [\frac{2\pi}{3},\frac{5\pi}{3}]$ qui est donc composé de classes de conjugaison paraboliques (sauf à ses extrémités).

Afin d'étudier explicitement d'autres points de l'image, on utilise le paramétrage de la partie 5.3 en tandem avec la formule pour la trace de la fin de la même section. Cette formule

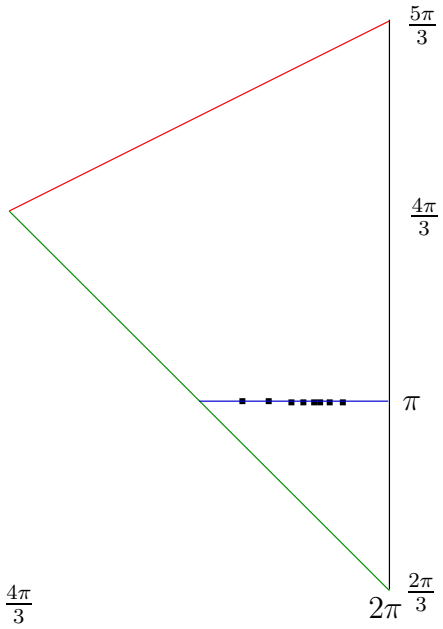

Figure 5.22: Les groupes $\tilde{\Gamma}(p,t)$ de Mostow dans le polygone du moment

se simplifie particulièrement dans le cas présent grâce aux valeurs des angles; on obtient après simplifications, avec les notations de la section 5.3 (et notant τ la trace de A_2):

$$\begin{cases} \frac{2}{3}Re(\tau) &= 1+2\frac{y^2}{r^2}-(\frac{y}{r}\cos\varphi-\sin\varphi)^2 \\ \frac{2}{\sqrt{3}}Im(\tau) &= (\cos^2\varphi-\sin^2\varphi)(1-\frac{y^2}{r^2})+6\cos\varphi\sin\varphi\frac{y}{r} \end{cases}$$

Ceci permet en principe de paramétrer explicitement les points de l'image, ce dont on n'a pas besoin pour l'instant (il nous faudra bien sûr des expressions algébriques pour déterminer les propriétés arithmétiques de chaque groupe). On a choisi comme premier point à tester un point proche du centre du triangle avec des coordonnées favorables, à savoir $(\frac{5\pi}{3},\frac{4\pi}{3})$. On a examiné dans ce groupe les mots de longueur maximale 5; aucune nouvelle classe d'elliptiques n'est apparue. On a également fait tourner la procédure Dirichlet de Deraux avec ces générateurs; après 5 étapes (quelques jours de calcul) celle-ci a produit deux bisecteurs cospinaux, à savoir ceux définis par les paires de mots $\{433121, 434421\}$ et $\{434433434, 343443121\}$ (utilisant la notation en chiffres $1 = A$, $2 = B$, $3 = B^{-1}$, $4 = A^{-1}$). L'occurrence de bisecteurs cospinaux dans la construction de Dirichlet est spéciale. Les mots eux-mêmes n'ont pas d'intérêt particulier (on vérifie ici que trois de ces mots sont dans les classes de conjugaison de A, B et AB et que le quatrième est loxodromique). Par contre l'intersection des deux bisecteurs correspondants (une partie d'un $\mathbb{C}$-plan) donne une transformation de cycle dans le cadre de Poincaré, et cette transformation de cycle (une réflexion complexe) pourrait être très intéressante; dans les exemples de Mostow les conditions de discrétude proviennent de deux telles transformations. Malheureusement, on n'a pas encore écrit les cycles correspondants pour l'instant, mais cela semble être un chemin prometteur.

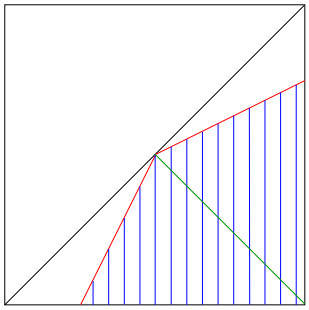

Figure 5.23: Le polygone image pour $\{\frac{\pi}{2}, -\frac{\pi}{2}\}$,$\{\frac{\pi}{2}, -\frac{\pi}{2}\}$: familles $\mathbb{R}$-fuchsiennes

5.5.2 Familles contenant des groupes $\mathbb{R}$-fuchsiens

Rappelons qu'une transformation elliptique de $H^2_{\mathbb{C}}$ stabilise un $\mathbb{R}$-plan si et seulement si ses angles sont de la forme $\{\theta, -\theta\}$ (ou $\{0, \pi\}$, voir le chapitre 1). On choisit un exemple simple, donné par les paires d'angles $\{\frac{\pi}{2}, -\frac{\pi}{2}\}$ et $\{\frac{\pi}{2}, -\frac{\pi}{2}\}$; le polygone image, représenté sur la figure 5.23, est alors assez grand pour permettre beaucoup de possibilités. La première idée est de considérer des produits qui sont aussi de la forme $\{\theta, -\theta\}$; ceci semble produire des groupes $\mathbb{R}$-fuchsiens (dans les exemples que l'on a étudiés). Ce qui est plus surprenant est que ce type d'angles apparaît également quand on essaie de les éviter. On a essayé deux autres exemples, considérant les fibres au-dessus des points $\{\pi, \frac{\pi}{2}\}$ et $\{\frac{2\pi}{5}, \frac{6\pi}{5}\}$. Dans les deux cas, le même phénomène se produit lorsqu'on examine les mots elliptiques dans le groupe: on rencontre une classe de conjugaison (celle de 122422 dans le premier cas et 1243 dans le second) qui a des angles $\{\theta, -\theta\}$ avec $\theta \notin \pi\mathbb{Q}$ (ce qui semble normal puisqu'on part d'un point arbitraire de la fibre). Ce qui est frappant est que les angles restent de la forme $\{\theta, -\theta\}$ lorsqu'on se déplace dans la fibre (jusqu'à ce qu'ils arrivent à 0 et que le produit devienne loxodromique). On a vérifié qu'aucun de ces groupes n'est $\mathbb{R}$-fuchsien, mais la forme particulière des angles indique qu'ils doivent avoir un sous-groupe $\mathbb{R}$-fuchsien. Lorsqu'on parcourt la fibre, θ parcourt un certain intervalle; un autre aspect frappant est que dans le premier exemple le maximum est $\frac{\pi}{4}$, et qu'il doit donc y avoir des choses à dire sur la configuration qui réalise ce maximum.

Bibliography

[A] M. F. Atiyah; *Convexity and commuting Hamiltonians*. Bull. London Math. Soc. **14(1)** (1982), 1–15.

[AMM] A. Alekseev, A. Malkin, E. Meinrenken; *Lie group valued moment maps*. J. Diff. Geom. **48(3)** (1998), 445–495.

[AW] S. Agnihotri, C. Woodward; *Eigenvalues of products of unitary matrices and quantum Schubert calculus*. Math. Res. Lett. **5(6)** (1998), 817–836.

[BGS] W. Ballmann, M. Gromov, V. Schroeder; Manifolds of Nonpositive Curvature. Birkhaüser Progress in Math. vol. 61, 1985.

[Be] P. Belkale; *Local systems on $P^1 - S$ for S a finite set*. Compositio Math. **129(1)** (2001), 67–86.

[Bi1] I. Biswas; *A criterion for the existence of a parabolic stable bundle of rank two over the projective line*. Internat. J. Math. **9(5)** (1998), 523–533.

[Bi2] I. Biswas; *On the existence of unitary flat connections over the punctured sphere with given local monodromy around the punctures*. Asian J. Math. **3(2)** (1999), 333–344.

[CG] S. Chen, L. Greenberg; *Hyperbolic spaces*. In Contributions to Analysis. Academic Press, New York (1974), 49–87.

[D1] M. Deraux; *Dirichlet domains for the Mostow lattices*. To appear in Experimental Math..

[D2] M. Deraux; *Deforming the $\mathbb{R}$-Fuchsian $(4,4,4)$-triangle group into a lattice*. Preprint, 2005.

[D3] M. Deraux; *Dirichlet domains in complex hyperbolic space*, java applets, `http://www-fourier.ujf-grenoble.fr/~deraux/java`.

[DFP] M. Deraux, E. Falbel, J. Paupert; *New constructions of fundamental polyhedra in complex hyperbolic space*. Acta Math. **194** (2005), 155–201.

[DM] P. Deligne, G. D. Mostow; Commensurabilities among lattices in $PU(1,n)$. Annals of Mathematics Studies **132**. Princeton University Press (1993).

[FMS] E. Falbel, J.-P. Marco, F. Schaffhauser; *Classifying triples of Lagrangians in a Hermitian vector space*. Topology Appl. **144** (2004), 1–27.

[FP] E. Falbel, J. Paupert; *Fundamental domains for finite subgroups in $U(2)$ and configurations of Lagrangians*. Geom. Dedicata **109** (2004), 221–238.

[FW] E. Falbel, R. Wentworth; *Eigenvalues of products of unitary matrices and Lagrangian involutions*. To appear in Topology.

[F] W. Fulton; *Eigenvalues, invariant factors, highest weights, and Schubert calculus*. Bull. Amer. Math. Soc. **37(3)** (2000), 209–249.

[G] W.M. Goldman; Complex Hyperbolic Geometry. Oxford Mathematical Monographs. Oxford Science Publications (1999).

[GS1] V. Guillemin, S. Sternberg; *Convexity properties of the moment mapping*. Invent. Math. **67(3)** (1982), 491–513.

[GS2] V. Guillemin, S. Sternberg; *Convexity properties of the moment mapping II*. Invent. Math. **77(3)** (1984), 533–546.

[Kl1] A. Klyachko; *Stable bundles, representation theory and Hermitian operators*. Selecta Math. (NS) **4(3)** (1998), 419–445.

[Kl2] A. Klyachko; *Vector bundles, linear representations, and spectral problems*. Proceedings of the International Congress of Mathematicians, Vol. II (Beijing, 2002), 599–613, Higher Ed. Press, Beijing (2002).

[Ko] V. P. Kostov; *The Deligne-Simpson problem–a survey*. J. Algebra **281** (2004), 83–108.

[M1] G. D. Mostow; *On a remarkable class of polyhedra in complex hyperbolic space*. Pacific J. Math. **86** (1980), 171–276.

[M2] G. D. Mostow; *Generalized Picard lattices arising from half-integral conditions*. Publ. Math. IHES **63** (1986), 91–106.

[N] A. J. Nicas; *Classifying pairs of Lagrangians in a Hermitian vector space*. Topology Appl. **42** (1991), 71–81.

[P] J. R. Parker; Notes on complex hyperbolic geometry, preliminary version (2003).

[Sa] J. K. Sauter; *Isomorphisms among monodromy groups and applications to lattices in $PU(1,2)$*. Pacific J. Math. **146(2)** (1990), 331–384.

[Sf] F. Schaffhauser; Decomposable representations and Lagrangian submanifolds of moduli spaces associated to surface groups. Thesis, Université Paris 6, 2005.

[Sz1] R. E. Schwartz; *Complex hyperbolic triangle groups*. Proceedings of the International Congress of Mathematicians, Vol. II (Beijing, 2002), 339–349, Higher Ed. Press, Beijing, 2002.

[Sz2] R. E. Schwartz; Spherical CR geometry and Dehn surgery. Research monograph, 2004.

[W1] A. Weinstein; *Poisson geometry of discrete series orbits, and momentum convexity for noncompact group actions*. Lett. Math. Phys. **56(1)** (2001), 17-30.

[W2] A. Weinstein; *The geometry of momentum*. Preprint, arXiv:math.SG/0208108 (2002).